THÈSE EN COTUTELLE

PRÉSENTÉE POUR OBTENIR LE GRADE DE

DOCTEURE DE

L'UNIVERSITÉ DE BORDEAUX

ET DE L'UNIVERSITE EUSKAL HERRIKO UNIBERTSITATEA

ÉCOLE DOCTORALE SCIENCES CHMIQUES

ÉCOLE DOCTORALE DU PARTENAIRE BIOLOGIE MOLÉCULAIRE ET BIOMÉDECINE

CHIMIE ANALYTIQUE ET ENVIRONNEMENTALE

Par Ana REY SOGO

Rôle des contaminants émergents dans la promotion du transfert horizontal de gènes de résistance aux antimicrobiens: approche multi-échelle en contexte environnemental

---

Role of emerging contaminants in promoting horizontal transfer of antimicrobial resistance genes: a multiscale approach in environmental context

Sous la direction de:

Itziar ALKORTA CALVO et Hélène BUDZINSKI

Soutenue le 30/06/2026

Membres du jury:

M. Eric FOUQUET, Professeur des universités, Université de Bordeaux, Examinateur.
M. Nestor ETXEBARRIA LOIZATE, Professeur des universités, Euskal Herriko Unibertsitatea, Examinateur.
Mme. Elisabeth GROHMANN, Professeur des universités, Berlin University of Applied Sciences, Rapporteure.
Mme. Matxalen LLOSA BLAS, Professeure des universités, University of Cantabria, Rapporteure.
M. Manel CAMPS, Professeur des universités, UC Santa Cruz, Examinateur.

Ana Rey Sogo presents the following thesis dissertation to obtain the degree of Doctor in Molecular Biology and Biomedicine from the University of the Basque Country (Euskal Herriko Unibertsitatea, EHU) & Analytical and Environmental Chemistry from the University of Bordeaux (Université de Bordeaux, UBx).

Role of emerging contaminants in promoting horizontal transfer of antimicrobial resistance genes: a multiscale approach in environmental context

El papel de los contaminantes emergentes en la promoción de la transferencia horizontal de genes de resistencia a los antimicrobianos: un enfoque a múltiples escalas en el contexto medioambiental

Rôle des contaminants émergents dans la promotion du transfert horizontal de gènes de résistance aux antimicrobiens: approche multi-échelle en contexte environnemental

---

Supervisors:
Dra. Itziar Alkorta Calvo
Department of Biochemistry and Molecular Biology
Faculty of Science and Technology (EHU)
Dra. Hélène Budzinski
EPOC – LPTC, UMR 5805 CNRS (UBx)

Titre: Rôle des contaminants émergents dans la promotion du transfert horizontal de gènes de résistance aux antimicrobiens: approche multi-échelle en contexte environnemental

Résumé :

La propagation mondiale de la résistance aux antimicrobiens (RAM) par le transfert génétique horizontal (TGH) et par le transfert conjugatif constitue l'un des défis les plus urgents en microbiologie environnementale et en santé publique. Alors que les antibiotiques sont depuis longtemps reconnus comme des facteurs favorisant la sélection et la propagation de la RAM, le rôle des contaminants émergents (par exemple, les produits chimiques industriels, les désinfectants, les produits de soins personnels) en tant que promoteurs de la conjugaison bactérienne à des concentrations pertinentes pour l'environnement reste mal compris. Cette thèse comble cette lacune grâce à une approche intégrative à plusieurs échelles combinant la modélisation prédictive basée sur l'apprentissage automatique (ML), l'expérimentation in vitro sur trois systèmes de conjugaison et l'évaluation in situ sur le terrain dans un estuaire influencé par les eaux usées.

Dans le premier chapitre, une série de modèles d'apprentissage automatique (régression linéaire, forêt aléatoire et *eXtreme Gradient Boosting*) a été développée et évaluée à l'aide d'un ensemble de données sélectionnées avec soin, comprenant les effets publiés de facteurs de stress chimiques sur des expériences de conjugaison. Le modèle le plus performant, le régresseur XGB, a atteint un R^2 de validation interne de 0,719, démontrant ainsi une capacité prédictive significative. L'analyse de l'importance des caractéristiques a révélé que la concentration chimique, les espèces bactériennes utilisées dans les expériences et les empreintes structurelles constituaient les prédicteurs dominants. Ces résultats établissent un cadre pour l'évaluation des risques liés au TGH et identifient les limites de la capacité prédictive actuelle, soulignant la nécessité de disposer d'ensembles de données expérimentales plus vastes et plus homogènes afin d'étendre l'applicabilité du modèle.

Dans le deuxième chapitre, les effets de douze contaminants émergents préoccupants (CEPs) issus de six groupes fonctionnels sur le transfert conjugatif ont été caractérisés à l'aide de deux systèmes de conjugaison intra-espèces d'*Escherichia coli* partageant le même receveur HMS174, mais différant par le souche donneuse et le groupe d'incompatibilité (Inc) plasmidique (IncF/K12 et IncP/UB1637). Les deux systèmes ont réagi à une exposition aux CEPs à des concentrations comprises entre 0,001 et 0,01 µg mL^{-1}, mais le système IncP a systématiquement montré une induction plus forte et plus reproductible. Cette différence de sensibilité a été attribuée expérimentalement au type de plasmide et expliquée sur le plan mécanistique par

l'interaction de trois facteurs : la fréquence de transfert basale plus élevée de l'IncF, qui laisse une induction apparente moins marquée ; l'hétérogénéité de la population cellulaire ; et le système de régulation intrinsèque du plasmide. Les mécanismes moléculaires ont été élucidés plus en détail pour des CEPs individuelles, mettant en évidence des voies spécifiques à chaque composé.

Dans les chapitres trois et quatre, l'étude a été étendue à un contexte environnemental in situ, en caractérisant le plasmide mobile présent en quatre points d'échantillonnage couvrant les effluents des stations d'épuration (STEP) et les eaux réceptrices vierges. L'intégration des plasmides capturés, la qPCR des gènes liés à la RAM et le contexte chimique du site ont démontré que les sites de rejet des effluents des STEP présentaient des taux élevés de capture et de diversité des plasmides. De plus, l'exposition du système de conjugaison in vitro IncF/HMS174 aux effluents des STEP a modulé le transfert conjugatif, établissant ainsi un lien mécanistique entre le mélange complexe de facteurs de stress chimiques et les répercussions in situ du TGH.

Dans l'ensemble, cette thèse démontre que les CEPs, à des concentrations pertinentes sur le plan environnemental, constituent un facteur de risque modeste mais réel pour la propagation de la RAM par conjugaison, dont l'ampleur est déterminée par l'interaction entre l'identité chimique, l'architecture régulatrice des plasmides et l'hétérogénéité au niveau de la population. La diversité mécanistique spécifique à chaque composé mise en évidence souligne l'importance d'étudier les substances chimiques individuellement, tandis que l'exposition à des mélanges d'effluents et le plasmide mobile in situ soulignent que le risque réel est façonné par la complexité chimique et le contexte écologique d'une manière que les expériences en laboratoire portant sur un seul composé ne peuvent pas pleinement saisir. Ces résultats plaident en faveur de l'intégration du potentiel de promotion du TGH dans les cadres d'évaluation des risques environnementaux liés aux contaminants émergents, ainsi que du développement de tests de conjugaison multiplasmidiques standardisés comme outils réglementaires pour l'évaluation des menaces chimiques pesant sur le résistome environnemental.

Mots clés :
Résistance aux antimicrobiens, Transfert horizontal de gènes, Contaminants émergents préoccupants, Conjugaison bactérienne, *One Health*

Title: Role of emerging contaminants in promoting horizontal transfer of antimicrobial resistance genes: a multiscale approach in environmental context

Abstract:

The global dissemination of antimicrobial resistance (AMR) through horizontal gene transfer (HGT), and through conjugative transfer, represents one of the most urgent challenges in environmental microbiology and public health. While antibiotics have long been recognized as drivers of AMR selection and spread, the role of contaminants of emerging concern (CECs; e.g., industrial chemicals, disinfectants, personal care products) as promoters of bacterial conjugation at environmentally relevant concentrations remains insufficiently understood. This thesis addresses that gap through a multiscale, integrative approach combining machine learning (ML)-based predictive modelling, in vitro experimentation across three conjugation systems, and in situ field assessment in a wastewater-influenced Estuary.

In the first chapter, a suite of ML models [*i.e.,* linear regression, random forest, and extreme gradient boosting (XGB)]was developed and evaluated using a curated dataset of published effects of chemical stressors on conjugation experiments. The best-performing model XGB regressor achieved an internal validation R^2 of 0.719, demonstrating meaningful predictive capacity. Feature importance analysis revealed that chemical concentration, bacterial species used in the experiments and structural fingerprints were the dominant predictors. These findings establish a framework for HGT risk assessment and identify the boundaries of current predictive capacity, underscoring the need for larger, more homogeneous experimental datasets to extend model applicability.

In the second chapter the effects of twelve CECs from six functional groups on conjugative transfer using two intraspecies *Escherichia coli* mating systems sharing the same recipient HMS174 but differing in donor background and plasmid incompatibility (Inc) group (IncF/K12 and IncP/UB1637) were characterized. Both systems responded to CEC exposure at 0.001-0.01 μg mL^{-1}, but the IncP system consistently showed stronger and more reproducible induction. This differential sensitivity was experimentally attributed to plasmid type and mechanistically explained by the interplay of three factors: the higher basal transfer frequency of IncF, leaving less apparent fold-change induction; the cell population heterogenicity; and the plasmid intrinsic

regulatory system. Molecular mechanisms were further elucidated for individual CECs demonstrating compound-specific pathways.

In the third and fourth chapters the investigation was extended to an in situ environmental context, characterizing the resistome and mobilizable plasmidome at four sampling points spanning wastewater treatment plants (WWTPs) effluents and receiving waters to assess the hydraulic continuum. Integration of captured plasmids, qPCR of AMR related genes and site chemical context demonstrated that WWTP effluent discharge locations harbored high rates of plasmid capture and diversity. Furthermore, exposure of the *in vitro* IncF/HMS174 conjugation system to WWTP effluent modulated conjugative transfer providing a mechanistic link between complex chemical stressors mixture and in situ HGT repercussion.

Collectively, this thesis establishes that CECs at environmentally relevant concentrations constitute a modest but real risk factor for conjugation-driven AMR dissemination, whose magnitude is determined by the interplay of chemical identity, plasmid regulatory architecture, and population-level heterogeneity. The compound-specific mechanistic diversity uncovered highlights the importance of studying individual chemicals, while the exposure to effluent mixtures and the in situ mobilizable plasmidome underscore that real-world risk is shaped by chemical complexity and ecological context in ways that single-compound laboratory-based experiments cannot fully capture. These findings argue for the integration of HGT-promoting potential into environmental risk frameworks for emerging contaminants, and for the development of standardized, multi-plasmid conjugation assays as regulatory tools for the assessment of chemical threats to the environmental resistome.

Keywords :
Antimicrobial Resistance, Horizontal Gene Transfer, Contaminants of Emerging Concern, Bacterial Conjugation, One Health

Título: El papel de contaminantes emergentes en la promoción de la transferencia horizontal de genes de resistencia a los antimicrobianos: un enfoque a múltiples escalas en el contexto medioambiental

Resumen:

La diseminación global de la resistencia a los antimicrobianos (RAM) mediante transferencia horizontal de genes (THG), y específicamente a través de transferencia conjugativa, representa uno de los desafíos más urgentes en microbiología ambiental y salud pública. Aunque los antibióticos han sido reconocidos desde hace tiempo como impulsores de la selección y propagación de la RAM, el papel de los contaminantes de preocupación emergente (CPEs; p. ej., compuestos químicos industriales, desinfectantes y productos de cuidado personal) como promotores de la conjugación bacteriana a concentraciones ambientalmente relevantes sigue siendo insuficientemente comprendido. Esta tesis aborda dicha laguna mediante un enfoque integrador y multiescala que combina modelización predictiva basada en *machine learning* (ML), experimentación *in vitro* en tres sistemas de conjugación y evaluación *in situ* en un estuario influenciado por aguas residuales.

En el primer capítulo, se desarrolló y evaluó un conjunto de modelos de ML [es decir, regresión lineal, bosque aleatorio y potenciación extrema del gradiente (XGB)] utilizando una base de datos curada con efectos publicados de estresores químicos sobre experimentos de conjugación. El modelo con mejor rendimiento, el regresor XGB, alcanzó un R^2 de validación interna de 0,719, demostrando una capacidad predictiva significativa. El análisis de importancia de variables reveló que la concentración química, las especies bacterianas empleadas en los experimentos y las huellas estructurales fueron las predictoras dominantes. Estos resultados establecen un marco para la evaluación del riesgo de THG e identifican los límites de la capacidad predictiva actual, subrayando la necesidad de conjuntos de datos experimentales más amplios y homogéneos para ampliar la aplicabilidad de los modelos.

En el segundo capítulo, se caracterizaron los efectos de doce CPE pertenecientes a seis grupos funcionales sobre la transferencia conjugativa utilizando dos sistemas de apareamiento intraespecífico de *Escherichia coli* que compartían el mismo receptor HMS174, pero diferían en el fondo genético del donador y en el grupo de incompatibilidad (Inc) del plásmido (IncF/K12 e IncP/UB1637). Ambos sistemas respondieron a la exposición a CPE a concentraciones de 0,001-0,01 $\mu g\ mL^{-1}$, pero el sistema IncP mostró de manera consistente una inducción más fuerte y reproducible. Esta sensibilidad diferencial se atribuyó experimentalmente al tipo de plásmido y se explicó mecanísticamente mediante la interacción de tres factores: la mayor frecuencia basal

de transferencia de IncF, que deja menos margen aparente de inducción; la heterogeneidad de la población celular; y el sistema regulador intrínseco del plásmido. Los mecanismos moleculares también fueron dilucidados para CPE individuales, demostrando rutas específicas según el compuesto.

En los capítulos tercero y cuarto, la investigación se extendió a un contexto ambiental *in situ*, caracterizando el resistoma y el plasmidoma movilizable en cuatro puntos de muestreo que abarcan efluentes de estaciones depuradoras de aguas residuales (EDAR) y aguas receptoras, con el fin de evaluar el continuo hidráulico. La integración de plásmidos capturados, qPCR de genes relacionados con la RAM y el contexto químico de cada emplazamiento demostró que las zonas de descarga de efluentes de EDAR albergaban altas tasas de captura y diversidad plasmídica. Además, la exposición del sistema de conjugación *in vitro* IncF/HMS174 a efluentes de EDAR moduló la transferencia conjugativa, proporcionando un vínculo mecanístico entre mezclas complejas de estresores químicos y las repercusiones *in situ* sobre la THG.

En conjunto, esta tesis establece que los CPE a concentraciones ambientalmente relevantes constituyen un factor de riesgo modesto, pero real, para la diseminación de la RAM impulsada por conjugación, cuya magnitud está determinada por la interacción entre la identidad química, la arquitectura reguladora de los plásmidos y la heterogeneidad a nivel poblacional. La diversidad mecanística específica de cada compuesto pone de relieve la importancia de estudiar sustancias químicas individuales, mientras que la exposición a mezclas de efluentes y el plasmidoma movilizable *in situ* subrayan que el riesgo en condiciones reales está modelado por la complejidad química y el contexto ecológico de formas que los experimentos de laboratorio basados en compuestos individuales no pueden captar completamente. Estos hallazgos respaldan la integración del potencial promotor de THG en los marcos de evaluación de riesgo ambiental de contaminantes emergentes, así como el desarrollo de ensayos estandarizados de conjugación con múltiples plásmidos como herramientas regulatorias para evaluar amenazas químicas al resistoma ambiental.

Palabras clave:

Resistencia a Antimicrobianos, Transferencia Horizontal de Genes, Contaminantes de Preocupación Emergente, Conjugación bacteriana, *One Health*

EPOC - UMR 5805 CNRS L'Equipe de Physico- et Toxico-Chimie
de l'environnement (LPTC)
Bâtiment A12 351 crs de la Libération 33405 Talence France

Departamento de Bioquímica.y Biología Molecular
Facultad de Ciencia y Tecnología, Dpto Biquímica y Biología Molecular (EHU)
Barrio Sarriena, s/n 48940 Leioa España

Funding and Projects involved:

This thesis was supported by the Pre-doctoral Research Staff Training Grant of the University of the Basque Country (EHU). Additional funding was provided by the Spanish State Research Agency (MCIN/AEI/10.13039/501100011033, grant PID2020-116495RB-I00) and the Basque Government (IT1578-22).

Research Centers and Collaborations involved



En busca de comprender:
no como meta,
sino como camino

Index

Agradecimientos ..... ¡Error! Marcador no definido.

List of Figures ..... **xiv**

List of Tables ..... **xvi**

List of Abbreviations ..... **xvii**

PART I — INTRODUCTION & STATE OF THE ART **1**

Antimicrobial resistance as a global health crisis: a One Health perspective **2**

The aquatic environment as a nexus of antimicrobial resistance dissemination 5

Mobile genetic elements, HGT, and the conjugative dissemination of antibiotic resistance **6**

Contaminants of emerging concern: environmental dynamics and selective pressure on resistance dissemination **9**

Structure of this thesis **10**

PART II — HYPOTHESIS & OBJECTIVES **13**

Hypothesis **14**

Objectives **14**

PART III — MAIN CHAPTERS **15**

CHAPTER 1 ..... **16**

Objectives 20

Material & Methods 21

Literature search, data extraction, and dataset construction 21

Environmental relevance of tested chemical concentrations 22

Model construction 22

Results & Discussion 25

Literature review 25

Exposure ranges used in conjugation assays and environmental context 26

Limited predictive power of concentration-dependent trends alone 28

Experimental Factors Influencing Bacterial Conjugation 31

Chemical structure enables improved prediction of conjugation outcomes 31

Implications for predictive screening of chemical impacts on conjugation 38

CHAPTER 2 ..... **40**

Objectives 46
Material & Methods 47
Bacterial strains, plasmids, and culture conditions. 47
Growth curves 49
Conjugation experiments 49
Exploratory application of the predictive model. 50
Molecular mechanisms underlying the effect of CECs on conjugative transfer 50
Data analysis 51
Statistical analysis 52
Results & Discussion 53
Inhibition effect of CECs on bacterial growth 53
Effect of CECs on conjugative plasmid transfer 56
Mechanistic basis of compound-specific responses 61
Exploratory application of the predictive model 68
CHAPTER 3 70
Objectives 74
Material & Methods 75
Study area 75
DNA extraction and High-throughput quantitative PCR (qPCR) 83
Bacteria and culture conditions 83
Effect of WWTP effluent on conjugative plasmid transfer 83
Statistical analysis 84
Results & Discussion 86
Environmental chemical and microbiological context 86
Bridging in situ and laboratory: conjugative transfer potential of WWTP effluent waters 89
Resistome profiling by quantitative PCR (qPCR) 92
CHAPTER 4 103
Objectives 105
Material & Methods 106
Bacteria and culture conditions 106
Exogenous plasmid capture assay and transconjugant isolation 106
Antimicrobial susceptibility test 107
Transconjugant restriction profiling and sequencing 108
Genome assembling, annotation and definition of plasmid entities 108
Annotation and definition of plasmid entities 109
Clonal cluster (CC) alignment and intra-cluster variability assessment 110
Phylogenetic analysis 110

Data and statistical analysis 111
Results & Discussion 112
Plasmid diversity and general characteristics of the river basin 112
Mobilizable plasmidome characterization 118
Inter-plasmid relatedness and assignment to plasmid individual identities 122
Plasmid relatedness and network structure across sampling sites 128
Other MGEs 130
ARG content of recovered plasmids 134
Relaxase phylogeny and plasmid evolutionary relationships 137
Beyond conjugative and mobilizable plasmids 142

PART IV — GENERAL DISCUSSION 146

PART V — CONCLUSIONS 152

PART VI — APPENDIX 155

Appendix A 156

Appendix B 166

Appendix C 174

Appendix D 180

References 186

List of Figures

Figure 1. Scheme on HGT main memchanisms, MGEs, gene capture tools and plasmids driving ARG dissemination. 7

Figure 2. Diagram of the thesis structure showing the four chapters and a visual summary of the key processes and methods addressed in each one. 12

Figure 3. PRISMA flow diagram 2020 adapted from work licensed under CC BY 4.0. 26

Figure 4. Distribution of chemical concentrations (mg L^{-1}) across functional categories. 28

Figure 5. Conjugation fold-change across tested concentrations (mg L^{-1}). 30

Figure 6. Cumulative distribution of models ranked solely by validation RMSE. 33

Figure 7. Selected feature set on model performance. 35

Figure 8. Model performance comparison between different feature sets. 37

Figure 9. Multilayered sensing and regulatory network linking xenobiotic exposure to bacterial conjugation. 43

Figure 10. Dose-response inhibition curve for antibiotics AUC-based 55

Figure 11. Effect of CECs belonging to six different functional groups on conjugative transfer. 57

Figure 12. Effect of plasmid type on conjugation frequency exposed to CECs. 60

Figure 13. Effect of CECs on reactive oxygen species (ROS) production in the donor (*E. coli* K-12) and recipient (*E. coli* HMS174) strains. 62

Figure 14. Gene expression of donor *E. coli* K12/IncF following exposure to CECs. 65

Figure 15. Chemical similarity of selected CECs to the training set and predictive model validation. 68

Figure 16. Proposed delimitation of the region to be protected biotope by the University of the Basque Country (EHU). 76

Figure 17. Delineation of the upper and lower Butroe catchments. 77

Figure 18. Simplified treatment flow diagrams of the WWTPs of Mungia (left) and Gorliz (right). 80

Figure 19. Overview of the study area and sampling sites. 81

Figure 20. Environmental context of the study area. 82

Figure 21. Preliminary data on cumulative concentration of pollutants found in the study area. 86

Figure 22. Preliminary detailed grouped data on cumulative concentration of pollutants found in the study area. 87

Figure 23. Effect of ellfuent in conjugation across seasons in *E. coli* K12/IncF (donor) and *E. coli* HMS174 (recipient). 90

Figure 24. Non-metric Multidimensional Scaling (NMDS) of resistome profiles across sites and seasons 93

Figure 25. Hierarchical clustering of ARGs and MGE genes across all sampling sites and seasons. 94

Figure 26. Heatmap of ARG, MGE and anthropogenic markers' abundance across sampling sites and seasons. 96

Figure 27. Differential ARG and MGE normalized abundance between Mungia (blue) and Gorliz (red) WWTP effluent across three hydrological sampling campaigns. 98

FIGURE 28. SPATIAL DISTRIBUTION PATTERNS ALONG THE HYDRAULIC CONTINUUM MUNGIA-ESTUARY-BAY..... 100
FIGURE 29. TRANSCONJUGANT RESISTANCE PROFILE..... 115
FIGURE 30. CORRELATIONS BETWEEN PLASMID SIZE AND GENE CARGO METRICS..... 120
FIGURE 31. FUNCTIONAL ANNOTATION BASED ON EGGNOG DATABASE OF SAMPLES BY SITE. 121
FIGURE 32. SEQUENCE ALIGNMENT OF SELECTED CLONAL CLUSTERS (CCS)..... 126
FIGURE 33. MAIN MASH NETWORK CONNECTING PLASMIDS ENTITIES..... 129
FIGURE 34. TOP TEN INSERTION SEQUENCES (IS) AND TRANSPOSON (TN) ELEMENTS. 131
FIGURE 35. UNIQUE INTEGRON DIAGRAM CASSETTE GENE PROFILES FOUND IN PLASMID ENTITIES. 133
FIGURE 36. ANTIMICROBIAL RESISTANCE PROFILE OF PLASMID BEARING-ARGS..... 136
FIGURE 37. MAXIMUM LIKEHOOD PHYLOGENY OF (A) MOBF RELAXASE AND (B) MOBP-RELAXASE PROTEINS. 141
FIGURE 38. FUNCTIONAL PROFILE OF NON TYPABLE CAPTURED PLASMIDS. 143
FIGURE 39. CHROMOSOMAL INSERTION SEQUENCES DETECTED IN *E. COLI* BW25113 TRANSCONJUGANTS. 144
FIGURE A1. CUMULATIVE EXPLAINED VARIANCE AS A FUNCTION OF THE NUMBER OF PRINCIPAL COMPONENTS FOR MACCS FEATURES OF ELECTED CHEMICAL STRESSORS DATAFRAME..... 165
FIGURE B1. PLASMID GENOMIC MAP OF PLASMID INCF USED IN THE STUDY..... 166
FIGURE B2. GROWTH CURVES OF BACTERIAL STRAINS INVOLVED IN THE CONJUGATION EXPERIMENTS. 168
FIGURE D1. COLONY GROWTH OF TRANSCONJUGANTS OBTAINED FROM EXOGENOUS PLASMID CAPTURE ASSAYS. 180
FIGURE D2. RESTRICTION PROFILING ELECTROPHORESIS OF DNA FROM PLASMID EXTRACTIONS. 181
FIGURE D3. BINOMIAL DISTRIBUTION OF MASH DISTANCE ON SEQUENCED PLASMIDS. 184
FIGURE D4. MASH NETWORK WITH A DISTANCE BETWEEN 0.001 AND 0.30 INTEGRATING ALL PLASMIDS. 185

List of Tables

TABLE 1. TOP FIVE EXTREME GRADIENT BOOSTING (XGB) MODELS FOR PREDICTING CONJUGATION EFFECT OF CHEMICAL STRESSORS. 32

TABLE 2. EFFECT OF ADDING FEATURES TO THE BASELINE MODEL ON PREDICTIVE PERFORMANCE. 36

TABLE 3. PHYSICOCHEMICAL PROPERTIES AND ENVIRONMENTAL FATE OF THE SELECTED COMPOUNDS 48

TABLE 4. GROWTH INHIBITION OF *E. COLI* STRAINS USED IN THE CONJUGATION EXPERIMENTS. 54

TABLE 5.DIFFERENTIAL RELEVANT GENES ENCODED IN DONOR *E. COLI* K12/INCF STRAIN 59

TABLE 6. HYDROMORPHOLOGICAL CHARACTERISTIC OF THE BUTROE RIVER BASIN. 75

TABLE 7. GENERAL CHARACTERISTICS AND CATCHMENT PROFILE OF THE TWO STUDIED WWTPS. 79

TABLE 8. CONCENTRATIONS OF SELECTED COMPOUNDS IN WWTP EFFLUENTS (NG L^{-1}). 89

TABLE 9. PLASMID CAPTURE ANTIBIOTIC STRATEGY. 112

TABLE 10. CLONAL CLUSTER (CC) CLASSIFICATION. 122

TABLE 11. PLASMID RECOVERY AND DIVERSITY ACROSS SAMPLING SITES. 127

TABLE 12. CHARACTERISTICS OF REPRESENTATIVE PLASMIDS FOR EACH CLONAL CLUSTER (CC) DETECTED ACROSS SAMPLING SITES. 127

TABLE A1. REFERENCES FROM THE LITERATURE SYSTEMATIC REVIEW ELECTED FOR THE STUDY. 157

TABLE A2. USAGE GROUP AND SUBGROUP CATEGORIZATION. ONE SUBGROUP MAY BELONG TO MORE THAN ONE USAGE GROUP. 164

TABLE A3. PERFORMANCE OF LINEAR REGRESSION (LR) MODELS PREDICTING THE RESPONSE VARIABLE TRANSFER FREQUENCY BASED ON REPORTED EXPERIMENTAL CONDITIONS. 165

TABLE B1. GROWTH INHIBITION (%) AT FIXED CONCENTRATIONS EXTENDED (AUC- AND µ-BASED). 169

TABLE B2. CONJUGATION FREQUENCY ON SYSTEMS I AND II EXPOSED TO 0.01 µG mL^{-1} 170

TABLE B3. CONJUGATION FREQUENCY ON SYSTEMS I AND II EXPOSED TO 0.001 µG mL^{-1} 171

TABLE B4. PRIMERS FOR GENE EXPRESSION ANALYSIS 172

TABLE C1. EXTENDED CHARACTERISTICS OF MUNGIA AND GORLIZ WWTPS. 174

TABLE C2. EXTENDED INFORMATION OF QUANTIFIED GENES FOR RESISTOME ANALYSIS 175

TABLE D1. REPLICON TYPE NUMBER FOUND BY SITE. 182

List of Abbreviations

A	
ACONV	Anticonvulsant
AMR	Antimicrobial resistance
ANLGC	Analgesic
ANTDEP	Antidepressant
ANTHIST	Antihistamine
ANTNP	Antineoplastic
ARB	Antibiotic-resistant bacteria
ARG	Antimicrobial resistance gene
AUC	Area under curve
AZI	Azithromycin
AZO	Azoxystrobin
B	
BB	Beta-blocker
BC	Benzalkonium chloride
Bertz CT	Bertz complexity index
BPF	Bisphenol F
C	
CBZ	Carbamazepine
CEC	Contaminants of Emerging Concern
CFU	Colony Forming Unit
CGD	Center for Global Development
CID	PubChem Compound identifier
COG	Clusters of Orthologous Groups
D	
DCF	2',7'-dichlorofluorescein
E	
E. coli	*Escherichia coli*
EC_{50}	Half maximal effective concentration
eggNOG	Evolutionary genealogy of genes: Non-supervised Orthologous Groups
EPA	Environmental Protection Agency
EU	European Union
EUCAST	European Committee on Antimicrobial Susceptibility Testing
F	
4PL	Four-parameter logistic model
FAO	Food and Agriculture Organization of the United Nations
FC	Fold-change
G	
GFP	Green Fluorescence protein
H	
HGT	Horizontal gene transfer
I	
IMZ	Imazalil
Inc	Incompatibility
IS	Insertion sequence
K	
KAN	Kanamycin
L	
LB	Lysogeny broth
LogP	Logarithm of the partition coefficient
LR	Linear Regression
M	

MACCS	Molecular ACCess System
MAE	Mean Absolute Error
MASH	MinHash-based Average Similarity of Hashes
MEC	Measured environmental concentration
MGE	Mobile genetic element
MIT	Methylisothiazolinone
ML	Machine learning
MOB	Mobilization family

N

NMDS	Non-metric Multidimensional Scaling
NSAID	Non-steroidal anti-inflammatory drug

O

OCT	Octocrylene
ON	Overnight
OXB	Oxybenzone

P

PBS	Phosphate-buffered saline
PCA	Principal component analysis
PCP	Personal care product
PFAS	Per- and polyfluoroalkyl substances
PFBS	Perfluorobutane sulfonate
PFOS	Perfluorooctane sulfonate
PI	Propidium iodide
PPP	Plant protection product

Q

qPCR	Quantitative polymerase chain reaction
Q_{90}	Quartile 90
QAC	Quaternary ammonium compound

R

RF	Random Forest
R^2	Coefficient of determination
RIF	Rifampicin
RMSE	Root mean squared error
ROS	Reactive Oxygen Species
RT-qPCR	Reverse transcription quantitative polymerase chain reaction

S

SHAP	SHapley Additive exPlanations
SMILES	Simplified Molecular Input Line Entry System
SMX	Sulfamethoxazole

T

T4SS	Type IV secretion system
TF	Transfer frequency
TMP	Trimethoprim
Tn	Transposon
TPSA	Topological polar surface area

U

UAA	Utilized agricultural area
UNEP	United Nations Environmental Programme
USD	United States Dollars

V

VLX	Venlafaxine

W

WHO	World Health Organization
WOAH	World Organization for Animal Health
WWTP	Wastewater treatment plant

X

XGB	eXtreme Gradient Boosting

PART I
INTRODUCTION & STATE OF THE ART

Antimicrobial resistance as a global health crisis: a One Health perspective

Antimicrobial resistance (AMR) represents one of the most pressing threats to global public health of the twenty-first century. Antibiotics are the foundation of modern medicine, yet their effectiveness can be undermined by microorganisms' ability to withstand the action of antimicrobial agents. This can potentially turn routine infections into fatal ones and compromise the safety of surgical procedures, cancer chemotherapy and organ transplants, all of which depend on effective antimicrobial prophylaxis. The global burden of AMR is already substantial and its trajectory deeply concerning. In 2021, an estimated 4.71 million deaths were associated with bacterial AMR, of which 1.14 million were directly attributable to resistant infections. In absence of additional intervention, projections forecast 1.91 million deaths attributable to AMR and 8.22 million deaths associated with AMR globally by 2050, representing an increase of nearly 70% in attributable mortality relative to current estimates (Naghavi et al., 2024). Critically, this trajectory falls short of the 10% reduction in AMR mortality proposed under international targets, underscoring the inadequacy of current mitigation efforts. The burden is neither geographically nor demographically uniform: South Asia and Latin America and the Caribbean are projected to carry the highest all-age AMR mortality rates by 2050, and over 80% of the AMR-attributable projected deaths fall within adults aged 70 years and older (Naghavi et al., 2024). This divergence reflects the intersection of AMR with global demographic ageing reframing AMR not only as a threat to the infectious disease landscape but as a fundamental challenge to the sustainability of healthcare systems worldwide.

The consequences of AMR extend well beyond mortality and into the structural foundations of the global economy. The Center for Global Development (CGD) has estimated that, under a scenario of accelerated rise in resistance, direct healthcare costs could increase by 176 billion United States Dollars (USD) per year by 2050, while global economic output could be reduced by up to 1.67 trillion USD annually relative to the business-as-usual scenario (McDonnell et al., 2024). These projections are particularly striking when contrasted with the cost of intervention: integrating improved treatment of bacterial infections, development of new Gram-negative antibiotics, enhanced vaccination programs, and improved access to water and sanitation strategies could save up to 99 billion USD per year in healthcare expenditure and add nearly 960 billion USD annually to global GDP by 2050 (McDonnell et al., 2024).

Yet the ramifications of AMR are not confined to healthcare systems and economic output. Anthropogenic antibiotic use and waste discharge have substantially elevated the abundance and clinical relevance of antimicrobial resistance genes (ARGs) across virtually every

environmental compartment far beyond the background levels that predate the antibiotic era (Berendonk et al., 2015; Dcosta et al., 2011). Wildlife has emerged as a particularly revealing indicator of this environmental contamination through the detection of clinically relevant ARGs and antibiotic-resistant bacteria (ARB) in wild animals not receiving antibiotics (Laborda et al., 2022), reflecting the extent to which anthropogenic resistance determinants have penetrated natural ecosystems. Wildlife species appear to be net recipients of AMR overall, yet they simultaneously act as reservoirs and disseminators of resistance across ecosystems. Migratory species, particularly wild birds, can transport ARBs across geographic boundaries through their movement between anthropogenically impacted and remote environments (Vezeau & Kahn, 2024). In pararell, synanthropic animals such rodents that cohabit with humans and livestock represent more direct transmission routes, facilitating the transfer of ARB between wildlife, domestic animals, and humans (Doyle et al., 2025; Laborda et al., 2022).

For much of the twentieth century, AMR was conceptualized primarily as a clinical problem, an inevitable evolutionary response of pathogens to therapeutic antibiotic pressure within hospital and community settings. This perspective, while not incorrect, proved fundamentally insufficient to account for the global epidemiology of ARB. Expectations on the evolution of ARBs outpaced based on clinical antibiotic use alone revealing a capacity for dissemination beyond the clinic (Berendonk et al., 2015; Laxminarayan et al., 2013). Resistance genes were appearing in pathogens that had never been directly exposed to the selecting antibiotic and identical resistance determinants were being recovered simultaneously from human patients, livestock, and environmental samples regardless geographic location (Andersson & Hughes, 2011; Ochman et al., 2000).

Together, the acceleration of globalization through the intensification of international trade, mass human mobility, and industrialized food production acted as a critical catalytic force, collapsing the geographical and sectorial barriers that had previously contained resistance within localized clinical or agricultural settings (Berndtson, 2020).Simultaneously, hydrological networks provide a continuous and largely unmanaged dispersal route through which ARB and ARGs could move across landscapes, connecting anthropogenic point sources with natural water bodies and ultimately with distant receiving environments (Berendonk et al., 2015; Hendriksen et al., 2019). The cumulative weight of this evidence moved to one conclusion: AMR is not a problem that crosses boundaries between sectors and ecosystems, it is a problem that is constituted by those crossings, and that therefore cannot be resolved within any single discipline or geography in isolation.

This recognition gave rise to the One Health framework as the conceptual and operational response to the complexity of AMR. Formally endorsed by the WHO, FAO, UNEP, and WOAH in the Quadripartite Joint Plan of Action on AMR (2022), One Health recognizes that the drivers, reservoirs, and dissemination routes of resistance are shared across human medicine, veterinary practice, food production, and the natural environment (FAO et al., 2022). Critically, that the environmental compartment is not a passive recipient of resistance from clinical and agricultural sources but an active arena of selection, evolution, and dissemination in its own (Larsson & Flach, 2022). Effective mitigation therefore requires integrated surveillance and intervention across all these domains simultaneously. In particular, the European Union (EU) has increasingly recognized this environmental dimension of AMR in its regulatory framework: the EU One Health Action Plan against AMR (European Commission, 2017), the EU Pharmaceutical Strategy, and the revised Urban Wastewater Treatment Directive (European Parliament and Council of the European Union, 2024) all include provisions addressing the environmental dissemination of antimicrobials and resistance determinants, reflecting a growing policy consensus that AMR surveillance and intervention must extend beyond the clinic into the environment.

Together, these pressures define a narrowing window of action underpinned by three structural factors. First, the antibiotic development pipeline remains critically insufficient. Although the number of antibacterial agents in clinical development increased from 80 in 2021 to 97 in 2023, fewer than half target WHO priority pathogens and only 12 meet innovation criteria (Global Coordination and Partnership (GCP), 2025). In fact, AMR research and development lags behind other fields such as cancer or HIV research, and the withdrawal of large pharmaceutical companies from the antibacterial space has created a structural innovation gap that current investment has not closed (Simpkin et al., 2017). Second, climate change is acting as an independent amplifier of AMR dissemination. Rising temperatures enhance bacterial growth rates and dissemination of ARGs. Global analyses confirm that temperature is positively and independently correlated with resistance rates across most bacterial species and antibiotic classes (MacFadden et al., 2018). Extreme weather events further disrupt sanitation infrastructure and promote the mixing of ARB across environmental compartments (van Bavel et al., 2024). Third, environmental AMR surveillance remains fragmented, methodologically inconsistent, and geographically incomplete. The chemical and biological pressures shaping resistance dynamics in aquatic environments are poorly characterized, and regulatory frameworks governing WWTP effluent quality do not yet incorporate microbiological or molecular AMR endpoints (Larsson & Flach, 2022). Addressing these gaps is not merely a

scientific priority but a public health imperative (Manaia, 2023): the window for prevention-oriented action in the environment is open, but it will not remain so indefinitely.

The aquatic environment as a nexus of antimicrobial resistance dissemination

Aquatic environments occupy a uniquely vulnerable position in the AMR crisis. Unlike other environmental compartments, water bodies act simultaneously as recipients, reactors, and distributors of resistance determinants: they receive continuous inputs of ARB, ARGs, and antimicrobial residues from multiple anthropogenic sources. Therefore, they provide appropriate physical and chemical conditions for horizontal gene transfer (HGT) and resistome expansion and its distribution through hydrological connectivity, linking point sources of contamination with distant receiving environments including coastal waters, groundwater, and drinking water catchments (Berendonk et al., 2015; Manaia et al., 2018).

Within this network, wastewater treatment plants (WWTPs) occupy a position of particular significance. As convergence points for domestic, hospital, industrial, and agricultural wastewater streams, WWTPs concentrate the combined AMR burden of entire catchments into a single discharge point. Urban WWTPs are convergence points for diverse wastewater sources with elevated levels of ARB and ARGs, and provide appropriate conditions including high organic matter, nutrients, and abundant and diverse microbial populations that proliferate ARB and ARGs in wastewater (Muoghalu et al., 2025). The scale of this concentration is substantial and although conventional biological treatment reduces this burden significantly, big efforts are being made to develop new removal strategies. Previous studies showed removal efficiencies for total ARG abundance typically range from 63.2 to 94.2%, yet the ARGs remaining in effluent include high-risk subtypes co-occurring with mobile genetic elements (MGEs) and carried by WHO priority pathogens, indicating that even substantially reduced effluent ARG loads retain meaningful dissemination potential (Luo et al., 2025). Critically, no currently implemented wastewater treatment option is capable of total elimination of ARGs in effluents, and in most jurisdictions globally the dissemination of microbial contaminants within effluent is not controlled or regulated, leaving WWTPs as persistent point sources of AMR-relevant material into receiving water bodies regardless of treatment performance (Drane et al., 2024; Manaia et al., 2018).

The downstream consequences of this continuous discharge are well documented: ARGs and ARB from WWTP effluent enter receiving rivers and coastal waters where they interact with resident microbial communities, undergo further selection under residual antibiotic

concentrations, and are incorporated into sediment reservoirs and biofilm communities that can maintain resistance gene pools for extended periods independent of the original bacterial hosts (Drane et al., 2024; Haenelt et al., 2023; Su et al., 2024). The result is a hydraulic continuum of AMR dissemination that connects the clinical, industrial, and domestic sources of resistance at the catchment head to the ecological and public health consequences at the receiving end.

The nature of this downstream resistome is shaped not only by the quantity and diversity of ARGs discharged but by the chemical and biological conditions of the receiving environment (Su et al., 2024). Experimental and field evidence consistently demonstrates that environmentally relevant antibiotic concentrations cause decreased taxonomic diversity and biofilm structural integrity, while simultaneously driving increased abundance of resistance, virulence, and MGEs (Flores-Vargas et al., 2023). In other words, sustained chemical pressure does not merely select for resistance within existing communities, it improves their ecological diversity while amplifying their resistance gene content, a trade-off with potentially far-reaching consequences for the functional integrity of aquatic ecosystems. These pressures reshape bacterial communities, notably favoring Proteobacteria, Bacteroidota, and Firmicutes while MGEs drive resistance dissemination (Flores-Vargas et al., 2023), effectively rewiring community composition around resistance traits at the expense of broader ecological diversity. The intensity of selective pressure appears to determine the degree to which taxonomic diversity is displaced by resistance-enriched populations (Sivalingam et al., 2024). Among the conditions that modulate this selective landscape, the presence of contaminants of emerging concern (CECs) at sub-inhibitory concentrations in WWTP effluents has emerged as a potentially important but insufficiently characterized driver of HGT dynamics, a dimension of the aquatic AMR problem that forms the central focus of this thesis.

Mobile genetic elements, HGT, and the conjugative dissemination of antibiotic resistance

The extraordinary speed at which ARB has spread across bacterial populations is principally attributable to HGT: the inter-cellular exchange of genetic material across lineages and, in many cases, across species boundaries (Davies, 1996). Horizontal gene transfer encompasses three main mechanistically distinct processes, namely transformation, transduction, and conjugation (Álvarez-Rodríguez et al., 2020; Figure 1). Transformation involves the uptake of naked extracellular DNA from the environment by naturally competent bacteria, and while important in certain ecological contexts, is generally considered a relatively minor contributor to ARG dissemination at the community level given its dependence on DNA stability and recipient competence (Johnston et al., 2014). Transduction involves bacteriophage-mediated transfer of bacterial DNA between cells and has gained renewed attention as a mechanism of ARG spread

in environments with high phage diversity, though its contribution to clinically relevant resistance transfer remains debated (Touchon et al., 2017). Conjugation, by contrast, is widely regarded as the dominant mechanism of ARG dissemination in natural and engineered environments: it involves the direct, contact-mediated transfer of DNA, typically plasmids, from a donor to a recipient cell through a dedicated secretion apparatus, and operates across a remarkably broad host range, including between distantly related taxa (Garcillán-Barcia et al., 2025). Two additional mechanisms of genetic transfer related to conjugation are intercellular nanotubes and membrane vesicles, which are conducted through direct cell–cell physical interactions and the release and uptake of extracellular vesicles, respectively (Douglas & Langille, 2019).

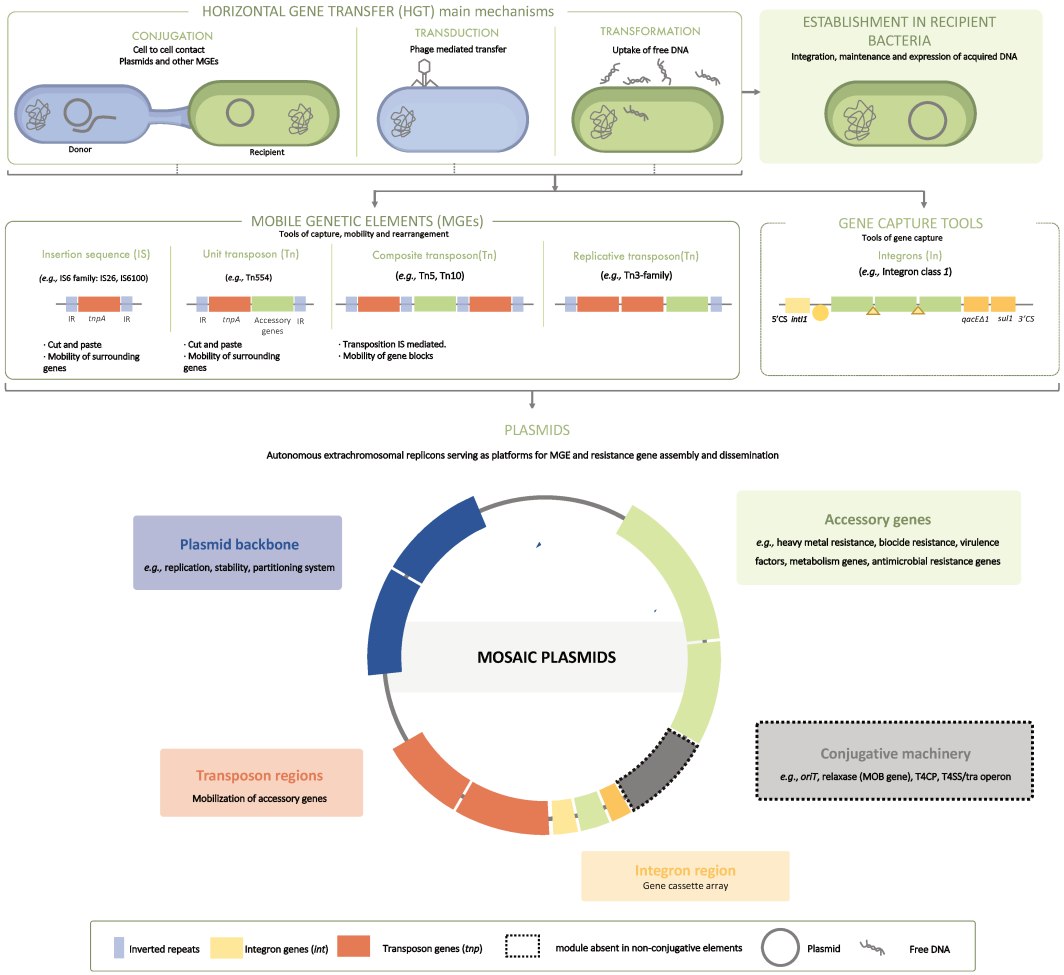

Figure 1. Scheme on HGT main memchanisms, MGEs, gene capture tools and plasmids driving ARG dissemination.

The efficiency and ecological reach of conjugative transfer are substantially amplified by the architecture of the MGEs that participate in it (Figure 1). Integrons are site-specific recombination platforms that capture, excise, and rearrange gene cassettes through integrase-mediated recombination, enabling the rapid assembly of multi-resistance arrays on a single

genetic platform (Mazel, 2006). Class 1 integrons are strongly associated with clinical and environmental resistance and are frequently embedded within transposable elements that further expand their dissemination potential (Gillings, 2014). Insertion sequences (ISs) are the simplest autonomous transposable elements, encoding only the transposase required for their own mobility, but their capacity to mediate chromosomal rearrangements, activate adjacent genes, and promote the co-mobilization of flanking resistance determinants makes them major drivers of ARG reshuffling between genetic contexts (Vandecraen et al., 2017). Composite transposons, formed when two IS elements flank a cargo region, can mobilize ARGs and entire resistance cassettes between plasmids, chromosomes, and other MGEs, generating the mosaic resistance gene architectures that characterize clinically problematic strains (Siguier, Gourbeyre and Chandler, 2014; Figure 1). Together, these elements act as a nested system of mobility: integrons shuffle cassettes within platforms, ISs and transposons move platforms between replicons, and conjugative plasmids transfer entire assemblies between cells and species.

Among the MGEs that mediate conjugative ARG dissemination, plasmids are the primary vehicles of ecological and clinical concern. A conjugative plasmid is defined by the presence of three functional modules: a replication region containing rep genes that govern plasmid DNA synthesis and copy number control; a maintenance region encoding partition and stability systems that ensure faithful segregation during cell division; and a conjugative transfer region containing *tra* genes that encode the Type IV Secretion System (T4SS) responsible for mating pair formation and the relaxase-*oriT* complex that initiates and executes single-stranded DNA transfer into the recipient cell (Álvarez-Rodríguez et al., 2020; Garcillán-Barcia et al., 2023). The relaxase recognizes the origin of transfer (*oriT*), nicks one DNA strand at a conserved site, and forms a covalent bond with the 5′ end of the nicked strand, which is then translocated through the T4SS into the recipient. This modular architecture is the fundamental unit of plasmid-mediated ARG dissemination, and understanding its organization is essential for interpreting how different plasmid types contribute differentially to resistance spread across environments.

Two complementary classification systems have been developed to organize the diversity of conjugative plasmids. The incompatibility (Inc) group system, the oldest and most widely used in clinical and environmental epidemiology, classifies plasmids based on their replication systems: two plasmids belonging to the same Inc group cannot stably coexist in the same cell because they compete for shared replication and partitioning machinery. In accordance with replicon typing methods, incompatible plasmids are currently classified into 27 types, with IncA, IncC, IncF, IncL, IncM, IncH, and IncP being among the most widely distributed and conjugatively active groups in Gram-negative bacteria Frontiers (Villa & Carattoli, 2020). The MOB

classification system, developed as a complementary and phylogenetically more robust framework, classifies plasmids based on the sequence of their relaxase. Comparison of relaxase sequences across the plasmid universe has resolved six MOB families: MOBF, MOBH, MOBQ, MOBC, MOBP, and MOBV, each with distinct phylogenetic relationships and biological characteristics (Garcillán-Barcia et al., 2009). These two systems are complementary rather than redundant: Inc group typing captures replication-based plasmid identity and is the standard for epidemiological tracking, while MOB typing captures the evolutionary history of the transfer machinery and enables phylogenetic inference across plasmid families.

The ecological and epidemiological significance of a given plasmid group in environmental AMR dissemination is shaped by the intersection of its host range, transfer efficiency, and ARG cargo. These are properties that differ substantially across Inc groups and that determine how susceptible different plasmid types are to modulation by chemical stressors in the receiving environment, a question that is developed in detail in the experimental chapters of this thesis.

Contaminants of emerging concern: environmental dynamics and selective pressure on resistance dissemination

The chemical landscape of aquatic environments has been fundamentally transformed by anthropogenic activity. Beyond the classical suite of regulated pollutants, a structurally and functionally diverse array of chemical substances, collectively termed contaminants of emerging concern (CECs), now permeates freshwater and coastal systems worldwide. The term CECs, which gained traction in the early 2000s to describe the progressive discovery of new pollutant classes in environmental matrices, encompasses a broad chemical space including pharmaceuticals, personal care products (PCPs), industrial biocides, plasticizers, flame retardants, pesticides, and their transformation products (Richardson & Ternes, 2018). These substances share neither a common chemical structure nor a single biological mode of action but are united by their capacity to reach aquatic environments at biologically relevant concentrations and by the inadequacy of existing regulatory frameworks to address their environmental dynamics (Z. Wang et al., 2020).

This chemical transformation of the aquatic environment is not merely a local or regional phenomenon: it represents a manifestation of a global-scale perturbation that has been formally recognized within the planetary boundaries framework. The concept of planetary boundaries, introduced by Rockström et al. (2009) and subsequently refined by Steffen et al. (2015) defines the biophysical limits within which humanity can safely operate without triggering abrupt or irreversible changes in Earth system functioning. Of the nine boundaries originally proposed,

that of novel entities has been assessed as already transgressed (Persson et al., 2022). This assessment explicitly includes pharmaceuticals and biocides among the chemical classes driving the transgression, situating the environmental contamination by CECs not as an isolated ecotoxicological concern but as a component of a planetary-scale chemical pressure on biological systems (Alkorta & Garbisu, 2025).

The biological relevance of these environmental CEC concentrations to AMR dynamics has emerged as a rapidly growing area of research. At the concentrations at which CECs typically occur in WWTP-impacted environments, direct toxicity to microbial communities is rarely the primary concern. Rather, it is their capacity to co-select for antibiotic resistance through mechanisms that operate independently of antibiotic exposure that has emerged as the critical biological interface between chemical pollution and AMR dissemination. Co-selection refers broadly to the process by which exposure to a non-antibiotic agent selects for antibiotic resistance, and can operate through three distinct mechanisms: cross-resistance, in which a single resistance determinant (*e.g.,* a multi-substrate efflux pump) confers reduced susceptibility to both the selecting agent and one or more antibiotics; co-resistance, in which genes conferring resistance to distinct agents are physically linked on the same genetic element and thus inherited together; and co-regulation, in which the transcriptional response to one agent activates resistance to another (Murray et al., 2024). Critically, co-selective pressure has been documented at sub-inhibitory concentrations (*i.e.,* below those required for growth inhibition) raising the possibility that the range of chemical compounds capable of driving resistance dissemination in real environmental matrices is far broader than antibiotic-centric risk frameworks would predict (Bengtsson-Palme & Larsson, 2016; Gullberg et al., 2011). WWTPs occupy a pivotal position in this interface: they are simultaneously the primary point of entry of CECs into aquatic environments and the site at which microbial communities are most intensively exposed to complex chemical mixtures under conditions that favor HGT, making them the logical focus for investigating the intersection of chemical pollution and AMR dissemination (Berendonk et al., 2015; Larsson & Flach, 2022)

Structure of this thesis

This thesis is organized into four experimental chapters, each addressing a distinct but interrelated dimension of the central hypothesis (Figure 2). Chapter 1 develops a machine learning (ML) framework for the prediction of CECs capable of modulating conjugative transfer frequency, providing the computational foundation for compound prioritization in subsequent experimental work. Chapter 2 characterizes the differential effects of selected CECs on conjugative transfer in IncP-1 and IncF plasmid systems, establishing the compound- and

plasmid-specific nature of the modulatory effects documented. Chapter 3 integrates resistome analysis and conjugative transfer potential assessment in real WWTP effluents from Mungia and Gorliz, providing field-relevant evidence for the intersection of chemical contamination and ARG dissemination under One Health conditions. Chapter 4 extends this analysis to the mobilizable plasmidome of the Butroe river catchment, characterizing the pool of MGEs available for horizontal transfer across environmental and clinical interfaces. Together, these four chapters provide a multi-scale assessment of the role of chemical stressors in modulating ARG dissemination in aquatic environments, from molecular mechanism to catchment-level ecology.

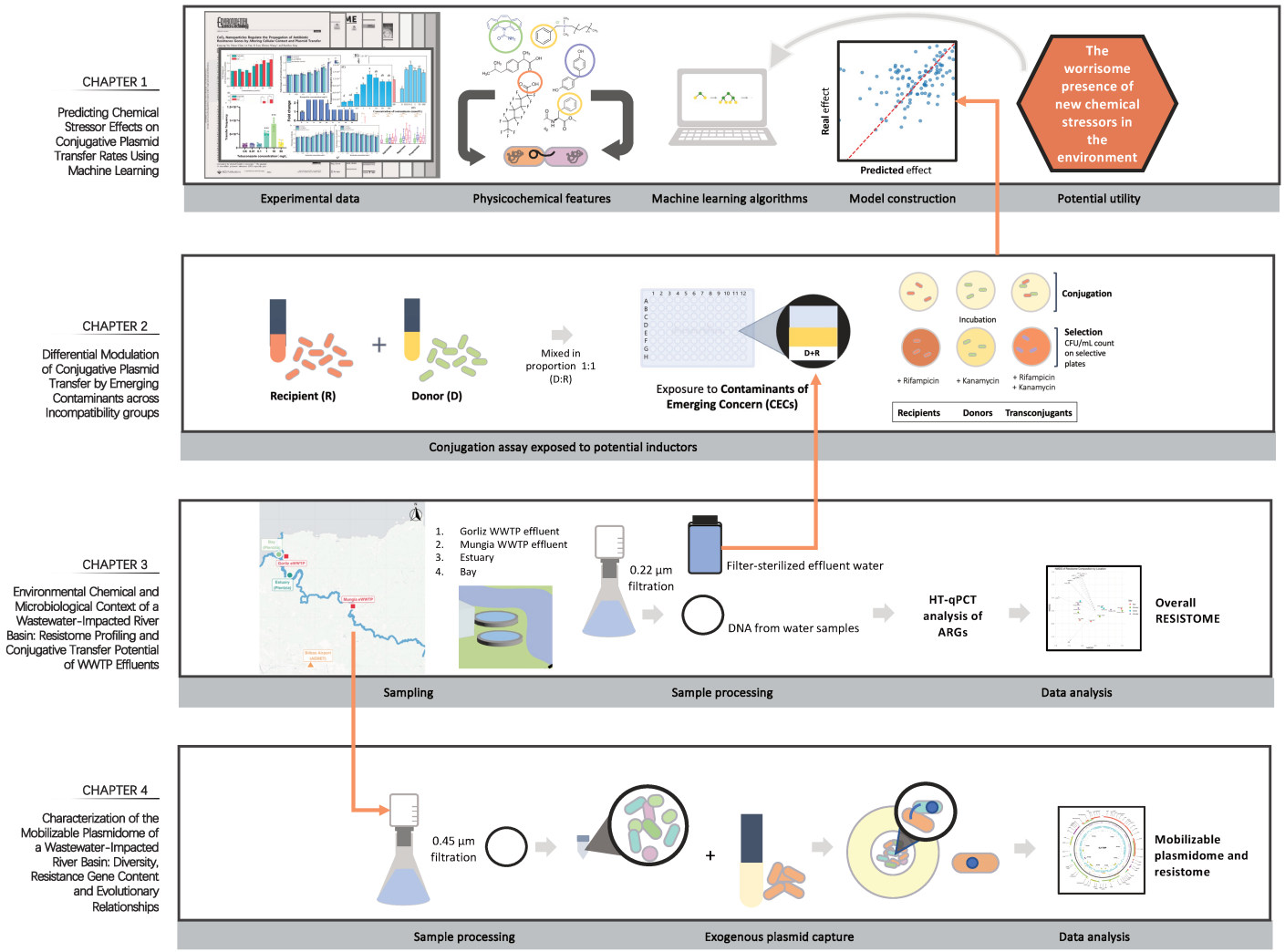

Figure 2. Diagram of the thesis structure showing the four chapters and a visual summary of the key processes and methods addressed in each one.

PART II
HYPOTHESIS & OBJECTIVES

Hypothesis

Contaminants of emerging contaminants (CECs) present in wastewater treatment plants (WWTPs) effluents modulate the frequency of plasmid-mediated conjugative transfer in a compound- and plasmid-specific manner, thereby contributing to the environmental dissemination of antimicrobial resistance genes (ARGs) in wastewater-impacted aquatic ecosystems.

Objectives

1. To assess the role of environmentally relevant chemical stressors as modulators of plasmid-mediated conjugative transfer, establishing the mechanistic and chemical basis through which sub-inhibitory CEC concentrations drive the environmental dissemination of ARGs.

2. To develop and validate a machine learning-based predictive framework capable of identifying CECs concern with potential to alter conjugative transfer frequency, using molecular structure descriptors as primary predictive features, and to evaluate its applicability as a screening tool for HGT risk assessment.

3. To characterize the compound- and plasmid-specific effects of environmentally relevant CECs on conjugative plasmid transfer across clinically and environmentally significant Inc groups, and to investigate the mechanistic pathways through which selected CECs modulate transfer frequency under controlled laboratory conditions.

4. To evaluate the role of WWTP effluent as driver of ARG dissemination in a coastal catchment by characterizing the chemical modulation of conjugative plasmid transfer, the composition and treatability of the effluent resistome, and the spatial and hydrological dynamics governing ARG and MGE distribution from point sources to open coastal receiving environments.

5. To characterize the mobilizable plasmidome of a WWTP-impacted coastal catchment, encompassing WWTPs, estuarine and marine environments, through culture-based capture and sequencing, and to identify the ecological and evolutionary determinants governing ARG mobilization across this environmental continuum, with implications for public health surveillance and evidence-based AMR governance.

PART III
MAIN CHAPTERS

CHAPTER 1

Predicting Chemical Stressor Effects on Conjugative Plasmid Transfer Rates Using Machine Learning

Antimicrobial-resistant bacteria represent one of the most serious and expanding threats to global public health. According to the latest WHO report, one out of every six laboratory-confirmed bacterial infections worldwide was resistant to antibiotic treatment in 2023 (World Health Organization, 2025). Because AMR emerges and spreads across interconnected human, animal, and environmental reservoirs, understanding the processes that drive its dissemination requires a systems-level perspective provided by the One Health framework (McEwen & Collignon, 2018).

A central process underlying the spread of ARGs is HGT, particularly conjugation. Conjugative plasmids (*e.g.,* IncP, IncW, and other broad-host-range plasmids) facilitate ARG movement across diverse bacterial taxa and environmental niches and are considered major drivers of plasmid-mediated ARG dissemination (Garcillán-Barcia et al., 2025; Klümper et al., 2015; G. Liu et al., 2022). Despite increasing research efforts, the dynamics of plasmid-mediated ARG spread and the factors that modulate conjugation remain incompletely understood.

Attention has been directed toward chemical pollutants present in the environment that may adversely affect ecosystem and human health. These include substances not usually monitored with potential to have an adverse impact on humans or the environment, commonly known as CECs (Environmental Protection Agency (EPA), 2024). Such chemicals encompass a broad range of synthetic and naturally occurring compounds, including pharmaceuticals, personal care products, industrial chemicals, nanomaterials, and disinfection by-products.

Beyond their toxicological relevance, accumulating evidence suggests that CECs can also interfere with microbial processes central to ARG dissemination. While antibiotics are well known to select for ARG-encoding plasmids and promote their spread via conjugation, recent works indicate that non-antibiotic chemicals can also modulate HGT and conjugation dynamics in both clinical and environmental settings (He et al., 2024; Klümper et al., 2017; Stanton et al., 2024; Yu et al., 2021). Multiple studies have reported that certain CECs influence bacterial conjugation frequencies through, for example, oxidative stress induction, enhanced reactive oxygen species production, or alterations of cell membrane properties (Y. Wang et al., 2021). However, available evidence remains scattered and highly chemical-specific, as certain compounds act primarily at the cell membrane, whereas others penetrate cells and elicit distinct intracellular responses, leading to heterogeneous effects on conjugation.

In addition, experimental conditions influencing conjugation outcomes vary widely across studies, including donor–recipient combinations, used plasmids, exposure concentrations, incubation time, and temperature. This variability makes it difficult to draw generalizable conclusions regarding which chemicals promote or inhibit conjugative transfer (Rodriguez-Grande et al., 2023). Although best practices for *in vitro* platforms to assess chemical pollutant effects on plasmid transfer have been proposed (L. G. Li & Zhang, 2023), a systematic framework to compare chemicals and predict their impact on conjugation remains lacking. Within this context, it is unfeasible to experimentally test each chemical and its derivatives, given the time and cost required, the large number of compounds in circulation, and the wide range of concentrations in diverse environmental settings. Consequently, there is a pressing need for predictive and scalable approaches to support risk assessment and chemical regulation, as current methodologies do not allow for efficient screening of chemicals for their potential to enhance ARG transfer.

Importantly, many of the mechanisms by which chemical stressors influence conjugative plasmid transfer, including membrane perturbation, oxidative stress induction, and intracellular stress responses, are closely linked to fundamental physicochemical properties of

the compounds involved, such as molecular size, polarity, functional groups, and lipophilicity (Y. Liu et al., 2020). In addition, whether a compound can interact with intracellular targets or primarily affects the cell envelope depends on its ability to traverse bacterial membranes, which is likewise governed by its chemical structure and associated physicochemical properties (Smułek & Kaczorek, 2022). These properties are inherently encoded in chemical structure and can be captured using molecular descriptors and fingerprints (Niazi & Mariam, 2023). As a result, chemical structure provides a mechanistically informed basis for predicting how different compounds may modulate conjugation outcomes across experimental systems.

Machine learning approaches using chemical descriptors, such as Molecular ACCess System (MACCS) and Morgan fingerprints, as well as physicochemical properties, offer the potential for scalable prediction of biological effects (Niazi & Mariam, 2023). Given the growing body of data regarding chemical effectors on plasmid transfer reported in the literature, ML provides an opportunity to integrate molecular descriptors derived from *in vitro* conjugation assays, enabling systematic prediction even when available data are fragmented or variable (Rodríguez-Pérez et al., 2022). Such predictive frameworks could support early-stage chemical screening by identifying compounds and concentration ranges likely to promote or suppress plasmid-mediated ARG transfer, and guide targeted experimental validation. By enabling the prioritization of chemical stressors with a higher potential to influence ARG dissemination, this approach can contribute to mitigation strategies aimed at limiting the environmental spread of antimicrobial resistance. Based on this, we here tested the hypothesis that chemical structure, encoded through molecular descriptors, provides predictive information on conjugative plasmid transfer beyond exposure concentration alone. Building on this premise, we aimed to develop a scalable predictive framework that integrates chemical structure, concentration, and biological context to anticipate chemical modulation of plasmid-mediated ARG transfer through ML approaches.

To this end, we first developed a comprehensive dataset through a systematic synthesis of published conjugation studies reporting the effects of individual chemical compounds at different concentrations on plasmid-mediated ARG transfer. This dataset encompasses multiple conjugative plasmids and a broad range of donor–recipient combinations, reflecting the diversity of experimental systems used in the literature. However, data availability across plasmids was highly uneven. Among all reported systems, the broad-host-range plasmid RP4 was the most frequently studied and was associated with the largest number of tested chemicals, providing sufficient data density to support robust quantitative modeling. Accordingly, this study focuses on RP4-mediated conjugation as a representative system to

develop and evaluate a predictive framework linking chemical properties and exposure concentrations to conjugation outcomes. While the present analysis focuses on RP4 due to its comparatively high data availability and experimental consistency across studies, the modeling framework itself is not plasmid-specific. Given sufficient and comparable data density, the same approach can be extended to other conjugative plasmid systems to evaluate chemical modulation of HGT. Within this modeling framework, chemical compounds were classified by functional group and Simplified Molecular Input Line Entry System (SMILES) derived molecular descriptors considering not only their chemical composition and functional groups but also their three-dimensional structures, which can influence how compounds interact with or enter cells. Multiple ML-based algorithms, including linear regression (LR), random forest (RF), and Extreme Gradient Boosting (XGB), were evaluated. SHapley Additive exPlanations (SHAP) analysis was used to identify key predictors shaping conjugation responses. This framework provides a scalable, data-driven approach for screening and prioritizing chemicals with the potential to enhance or inhibit conjugative ARG spread and is transferable to other types of plasmid systems given sufficient data.

Objectives

i. To construct a curated dataset of published conjugation studies reporting the effects of individual chemical compounds on plasmid-mediated ARG transfer, and to develop a machine learning-based predictive framework integrating chemical structure, exposure concentration, and biological context to anticipate chemical modulation of conjugative transfer.

ii. To evaluate and compare the predictive performance of linear regression, random forest, and extreme gradient boosting algorithms, and to identify the key molecular descriptors driving model predictions through SHAP analysis.

iii. To assess the scalability and potential transferability of the framework as a generalizable tool for chemical screening and prioritization in ARG dissemination risk assessment.

Material & Methods

Literature search, data extraction, and dataset construction

To systematically capture and harmonize experimental evidence on chemical effects on plasmid-mediated conjugation, a comprehensive systematic literature review was conducted in two stages: (i) early-stage screening and (ii) later-stage screening with full-text assessment according to predefined eligibility criteria. Scopus (Elsevier) and Web of Science (Clarivate Analytics) databases were selected to maximize coverage and reduce database-specific bias. Search queries combined terms related to conjugation with terms describing chemical exposure (Appendix A, Text A1). Briefly, research was restricted to peer-reviewed research articles from 2015 to 2025. Records were imported into Rayyan (Ouzzani et al., 2016) to facilitate title/abstract and full-text screening and to record inclusion and exclusion decisions.

An initial broad literature synthesis covering conjugation experiments involving multiple plasmid types was performed to assess data availability across systems. However, eligibility for quantitative modeling was restricted to primary research articles reporting *in vitro*, broth-based conjugation assays in which the effect of individual chemical compounds was tested, using the RP4 plasmid under controlled experimental conditions, due to its high frequency of use and data availability across studies. Restricting quantitative analysis to RP4-based systems ensured consistency across studies and comparability of conjugation outcomes for subsequent modeling.

Only studies reporting quantitative data were included. Eligible studies reported conjugation assays´ outcome expressed as conjugation transfer frequency (TF) (Eq. 1), or relative to a control group as fold-change (FC) (Eq. 2), were included.

$$\mathrm{TF} = \frac{\mathrm{CFU}_{\mathrm{transconjugants}}/\mathrm{mL}}{\mathrm{CFU}_{\mathrm{recipient}}/\mathrm{mL}} \qquad \text{Eq. 1}$$

$$\mathrm{FC} = \frac{\mathrm{Transferfrequency}_{\mathrm{exposure}}}{\mathrm{Transferfrequency}_{\mathrm{control}}} \qquad \text{Eq. 2}$$

Data were extracted either directly from tables when available or digitized from published plots when numerical values were not explicitly reported using WebPlotDigitizer (v5.2) (Rohatgi, 2024). All extracted data were compiled into a standardized table for downstream analysis. Studies were excluded if they did not test the effect of a single chemical substance, could not be linked to a PubChem compound identifier (CID), or did not report the tested

concentration. To ensure a consistent response variable across studies, TF values were converted to FC relative to the corresponding control condition when required. Each TF and FC data point was assigned to a unique CID and a concentration expressed in mg L^{-1} corresponding to the chemical tested. Moreover, CECs were identified within the list of chemicals tested, and all chemical stressors were assigned to at least one categorical group for posterior analysis based on use as reported in the NORMAN SusDat database (NORMAN Network, 2025).

To characterize the resulting dataset prior to model construction, basic descriptive statistics (*i.e.,* mean, standard deviation, and linear regression) on log_{10}-transformed tested concentrations and FC values were computed. These analyses were used to summarize the types and distribution of chemical concentrations tested, the number of compounds studied per chemical category, and overall trends in reported plasmid transfer responses.

Environmental relevance of tested chemical concentrations

To contextualize laboratory conjugation assays within environmentally relevant exposure ranges, Measured Environmental Concentration (MEC) data were extracted from a validated database compiled on behalf of the German Environment Agency (Graumnitz & Jungmann, 2021), which includes harmonized concentration data for pharmaceuticals and other chemicals measured globally between 1981 and 2020. Only positively validated measurements, assessed according to the quality criteria described in the accompanying technical report, were included in the dataset (https://www.umweltbundesamt.de/sites/default/files/medien/6232/dokumente/pharms-uba_v3_2021_0.xlsx).

To ensure compatibility with the conjugation assay dataset, MEC values were filtered according to predefined criteria, including matching chemical identity, consistent units (µg L^{-1}), environmental matrix (surface water), and geographic region (Europe). Extreme values and uncharacterized maxima were excluded to avoid disproportionate influence of outliers. The resulting filtered MEC dataset was used to systematically compare environmentally observed concentration ranges with those applied in laboratory conjugation assays, across chemical classes and functional groups.

Model construction

Guided by the premise that chemical structure and associated physicochemical properties underpin many of the mechanisms influencing conjugative plasmid transfer, the objective of

the modeling was to predict plasmid transfer response to chemical exposure. The response variable was the FC and TF in plasmid transfer. Candidate predictors included chemical concentration, donor–recipient species involved in the conjugation assays, chemical use category, and descriptors associated with chemicals (*i.e.,* physicochemical descriptors and chemical fingerprints). All data processing and modeling workflows were implemented in Python, and scripts are publicly available in a GitHub repository https://github.com/Sogoana/chemical-stress-conjugation-analysis.

Candidate features

To capture chemical structure in a quantitative and model-compatible manner, canonical SMILES representations of the tested compounds in the literature were retrieved from PubChem using their CID. Chemical descriptors were computed using RDKit 2025.03.4 for Python 3.12. MACCS keys, Extended-Connectivity Fingerprints (ECPF4), also referred to as Morgan fingerprints, and additional physicochemical descriptors were generated, capturing both functional group composition and aspects of molecular geometry that can influence compound behavior. Both MACCS keys and Morgan Fingerprints are binary fingerprint representations, whereas physicochemical descriptors are composed of continuous features including molecular weight, logarithm of the Partition Coefficient (LogP), topological polar surface area (TPSA), number of hydrogen bond donors and acceptors, fraction of sp3 hybridized carbons (fractionCSP3), number of rotatable bonds, ring count, Bertz complexity index (Bertz CT), and connectivity indices (Chi0 and Chi1).

Data processing

To reduce redundancy and limit collinearity among predictors prior to model training, chemical descriptors were pre-processed to reduce redundancy. For MACCS keys, principal component analysis (PCA) was applied to reduce dimensionality, retaining the principal components (PC) that explained at least 90% of variance to balance dimensionality reduction with information retention. In the remaining descriptor sets, features with pairwise similarity greater than 90% were removed to avoid collinearity. All continuous chemical descriptors were standardized prior to analysis using the StandardScaler method from scikit-learn 1.7.0 (Bishop et al., 2011) to obtain the standard score, whereas binary features were left unscaled to preserve their categorical nature. In brief, each variable was centered at zero mean and unit variance, according to Eq. (3), where z is the original descriptor, is the mean of the variable, and is the standard deviation. This transformation prevents numerical descriptors with larger magnitudes from dominating the analysis and ensures comparability across scale-sensitive

models.

$$z = \frac{x-\mu}{\sigma} \qquad \text{Eq. 3}$$

Concentration values and the response variable were $\log_{10}$-transformed prior to modeling. To prevent data leakage, training and validation sets were kept strictly separated throughout the workflow. Dimensionality reduction, feature standardization, and data transformation steps were fitted exclusively on the training data and subsequently applied to the validation set.

Model training and evaluation

To systematically evaluate the predictive contribution of different feature sets and model types, all possible combinations of the processed feature sets were generated and used as inputs for model training. A total of 378 predictive models were evaluated, corresponding to 126 distinct feature set configurations combined with three model families: LR, RF, and XGB. Hyperparameters for RF and XGB models were optimized using grid search with cross-validation on the training data. Models were trained using identical training–validation splits to ensure fair comparison across feature sets and model families.

Performance metrics

Model performance was evaluated on validation root mean squared error (RMSE) and coefficient of determination (R^2). RMSE was treated as the primary evaluation metric due to its direct interpretability in $\log_{10}$ fold-change units, providing an estimate of the magnitude of prediction error. R^2 was used as a complementary metric to quantify the proportion of variance that can be explained by the model. To assess overfitting (OF), the difference between training and validation on R^2 was computed for each model.

Model selection strategy

To balance predictive performance and model interpretability, model selection followed a multicriteria approach based on the above-mentioned performance metrics. First, models were filtered to retain a minimum R^2 threshold (R^2 >0.6), ensuring sufficient explanatory power. Among the remaining models, validation RMSE was minimized, with preference given to models exhibiting lower OF. Lastly, models with reduced feature-set complexity were favored to enhance interpretability and generalizability when RMSE and R^2 were comparable.

Importances and SHAP values

To interpret model predictions and identify the chemical features driving conjugation responses, feature relevance was assessed using two complementary approaches: feature

importance scores provided by the learning algorithms and SHAP values (Lundberg & Lee, 2017).

Results & Discussion

Literature review

From the systematic literature review, 4,625 records were retrieved, of which 336 studies were assessed for full-text eligibility (Figure 3). To ensure comparability, the analysis was restricted to broth-based conjugation assays using the plasmid RP4 (65% of the eligible articles), and conjugation outcomes were harmonized and expressed as fold-change (FC). Based on these criteria, 73 articles were retained for quantitative analysis (Appendix A, Table A1), comprising 163 unique chemical compounds, and yielding 1,443 processed data points. To reduce redundancy in FC values, observations corresponding to controls (concentration of 0 mg L^{-1}) were excluded. The final dataset used for statistical analysis and model construction comprised 1,198 data points consisting of chemical, concentration, FC, and experimental metadata (Data available at https://github.com/Sogoana/chemical-stress-conjugation-analysis).

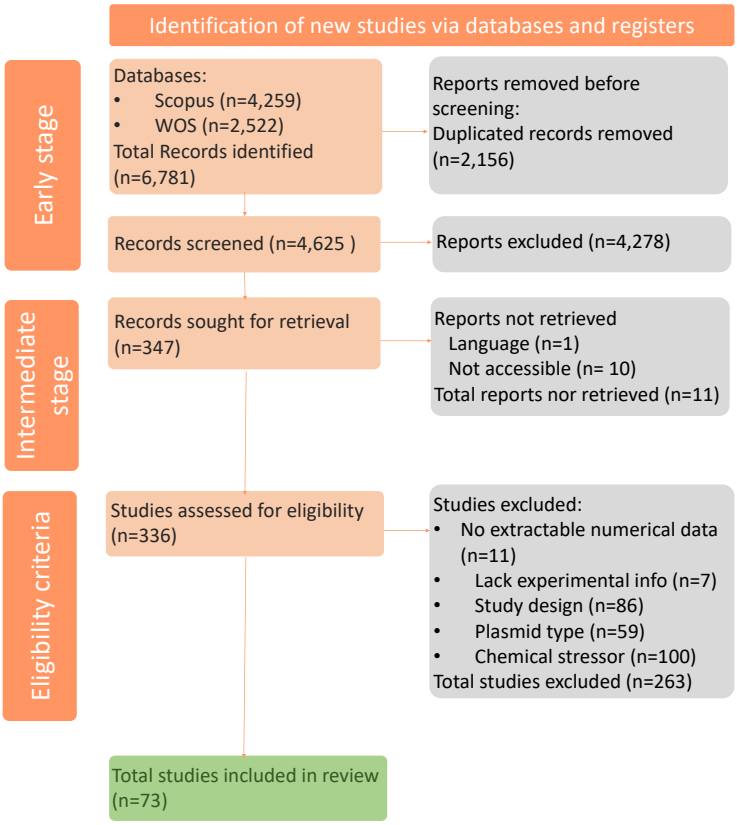

Figure 3. PRISMA flow diagram 2020 adapted from work licensed under CC BY 4.0.

Process of study selection, including identification of records through databases and registers, screening of records, assessment of eligibility, and final inclusion in the review. The identification stage is divided into three steps: early stage, intermediate stage, and eligibility assessment.

Each chemical compound was then assigned to one or more major use categories based on the NORMAN SusDat database (consulted in 2025), including biocides, food additives, industrial chemicals, disinfection by-products, natural products, and non-antibiotic pharmaceuticals. An additional antimicrobial category was defined to capture compounds with direct antimicrobial activity, and nanomaterials were retained as a separate group due to their distinct physicochemical properties (Mansor & Xu, 2020). In addition, compounds were further classified into more specific subcategories (Appendix A, Table A2).

Exposure ranges used in conjugation assays and environmental context

The concentrations of chemicals used in the conjugation assays varied widely, spanning 10^{-4} to 10^{5} mg L^{-1} (Figure 4A). Substantial heterogeneity was observed both within and between the major chemical categories; however, all categories encompassed broad concentration ranges, providing sufficient variability for subsequent quantitative and ML-based analyses.

When placing these laboratory exposure ranges into an environmental context, tested

concentrations were compared with MECs derived from surface waters (Figure 4B). This comparison was restricted to pharmaceuticals, for which sufficient environmental monitoring data are available, and resolved to exposure ranges at the level of individual pharmaceutical subgroups (Graumnitz & Jungmann, 2021). Although many studies state that they cover concentrations that could be found in environmental and clinical settings, the mean tested concentrations for most pharmaceutical groups exceeded typical environmental occurrence by several orders of magnitude, indicating that experimental designs frequently incorporate high-exposure scenarios (Figure 4B). For most pharmaceutical classes, concentrations tested in conjugation experiments substantially exceeded even the 90th percentile (Q_{90}) of the combined distribution of MECs of monitored pharmaceuticals. In contrast, the concentration ranges tested for transformation products (TPs) largely fell below this Q_{90} threshold. This pattern reflects the predominantly environmental focus of TP studies, as these compounds typically occur at lower concentrations than their parent pharmaceuticals and might therefore be more often investigated under environmentally realistic exposure conditions.

Taken together, these comparisons indicate that current conjugation assays predominantly explore high or worst-case exposure scenarios, such as those relevant to clinical or point-source contexts, whereas environmentally realistic concentration ranges remain comparatively underrepresented. This underscores the importance of explicitly accounting for concentration when interpreting and modeling chemical effects on plasmid transfer. Despite its dominance by high exposure scenarios, the dataset is sufficient for the planned analysis, as we intend to contextualize experimental exposure levels rather than immediately assess environmental risk.

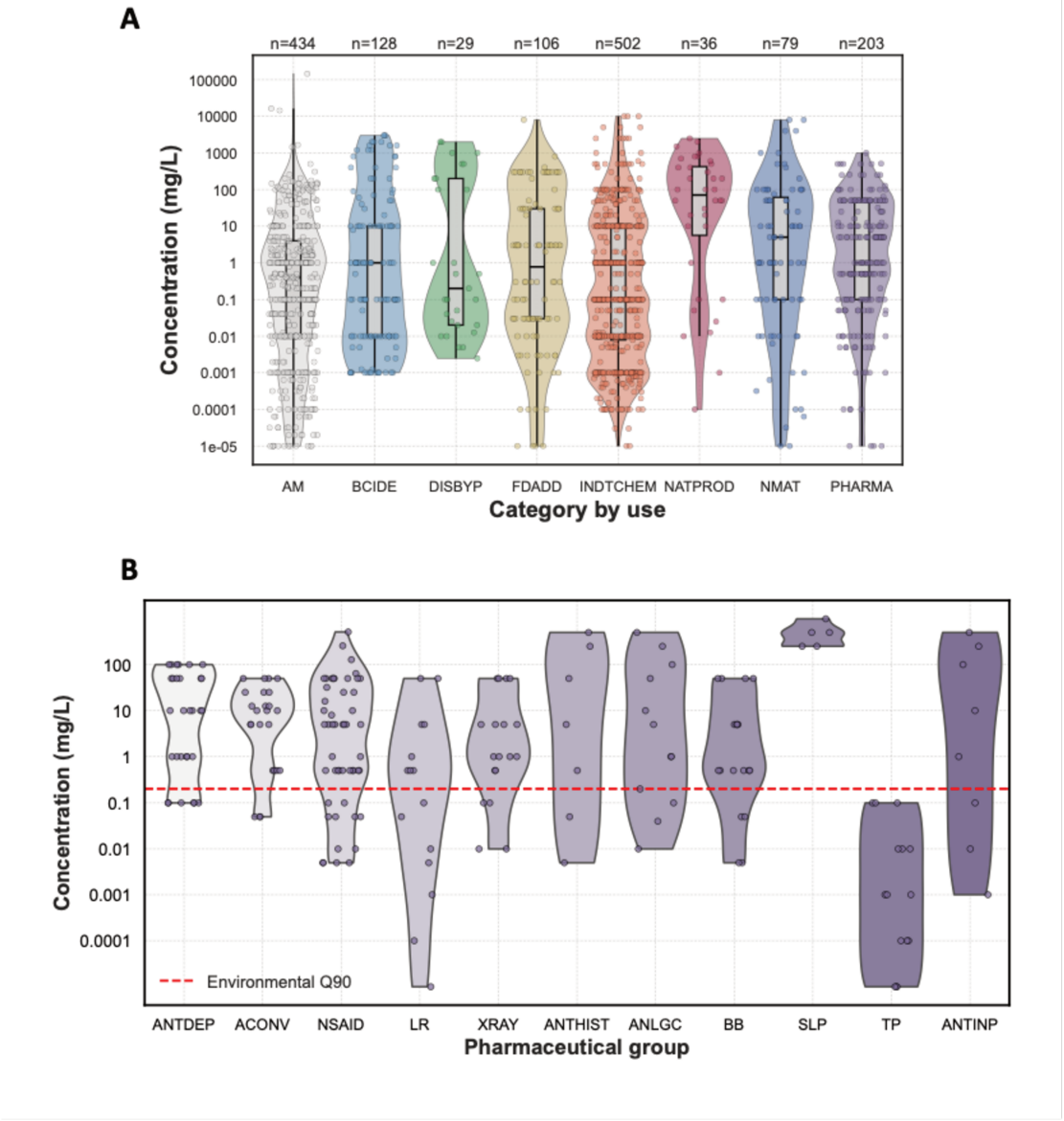

Figure 4. Distribution of chemical concentrations (mg L^{-1}) across functional categories.

(A) Main categories (AM: antimicrobials; BCIDE: biocides; DISBYP: disinfection byproducts; FDADD: food additives; INDTCHEM: industrial chemicals; NATPROD: natural products; NMAT: nanomaterials; PHARMA: non-antibiotic pharmaceuticals). Sample sizes for each category are indicated above the violins. (B) PHARMA subcategories (ANTDEP: antidepressants; ACONV: anticonvulsants; NSAID: non-steroidal anti-inflammatory drugs; LR: lipid regulators; XRAY: contrast agents; ANTHIST: antihistamines; ANLGC: analgesics; BB: beta-blockers; TP: transformation products, ANTNP: antineoplastics). The dashed line indicates the measured environmental concentration (MEC) Q_{90} of pharmaceuticals monitored in surface waters. Concentration (mg L^{-1}) is shown on a logarithmic scale.

Limited predictive power of concentration-dependent trends alone

To evaluate whether chemical concentration alone can explain variation in conjugative plasmid transfer, concentration–response patterns were examined across the compiled

dataset. *In vitro* conjugation data were successfully extracted from the literature and typically spanned a wide range of exposure concentrations as described above. A heterogeneous response was observed across chemical concentration and groups (Figure 5). When concentration–response relationships were evaluated across the entire dataset, overall explanatory power remained very low (global R^2=0.0516, Figure 5A), indicating the absence of a generalizable concentration–response relationship for chemical pollutants.

Across individual chemical groups, food additives, nanomaterials, and biocides led to increasing plasmid transfer rates with rising concentrations, suggesting a stimulatory effect (Figure 5B). In contrast, non-antibiotic pharmaceuticals and antimicrobials displayed a decreasing response with increasing concentrations (Figure 5B). The inhibitory effects of antimicrobials on conjugation are particularly noteworthy, as these compounds directly suppress microbial growth, which is reflected in lower bacterial numbers and thus cell-cell encounters, effectively reducing plasmid transfer probabilities at higher concentrations (Figure 5B). By comparison, industrial chemicals, which represent a more chemically diverse category, did not follow a consistent trend, and instead exhibited highly variable responses across concentrations.

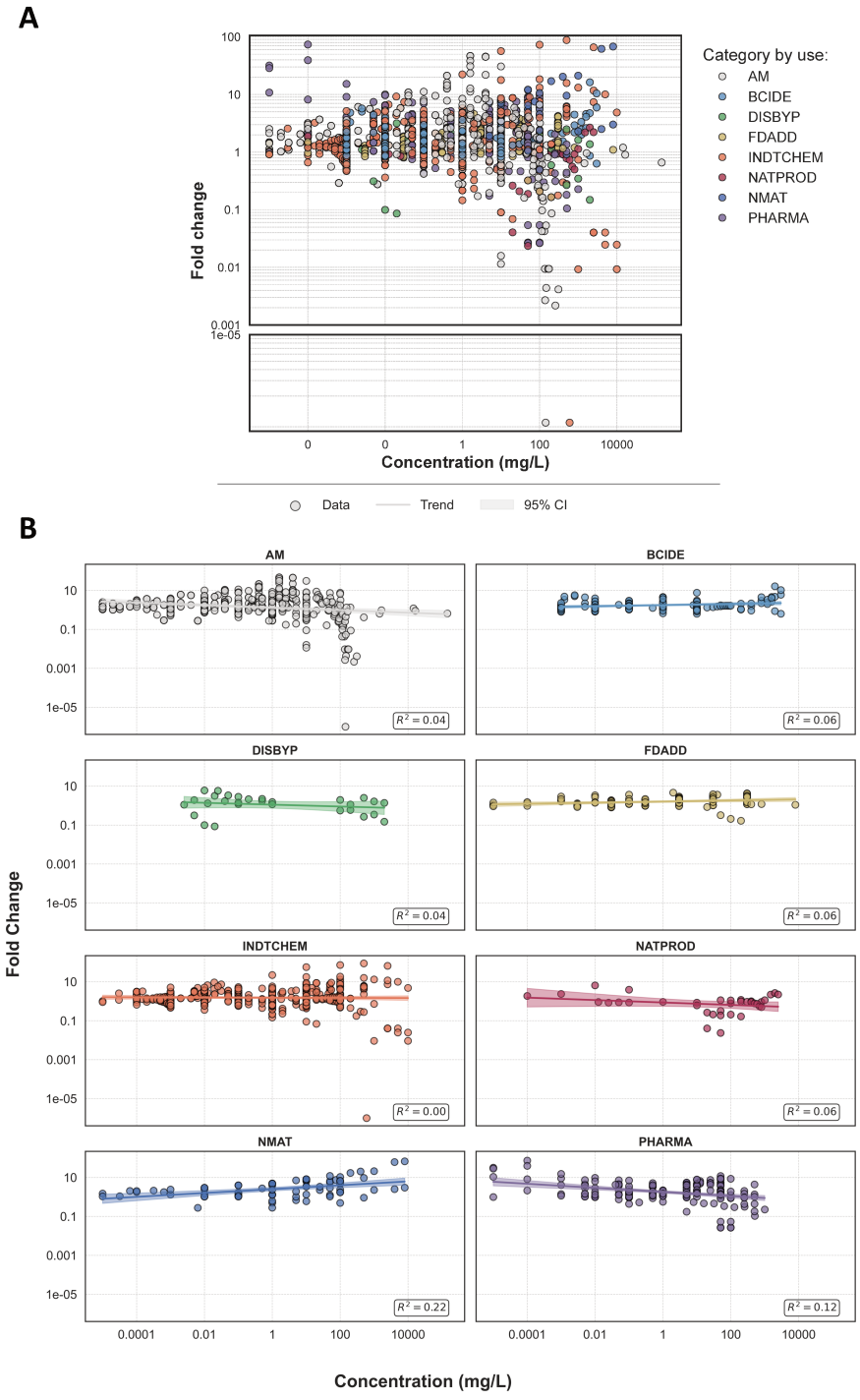

Figure 5. Conjugation fold-change across tested concentrations (mg L^{-1}).

(A) Eight major compound categories (AM: antimicrobials; BCIDE: biocides; FDADD: food additives; NMAT: nanomaterials; DISBYP: disinfection byproducts; PHARMA: non-antibiotic pharmaceutical) distribution. (B) Individual trends in plasmid transfer per category. Shaded areas indicate the 95% confidence interval. The coefficient of determination (R^2) shown in the lower-right corner of each panel quantifies the proportion of variance in fold-change explained by the regression. Data was extracted from the systematic review and $\log_{10}$ transformed.

Across all chemical groups, independent of trend direction, R^2 values ranged from 0.000365 to 0.123, demonstrating that, despite weak group-level tendencies, no robust generalization due to weak effect sizes can be drawn. Taken together, although concentration is biologically relevant, it cannot by itself predict modulation of conjugation frequency, underscoring the need to account for additional chemical- and system-specific factors to capture the complexity of chemical effects on bacterial conjugation.

Experimental Factors Influencing Bacterial Conjugation

To assess whether variability in experimental conditions could explain differences in reported conjugation outcomes, metadata describing *in vitro* conjugation assay settings were compiled. These included species relationships, mating duration, and incubation temperature. In total, 59 control groups were extracted from 51 published studies. Among the selected studies, mating time, incubation temperature, and species combinations showed the greatest variability across experiments. In contrast, cell density and donor:recipient ratios were largely consistent, with most studies using approximately 10^8 cells mL^{-1} and a 1:1 ratio, respectively. Similarly, conjugation assays were predominantly conducted in nutrient-rich LB or PBS media, accounting for more than 90% of the included studies. Despite these experimental parameters having been previously identified as influential determinants of conjugation efficiency (Johnsen & Kroer, 2007; Rodriguez-Grande et al., 2023), LR models applied to the three most variable factors, namely mating duration, incubation temperature, and species relationship, were unable to explain the observed variance in conjugation frequencies (Appendix A, Table A3). Validation R^2 values ranged from -0.034 to -0.88 when evaluating models based on time, temperature, species, and combinations of all these parameters. This lack of explanatory power suggests that bacterial conjugation dynamics are governed by non-linear relationships and more complex interactions among experimental and chemical factors. However, due to the limited number of studies reporting systematic variation across these parameters, more flexible non-linear modeling approaches could not be robustly applied.

Chemical structure enables improved prediction of conjugation outcomes

Because neither concentration nor experimental metadata alone was sufficient to explain variation in conjugation outcomes, we next evaluated whether incorporating chemical structural information improved predictive performance.

Model performance improves when chemical descriptors are included

To test whether chemical structure improves predictive performance beyond concentration alone, chemical stressors were first grouped into broad usage-based categories

and described using SMILES-derived molecular descriptors. Dimensionality reduction was applied to MACCS keys using 30 PCs that explained at least 90% of the variance (Appendix A, Figure A1). In parallel, 1536 Morgan fingerprints were included after removal of highly correlated features.

These 5 chemical-related descriptor classes (Usage Group, Usage Subgroup, MACCS keys, Morgan fingerprints & physiochemical descriptors) were combined with chemical concentration and the donor–recipient species relationship (intra- vs. interspecies), resulting in seven descriptor categories considered for modeling of plasmid transfer FC. All possible combinations of these descriptor classes were iteratively evaluated to identify feature sets that best explained variance in conjugation FC under chemical stress. This resulted in 126 distinct feature sets, excluding the empty set and the species-only set, as these did not include any chemical information.

Three predictive modeling approaches were evaluated: LR as a baseline method, and two ML approaches, RF and XGB. These algorithms were applied across the 126 distinct feature-set combinations, resulting in a total of 378 trained and evaluated models. Across feature sets, the highest predictive performance was consistently achieved using XGB. When ranked by validation RMSE, the 40 best-performing models all originated from different XGB-based feature sets (Figure 6), with the first RF-based model appearing only at rank 41. Moreover, the best-performing models, when jointly considering R^2, RMSE, OF (overfitting score, defined as the difference between training and validation R^2), and prediction bias, were exclusively derived from the XGB approach (Table 1). In contrast, LR consistently showed the weakest performance across feature sets (Figure 6).

Table 1. Top five extreme gradient boosting (XGB) models for predicting conjugation effect of chemical stressors.

Feature set	R^2	RMSE	OF	Bias	Model
Concentration, Morgan FPs, species relation	0.718	0.279	0.126	-0.0094	XGB
Concentration, physicochemical features, PCs, and species relation	0.714	0.282	0.230	--0.0084	XGB
Concentration, Morgan FPs, species relation and subcategory by use	0.714	0.282	0.150	-0.010	XGB
Concentration, Morgan FPs, species relation and subcategory by use	0.701	0.289	0.164	-0.010	XGB

Concentration, Morgan FPs, species relation, physicochemical features, category, and subcategory by use	0.700	0.290	0.254	-0.0093	XGB

Ranking based on validation performance parameters (*i.e.,* coefficient of determination (R^2), root mean squared error (RMSE), difference between validation and training performance, here referred to as overfitting (OF) and Bias) across feature sets.

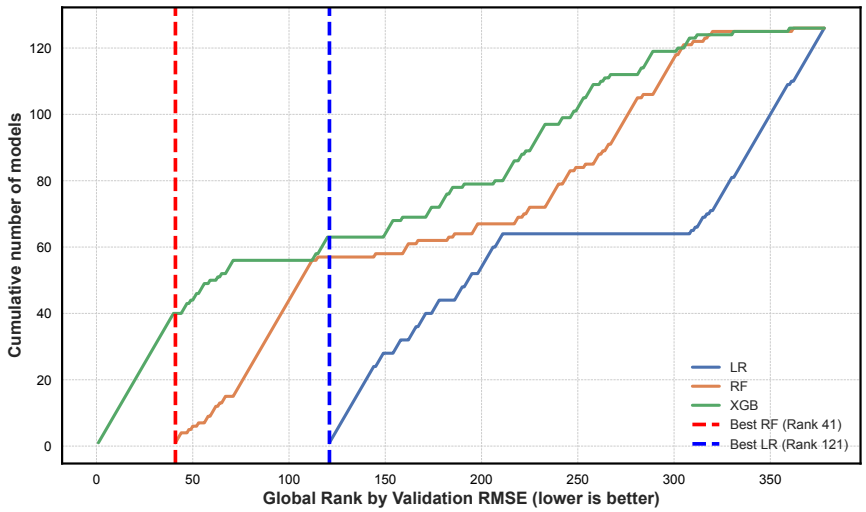

Figure 6. Cumulative distribution of models ranked solely by validation RMSE.

Lines indicate the cumulative number of logistic regression (LR), random forest (RF), and extreme gradient boosting (XGB) models across the global performance ranking. The dashed vertical lines indicate the rank of the best-performing RF model (Rank 41) and of the best-performing LR model (Rank 121).

The superior performance of XGB relative to RF and LR is consistent with the structure of the conjugation system under study. XGB is particularly well-suited to modeling non-linear relationships and higher-order interactions because it sequentially builds models and fits the residual error from previous models. This allows it to gradually learn weak effects that can collectively contribute to predictive accuracy (Chen & Guestrin, 2016; Friedman, 2001). Such interactions are expected when chemical structure, concentration, and biological context jointly influence conjugation dynamics. In contrast, RF builds many deep trees independently and averages their predictions to reduce variance (Breiman, 2001) so it may smooth out weak signals particularly in high-dimensional settings (Efron & Hastie, 2016). Ultimately, LR cannot capture features interactions explaining its poorer performance while still serving as a useful benchmark (Hastie et al., 2009; Kwapien et al., 2022).

Structural fingerprints consistently contribute to predictive performance

Several XGB models achieved comparable validation performance, with RMSE values between 0.28 and 0.29 and R^2 values ranging from 0.70 to 0.72. Because differences in RMSE

were biologically negligible, model selection prioritized low OF and feature-set simplicity. Based on these criteria, the optimal model combined chemical concentration, donor–recipient species relationship, and Morgan fingerprints, achieving a validation R^2 of 0.718, RMSE of 0.279, an OF score of 0.126, and minimal bias of 0.0094 (Table 1).

Chemical concentration and species relationship were present in all top-performing models, while Morgan fingerprints were additionally included in four of the five best models (Table 1). This indicates that chemical structural information captures relevant determinants of chemical stressor effects on bacterial conjugation. Morgan fingerprints consistently outperformed alternative chemical representations, including MACCS keys, physicochemical descriptors, and categorical classifications based on chemical use or sub-class, in predicting modulation of plasmid transfer.

The strong contribution of Morgan fingerprints is consistent with their ability to encode local chemical environments and substructural motifs that directly influence biological interactions. Many mechanisms by which chemical stressors affect conjugation, such as membrane perturbation, redox activity, and induction of cellular stress responses, are driven by localized functional groups rather than by global physicochemical properties or coarse use categories (Jiang et al., 2022). By capturing these local structural features, Morgan fingerprints allow the model to distinguish compounds with similar usage or bulk properties but divergent effects on conjugation dynamics (Lin et al., 2025; Rogers & Hahn, 2010).

Despite the strong predictive performance, residual unexplained variance remained, as reflected in the predicted *versus* observed relationship (Figure 7A) and the observed RMSE values. This indicates that additional biological and experimental factors contribute to conjugation dynamics under chemical stress. Such factors likely include bacterial physiological state, activation of stress-response pathways, and subtle differences in experimental implementation that are not consistently reported. Metadata describing growth phase, physiological stress status, and precise exposure conditions are often underreported or inconsistently documented across studies. More standardized and detailed reporting of experimental metadata would likely improve model performance and generalizability by enabling a more complete representation of the biological context in which chemical stressors modulate conjugative plasmid transfer.

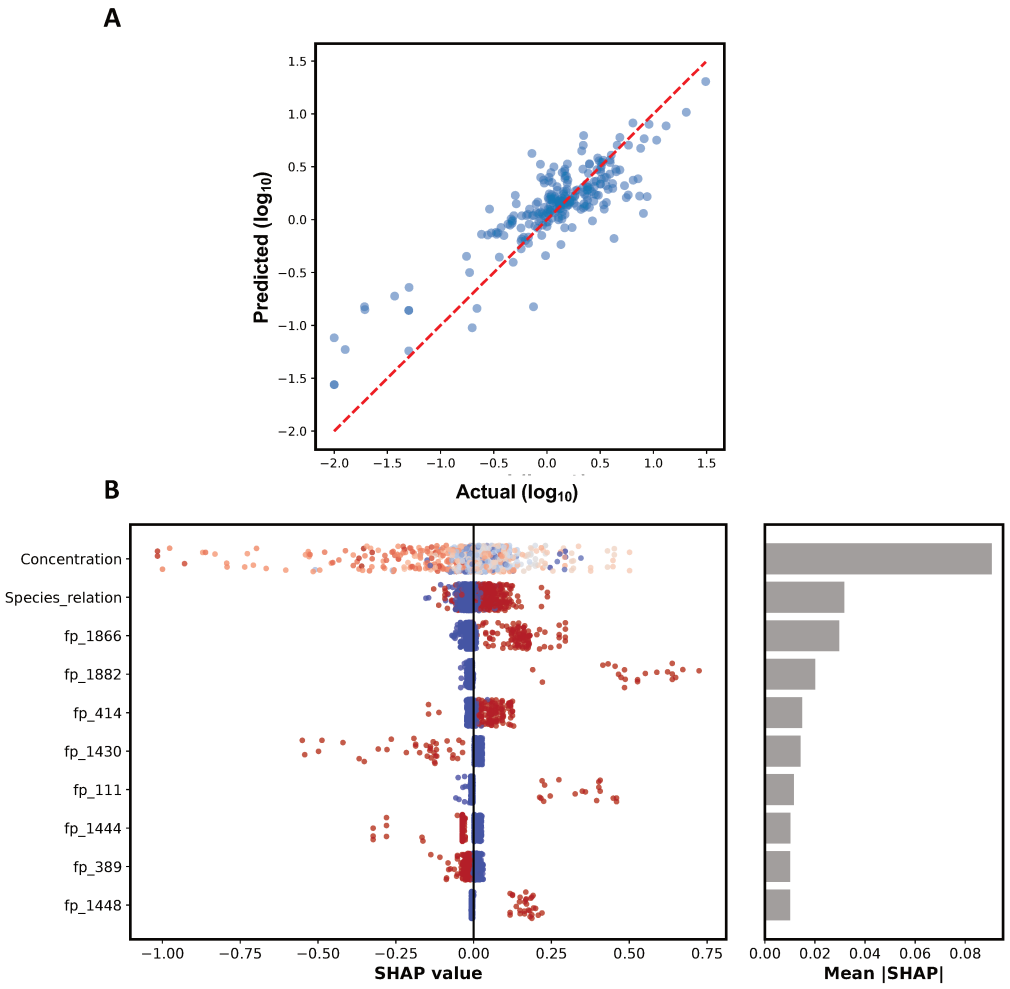

Figure 7. Selected feature set on model performance.

(A) SHAP summary plot showing the ten most influential input variables ranked by mean absolute SHAP values. Each dot represents individual samples, showing the distribution of SHAP values for each feature (row). The horizontal position indicates the magnitude and direction of the contribution to the model output, with positive values increasing and negative values decreasing the predicted conjugation fold-change (FC) response. The vertical dispersion reflects the density of observations. Point color represents the normalized feature value (blue: low, red: high). Vertical line marks zero contribution. The bar plot on the right shows the mean absolute SHAP value for each feature. (B) Scatter plot comparing observed values with XGB predictions on the validation set. The red dashed line represents the line of identity (perfect prediction).

Interpreting model predictions using SHAP analysis

To elucidate the drivers underlying model predictions, SHAP values were used to quantify the contribution of individual features to the XGB model outputs. This approach enables interpretation of both global feature importance and feature-specific effects on predicted conjugation responses. Across the model, concentration emerged as the strongest predictor, with increasing concentrations consistently associated with lower predicted conjugation rates (Figure 7B). This pattern aligns with biological expectations, as elevated exposure to chemical

stressors, particularly those with antimicrobial activity, can suppress bacterial growth and thereby limit opportunities for plasmid transfer (Headd & Bradford, 2020).

Despite its dominant SHAP contribution (mean absolute SHAP value=0.09), concentration alone exhibited limited predictive capacity, as models relying exclusively on concentration showed poor overall performance (Table 2, Figure 8). Similarly, only adding categorical classification of chemicals based on use did not capture substantial variance in conjugation outcomes (Table 2), indicating that coarse chemical grouping fails to reflect the mechanistic diversity underlying chemical–microbe interactions.

Table 2. Effect of adding features to the baseline model on predictive performance.

Feature set	R^2	RMSE	OF	Bias
Concentration	0.0516	0.513	0.176	-0.025
Concentration and main category by use	0.173	0.479	0.275	-0.019
Concentration and subcategory by use	0.200	0.471	0.249	-0.021
Concentration and FPs	0.649	0.312	0.136	-0.010
Concentration, FPs, and species relation	0.718	0.279	0.126	-0.0094

Feature sets are built on the baseline concentration feature and progressively include main category by use, subcategory by use, Morgan fingerprints (FPs), and species relation, ordered by improved model performance. Performance metrics reported for each model include coefficient of determination (R^2), root mean squared error (RMSE), difference between validation and training performance (overfitting, OF), and Bias.

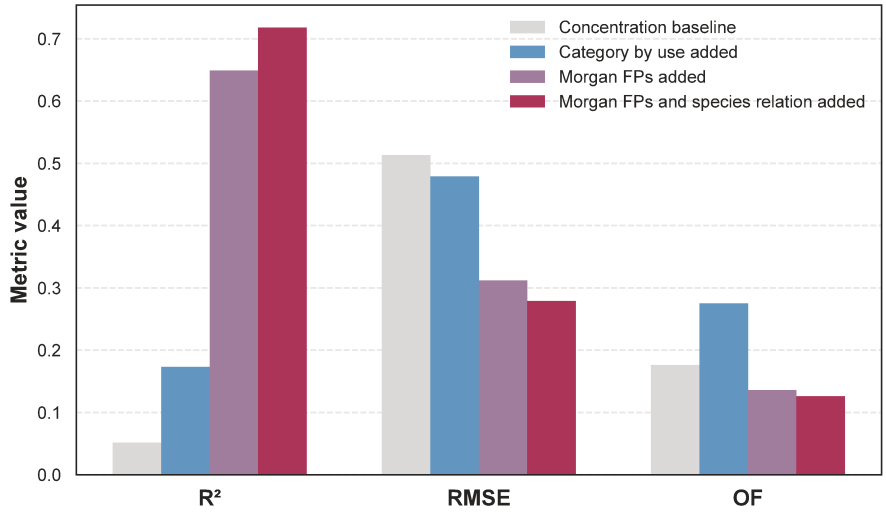

Figure 8. Model performance comparison between different feature sets.

Evaluated parameters included coefficient of determination (R^2), root mean squared error (RMSE), and the difference between validation and training performance (OF). Model outperformed when higher score in R^2 and lower RMSE and OF. Outperformance was achieved when the model scored higher in R^2 and had a lower RMSE and OF.

Species-related information in conjugation assays emerged as the second most influential predictor of plasmid FC. The species relationship feature showed a mean absolute SHAP value of 0.031 (Figure 7A). During model training, assays were encoded as a binary variable distinguishing interspecies from intraspecies conjugation. Examination of the SHAP summary plot revealed a clear separation between these two classes, with interspecies assays predominantly associated with positive SHAP values (mean SHAP value =0.046) and intraspecies assays with negative SHAP values (mean SHAP value =−0.017). This indicates that the model systematically associated interspecies conjugation with higher predicted transfer rates, while intraspecies conjugation tended to suppress predicted outcomes.

The strong contribution of donor–recipient species relationship identified by SHAP analysis is consistent with established conjugation biology for broad-host-range plasmids such as RP4. Although IncP plasmids can transfer across diverse taxa, transfer efficiency and stable establishment are strongly constrained by recipient-associated barriers, including restriction–modification systems, entry and surface exclusion, and host-specific regulatory interactions (Dimitriu, 2022; Dimitriu et al., 2019). Experimental studies have shown that recipient permissiveness can vary by orders of magnitude even among closely related strains, making host context a dominant determinant of observed conjugation frequencies for RP4 (Dimitriu et al., 2019). In interspecies conjugation, chemical stressors may differentially affect donor and

recipient physiology, such that stress responses acting on only one partner or eliciting distinct responses in each partner can combine to amplify effects on mating pair formation, plasmid transfer, or establishment, whereas in intraspecies systems, more similar stress responses may partially overlap and dampen net effects. The systematic association of interspecies conjugation with higher predicted transfer rates in the present model therefore reflects biologically meaningful constraints on plasmid establishment rather than experimental noise and provides a mechanistic basis for why chemical stressors may differentially modulate conjugation outcomes depending on donor–recipient compatibility (Klümper et al., 2019).

In addition, chemical structure descriptors encoded as Morgan fingerprints were major contributors to model performance. Immediately following species relationship, several fingerprint bits ranked among the most influential features, with fp_1866 showing a mean absolute SHAP value comparable to that of species relationship, followed by fp_1882, fp_414, and other fingerprint-derived features. Morgan fingerprints encode local chemical environments through circular atom neighborhoods, enabling representation of substructural features rather than coarse chemical classes (Rogers & Hahn, 2010). Although individual fingerprint bits are not directly interpretable due to hashing and bit collisions, SHAP analysis allows their relative importance for model predictions to be quantified (Lundberg & Lee, 2017). The consistent prominence of multiple fingerprint-derived features among the top-ranked predictors indicates that localized chemical structure plays a central role in shaping conjugation under chemical stress, complementing global predictors such as concentration and species-related metadata.

Implications for predictive screening of chemical impacts on conjugation

Together, these results demonstrate the potential of machine-learning approaches as scalable tools to screen and prioritize chemical stressors based on their capacity to modulate plasmid-mediated gene transfer. By integrating chemical structure descriptors, particularly Morgan fingerprints, with concentration and experimental metadata, the model captures relationships between molecular features and conjugation dynamics that are not accessible through concentration-based or categorical analyses alone.

The strong contribution of structural fingerprints underscores the importance of molecular-level determinants in shaping biological responses and enables discrimination between compounds with similar use classifications but divergent effects on conjugation. Such *in silico* screening frameworks can substantially reduce experimental burden by guiding hypothesis-driven testing and prioritizing compounds and exposure scenarios most likely to

influence HGT This could, if validated, also have potential for inclusion in ecotoxicological assessment of chemicals based on predicted effects.

At the same time, residual unexplained variance highlights the complexity of conjugation dynamics and the influence of biological and experimental factors that are not consistently reported. Reporting bias toward positive results and limited metadata availability likely constrain model generalizability. Future efforts would therefore benefit from more standardized reporting of conjugation assays, including negative outcomes and detailed experimental context, as well as expanded datasets encompassing broader chemical and biological diversity. These advances would strengthen predictive performance and support the development of robust tools to assess chemical contributions to antimicrobial resistance dissemination across One Health settings.

Although the present study focuses on a single, well-characterized plasmid system, future extensions of this framework may integrate sequence-based machine learning approaches (Gustavsson et al., 2024; Inda-Díaz et al., 2026; Lund et al., 2025) to broaden applicability across plasmid families. Recent advances in transformer-based models trained on >700.000 plasmid sequences have demonstrated strong performance in predicting host range, plasmid compatibility, and structure–function relationships (Parras-Moltó et al., 2025). Coupling such sequence-informed models with the chemical-effect prediction framework developed here could enable inference of chemical modulation of conjugation across diverse plasmid–host systems, even where direct experimental data remain sparse, provided appropriate validation data are available.

CHAPTER 2

Differential Modulation of Conjugative Plasmid Transfer by Emerging Contaminants across Incompatibility groups

The global dissemination of AMR represents one of the most pressing threats to public health, with HGT mediated by conjugative plasmids constituting the primary mechanism by which resistance genes spread across bacterial populations and ecological niches. While the selective pressure exerted by antibiotics on resistance gene dissemination is well established, growing evidence indicates that a broader class of environmental pollutants (here collectively termed CECs) can also modulate conjugative transfer independently of antibiotic selection. Contaminants of emerging concern encompass chemically diverse compounds including pharmaceuticals, non-antibiotic drugs, plant protection products (PPP), industrial chemicals, personal care products (PCPs), and disinfectants, all of which are detected at sub-inhibitory concentrations in wastewater, surface water, and agricultural soils. Wastewater treatment plants represent critical nexus points where these compounds converge with dense and phylogenetically diverse bacterial communities, creating conditions that are highly permissive for plasmid-mediated HGT.

The epidemiological landscape of conjugative plasmids differs markedly between clinical and environmental settings. Among the diverse Inc groups, IncF and IncP-1 are the most relevant to the clinic-environmental interface, as each differs fundamentally in ecological niche, host range, and regulatory architecture governing conjugative transfer. IncF plasmids are the most clinically prevalent group in Enterobacteriaceae, serving as the primary vehicles for the global dissemination of extended-spectrum beta-lactamases and carbapenemases including *bla*$_{CTX}$-M, *bla*$_{NDM}$, and *bla*$_{KPC}$, particularly in high-risk pandemic clones such as *E. coli* ST131 and *Klebsiella pneumoniae* ST258 (Mathers et al., 2015). Their narrow host range, restricted predominantly to Enterobacteriaceae, combined with their genomic plasticity to accumulate AMR and virulence determinants, has enabled the coevolution of persistent and stable epidemic lineages bearing distinct resistance profiles (Pitout & Chen, 2023). The regulatory network governing IncF conjugative transfer reflects this intimate association with clinical hosts: transfer is controlled by a host-coupled architecture in which the plasmid-encoded activator TraJ, whose expression is subject to modulation by multiple host factors including the redox-responsive ArcB/ArcA system, drives transcription from the P_Y promoter (Lu et al., 2019). Meanwhile, the plasmid encoded FinOP antisense RNA system provides an additional layer of post-transcriptional repression (Figure 9A). This multi-layered architecture renders IncF conjugation inherently responsive to the physiological state of the donor cell, and thus potentially susceptible to modulation by environmental stressors that perturb host metabolism.

In contrast, IncP-1 plasmids are characterized by an exceptionally broad host range spanning phylogenetically distant Gram-negative genera, positioning them as key mediators of gene flow between environmental and clinical bacterial populations. They are consistently recovered from WWTPs, contaminated soils, and agricultural environments (Heuer et al., 2012; Schlüter et al., 2007), where their modular accessory architecture adapts to local selective pressures by accumulating resistance determinants to nearly all clinically relevant antimicrobial classes alongside heavy metal and quaternary ammonium compound (QAC) resistance genes. This plasticity underpins a shared pool of resistance determinants distributed across diverse bacterial species, making IncP-1 plasmids a critical bridge in the One Health continuum connecting environmental reservoirs to human pathogens. At the regulatory level, IncP-1 plasmids employ an autonomous repressor circuit in which four plasmid-encoded global regulators (KorA, KorB, TrbA and KorC) control plasmid gene expression directly at the DNA level without requiring host regulatory inputs, with KorA, KorB and TrbA cooperatively repressing the P_{tra} and P_{trb} promoters (Figure 9A) (Kostelidou et al.,

1999). Yet this autonomy is not absolute: the recently identified plasmid-encoded sensor GlsS32.8, conserved across globally distributed IncP-1α plasmids, detects intracellular glutamine depletion and triggers derepression of the transfer circuit under metabolic stress, indicating that IncP-1 transfer is additionally responsive through distinct specific mechanisms (Huang et al., 2025).

The molecular mechanisms by which CECs modulate conjugative transfer frequency have been partially elucidated through studies employing model conjugative plasmids *in vitro.* Mainly, the effect of CECs on HGT was attributed to stress levels, ROS production, and cell membrane permeability (G. Feng et al., 2021). At the cellular level, xenobiotic exposure can trigger multiple stress responses depending on the physicochemical properties of the compound as summarized in Figure 9B: membrane and envelope stress activates the CpxAR and related two-component systems, which among other effects destabilize the IncF transfer activator TraJ via the HslVU protease (Lau-Wong et al., 2008); oxidative stress alters the redox state of the membrane quinone pool, modulating ArcB/ArcA activity and thereby influencing P_Y-driven *tra* gene expression in IncF-carrying cells (Loui et al., 2009; Virolle et al., 2020); direct DNA damage induces the SOS response via RecA, which has been linked to induction of transfer gene expression (Memar et al., 2020); and perturbation of intracellular nitrogen metabolism (specifically, depletion of glutamine pools through increased cellular demand) in which the IncP-1 sensor GlsS32.8 is involved (Huang et al., 2019). Importantly, membrane permeabilization may also facilitate conjugative transfer, at least transiently, by enhancing mating pair formation efficiency. These pathways are not mutually exclusive and may produce opposing or synergistic effects depending on the CEC class, concentration, and exposure time (Figure 9B). Notably, several of these inputs are system-specific: ArcA-P directly activates the P_Y promoter in IncF but has no equivalent binding sites in IncP-1 transfer promoters, whilst GlsS32.8 is absent from IncF plasmids, suggesting that the two plasmid types may respond differentially to the same environmental perturbation.

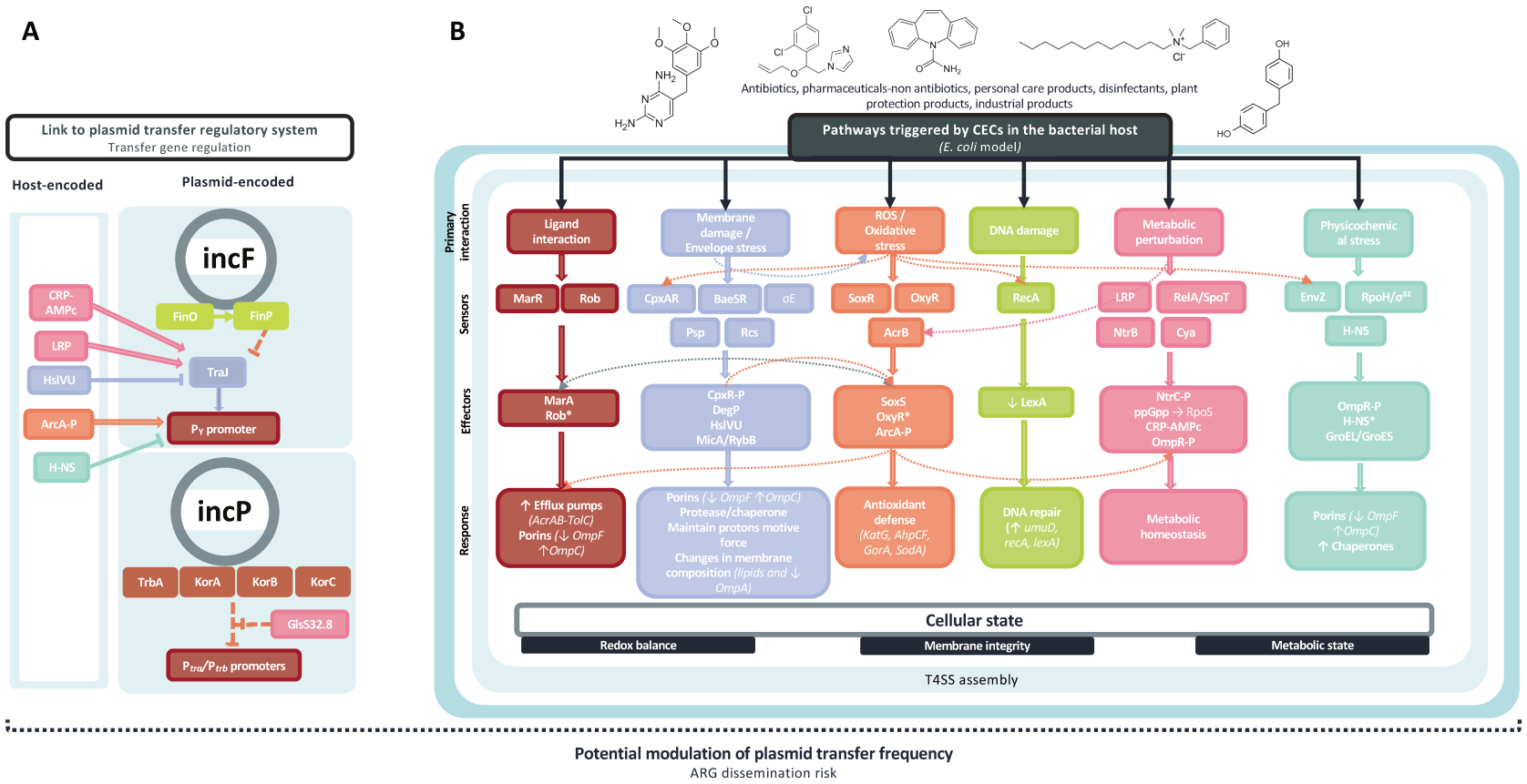

Figure 9. Multilayered sensing and regulatory network linking xenobiotic exposure to bacterial conjugation.

(A) Integration of host-encoded stress responses and plasmid-specific regulatory systems controlling conjugative transfer in IncF and IncP-1 plasmids. Host factors influence transfer through global physiological changes, whereas plasmid-encoded regulators control transfer gene expression via the P_Y promoter (IncF) and the P_{tra}/P_{trb} promoters (IncP-1). (B) Pathways triggered by CECs in the bacterial host (model: *E. coli*). Four functional layers (xenobiotic-primary interactions, sensors, regulatory effectors, and cellular responses) converge on T4SS assembly and potential modulation of plasmid transfer frequency. Each color represents an individual pathway; arrows indicate directional interactions.

The contrasting regulatory architectures of IncF and IncP-1 plasmids raise a fundamental question with direct One Health implications: do these mechanistic differences translate into qualitatively distinct responses when bacterial communities are exposed to CECs characteristic of environmental hotspots such as WWTPs? Despite the growing body of evidence linking individual CECs to enhanced conjugative transfer, the existing literature is substantially limited by interexperimental variability. Studies differ in bacterial strains, plasmid systems, growth conditions, exposure concentrations, and conjugation protocols, making direct mechanistic comparison across compound classes and plasmid types exceedingly difficult. Critically, comparative studies examining whether distinct regulatory architectures confer differential susceptibility to CECs within a standardized experimental framework remain scarce, highlighting an important gap in our mechanistic understanding of CEC-driven AMR dissemination.

The preceding chapter of this thesis established a ML model trained on experimental conjugation assays with the IncP-1 plasmid RP4 to predict the effect of environmental stressors on conjugative transfer frequency. The experimental dataset generated here provides an independent basis for partial external validation of model generalizability to novel chemical perturbations.

The present chapter extends this framework to a systematic experimental comparison of two biologically and epidemiologically distinct conjugative systems: the IncF-like plasmid and the IncP-1 plasmid. This controlled design allows differential responses to CECs to be attributed to the regulatory architecture of each plasmid type rather than to strain-specific factors. Both systems were assessed against a panel of twelve CECs spanning six functional classes (*i.e.,* antibiotics, non-antibiotic pharmaceuticals, PPP, industrial chemicals, PCPs, and disinfectants) at two concentrations spanning those reported in environmental hotspots, under identical experimental conditions, with *E. coli* HMS174 as the common recipient. To further control for donor strain background effects, the IncF-like plasmid was additionally introduced into the IncP-1 donor strain *E. coli* UB1637, enabling direct comparison of plasmid-type-specific responses under identical cellular backgrounds. This standardized multi-compound, multi-plasmid design not only maximizes the comparability of responses across chemically diverse CECs but also reflects the ecological reality of natural environments such as WWTPs, where IncF and IncP-1 plasmids coexist within the same microbial communities simultaneously exposed to complex contaminant mixtures. The aims of this chapter are therefore threefold: (i) to determine whether CEC exposure differentially modulates conjugative transfer in a plasmid-type-dependent manner, (ii) to evaluate these responses in relation to the

distinct regulatory circuits of each plasmid type, and (iii) to assess the broader implications for the role of environmental contamination in AMR dissemination across the One Health continuum.

Objectives

The specific objectives of this chapter are:

i. To systematically evaluate the effect of 12 structurally and functionally diverse contaminants of emerging concern (CECs) on the conjugation efficiency of the broad-host-range IncP plasmid RP4 and an IncF-like plasmid under standardized *in vitro* conditions.

ii. To assess whether the observed effects on conjugation are plasmid-dependent by comparing the response of IncP- with that of an IncF-like plasmid under identical experimental conditions.

iii. To determine whether any plasmid-dependent differences in conjugation modulation are attributable to the plasmid backbone itself, independently of the bacterial strain background.

iv. To identify molecular mechanisms that trigger conjugation transfer modulation, contributing to a mechanistic understanding of how CECs may shape HGT dynamics.

v. To evaluate the capacity of the predictive model developed in Chapter 1 by machine learning to generalize to the external CEC dataset.

Material & Methods

Bacterial strains, plasmids, and culture conditions.

Three conjugative systems were used in this study, all sharing *E. coli* HMS174 as the common recipient. The donor strains were *E. coli* UB1637 harboring the Green Fluorescence Protein (GFP)-tagged IncP-1 plasmid RP4 (RP4::*gfp*; kindly provided by Uli Klümper), originally described in *Pseudomonas putida* KT2442 (Musovic et al., 2010), and *E. coli* UB1637 and *E. coli* K12, both harboring the same IncF-like plasmid, which shares 9.98% query coverage and 92% nucleotide identity to pOX38 (*E. coli* K-12 MG1655, OQ683454.1), a well-characterized mini-F derivative. Both RP4 and the IncF-like plasmid conferred resistance to kanamycin (KAN, PanReac AppliChem), the recipient *E. coli* HMS174 carried a chromosomally encoded rifampicin (RIF, PanReac AppliChem) resistance marker. Prior to experimental use, the IncF-like plasmid sequence was extracted from the complete genome assembly (see Comparative genome analysis within this Chapter 2) and inspected to confirm the structural integrity of the fertility inhibition system. Both *finO* (399 nt) and *finP* (79 nt) *loci* were identified as intact, with no IS disrupting both gene, indicating that the fin system was structurally functional (Appendix B, Figure B1).

For all experimental assays both donor and recipient strains were grown overnight (*ON*) in Lysogeny Broth (LB) Lennox supplemented with the appropriate selective antibiotic (KAN, 20 µg mL^{-1} or RIF, 50 µg mL^{-1}) with orbital shaking at 220 rpm and 37°C. On the day of each experiment, *ON* cultures were cultured further by inoculating 75 µL into 3500 µL of fresh LB and grown under the same conditions for two hours until OD_{600} reached approximately 0.5 (~10^8 cells mL^{-1}).

All twelve compounds tested as CECs were obtained from Sigma-Aldrich at the highest available purity: trimethoprim (TMP), sulfamethoxazole (SMX), carbamazepine (CBZ), venlafaxine hydrochloride (VLX), azoxystrobin (AZO), imazalil (IMZ), methylisothiazolinone (MIT), benzalkonium chloride (BC), bisphenol F (BPF), potassium perfluoro-1-butanesulfonate (PFBS), oxybenzone (OXY) and, octocrylene (OCT). Detailed physicochemical properties are further described in Table 3.

Table 3. Physicochemical properties and environmental fate of the selected compounds

Compound identification			Hydrophobicity		Acid-base speciation		Aqueous solubility	Persistence & removal
Compound	Abb.	Class	MW (g/mol)	log Kow	pKa	Ionization at pH7	Solubility	t1/2 water
Trimethoprim	TMP	Antibiotic (DHFR* inhibitor)	290,3	0,91	7.12 (20°C)	~50% cationic	400	5–30 d
Sulfamethoxazole	SMX	Antibiotic (sulfonamide)	253,3	0,89	1.6 / 5.7 (amphoteric)	Anionic	610	85–100 d
Venlafaxine	VLX	Antidepressant (SNRI*)	277,4	3,2	9.4 (base)	Cationic	572	60–100 d
Carbamazepine	CBZ	Antiepileptic	236,3	2,45	n/a (neutral)	Neutral	112	47–82 d
Benzalkonium chloride	BC	Disinfectant (QAC)	350	1,5	n/a (permanent cation)	Cationic	500000	2–60 d
Methylisothiazolinone	MIT	Disinfectant/biocide	115,2	-0,49	n/a (neutral)	Neutral	500000	<7 d
Octocrylene	OCT	UV filter (acrylate)	361,5	6,88	n/a (neutral)	Neutral	0,003	Months–years
Oxybenzone	OBZ	UV filter (benzophenone)	228,3	3,79	n/a (neutral)	Neutral	6	~2.4 years
Bisphenol F	BPF	Industrial chemical	200,2	2,91	9.2 / 10.5 (phenol)	Neutral	5,4	Hours–days
Perfluorobutanesulfonate	PFBS	PFAS* (short-chain)	300,1	-0,18	<0 (strong acid)	Anionic	500000	Non-degradable
Imazalil	IMZ	Fungicide (imidazole)	297,2	3,82	6.53 (base)	~50% cationic	180	120–190 d (soil)
Azoxystrobin	AZO	Fungicide (strobilurin)	403,4	2,5	n/a (neutral)	Neutral	6	11–26 d (water)

Source: PubChem. *DHFR: Dihydrofolate reductase, SNRI: Serotonin-norepinephrine reuptake inhibitor, PFAS: per- and polyfluoroalkyl substances

Growth curves

To assess the potential inhibitory effect of the selected CECs on bacterial growth, *ON* cultures were diluted in fresh LB to an OD_{600} of 0.15. Serial dilutions of each compound were prepared in LB and combined with the bacterial suspension in 96-well microplates to a final volume of 150 µL (10 µL bacterial inoculum + 140 µL compound dilution in LB). OD_{600} was monitored over 20 h using a TECAN plate reader with continuous orbital shaking, recording absorbance every 15 min. Wells containing LB without bacteria were included in each plate as blank controls and used for background subtraction. Each compound was tested across concentrations ranging from 0.001-28 µg mL^{-1}.

Conjugation experiments

Three conjugative systems were used in this study. This design yielded three independent conjugation systems: (i) *E. coli* UB1637 (RP4) × *E. coli* HMS174, (ii) *E. coli* UB1637 (IncF-like) × *E. coli* HMS174, and (iii) *E. coli* K12 (IncF-like) × *E. coli* HMS174. Systems (ii) and (iii) were included to control for donor strain background effects on conjugative transfer. The conjugation system used was previously described by Arbé-Carton et al. (2023) with modifications. First, 100 µL of donor and 100 µL recipient (ratio 1:1) were mixed in a well of a sterile 96-filter-well plate (0.22 µm; Merck, Darmstadt). The plate was adapted to vacuum manifold (MultiScreenHTS) and vaccum (between 5-10 mm Hg) was applied to attach the cells from the filter. Then cells were exposed to 0.01 and 0.001 µg mL^{-1} to the elected CECs by adding to each well 150 µL of LB solved concentration of the contaminants. Every conjugation was referred to a control group. The 96-filter-well plates were incubated at 37°C for 4 h onto a LB-agar plate to ensure nutrients to the mating system. After conjugation time, the 150 µL of LB containing solved CECs was removed by vacuum filtration as described above. For cell detachment from the filter, 200 µL of saline buffer [0.8% (w/v) NaCl) was added to each well and bacteria were resuspended by pipette mixing. Next, adequate dilutions for colony counting were inoculated into selective LB-agar plates by drop plate method with 10 µL for each dilution (Blau et al., 2020). Plates were incubated *ON* (14-24 h). Colony Forming Units (CFUs) were counted, and conjugative efficiency was determined as the number of transconjugants (CFU mL^{-1}) referred to the number of recipients (CFU mL^{-1}). Fold-changes for each condition was calculated referring each exposure to their control group to minimize external factors affecting the conjugation process and the tested compound. To confirm the presence of transconjugants random colonies were picked and plasmid-encoded genes were amplified by PCR using OneTaq 2x MasterMix (New England Biolabs, USA)

Exploratory application of the predictive model.

The XGB model developed in Chapter 1 in which a set of descriptors could potentially be used to predict the effect of chemical stressors on conjugative transfer, was applied to the 12 CECs characterized in this chapter. External compounds were preprocessed following the identical pipeline used for the internal dataset.

Predictive performance was evaluated using R^2, RMSE, MAE, Pearson correlation coefficient, and the Concordance Correlation Coefficient (CCC), all computed in $\log_{10}$-transformed space. Per-compound analysis was performed by computing the mean absolute error (MAE) for each compound across the two tested concentrations. Chemical similarity between each external compound and the training set was quantified by the Tanimoto coefficient computed on Morgan circular fingerprints, identifying the nearest neighbor and the mean similarity across the five closest compounds. Predicted dose-response curves were generated by applying the model across a concentration range of 10^{-4} to 10^{3} mg L^{-1} (60 evenly spaced points in $\log_{10}$ scale) while keeping all other features fixed at the values corresponding to each compound. All analyses were performed in Python 3 using scikit-learn (v1.7.0) 0 (Bishop et al., 2011), and joblib for saving and loading trained models to ensure reproducibility.

Molecular mechanisms underlying the effect of CECs on conjugative transfer

Determination of reactive oxygen species (ROS)

The 2',7'-Dichlorofluorescein diacetate (DCFH-DA, Invitrogen; Carlsbad, California, USA) was used to quantify intracellular ROS generation according to previous studies (Y. Wang et al., 2019). Specifically, the donor and receipt suspensions were diluted to an OD_{600}=0.2 (approximately 10^7 CFU/mL) and stained by DCFH-DA (at the final concentration of 20 µM) for 30 min at 37°C in darkness. Next, the bacteria suspensions were washed in PBS and then treated with the elected contaminants in concentrations ranging from 0.001 to 10 µg mL^{-1} for 1.5 h. 1.5% H_2O_2 was set as positive control. Afterwards, all the samples were transferred into black 96-well plates (100 µL per well) and the fluorescence intensity (wavelength of excitation 485 nm/emission 535 nm) was measured after oxidation of DCFH-DA into 2',7'-Dichlorofluorescein (DCF) in the Infinite® 200 PRO microplate reader. Relative fold-changes in ROS production were calculated as treated samples divided by untreated samples.

Assessment of membrane permeability integrity

Donor and receipt suspensions were diluted to an OD_{600}=0.2 (approximately 10^7-10^8 CFU/mL) and washed by centrifuge at 5000 x g for 10 min and resuspended in filtered PBS

with the dissolved contaminant in concentrations ranging from 0.001 to 10 μg mL^{-1} for 1.5 h. For positive control cells were boiled for 15 minutes at 80°C. Afterwards, all the samples were transferred into 96-well plates diluted 1/10 (100 μL per well) and Propidium iodide (PI) was added to a final concentration of 20 μM. Staining for 15-30 min in darkness. Fluorescence intensity of IP (wavelength of excitation 535 nm/emission 620 nm) was measured in the in Infinite® 200 PRO microplate reader. The untreated group evaluated the level of IP uptake by the cell production measuring the ratio of the fluorescence intensity of treated samples.

Quantification of gene expression presumably involved in the conjugation process

The transcription of genes associated with conjugative transfer was evaluated using quantitative reverse transcription polymerase chain reaction (RT-qPCR). Donor *E. coli* HB101 was exposed to 0.1 and 10 μg mL^{-1} of the elected compounds for 4 h in PBS. The total RNA was extracted using Bacterial RNA extraction Kit (EZNA Bacterial, China) following manufactures' protocol with modifications. Briefly, after first RNA purification we applied a second DNase digestion to ensure no amplification on control tubes during RT-qPCR. After RNA double digested elution in ddH_2O, cDNA (qPCR template) synthesis step was immediately followed (Transgen Biotech, China) using 200 ng RNA. Quantitative PCR (qPCR) was carried out to quantify the expression of outer membrane protein genes (*ompA, ompC, ompF*), stress response gene (*rpoS, oxyR, soxS, soxR, sodA, sodC, marA, ompR, recA)*, SOS response genes (*umuD, lexA*) horizontal transfer global regulator plasmid transfer genes (*traM, traJ, trbB, trbA*). Gene expression was quantified referred to the housekeeping gene *gapA*. Primers used in this study are listed in Appendix B, Table B4.

Data analysis

Growth curves

Raw OD_{600} values were blank-corrected where applicable. Technical replicates were averaged prior to biological replicate aggregation. Growth inhibition was quantified using two complementary metrics: the area under the growth curve (AUC), calculated by numerical integration (trapezoid method) over the full 20 h period, and the maximum specific growth rate (μ, h^{-1}), estimated by fitting the modified Gompertz model to each growth curve . Where Gompertz fitting failed to converge (R^2<0.90), μ was estimated from the log-linear slope of the exponential phase using a sliding window approach. Percentage inhibition for each metric was calculated relative to the untreated control (concentration=0). Dose-response curves were fitted using a four-parameter logistic model (4PL) and half maximal effective concentration (EC_{50}) values were derived for compounds exhibiting >10% inhibition at the highest

concentration tested. All analyses were performed in Python v3.12.10 using SciPy v1.16.0 (Virtanen et al., 2020), and matplotlib v3.10.3 (Hunter, 2007).

Comparative genome analysis

Complete genome sequencing was done for the two *E. coli* donor strains using long read sequencing technology (Oxford Nanopore Technology). Assembly was done using Flye v2.9.6-b1802 (Kolmogorov et al., 2019) and circularity was checked using Bandage. Final assemblies were annotated using Bakta v.1.11.4 full database v6.0 (Schwengers et al., 2021). Annotations output were used for genome comparison using Roary v3.13 (Page et al., 2015) executed in Docker (sangerpathogens/roary). We generated the presence/absence of differential genes in each genome. Manual curing was done to retain functionally relevant genes that could be involved in the conjugation process: oxidative stress, membrane regulation, two component system (*i.e., arcA, arcB, cpxA, cpxR, ompC, ompF, rpoS, hns, hfq, marA, soxR, soxS, sodA, sodB, sodC, oxyR*). Global alignment between genomes was done using MUMmer4 (Marçais et al., 2018) in the Docker container (staphb/mummer4) using *E. coli* containing IncF-like plasmid as reference. Results were visualized by using Artemis Comparison Tool (Carver et al., 2005).

Statistical analysis

Statistical analyses were performed using R v4.2.3 (2023-03-15). Non-parametric tests were applied throughout, as normality could not be assumed given the small sample size (n=3–6 independent biological replicates), as confirmed by Shapiro–Wilk testing and visual inspection of Q–Q plots and histograms.

For conjugation experiments and RT-qPCR gene expression analysis, the Wilcoxon rank-sum test was used. For ROS production and membrane permeability assays, the Friedman test was applied to assess concentration-dependent trends across the full exposure range. Post-hoc comparisons between each concentration and the untreated control were performed using the Wilcoxon signed-rank test against $\mu=1$. In all cases, p-values arising from multiple comparisons were corrected using the Benjamini–Hochberg (BH) method to control the false discovery rate (FDR). Differences with $p_{adj}<0.05$ were considered statistically significant. Where statistical significance was not reached, results are interpreted in conjunction with effect size (fold-change) and consistency of direction across replicates.

Results & Discussion

Inhibition effect of CECs on bacterial growth

To assess the potential inhibitory effect of CECs on bacterial growth, growth inhibition was quantified as both the area AUC and the specific growth rate (μ) obtained from a linear fit of ln-transformed growth data for concentrations ranging from 0 to 10 μg mL^{-1} (Table B1). Although inhibition was initially assessed using both AUC and μ-based growth rate models, subsequent analyses focused on AUC-derived values, as they exhibited a better fit to the observed growth dynamics and reduced variability across replicates. This step was critical to ensure that any observed effect on plasmid transfer frequency could not be attributed to a reduction in donor or recipient cell viability rather than to a direct effect on the conjugation process itself. In particular, OCT was excluded from growth inhibition analysis due to optical interference at OD_{600} attributable to the physicochemical properties of the compound; growth inhibition data for OCT are therefore not reported.

At the concentrations employed in the conjugation experiments (0.001 and 0.01 μg mL^{-1}, Appendix B, Figure B2), AUC-based growth inhibition remained below 14% across all compounds and strains tested (*E. coli* HMS174, *E. coli* K12/IncF and *E. coli* UB1637/IncP; Table 4). Among the CECs evaluated, BC, MIT, TMP and SMX are recognized as agents with direct antimicrobial activity: BC and MIT as broad-spectrum biocidal disinfectants, and TMP and SMX as clinically used antibiotics. Therefore, they were assessed regarding their potential to compromise bacterial viability at the working concentrations. Disinfectant BC exhibited the highest AUC-based inhibition, reaching 12.3% and 10.3% in *E. coli* HMS174 at 0.001 and 0.01 μg mL^{-1} respectively, while remaining below 4% in the donor strains. MIT showed negligible inhibition in *E. coli* HMS174 and *E. coli* UB1637/IncP (<3%) and produced negative AUC values in *E. coli* K12/IncF (−10.1% and −9.5%), suggesting a mild hormetic growth stimulation at subinhibitory concentrations in this strain (Agathokleous & Calabrese, 2019). The antibiotics TMP and SMX showed negligible AUC-based inhibition at the working concentrations (<3% across all strains), consistent with their EC_{50} values falling well above the conjugation range. For these two compounds, full dose-response curves were successfully fitted using a 4PL across the complete concentration range tested, and half maximal effective concentration (EC_{50}) values were determined for each strain (Figure 10); in all cases, proposed conjugation working concentrations fell well below the derived EC_{50} values. The lowest values corresponded to TMP exposure, with EC_{50} values of 0.12, 0.20, and 15.73 μg mL^{-1} for *E. coli* HMS174, K-12/IncF, and UB1637/IncP, respectively. Notably, the UB1637/IncP system remained relatively

insensitive to this antibiotic suggesting differential genomic response. This phenotype may reflect host-plasmid interactions or compensatory adaptation mechanisms mitigating the effect of TMP (Durão et al., 2018). For disinfectants MIT and BC, a complete sigmoidal dose-response curve could not be resolved within the tested concentration range for all strains. AUC-based inhibition at the working concentrations was nonetheless confirmed to be below 13%, supporting the suitability of these concentrations for conjugation experiments.

Table 4. Growth inhibition of *E. coli* strains used in the conjugation experiments.

	***E. coli* HMS174**		***E. coli* K12/IncF**		***E. coli* UB1637/IncP**	
	Concentration (μg mL^{-1})					
	0.001	**0.01**	**0.001**	**0.01**	**0.001**	**0.01**
Antibiotics						
TMP	0.15	0.02	-1,38	2,76	0.48	0.54.
SMX	0.0	0.0	-2,89	-9,11	2,97	3,90
Pharmaceuticals non antibiotics						
CBZ	*2,56*	*2,57*	*13,58*	*13,62*	1,75	1,36
VLX	5.16	2.83	-9.31	-13	3.4	3.5
Disinfectants						
BC	12.34	10.25	-8,50	-11,18	3.18	2.71
MIT	2.73	2.85	-10,09	-9,52	2.05	1.4
Plant protection products (PPPs)						
AZO	-0,16	0.83	-2,45	-5,68	3.12	4.23
IMZ	1.54	2.31	-2,44	-3,18	6.85	2.35
Industrial chemicals						
BPF	-1.2	-0.8	0.1	2.7	2.2	3.1
PFBS	12.6	0.0	-0.7	-1.4	1.5	2.6
Personal care products (PCPs)						
OCT	-2.1	-0.4	-0.2	4.5	2.1	1.4
OXB	3.7	4.2	-0.9	2.9	0.2	1.1

Growth inhibition based on the AUC when strains were exposed to CECs to concentrations used in the conjugation experimental design.

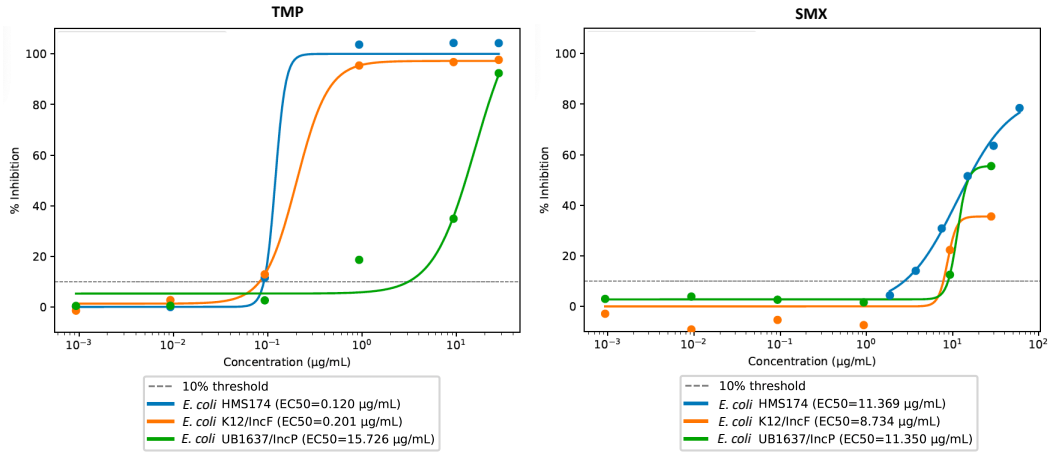

Figure 10. Dose-response inhibition curve for antibiotics AUC-based

Percentage inhibition (%) based on AUC for antibiotics trimethoprim (TMP) and sulfamethoxazole (SMX). Horizontal dashed line represents 10% inhibition threshold.

Notably, several CECs —AZO, MIT, VLX, BPF and PFBS— produced negative AUC inhibition values (*i.e.,* apparent growth stimulation) at subinhibitory concentrations in *E. coli* K12/IncF, ranging from -1% to -13%. This pattern is consistent with hormetic responses as seen for MIT, whereby exposure to low concentrations of stressors can paradoxically stimulate bacterial growth, potentially through upregulation of unrelated stress response pathways (Migliore et al., 2013). These values fell within a range indistinguishable from experimental variability and did not represent true inhibition, they do not compromise the interpretation of the conjugation results. The pharmaceutical CBZ showed negligible inhibition in *E. coli* HMS174 and *E. coli* UB1637/IncP (<4%) at the working concentrations; however, inhibition reached 11.8% and 13.9% in *E. coli* K12/IncF at 0.006 and 0.056 µg mL^{-1} respectively, indicating a mild strain-specific sensitivity at these concentrations. In addition, PFBS showed inhibition reached 12.6% at 0.001 µg mL^{-1} for *E. coli* HMS174 but this value was not consistent across concentrations suggesting an experimental outlier. The remaining CECs showed no appreciable AUC-based inhibition at the working concentrations (<7% across all strains), and dose-response modelling was not applicable given the absence of concentration-dependent inhibitory activity within the tested range. In all cases, growth inhibition remained below 14%, and the selected working concentrations were considered appropriate for conjugation experiments.

Effect of CECs on conjugative plasmid transfer

To evaluate the effect of CECs on plasmid transfer, we conducted intragenera mating assays using two conjugative systems sharing the same recipient, *E. coli* HMS174: (i) donor *E. coli* K12 carrying an IncF-like plasmid and (ii) donor *E. coli* UB1637 carrying an IncP-like plasmid. Each system was exposed to CECs from six functional groups at two subinhibitory concentrations (0.001 and 0.01 μg mL^{-1}). The use of two plasmid Inc groups was deliberate, as IncF and IncP plasmids differ substantially in their host range, transfer machinery and regulatory responses to environmental stressors (Rozwandowicz et al., 2018).

The IncP/UB1637 system showed the strongest and broadest response to CEC exposure. Specifically, BC produced the highest induction at both concentrations (mean fold-change 5.42 ± 3.56 at 0.01 μg mL^{-1} and 3.09 ± 2.26 at 0.001 μg mL^{-1}, Figure 11) followed by VLX, which showed a marked concentration-dependent pattern in the opposite direction to what would be expected from standard dose-response relationships, with higher induction at the lower concentration (6.38 ± 2.20 at 0.001 μg mL^{-1} vs 2.79 ± 1.63 at 0.01 μg mL^{-1}). TMP and SMX also produced consistent induction across both concentrations (TMP: 4.29 ± 1.94 and 4.05 ± 1.97; and SMX: 2.31 ± 0.56 and 2.51 ± 0.20, at 0.01 and 0.001 μg mL^{-1} respectively). In concordance, the inducer effect of antibiotics at subinhibitory concentrations was already well documented (M. Ding et al., 2022). Additionally, MIT showed moderate but consistent induction (2.99 ± 0.81 and 3.70 ± 0.94), while BPF and PFBS displayed high variability at the lower concentration (3.78 ± 3.76 and 4.31 ± 3.88 respectively), suggesting heterogeneous responses across biological replicates. AZO and OXB produced the most modest effects in this system (AZO: 1.17 and 1.69; OXB: 1.17 and 1.68 at 0.01 and 0.001 μg mL^{-1}, respectively). In line with previous reports collected in Chapter 1, no dose-dependent pattern could be drawn across exposure groups (Figure 5), indicating the absence of a generalizable concentration–response relationship for chemical pollutants in a systematic experimental design in which inter-experimental experimental conditions (*i.e.,* temperature, mating time or medium) do not play a major role.

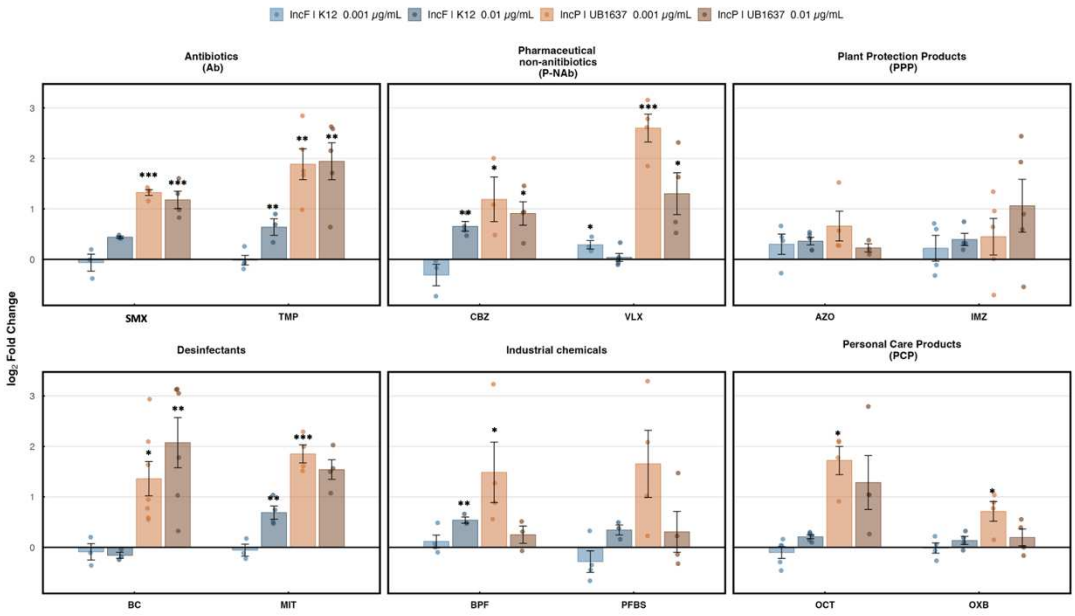

Figure 11. Effect of CECs belonging to six different functional groups on conjugative transfer.

Two mating systems were stablished depending on the donor strain and plasmid tested (*E. coli* IncF/K12 and *E. coli* IncP/UB1637) and the recipient *E. coli* HMS17. Two different concentrations were tested: 0.001 and 0.01 µg mL^{-1}. Conjugation fold-change data was log_2 transformed. Asterisks indicate significant deviation from the unexposed control (*p< 0.05, **p<0.01, ***p<0.001).

In agreement with previous studies, the promoting effect of CBZ, BPF, AZO, BC, and PFBS on conjugative transfer has been reported for the same IncP-1 RP4 plasmid. Carbamazepine at environmentally relevant concentrations has been shown to enhance RP4-mediated plasmid conjugation (Y. Wang et al., 2019) and bisphenol compounds including BPF have similarly been demonstrated to promote conjugative transfer within and across bacterial genera (Xiong et al., 2024; Yang et al., 2024). The fungicide AZO has been reported to enhance RP4 conjugative transfer frequency by upregulating plasmid transfer-related genes (Zhang et al., 2023). Regarding BC, sub-inhibitory concentrations have been shown to promote conjugative transfer of RP4 and pKJK5 (IncP-1) plasmids (Schmidt et al., 2022; Zhu et al., 2023). The strong induction of IncP transfer by BC at 0.001-0.01 µg/mL observed here confirm this effect in environmentally relevant concentrations in the intraspecies *E. coli* system. For PFBS, while most existing evidence on perfluorooctane sulfonate (PFAS)-enhanced conjugation concerns long-chain compounds such as perfluorooctane sulfonate (PFOS) (Yin et al., 2023), short-chain PFAS have been shown to exert stronger effects on plasmid transfer than their long-chain counterparts (Han et al., 2025), supporting the relevance of the PFBS induction reported here.

The IncF/K12 system showed a more restricted response, with significant but moderate induction confined to the higher concentration tested (0.01 μg mL^{-1}): TMP (1.58 ± 0.30), CBZ (1.58 ± 0.22), MIT (1.63 ± 0.31) and BPF (1.46 ± 0.11) (Figure 11). BC was the only compound that consistently failed to induce transfer in this system (0.90 ± 0.07 and 0.95 ± 0.19), suggesting a moderate inhibitory or neutral effect on IncF transfer at subinhibitory concentrations. At 0.001 μg mL^{-1}, most compounds produced fold-changes close to 1, indicating no meaningful modulation of transfer at the lower concentration in the IncF/K12 system.

For disinfectant MIT and PCPs OCT and OXB, to our knowledge no prior study has reported effects on conjugative plasmid transfer. For MIT, while direct evidence for conjugation induction is limited, its mechanism of action in disruption of the metabolic pathways and sublethal stress that may influence in the regulatory pathway for the modulation of conjugative transfer, including alterations in membrane permeability (G. Feng et al., 2021; Xu et al., 2026). The induction of IncP-1 plasmid transfer observed here represents a novel finding warranting further mechanistic investigation.

Subinhibitory concentrations of anthropogenic compounds have increasingly been recognized as drivers of HGT, with effects that are often non-monotonic and not predictable from standard dose-response relationships (Alav & Buckner, 2024). Noteworthy, the effect of CECs on both systems were consistently different under identical conditions. As observed in this study, P. Ding et al. (2022) had already reported the differential effect of several antidepressants (*i.e.,* sertraline, duloxetine, fluoxetine, bupropion escitalopram and agomelatine) in conjugative transfer modulation using RP4 and clinical isolated pMS6198A plasmids. The differential response between systems under identical experimental conditions suggests either a plasmid type effect or a donor genomic background effect, in which the molecular machinery of the IncP/UB1637 system may be more responsive to environmental chemical stress. To disentangle these two possibilities, a third conjugative system was established.

Plasmid-type effect on differential CEC sensitivity

To test the differential sensitiveness of CECs on plasmid transfer, a third conjugative system was used to discard the potential effect of genomic background after identifying potential gene differences in the genome alignment analysis (Table 5). Genes involved in stress pathways (*e.g., hsc*), DNA damage (*e.g., gad*) and xenobiotic transport (*e.g., mdt*) could contribute to the lower sensitivity of this strain to the effect of CECs.

Table 5.Differential relevant genes encoded in donor *E. coli* K12/IncF strain

Gene	Biological function
hsc	Response to stress
dctR	Cellular stress response to acidic pH
hdeB	Cellular stress response to acidic pH
hdeA	Cellular stress response to acidic pH
gadE	Cellular stress response to acidic pH
mdtE	Xenobiotic transport
mdtF	Xenobiotic transport
gadW	DNA damage response
gadX	DNA damage response

The differential response observed between the IncF/K12 and IncP/UB1637 conjugative systems could therefore be attributed to two non-exclusive factors: the Inc group of the plasmid (IncF vs IncP), or intrinsic differences in the genomic background of the donor strains (*E. coli* K12 vs *E. coli* UB1637). To discriminate between these two explanations, a third mating system was established using the IncF plasmid transferred into the UB1637 donor background (IncF/UB1637), allowing the plasmid variable to be held constant while the strain background varied. This approach follows the rationale that plasmid transfer regulatory networks are influenced both by plasmid-encoded factors and by host chromosomal regulators, which may differ between strains (Rozwandowicz et al., 2018). Given the constraints of the experimental design, this comparison was conducted at a single concentration (0.001 μg mL^{-1}) for a subset of eight compounds representing all functional groups.

All five compounds produced fold-changes close to 1 in the IncF/UB1637 system, with means ranging from 0.94 ± 0.43 (BPF) to 1.56 ± 0.94 (OCT), and none reaching statistical significance after BH correction (p_{adj} >0.05, Figure 12). Crucially, these values were markedly lower than those observed in the IncP/UB1637 system and concentration where TMP, VLX, BC and MIT produced mean fold-changes of 4.05 ± 1.97, 6.38 ± 2.20, 3.09 ± 2.26 and 3.70 ± 0.94, respectively (Figure 12). Critically, Kruskal-Wallis significant differences for TMP, CBZ and MIT were detected between both strain' groups. On the other side, the absence of significant induction in the IncF/UB1637 system, despite sharing the UB1637 host background with the highly responsive IncP system, strongly suggests that the differential CEC sensitivity observed

between the two main systems is driven primarily by plasmid-intrinsic properties rather than by donor strain effects.

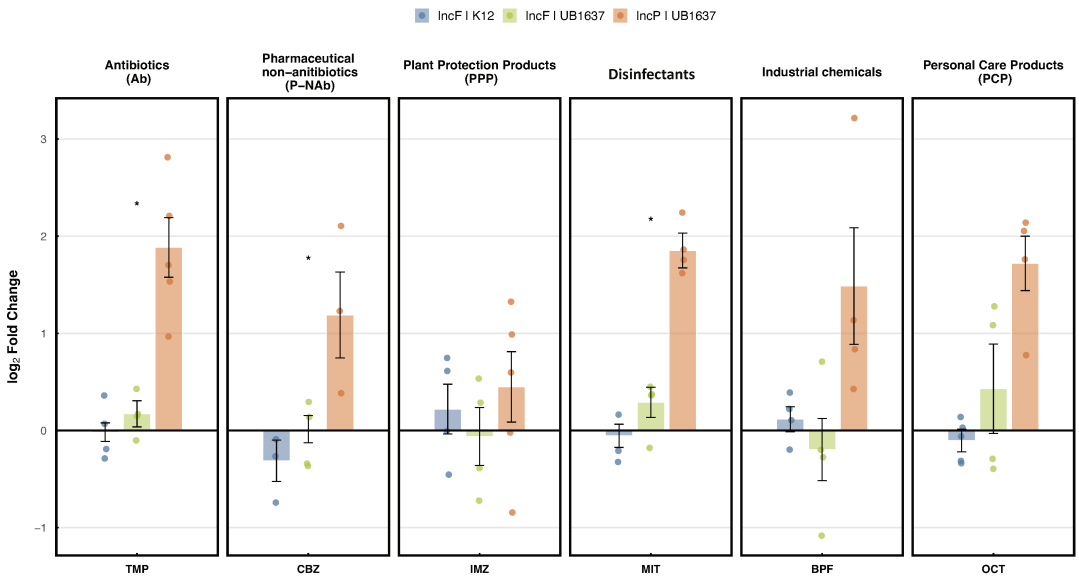

Figure 12. Effect of plasmid type on conjugation frequency exposed to CECs.

Exposure to selected emerging contaminants at 0.001 µg mL^{-1}. Bars represent mean log_2 fold-change relative to the unexposed control. Two donors of IncF-like plasmid (*i.e., E. coli* K12 and *E. coli* UB1637) and one donor of IncP-like plasmid (*E. coli* UB1637) were harboring IncF-like plasmid for three experimental groups: IncF plasmid in donor *E. coli* K12 (blue), IncF plasmid in *E. coli* UB1637 (green), and IncP plasmid in UB1637 (orange). Error bars represent standard mean error (SEM). Asterisks indicate significant differences between IncF/UB1637 and IncP/UB1637 (*$p < 0.05$).

This finding is consistent with previous reports of plasmid-type-specific responses to chemical pollutants. Ding et al. (2022) reported stronger induction of IncP transfer compared to IncC under chemical exposure, and Raro et al. (2023) demonstrated that IncL, IncA/C, and IncX3 plasmids responded to ZnO and $CuSO_4$ while IncF and IncI1 did not. Collectively, these results support a hierarchy of plasmid sensitivity to chemical induction that likely reflects differences in the regulatory architecture governing transfer gene expression across Inc groups. Notably, the two systems also differed in their basal conjugation frequencies: approximately one order of magnitude higher in IncF/K12 ($\sim10^{-1}$) than in IncP/UB1637 ($\sim10^{-2}$-10^{-3}; Appendix B, Tables B2 and B3). This difference is consistent with the well-documented variability in transfer rates across plasmid Inc groups and strain backgrounds (Dimitriu et al., 2019; Frost & Koraimann, 2010). This inherent variability reinforces the importance of reporting both relative fold-changes to be allow direct comparable outcomes between systems and studies; and raw conjugation frequencies to identify potential limitations of the experimental design.

Mechanistic basis of compound-specific responses

Reactive oxygen species and membrane permeability

The promotion of conjugative plasmid transfer by sub-inhibitory chemical stressors has been mechanistically linked to two principal cellular responses: overproduction of ROS and perturbation of membrane integrity, both of which can converge on SOS response activation and derepression of conjugative transfer genes (Beaber et al., 2004; Y. Liu et al., 2020). However, growing evidence suggests that CEC-enhanced conjugation can occur in the absence of detectable oxidative stress or membrane disruption, implying that compound-specific, stress-independent pathways also contribute to transfer induction (Alav & Buckner, 2024). To systematically characterize the mechanistic basis of the conjugation-modulating effects observed here, intracellular ROS production (DCF assay) and membrane permeability (PI uptake) were quantified in both donor (*E. coli* K12/IncF) and recipient (*E. coli* HMS174) strains across the full concentration range (0.001-10 µg mL^{-1}; Figure 13). The CECs TMP, CBZ, MIT, and BPF were evaluated, all of which exhibited a moderate yet significant increase in plasmid transfer at 0.01 µg mL^{1}. BC was also included in the analysis due to its unexpected and contrasting effect on the conjugation process.

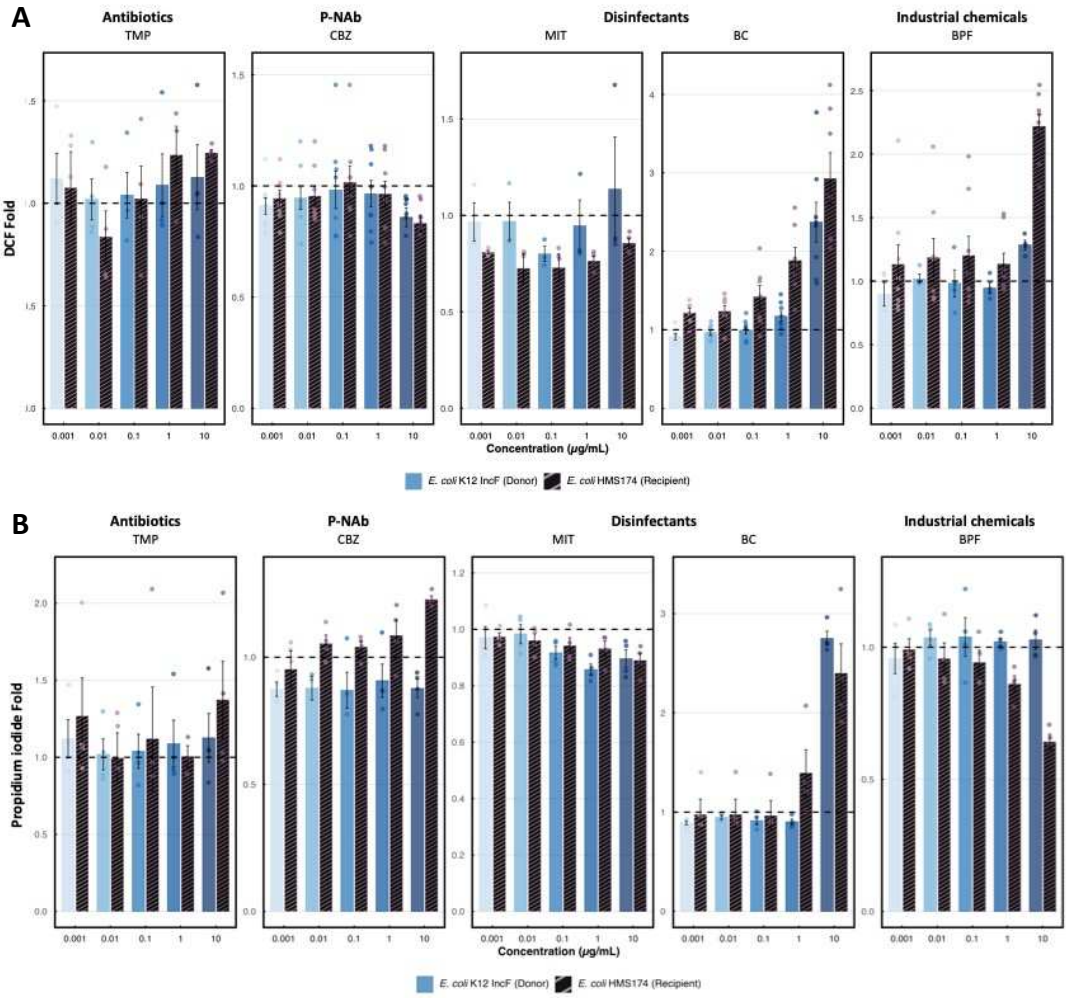

Figure 13. Effect of CECs on reactive oxygen species (ROS) production in the donor (*E. coli* K-12) and recipient (*E. coli* HMS174) strains.

(A) Fold-changes of fluorescence intensity of DCF and (B) PI uptake fold related to membrane integrity.

Of the five compounds evaluated, only BC produced significant, concentration-dependent responses in both assays. Induction of ROS in the recipient strain increased progressively from 1.22 ± 0.15-fold at 0.001 μg mL^{-1} to 2.93 ± 0.87-fold at 10 μg mL^{-1} (Friedman $p < 0.05$; Figure 13A), while membrane permeability reached 2.40 ± 0.59-fold at the same concentration. In the donor strain, both responses were detectable only at ≥1 μg mL^{-1}, with the strongest effects at 10 μg mL^{-1} (*i.e.,* ROS: 2.37 ± 0.72-fold; membrane permeability: 2.75 ± 0.15-fold), and no significant effect at lower concentrations. This concentration-response profile is consistent with the membrane-disrupting mechanism of QACs, which interfere with the electron transport chain and generate ROS as a secondary consequence of membrane damage (Tezel & Pavlostathis, 2015). Crucially, both responses occurred exclusively at

concentrations substantially above those at which BC modulated conjugative transfer (0.001–0.01 μg mL^{-1}), where neither ROS induction nor membrane perturbation were detectable in the donor strain consistent with the near neutral effect in conjugation modulation.

In contrast, disinfectant MIT produced a consistent reduction tendency in ROS detection in the recipient strain across all concentrations tested (0.73 to 0.81-fold; Figure 13A), alongside a progressive moderate decrease in membrane permeability in both strains (donor: 0.97 to 0.90-fold; recipient: 0.97 to 0.89-fold; Figure 13B). The absence of detectable membrane permeability alterations suggests that MIT did not induce severe envelope damage under the tested conditions. This contrasts with previous reports describing oxidative stress, membrane perturbation, and altered biofilm formation following sublethal MIT exposure in environmental bacteria (Nowak-Lange et al., 2022). Such discrepancies likely reflect strain-specific responses to MIT exposure, which may vary substantially depending on bacterial physiology and stress tolerance mechanisms. In addition, previous studies have suggested that some bacteria may partially tolerate or metabolically adapt to low MIT concentrations under certain conditions (Nowak-Lange et al., 2022). These observations highlight the importance of evaluating MIT effects in a strain-specific context, as bacterial responses to sublethal biocide exposure may differ substantially across species and physiological backgrounds.

Measurement of ROS or membrane permeability in the remaining CECs –TMP, CBZ, and BPF– was no significant or directionally consistent in either strain at any concentration tested (fold-changes 0.86–1.13 across all conditions; Figure 13). TMP lethality to oxidative DNA damage and thymineless death-like responses under strongly inhibitory conditions (Rao & Kuzminov, 2022). However, TMP primarily acts as a bacteriostatic inhibitor of folate metabolism, and its downstream physiological effects appear to vary substantially depending on exposure conditions, metabolic state, and bacterial strain background .

In contrast, CBZ has previously been reported to induce oxidative stress and increase membrane permeability in *E. coli* strains under comparable exposure conditions (Y. Wang et al., 2019) whereas no such effects were observed in the present study. Regarding bisphenol analogues, previous work by M. Feng et al. (2022) reported that trace-level bisphenols (including Bisphenol S and Bisphenol AF) exerted minimal effects on bacterial membrane integrity and oxidative damage, suggesting limited toxicity at environmentally relevant concentrations. In contrast, Yang et al. (2024) demonstrated that Bisphenol AF exposure can enhance conjugative transfer through mechanisms involving oxidative stress, membrane

disruption, and metabolic activation. The differential biological effects of bisphenol analogues highlight a compound-specific mechanism that may ultimately enhance plasmid transfer (Xiong et al., 2024).

The limited ROS-associated response observed in this study may be partially related to strain-specific stress tolerance mechanisms, in addition to intrinsic bacterial systems involved in ROS detoxification. In particular, the upregulation of multidrug efflux-associated genes, especially *mdtE* and *mdtF*, has been previously linked to enhanced resistance to diverse xenobiotics through active reduction of intracellular compound accumulation. Such efflux-mediated stress mitigation may represent a general adaptive response to chemical exposure and could indirectly modulate cellular conditions relevant to plasmid transfer processes by altering intracellular stress levels (Shi et al., 2022). In addition, the activation of acid- and stress-response regulators (*gadE*, *gadW*, *gadX*) may reflect broader protective physiological adaptations contributing to stress resilience. This hypothesis requires further investigation and was not directly addressed in this chapter.

Effects of CECs on SOS, Oxidative Stress, and Membrane-Associated Gene Expression

To further characterize the transcriptional basis of these responses, RT-qPCR gene expression analysis was performed exclusively in the donor strain (*E. coli* K12/IncF) exposed to TMP, CBZ, MIT and BPF at 0.1 and 10 μg mL^{-1}. The donor strain was selected as the mechanistically relevant cell type since the regulatory circuitry governing plasmid transfer gene expression resides in the plasmid-bearing donor. BC was excluded from this analysis due to insufficient RNA yield at the concentrations required for RT-qPCR, likely reflecting compound-induced conditions that compromised the stability of the RNA. Expression of 14 genes were quantified across five functional categories (Figure 14): oxidative stress regulators (*oxyR, soxR, soxS, sodA, sodC, marA*), SOS response genes (*recA, lexA, umuD*), the global stress sigma factor *rpoS*, outer membrane regulators (*ompA, ompC, ompF, ompR*), and conjugative transfer genes (*traJ, traM, trbA, trbB*).

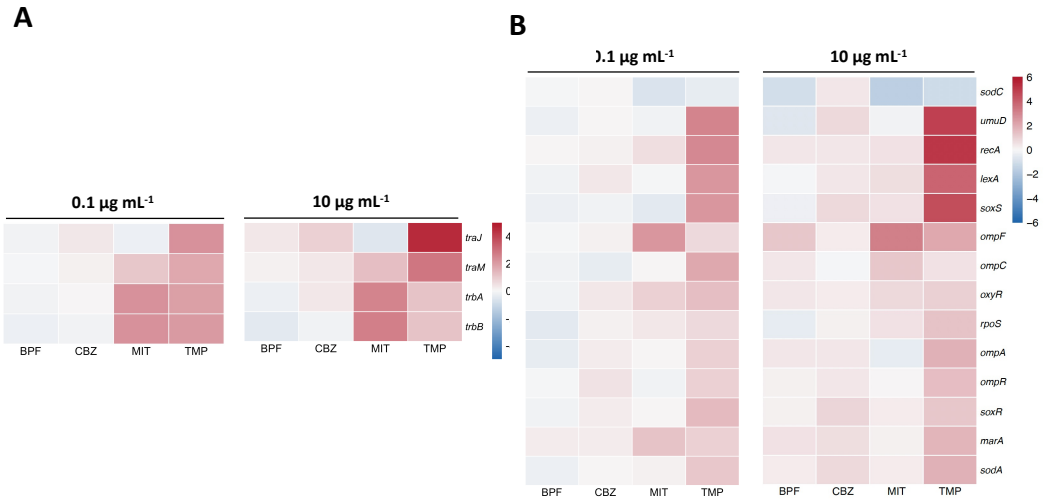

Figure 14. Gene expression of donor *E. coli* K12/IncF following exposure to CECs.

(A) Expression of conjugative transfer genes (*trbA, trbB, traJ, traM*) in donor *E. coli* K12/IncF. Values represent $\log_2$ fold-change relative to unexposed control. (B) Expression of bacterial stress response genes in donor *E. coli* K12/IncF. Genes include SOS response markers (*recA, umuD, lexA*), oxidative stress indicators (*soxS, sodC, sodA, soxR, oxyR*), membrane stress markers (*ompA, ompC, ompR*), and global regulators (*marA*, *rpoS*).

Genes involved in SOS response were upregulated by TMP exposure in a concentration-dependently manner : *recA* (median $\log_2$FC +3.07 and +5.18), *lexA* (+2.64 and +3.89) and *umuD* (+2.93 and +4.50) at 0.1 and 10 µg mL^{-1}, respectively; indicative of SOS activation through thymine starvation-induced replication fork stalling (Sangurdekar et al., 2011). Oxidative stress regulators were similarly induced: *soxS* (+2.76 and +4.75), *oxyR* (+1.56 and +1.00), *sodA* (+1.45 and +2.10), *marA* (+1.13 and +1.60) at .1 and 10 µg mL^{-1}, respectively (Figure 14B). In contrast, *sodC* was consistently repressed at both concentrations (−0.47 and −1.12) at 0.1 and 10 µg mL^{-1}, respectively; while the cytoplasmic Mn-SOD encoded by *sodA* was upregulated. This regulation is consistent with the regulatory circuit governing in *E. coli*: *sodA* expression is activated by the SoxRS regulon in response to intracellular superoxide, whereas *sodC* is regulated by RpoS and repressed under conditions that favor cytoplasmic stress responses over periplasmic defense (Strohmeier Gort et al., 1999). Outer membrane regulators were broadly upregulated (*ompC* +2.02; *ompA* +1.07 and +1.97; *ompR* +1.04 and +1.52) at 1 and 10 µg mL^{-1}, respectively; consistent with SOS-associated membrane remodeling. Although these transcriptional changes suggest activation of SOS and oxidative stress response pathways, no corresponding increase in ROS levels was detected under the experimental conditions. This discrepancy may reflect limitations in ROS detection sensitivity and/or efficient detoxification of reactive oxygen species by antioxidant systems, preventing intracellular accumulation to detectable levels.

Critically, conjugative transfer genes were concentration-dependently induced: *traJ* (+2.12 and +4.71), *traM* (+1.95 and +2.97), *trbA* (+1.75 and +1.14) and *trbB* (+2.00 and +1.08) at 1 and 10 μg mL^{-1}, respectively (Figure 14A); providing supportive evidence by which TMP promotes plasmid dissemination through SOS-mediated derepression of the conjugative transfer machinery, consistent with previous reports on RP4-mediated conjugation (Y. Liu et al., 2020).

Antiepileptic pharmaceutical CBZ showed a directionally consistent but low-amplitude transcriptional response across all categories, with no gene reaching statistical significance after BH correction. SOS genes showed modest upregulation, suggesting sub-threshold SOS engagement that does not fully activate the RecA–LexA autocleavage cascade. Conjugation genes were similarly modest, with *traJ* and *traM* reaching +0.80 and +0.67 log_2FC only at 10 μg mL^{-1}, three orders of magnitude above the conjugation-relevant concentrations used in the mating assays (Figure 14A). This weak transcriptional response contrasts with previous reports showing that CBZ can enhance conjugative transfer through plasmid-encoded regulatory pathways, including repression of korA and upregulation of *tra* and pili formation genes in RP4 systems (Y. Wang et al., 2019). These discrepancies likely reflect differences in plasmid architecture, bacterial host background, and exposure context, suggesting that CBZ-induced conjugation may be mediated by system-specific regulatory networks that are not fully captured by the gene set analyzed in this study.

Bisphenol F showed no significant transcriptional response in the transfer or any stress gene pathway at either concentration tested in the IncF/K12 system (Figure 14). The absence of a significant transcriptional response to BPF at 0.1 and 10 μg mL^{-1} indicates that bisphenol F does not strongly activate stress or transfer-related transcriptional programs in the IncF/K12 system. This aligns with previous studies reporting that bisphenol-mediated effects on bacterial conjugation are highly dependent on compound structure and experimental conditions and may not necessarily be reflected at the transcriptional level across all systems (Xiong et al., 2024; Yang et al., 2024). Particularly, M. Feng et al. (2022) reported direct transcriptional repression of the global transfer repressor *trbA* at lower, environmentally relevant concentrations without detectable membrane damage in the donor RP4 system. The latter mechanism is particularly relevant to the concentrations used in the present conjugation assays (0.001-0.01 μg mL^{-1}) and would predict de-repression of IncP transfer genes rather than IncF transfer genes, explaining the absence of detectable *traJ/traM* upregulation in the IncF/K12 donor. However, given that BPF did promote conjugation in the IncF system at 0.01 μg mL^{-1}, it is possible that bisphenol-mediated effects on membrane

fluidity or lipopolysaccharide composition may facilitate mating pair formation in a manner that is independent of transfer gene transcription (Nikaido, 2003).

Disinfectant MIT showed the highest inter-replicate variability of all compounds, particularly for outer membrane and conjugation genes, with extreme fold-changes in single replicates driving high median values for *ompF* (median log_2FC +2.52 and +3.08), *trbA* (+2.63 and +2.72) and *trbB* (+2.30 and +2.77) at 0.1 and 10 μg mL^{-1}, respectively (Figure 14). This variability is consistent with MIT's irreversible thiol-oxidizing mechanism, which may affect individual cells differentially depending on their instantaneous redox state, producing stochastic transcriptional responses across biological replicates. The apparent upregulation of *trbA* and *trbB* occurred in the absence of a coordinated SOS response and without a consistent induction of oxidative stress markers suggests that the observed transcriptional pattern is not fully explained by canonical stress-response pathways. Nonetheless, the high inter-replicate variability warrants caution, and further experiments are required to validate this observation.

Taken together, the ROS, membrane permeability, and gene expression data reveal distinct compound-specific profiles that only partially explain the observed conjugation phenotypes. First, TMP is associated with a clear SOS-related transcriptional response, with upregulation of key DNA damage regulators and stress-associated genes, consistent with a DNA replication stress mechanism. Second, CBZ elicits a low-amplitude and non-coordinated transcriptional response, suggesting sub-threshold activation of stress pathways that does not translate into a fully developed SOS or oxidative stress program under the conditions tested. Third, BPF and MIT induce limited or highly variable transcriptional responses in classical stress and transfer-related gene panels, despite promoting conjugation under certain conditions. This suggests that their effects may involve mechanisms that are not fully captured at the transcript level, potentially including subtle modulation of envelope properties or regulatory noise rather than strong activation of canonical stress pathways.

Despite this mechanistic heterogeneity observed at higher concentrations, all four CECs consistently enhanced IncF plasmid conjugation at 0.01 μg mL^{-1}, a concentration at which gene expression responses in the donor strain were not directly assessed. However, ROS production and membrane permeability measurements across the tested range did not indicate consistent activation of canonical stress responses in either strain. This dissociation between stress pathway engagement and conjugation enhancement at environmentally relevant concentrations represents a central observation of this study and suggests that

promotion of IncF plasmid transfer can occur in the absence of detectable population-level stress responses.

These findings have important implications for environmental risk assessment, as they indicate that the promotion of horizontal gene transfer by CECs may occur at concentrations that do not elicit measurable cellular damage and that are commonly detected in wastewater effluents, surface waters, and agricultural soils (Larsson & Flach, 2022). This implies that current frameworks may underestimate the potential role of low-level chemical exposure in shaping the dissemination of ARGs in environmental settings.

Exploratory application of the predictive model

Global performance

The XGB model developed in Chapter 1 over RP4 conjugation transfer was applied without retraining to the 12 CECs characterized in this chapter (n=24). Global predictive performance on the external set was lower than on the internal validation set (external: R^2=-0.886, RMSE=0.283; internal: R^2=0.719, RMSE=0.279; Figure 15A). This difference is partly attributable to the narrow fold-change range of the external compounds (1.2-6.4×, $\log_{10} \sim 0.07$-0.80), which reduces the discriminative signal available for evaluation, rather than reflecting a fundamental failure of the model.

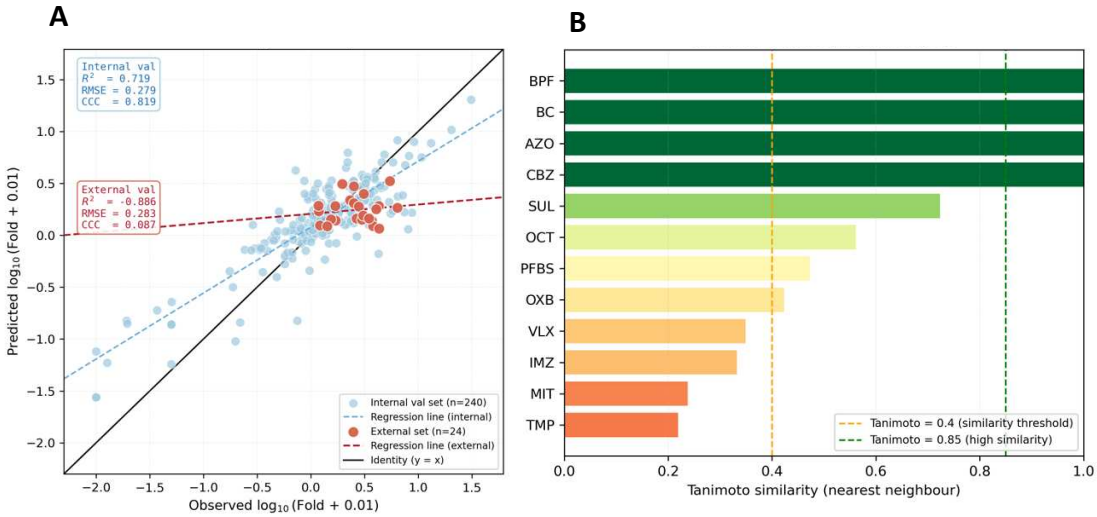

Figure 15. Chemical similarity of selected CECs to the training set and predictive model validation.

(A) Observed versus predicted $\log_{10}$ for the internal validation set (blue, n=240) and the external CEC set (red, n=24) using the best-performing XGB model (feature set: concentration + Morgan fingerprints + species relation; internal R^2=0.719). Dashed lines indicate regression lines for each set; solid black line indicates the identity line (y=x). (B) Tanimoto similarity of the 12 external CECs to their nearest neighbor in the training set, computed on Morgan

circular fingerprints (radius=2, 2048 bits). Bar colors reflect similarity score (green=high, red=low); dashed vertical lines indicate conventional similarity thresholds of 0.4 and 0.85.

Analysis of individual predictions revealed a clear pattern: 9 of the 24 observations were predicted with an absolute error below 0.15 log_{10} units (equivalent to <0.5× in original scale), while the remaining 15 showed larger deviations. Two independent factors explained most of the variability in prediction error. First, compounds with observed fold-change above 3× were systematically underestimated by the model, which tends to predict towards the center of the training distribution in the high-response range. Second, observations at 0.001 µg mL^{-1} were less accurately predicted than those at 0.01 µg mL^{-1} for the same compound, likely reflecting greater biological variability at sub-nanomolar concentrations rather than a limitation of the chemical representation.

The best-predicted compounds were BPF (MAE=0.009), SMX (MAE=0.029), IMZ (MAE=0.036), OXB (MAE=0.055), PFBS (MAE=0.067), CBZ (MAE=0.070), and AZO (MAE=0.088), all with observed fold-change in the range 1.2-3.1×. Notably, three of these (BPF, CBZ, AZO) had a Tanimoto similarity of 1.0 to compounds in the training set, confirming that chemical familiarity is a positive predictor of model performance. The poorest predictions corresponded to TMP, MIT, OCT, VLX, and PFBS at 0.001 mg L^{-1}, all showing fold-changes above 3× and/or low Tanimoto similarity to the training set (Figure 15B).

Overall, these results suggest that the model developed in Chapter 1 captures relevant chemical structure-activity relationships within its training domain, but its direct applicability to new CECs datasets is conditioned by the biological response range and the experimental heterogeneity inherent to the training data. The present analysis identifies compounds with moderate fold-change induction as the most reliably predicted class, and points to the systematic generation of experimental HGT data across a wider range of CECs and concentrations as the key requirement for improving external predictive performance.

CHAPTER 3

Environmental Chemical and Microbiological Context of a Wastewater-Impacted River Basin: Resistome Profiling and Conjugative Transfer Potential of WWTP Effluents

Antibiotic resistance is a natural evolutionary phenomenon that predates clinical antimicrobial use, but human activities have significantly accelerated its propagation through the environment (Larsson & Flach, 2022). Anthropogenically impacted aquatic environments receive a complex mixture of chemical stressors including a chemically diverse set of CECs alongside bacterial communities of both environmental and clinical origin, creating conditions that may modulate HGT (Jiang et al., 2022).

Conjugative plasmids are the primary vehicles of HGT in bacterial communities (Garcillán-Barcia et al., 2025). Their intrinsic transfer and replication machinery operates largely independently of the host genome, enabling them to cross phylogenetic boundaries that would otherwise be impermeable to genetic exchange. Beyond their autonomous transfer capacity, conjugative plasmids can additionally mobilize non-conjugative elements carrying host-beneficial traits and additional recombination tools, amplifying the reach of HGT across genera (Álvarez-Rodríguez et al., 2020). The ecology of this conjugative plasmid pool is shaped

by multiple interacting factors: the chemical selective pressures that modulate transfer frequency; the physical structure of the environment (*i.e.,* cell density, surface attachment and hydrodynamics) which determines the probability of the cell-to-cell contact that conjugation requires (Ruan et al., 2021; Thomas & Nielsen, 2005); and the evolutionary history of the plasmid pool itself, which determines the range of compatible host-plasmid combinations available for transfer at any given site and time (Benz & Hall, 2023; Norman et al., 2009).

The preceding chapters of this thesis demonstrated that, under controlled experimental conditions, structurally diverse CECs modulate conjugative transfer frequency in a compound-specific manner, implicating the intrinsic physicochemical properties of each contaminant as determinants of their differential effect on plasmid dissemination dynamics. These analyses further provided mechanistic insight into the distinct modes of action through which CECs interact with the bacterial stress response, the conjugative transfer apparatus, and membrane physiology of the model donor strain. However, by design, such reductionist experiments isolate individual chemical stressors and defined plasmid-host pairs from the ecological complexity that characterizes real-world microbial communities, where mixed contaminant profiles, fluctuating environmental conditions, and diverse plasmid pools coexist and interact simultaneously.

Whether the pro-conjugative effects characterized *in vitro* manifest under ecologically realistic conditions remains an open and critical question. In natural and engineered aquatic environments, conjugative plasmid transfer occurs within taxonomically diverse biofilm and planktonic communities exposed to complex chemical mixtures at concentrations that shift dynamically with hydrological regime, seasonal variation, and anthropogenic input (Abe et al., 2021; Beltrán de Heredia et al., 2023, 2025). Resolving this question requires moving beyond controlled model systems toward direct empirical characterization of the plasmid populations circulating in environments where CEC-mediated selective pressure operates at ecologically relevant concentrations.

Wastewater treatment plants and their receiving water bodies represent ideal systems for this investigation. In particular, WWTPs serve as hotspots for the emergence and dissemination of ARGs, concentrating pathogenic bacteria, MGEs, and a complex array of CECs derived from human activities (Berendonk et al., 2015). Despite ongoing improvements in contaminant removal during wastewater treatment, WWTP effluents routinely discharge complex mixtures of chemical stressors into receiving water bodies at sub-inhibitory

concentrations, including compounds with antimicrobial activity insufficient to kill bacteria but potentially sufficient to exert selective pressure on MGEs (Bengtsson-Palme & Larsson, 2016). This discharge is projected to intensify under climate change scenarios, where increased frequency of extreme precipitation events and combined sewer overflows will periodically bypass treatment capacity, delivering untreated or partially treated effluents directly into receiving waters (Hughes et al., 2021; J. Li et al., 2023). The resulting chemical gradients, extending from the WWTP outfall through downstream receiving waters, may sustain chronic selection for resistance over spatial scales that far exceed the immediate vicinity of the point source. The river or estuary downstream of a WWTP thus functions as a continuum of selective pressure, in which the local plasmid pool is shaped simultaneously by the CECs that escape treatment, the hydraulic connectivity that redistributes bacteria between sites, and the ecological interactions *(e.g.*, competition, predation and syntrophy) that determine which plasmid-host combinations persist and proliferate in the receiving community (Bottery, 2022; Sünderhauf et al., 2023).

To address these questions, we selected the Butroe river basin in the Basque Country (northern Spain) as a model system. The basin encompasses two municipal WWTPs with contrasting catchment characteristics discharging into a shared coastal receiving environment: Gorliz, serving a coastal urban-hospital population with strong seasonal fluctuations associated with tourism, and Mungia, serving an inland mixed urban-agricultural catchment. Critically, this configuration also allows the study of a water continuum: the receiving waters downstream of the Mungia WWTP discharge progress through a hydrologically connected estuarine-bay system, enabling the simultaneous assessment of point-source chemical gradients and their expected attenuation along the aquatic continuum. This spatial design, combined with sampling across three contrasting seasons, captures both the temporal variation in contaminant load and the spatial dilution and redistribution of chemical selective pressure from the WWTP outfall through the receiving coastal waters

This chapter addresses these questions through three complementary approaches. First, the chemical characterization of WWTP effluents and receiving waters, carried out as part of the collaborative HOBE project by members of the IBeA research team at the University of the Basque Country (EHU, https://www.ehu.eus/es/web/ibea). This analytical chemistry team in the context of Maddi Salvoch Vilches doctoral thesis project, provided the environmental contaminant context within which microbiological and conjugation data are interpreted. Second, filtered-sterilized WWTP effluent waters from Gorliz and Mungia were tested directly in the standardized conjugation platform developed in Chapter 2 across three sampling

seasons. This approach, building on previous assessments of conjugation modulation by wastewater matrices (Miao et al., 2025) extends the analysis to systematic seasonal and spatial comparison within a single river basin, using the same defined plasmid-host system as Chapter 2 to enable direct comparison between the effects of individual compounds and complex environmental mixtures on conjugative transfer frequency. Third, quantitative PCR targeting ARGs, MGE markers, and anthropogenic indicators was used to profile the resistome of all sampling points across seasons, establishing the *in situ* microbiological selective pressure landscape. Together, these three lines of evidence establish the environmental chemical and microbiological context of the Butroe river basin and bridge the gap between the controlled experimental conditions of preceding chapters and the ecological complexity of real wastewater-impacted environments.

Objectives

i. To evaluate the capacity of real WWTP effluent matrices to modulate conjugative plasmid transfer using the standardized conjugation platform developed in Chapter 2, enabling direct qualitative comparison between the effects of individual compounds and complex environmental mixtures on conjugation frequency.

ii. To profile the resistome of influents, effluents, and receiving waters across sampling seasons using quantitative PCR targeting ARGs, MGE markers, and anthropogenic indicators, and to compare resistome composition between WWTPs in relation to their catchment characteristics.

Material & Methods

Study area

Butroe river basin

The study area encompasses the Butroe river basin (175.15 km², mean annual flow 4.7 m³/s and moderate drainage density of 0.87 km/km^2), located in the province of Bizkaia, Basque Country, northern Spain (Docampo, 1989), Figure 16). The Butroe river originates in Bizkargui and flows approximately 30 km in a southeast-to-northwest direction before transitioning to estuarine waters at the Arbina dam in the municipality of Gatika. The subsequent 8.5 km corresponds to the Butroe estuary, which discharges into the Bay of Biscay at the municipality of Plentzia. The tidal regime is semidiurnal with mesotidal amplitudes ranging from approximately 1 m on neap tides to 4.5 m on spring tides. The climate is temperate mesothermal with a mean annual precipitation of 287 hm³/year distributed relatively evenly throughout the year, with a characteristic increase in autumn-winter rainfall. The main hydromorphological characteristics of the Butroe River basin are summarized in Table 6. These indices indicate moderately elongated basin, suggesting a progressive hydrological response and potentially gradual downstream transport of contaminants.

Table 6. Hydromorphological characteristic of the Butroe river basin.

Parameter	Value	Description
Basin area (km^2)	175.15	Total drainage area
Total drainage length (Km)	152	Sum of all network channels
Elongation ratio	0.66	Indicates elongated basin shape
Garvelius index	1.32	Degree of deviation from circular shape
Caquot index	1.19	Hydrological response

Source: Adapted from Docampo (1989), Table 1.

Ecological framework

The Butroe estuary and surrounding coastal system have been identified as an area of high ecological value, with formal proposals for its designation as a protected biotope initiated in 2012, though this designation remains pending (Figure 16). The area encompasses 14 Community Interest Habitats under Directive 92/43/EEC, including well-preserved estuarine marshes, coastal dune systems (European Council, 1992), and habitats of high ecological value. However, the area is also subject to significant anthropogenic pressures, particularly from urban development, highlighting its vulnerability to environmental impacts.

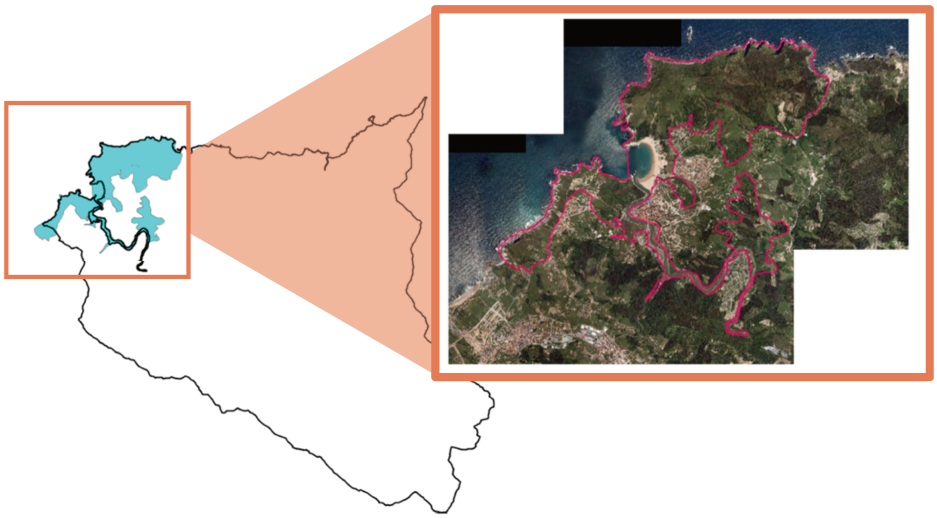

Figure 16. Proposed delimitation of the region to be protected biotope by the University of the Basque Country (EHU).

Source: Adapted from Fundación Interuniversitaria Fernando González Bernáldez (2011). Dictamen sobre las medidas de conservación y protección más adecuadas para la zona de Uribe Kosta-Butroe (Bizkaia). Gobierno Vasco, Departamento de Medio Ambiente, Planificación Territorial, Agricultura y Pesca. Octubre 2011.

Socioeconomic activity and anthropogenic pressures

The Butroe river basin encompasses a set of municipalities with contrasting demographic and land-use characteristics along its longitudinal gradient. The main urban center is Mungia (~17,700 inhabitants), located in the upper-middle basin (Figure 17), where urban development coexists with extensive livestock farming. Downstream, smaller rural municipalities such as Gatika, Barrika and Lemoiz are distributed along the river corridor and coastal fringe. The lower basin and estuarine zone include the coastal towns of Gorliz and Plentzia (~6,000 and ~4,000 inhabitants, respectively; Figure 17), which are characterized by strong seasonal population increases linked to tourism.

This spatial gradient is reflected in marked differences in land use and anthropogenic pressures across the catchment. The inland area, associated with the Mungia WWTP catchment, comprises six municipalities with a combined utilized agricultural area (UAA) of 1,703 ha, dominated by permanent pastures (87%) and substantial livestock farming activity: 1,996 cattle, 2,642 sheep and 573 goats (Eustat, 2020). This pastoral activity is concentrated along the Butroe river valley and its tributaries, representing a potential diffuse source of veterinary antimicrobial residues and manure-associated resistant bacteria entering the river through surface runoff. In contrast, the coastal catchment associated with the Gorliz WWTP includes four municipalities (Barrika, Lemoiz, Gorliz and Plentzia) with a much smaller UAA (298 ha) and markedly lower livestock densities (293 cattle and 415 sheep), reflecting the predominantly urban and coastal character of this zone. The municipality of Gorliz had a permanent population of 6,015 inhabitants in 2024 and received approximately 26,893 tourists during the same year (Instituto Nacional de Estadística, 2024), while Plentzia is virtually devoid of agricultural activity (12 ha UAA and 6 cattle heads). Overall, the Mungia catchment contains 6.8-fold more cattle and 6.4-fold more sheep than the Gorliz catchment, supporting the classification of the Mungia WWTP effluent as receiving mixed urban-rural influent and the Gorliz WWTP effluent as receiving predominantly urban-derived wastewaters.

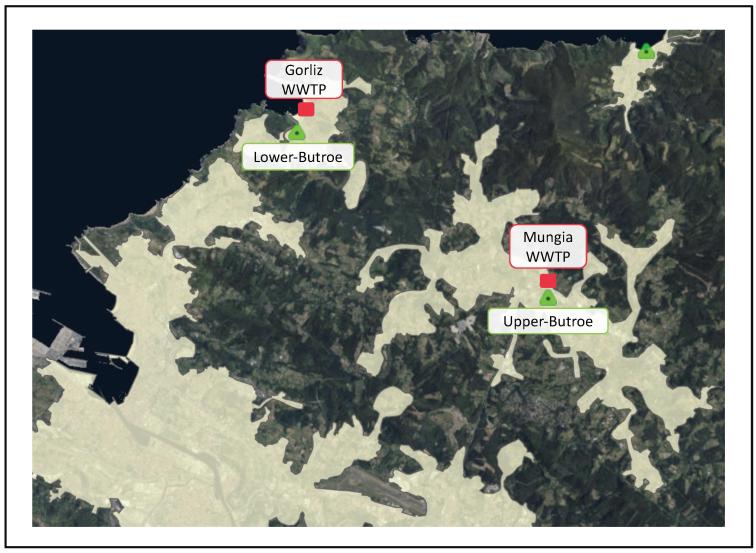

Figure 17. Delineation of the upper and lower Butroe catchments.

Source: Image modified from Agencia Vasca del Agua (URA)

Wastewater treatment plants (WWTPs)

Two WWTPs discharging into hydrologically distinct receiving environments within the Butroe catchment were selected as primary sampling sites. The Mungia WWTP serves the upper-middle basin catchment, receiving mixed urban-agricultural-industrial influent from six municipalities, and discharges treated effluent directly into the Butroe river approximately 15 km upstream of the estuary mouth. The Gorliz WWTP serves the lower coastal catchment, receiving predominantly urban influent from three municipalities including the Hospital de Gorliz (Osakidetza), and discharges via submarine outfall directly into the Bay of Biscay. Key characteristics of both plants are summarized in Table 7 and extended in Appendix C Table C1.

Table 7. General characteristics and catchment profile of the two studied WWTPs.

Feature	Mungia WWTP	Gorliz WWTP
Agglomeration code	ES16480690001010	ES16480770003010
Coordinates	43.361°N, 2.846°W	43.412°N, 2.939°W
Catchment type	Urban-agricultural-industrial	Urban-coastal-hospital
Served municipalities	6 (Upper Butroe)	3 (Lower Butroe/Coastal)
Connected load (h.e.)	21,616	18,446
Design capacity (h.e.)	21,884	44,000
Annual treated volume (m^3/yr)	2,600,000	1,700,000
Secondary treatment	Biological (activated sludge)	Biological (biofilm) + physico-chemical
N removal	Yes	No
P removal	Yes	No
UV disinfection	Yes	No
Discharge point	Butroe river (~15 km upstream estuary)	Bay of Biscay (Submarine outfall)
Receiving water body code	ES111R048020	ES111C000030

Data from URA discharge authorizations (Agencia Vasca del Agua (URA), 2019a, 2019b) and (European Environment Agency, 2026). h.e.: population equivalents.

The two plants differ substantially in treatment intensity: Mungia applies full biological treatment with nitrogen and phosphorus removal and UV disinfection, while Gorliz applies primary and secondary treatment only, without nutrient removal or disinfection (Figure 18). This difference is reflected in their respective regulatory emission limits, which do not include nitrogen or phosphorus thresholds for Gorliz (Appendix C, Table C3). The contrasting treatment levels, discharge pathways, and catchment profiles provide a natural comparative framework for assessing how WWTP effluent composition and treatment intensity influence conjugative plasmid transfer and the environmental resistome of the receiving water system.

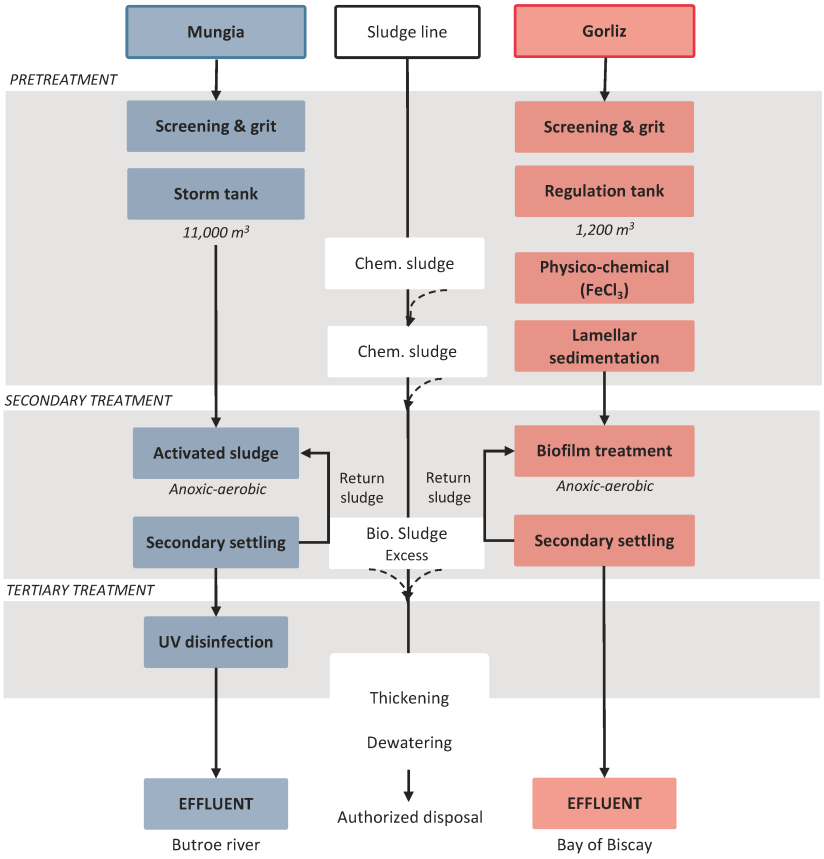

Figure 18. Simplified treatment flow diagrams of the WWTPs of Mungia (left) and Gorliz (right).

Sampling points and strategy

Sampling was conducted at two WWTP effluents: Mungia (hereafter Mungia) and Gorliz (hereafter Gorliz); and their receiving environments: the inner estuary of Plentzia (hereafter Estuary) and the coastal waters of the Bay of Biscay (hereafter Bay), at four time points across 2024: March, June, September, and November, representing winter, spring, summer, and autumn seasons, respectively (Figure 19). These sampling campaigns were designed to capture seasonal variability in environmental conditions, including water temperature, precipitation patterns, and associated shifts in microbial community composition.

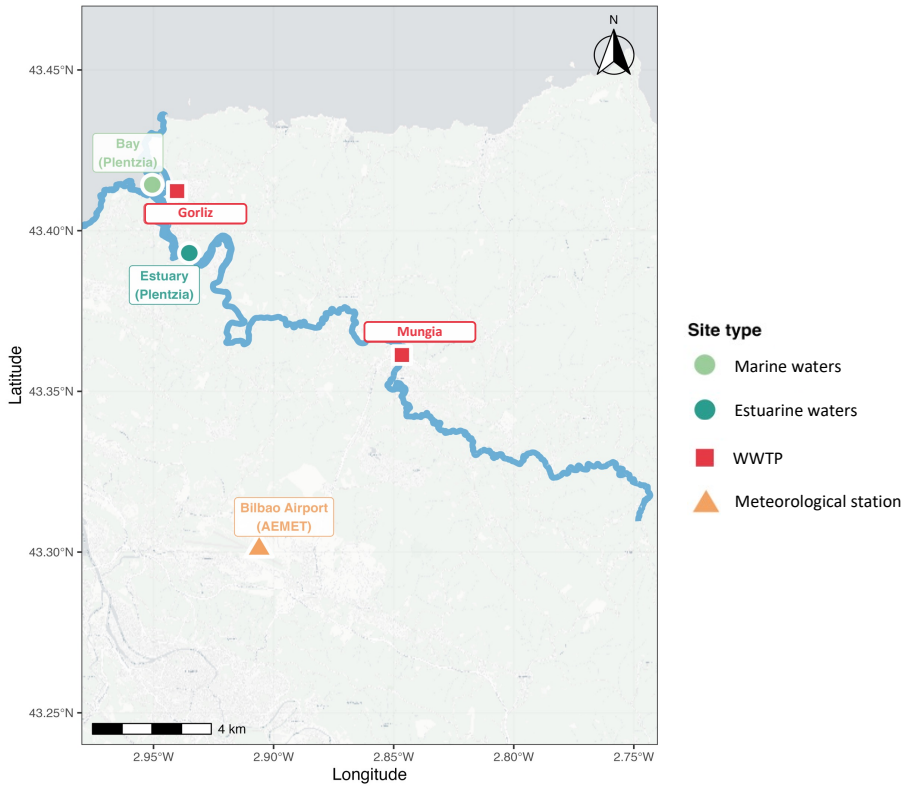

Figure 19. Overview of the study area and sampling sites.

Location of the sampling sites along the Butroe basin discharging into Plentzia Bay (northern Spain). Receiving waters are marked in circles: Bay and Estuary. Wastewater treatment plants (WWTP) are marked in squares. The meteorological station is marked in triangle (Bilbao airport, AEMET). The river course continuum is shown in blue. Basemap: CartoDB Positron.

Physicochemical conditions

Physicochemical conditions in the receiving water bodies were characterized using long-term monitoring data from the Butroe estuary carried out within the collaborative HOBE project, including surface water temperature, salinity, dissolved oxygen, and pH at two representatives' stations (Bay of Plentzia and inner estuary, Figure 20A). Seasonal dynamics in 2023 showed a clear temperature cycle ranging from approximately 10°C in winter to 22°C in late summer, with a marked salinity gradient between the coastal waters and the estuary which intensified during autumn rainfall events.

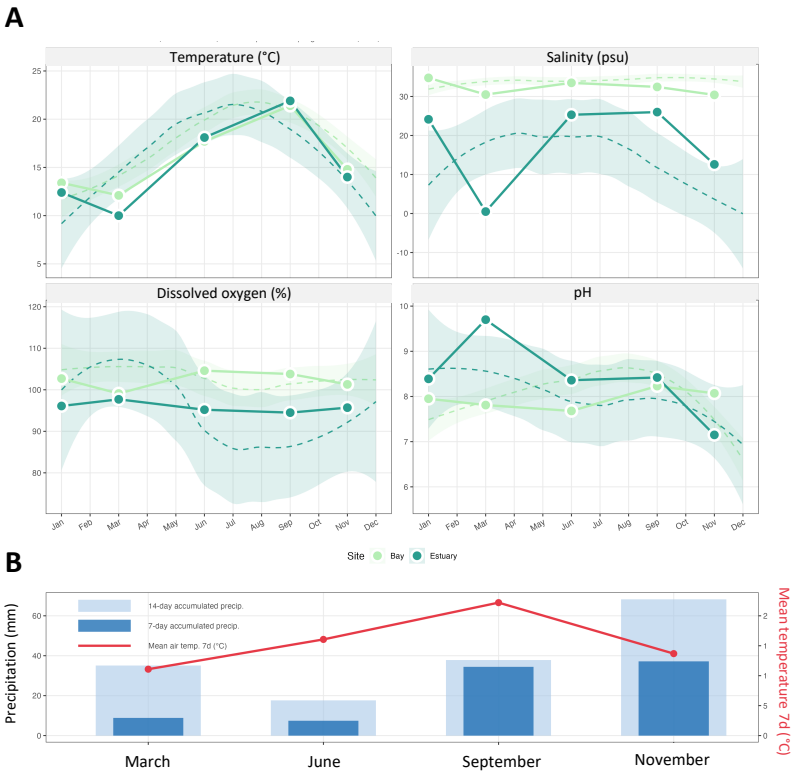

Figure 20. Environmental context of the study area.

(A) Seasonal physicochemical dynamics in the Butroe estuary system. Temperature (°C), salinity (psu), dissolved oxygen (%) and pH). Shaded curves correspond to 2023 baseline (± 95% CI). Lines and points correspond to 2024 sampling that comprehends this study. Source: data were collected during sampling campaign within the HOBE project. (B) Meteorological conditions prior to sampling day. Bars show accumulated precipitation 14 or 7 days before sampling day. Red line shows mean air temperature (Cº). Source: Data was extracted from AEMET database in the Bilbao Airport station.

Meteorological conditions

Meteorological conditions preceding each sampling campaign were characterized using daily precipitation and temperature data from the nearest meteorological station, Bilbao Airport (station 1082), located approximately 7 km from Mungia [Agencia Estatal de Meteorología (AEMET), 2026]. Accumulated precipitation in the 7 days prior to sampling ranged from 7.4 mm (June) to 37.2 mm (November), with the 14-day accumulation reaching 68.3 mm prior to the November sampling (Figure 20B).

Sample collection

Water samples were collected at four sampling sites using sterile polyethylene terephthalate (PET) bottles: the Butroe Estuary, Bay, and the effluent of the two WWTPs Mungia and Gorliz. At each WWTP effluent, 1 L of water was collected in duplicate, yielding two independent 1 L fractions: one designated for total DNA extraction and one for bacterial

community isolation. At Estuary and Bay, 3 L of surface water were collected in duplicate, yielding two independent 3 L fractions in each site for the same purposes. Water fractions collected for DNA extraction were filtered through 0.22 µm pore size polyethersulfone (PES) membrane (Gilson, Middleton, WI, USA) while those for bacterial community extraction were filtered through 0.45 µm pore size mixed cellulose membrane by vacuum filtration, until either the target volume was processed, or the membrane was clogged. Cellulose membranes designated for bacterial community extraction were processed immediately after filtration. PES membranes designated for DNA extraction were snap-frozen and stored at -40°C until further processing.

DNA extraction and High-throughput quantitative PCR (qPCR)

DNA extraction from PES membranes was performed using DNeasy Power Water Kit (Qiagen, Hilden, Germany) following manufacturer instructions. Quality and quantification on purified DNA were quantified using BioDrop spectrophotometer and concentration was adjusted to 10 ng μl^{-1} and sent to Resistomap Oy (Helsinki, Finland). The study examined a total of 34 target genes, including 24 ARGs, two genes associated with resistance to disinfectants (*qacEdΔ1*, *bacA*), 5 MGEs, and one gene associated with resistance to metal (*merA*) and other resistance markers (*mcr-1*) related gene fragments. Additionally, crAss64 viral marker were screened as an indicator of human fecal contamination and *intI1*, recognized anthropogenic proxy were included in the analysis. The 16S rRNA gene was also analyzed to estimate the overall bacterial load. Detailed information on tested genes can be found in Appendix C, Table C1.

Bacteria and culture conditions

For the WWTP effluent effect on conjugative plasmid transfer, *E. coli* K12 harboring an IncF-like plasmid was used as the donor strain, and *E. coli* HMS174 as the recipient (system i, adapted from Chapter 2). Both strains were grown in LB broth at 37°C with orbital shaking at 220 rpm *ON* prior to each experiment. Cells were harvested by centrifugation (6,000 × g, 4 min) and washed once with PBS (pH 7.4) before use.

Effect of WWTP effluent on conjugative plasmid transfer

Filter-sterilized WWTP effluent samples (0.22 µm pore size) were used to evaluate their effect on conjugative gene transfer, using the system described in Chapter 2 (system i). All experiments were performed within 72 h of filtration, using samples stored at 4°C that had not been subjected to freezing.

The conjugation protocol was adapted from Arbé-Carton et al. (2023) with modifications. Briefly, 100 µL of donor and 100 µL of recipient cell suspensions (1:1 ratio), both resuspended in PBS (pH 7.4), were combined in individual wells of a sterile 96-well filter plate (0.22 µm; Merck, Darmstadt, Germany). The plate was fitted onto a vacuum manifold (MultiScreenHTS) and a gentle vacuum (5-10 mmHg) was applied to retain cells on the membrane surface. Cells were then exposed to 150 µL of filter-sterilized WWTP effluent collected across three seasons (spring, summer, and autumn), while control wells received 150 µL of PBS. Plates were placed onto LB-agar plates to provide nutrients and incubated at 37°C for 4 h.

Following the conjugation period, the mating medium was removed by vacuum filtration. Cells were detached from the membrane by adding 200 µL of saline buffer (0.8% NaCl w/v) and resuspending by pipetting. Next, adequate dilutions for colony counting were inoculated into selective LB-agar plates by drop plate method with 10 µL for each dilution (Blau et al., 2020). Plates were incubated *ON* (14-24 h). Colony-forming units were enumerated, and conjugation efficiency was expressed as the ratio of transconjugants (CFU mL^{-1}) to recipients (CFU mL^{-1}). All experiments were performed in four biological replicates.

Statistical analysis

Quantitative PCR

All statistical analyses were performed in R v4.2.3. Prior to analysis, ARG and MGE abundances were log_{10}-transformed after normalization to 16S rRNA gene copy numbers. Hierarchical clustering of gene abundance profiles was performed using Euclidean distance and complete linkage, as implemented in the pheatmap package. Gene clusters were defined by cutting the resulting dendrogram at k=2.

Pairwise Spearman rank correlations between sites were computed on the paired dataset, where each observation represents one gene at one sampling site in one month (n=60–102 observations per pair depending on data availability). Permutation-based comparison of dependent Spearman correlations was used to formally test significance in prediction of resistome dynamics. Under the null hypothesis that the two WWTPs are interchangeable as predictors of downstream resistome composition, Mungia and Gorliz labels were randomly swapped row-wise across all Assay × Month observations (n=9,999 permutations, seed=42), generating a null distribution of rho differences. The two-tailed p-value was calculated as the proportion of permuted differences with absolute value equal to or greater than the observed difference (rho_Mungia − rho_Gorliz). Tests were performed for the full gene panel and for

each hierarchical cluster separately, using both the Estuary and the combined downstream environment (Estuary + Bay averaged per Assay × Month) as outcome variables.

Non-metric multidimensional scaling (NMDS) was performed on Euclidean distances between site × month resistome profiles using the metaMDS function from the vegan package (k=2, trymax=100, autotransform=FALSE, seed=42). Permutational multivariate analysis of variance (permanova) was used to formally test the effects of sampling Location and Month on resistome composition, implemented via adonis2 in vegan (999 permutations, Euclidean distance). Analyses were performed on the full dataset and on subsets (*i.e.,* excluding Bay, excluding November, and restricted to the two WWTP sites).

Results & Discussion

Environmental chemical and microbiological context

Chemical characterization of WWTP effluents

As part of the HOBE project, a comprehensive chemical characterization of water samples collected across the Butroe river basin was carried out by the collaborating analytical chemistry team. Preliminary data from this analysis, covering over 300 compounds across three sampling seasons, are presented here as contextual background for the microbiological and conjugation results described in subsequent sections. Detailed analytical methods and full compound-level results will be reported by our collaborators.

The detected compounds were classified into six functional groups: Pharmaceuticals (non-antibiotic), antibiotics, PPPs, industrial chemicals, PCPs, and disinfectants (Figures 21 and 22). Pharmaceuticals (non-antibiotics) dominated the total cumulative concentration across all sample types (~70%), followed by PPP (~20%) and industrial chemicals (~8%), while antibiotics represented less than 2% of the total load. This composition is broadly consistent with the profile reported for urban WWTP effluents in European river systems, where pharmaceuticals consistently represent the dominant contaminant fraction due to incomplete removal during conventional biological treatment (Chaber-Jarlachowicz et al., 2025; Verlicchi et al., 2012).

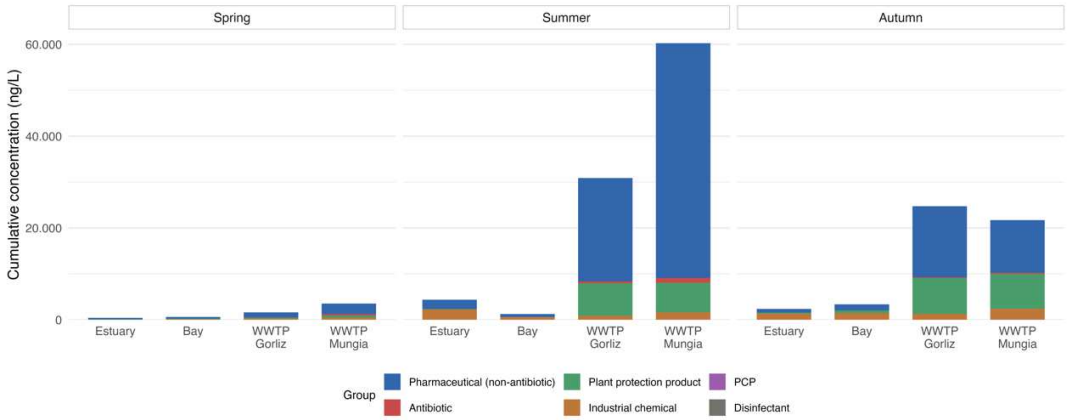

Figure 21. Preliminary data on cumulative concentration of pollutants found in the study area.

Data is divided into three seasons: spring, summer, and winter. The study area comprised four sites: Estuary, Bay and two wastewater treatment plants (WWTPs) Gorliz and Mungia. Sampling Samples corresponded to three seasons: spring, summer, and autumn as in the context of this study. CECs were divided into pharmaceuticals non antibiotics, plant protection products (PPP), PCP (Personal care products), Antibiotics, industrial chemicals, and disinfectants: Source: Preliminary data from Maddi Salvoch Vilches within the collaborative HOBE project by members of the IBeA research team at the University of the Basque Country (EHU).

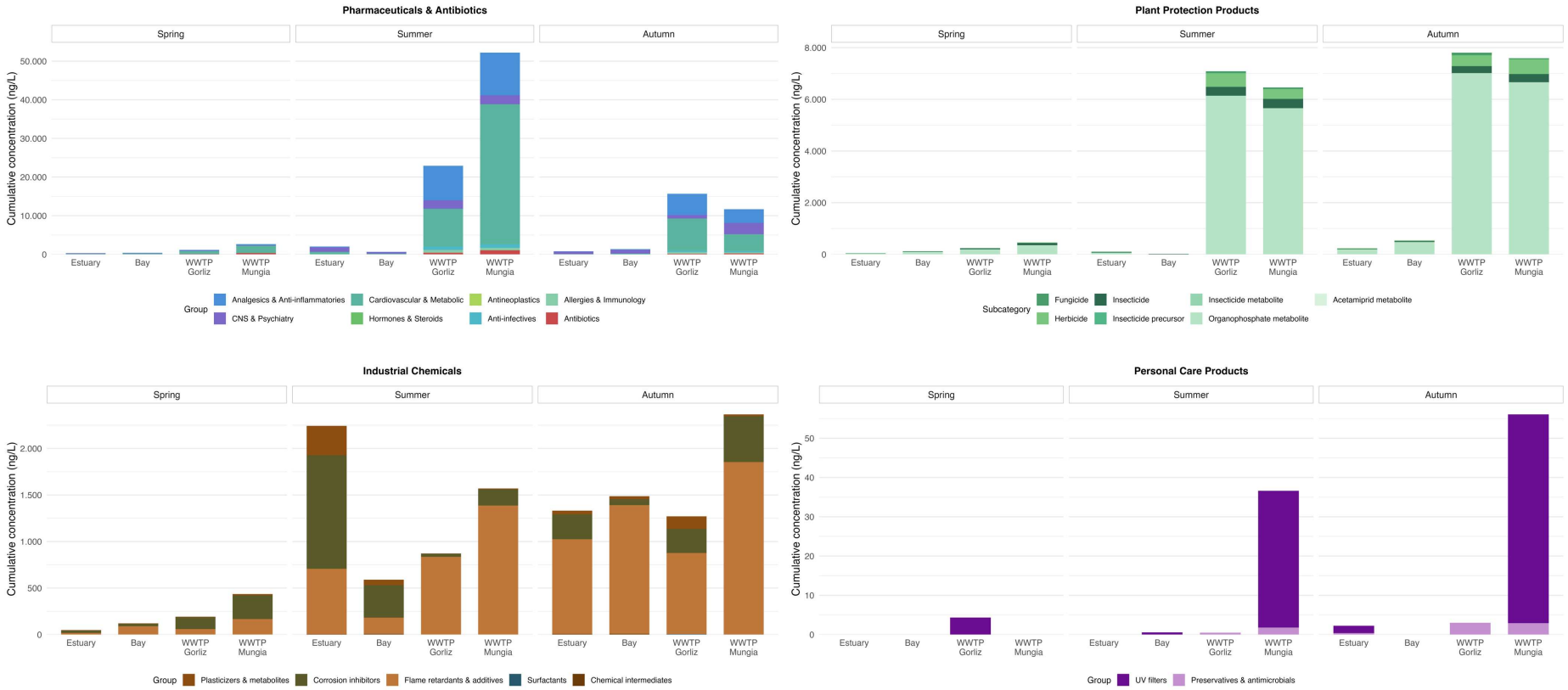

Figure 22. Preliminary detailed grouped data on cumulative concentration of pollutants found in the study area.

The study area comprised four sites: Estuary, Bay and two wastewater treatment plants (WWTPs) Gorliz and Mungia. Sampling corresponded to three seasons: spring, summer, and autumn as in the context of this study. CECs were divided into pharmaceuticals non antibiotics, plant protection products (PPP), PCP (Personal care products), antibiotics, industrial chemicals, and disinfectants. Each group is in addition subdivided into main subgroups defined from the found compounds. Source: Preliminary data from Maddi Salvoch Vilches within the collaborative HOBE project by members of the IBeA research team at the University of the Basque Country (EHU).

Both WWTP effluents showed marked seasonal variation in total contaminant load. Summer was characterized by the highest overall concentrations at both Gorliz and Mungia, with pharmaceutical loads at Mungia exceeding those of Gorliz by more than 2-fold during this period. On the contrary, PPP concentrations were proportionally highest in Autumn (~31–35% of the seasonal total), consistent with post-harvest agricultural activity and increased runoff previously observed in other studies (Schönenberger et al., 2022; Stehle & Schulz, 2015). spring presented the lowest overall contaminant loads at both plants' effluent, with a more stable chemical mixture. Mungia was consistently more concentrated than those of Gorliz across all seasons, likely reflecting differences in catchment profiles.

Two other sites, Estuary, and Bay were sampled to test the hydrological continuum of Mungia's effluent. The release of WWTP effluent into surface water has been considered a main cause of presence of micropollutants in comparison to other sources such as agriculture and industrial point discharges (Luo et al., 2025).

Among the CECs evaluated in Chapter 2, including their known transformation products and metabolites, the majority were detected in at least one sampling campaign, with the notable exception of disinfectants, which were not found in any effluent sample. Detected concentrations ranged from 10^1 to 10^2 ng L^{-1}, approximately one to two orders of magnitude below the exposure concentrations used in the controlled laboratory experiments (10^3 ng L^{-1}), suggesting that the environmental mixtures present in WWTP effluents represent sub-effect concentrations relative to those tested individually *in vitro*. Among the consistently detected compounds, carbamazepine and venlafaxine stood out for their presence across all seasons and both WWTPs (Table 8). This pattern is consistent with their recognized persistence in wastewater-impacted systems: carbamazepine is widely established in the scientific literature as a conservative wastewater tracer due to its ubiquitous occurrence and recalcitrance to conventional treatment (Clara et al., 2004; de Cravalho et al., 2024) while venlafaxine has been flagged for its persistence and ecotoxicological risk through the EU Watch List mechanism (Souza et al., 2022) reflecting similarly low removal efficiencies in WWTPs.

Table 8. Concentrations of selected compounds in WWTP effluents (ng L^{-1}).

	WWTP Gorliz			WWTP Mungia		
	Spring	Summer	Autumn	Spring	Summer	Autumn
Personal Care Products						
Benzophenone-1_neg *(metabolite)*	4.3	0.0	0.0	0.0	25.7	53.2
Pharmaceuticals (non-antibiotic)						
Carbamazepine	1.0	22.3	15.5	4.1	22.6	14.8
Venlafaxine	61.2	6.8	26.9	42.1	6.9	26.9
Plant Protection Products						
Azoxystrobin	0.0	4.7	2.2	0.0	12.2	4.3
Imazalil	0.0	5.2	1.8	0.0	5.2	1.3
Antibiotics						
Sulfamethoxazole	24.9	0.0	0.0	122.8	0.0	81.5
Trimethoprim	0.0	18.7	11.9	3.2	0.0	28.6

Source: Preliminary data provided by the collaborative HOBE project by members of the IBeA research team at the University of the Basque Country (EHU).

Although antibiotics represented a minor fraction of the total chemical load, their inherent antimicrobial activity is relevant as selective pressure for bacterial resistance. SMX and TMP were detected in WWTP effluents at low to mid ng L^{-1} concentrations, within the range typically reported for European WWTP effluents (Sabri et al., 2020; Verlicchi et al., 2012). Regarding SMX and TMP, SMX showed notably higher concentrations at Mungia than at Gorliz, particularly in spring and autumn, while TMP showed a more variable pattern between plants and seasons, suggesting differences in prescription rates or treatment efficiency between catchments. Conventional WWTP processes achieve only partial removal of both compounds resulting in their continuous discharge into receiving waters (Q. Liu et al., 2018). Even at the ng L^{-1} concentrations detected here, sub-inhibitory antibiotic concentrations have been shown to contribute to the maintenance and spread of corresponding resistance genes, including *sul1, sul2, dfrA*, and *dfrB* (Bengtsson-Palme & Larsson, 2016; Gullberg et al., 2011), all of which were detected in the qPCR analysis described in the last section within this chapter.

Bridging *in situ* and laboratory: conjugative transfer potential of WWTP effluent waters

The present results are broadly consistent with the findings of Hutinel et al. (2021) who used filter-sterilized municipal and hospital wastewaters as chemical matrices in conjugation assays with a complex bacterial donor community and a defined *E. coli* recipient, finding no

detectable increase in HGT rates with municipal effluent while hospital wastewater increased the relative proportion of sulfonamide-resistant transconjugants through an effect attributable to the chemical mixture rather than any single measured compound (Figure 23). In the present study, Mungia, a predominantly municipal catchment, showed similarly near-neutral conjugation modulation across all seasons. Meanwhile, Gorliz, which receives hospital effluent via a dedicated pumping station, displayed the most divergent seasonal response, including both the highest induction (Summer) and the strongest inhibition (Autumn) observed in this study. This plant-specific pattern is consistent with the hypothesis that healthcare-associated chemical inputs introduce a qualitatively distinct modulating potential relative to domestic wastewater, even when the hospital contribution represents a minor fraction of the total influent load, as was also the case in the Gothenburg system studied by Hutinel et al. (2021). Importantly, despite higher cumulative contaminant concentrations measured in Mungia, the contaminant mixture characterizing Gorliz appeared to exert a moderate stronger ecological influence.

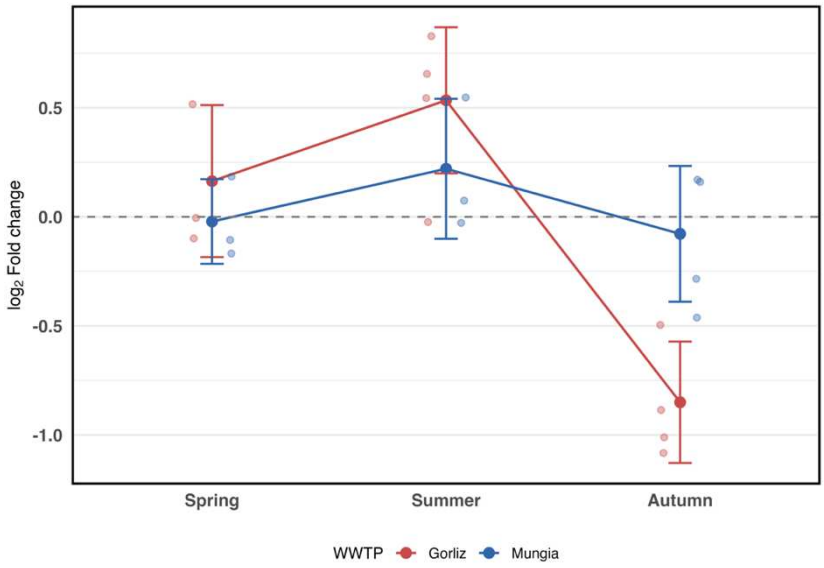

Figure 23. Effect of ellfuent in conjugation across seasons in *E. coli* K12/IncF (donor) and *E. coli* HMS174 (recipient).

Critically, the negative modulation observed during the autumn season was particularly noteworthy. Two compounds were detected exclusively during this sampling campaign in Gorliz : dimethyl phosphate, an organophosphate pesticide metabolite consistent with post-harvest agricultural runoff in the Butroe catchment, and ethyl 4-dimethylaminobenzoate (EDAB), an industrial photoinitiator. While the potential contribution of these compounds to the inhibitory conjugation response cannot be assessed from the current dataset, their exclusive occurrence in the inhibitory condition makes them candidates for further

mechanistic investigation. Neither compound has been previously reported to modulate conjugation frequency. Organophosphates have been shown to interfere with bacterial energy metabolism and induce oxidative stress at sub-lethal concentrations (Nguyen et al., 2020), processes that are known to influence conjugation efficiency. Photoinitiator can generate reactive oxygen species upon activation, potentially inducing oxidative stress in the recipient population (Nguyen et al., 2020). The autumn decline at Gorliz relative to Mungia may additionally reflect the combined effect of increased precipitation and withdrawal of seasonal population pressure associated with summer tourism, two factors that covary in this coastal catchment and cannot be independently resolved from the current dataset. Whether these compounds contributed individually or synergistically to the inhibitory effect cannot be resolved due to the complexity of the environmental mixture and controlled single-compound exposure experiments at environmentally relevant concentrations would be required to establish causality.

It is also important to note that the conjugation assay used here employed laboratory strains carrying an IncF plasmid as the transfer model, whereas the previous chapter demonstrated a differential chemical response between Inc groups, with IncP-1 type replicons showing greater sensitivity to chemical stressors than IncF. This potential plasmid-specific response means that the modest modulation observed here may underestimate the effect that the same effluent matrices would exert on other replicon groups, particularly IncP and IncN plasmids, which are more environmentally prevalent and, in the case of IncN, have been identified as the dominant conjugative elements captured from wastewater communities in filter mating assays (Hutinel et al., 2021).

Taken together, these results demonstrate that real WWTP effluents exert statistically detectable but quantitatively narrow effects on conjugative plasmid transfer frequency, with a seasonal pattern: near neutral in spring, mildly inductive in autumn, and inhibitory at Gorliz in November. These variations cannot be predicted from the chemical composition of the effluent alone. Critically, the overall modulation window observed here (fold-change 0.47–1.78) indicates that the chemical matrix of treated effluents is unlikely to be a primary driver of the ARG burden documented downstream, as conjugation frequencies remained close to baseline even under the most chemically loaded conditions. The characterization of the resistome by qPCR, presented in the following section, provides the microbiological counterpart to these chemical and HGT data under controlled conditions: while the conjugation assays address the potential for chemical modulation of plasmid transfer, the

qPCR profiles document the actual resistome and associated MGEs present in each WWTP and its fate along the receiving hydraulic continuum.

Resistome profiling by quantitative PCR (qPCR)

To profile the resistome across the four sampling sites of this study, 35 genetic markers were quantified by qPCR. The sampling design was structured around two complementary comparisons. First, the two WWTP effluents (Gorliz and Mungia) were compared to evaluate whether catchment characteristics shape effluent resistome composition. Second, given that Mungia discharges into a defined hydraulic continuum (flow from Mungia, Estuary and Bay) whilst Gorliz discharges directly into the marine environment without a connected downstream system, a longitudinal analysis along the Mungia–Estuary–Bay continuum was conducted to assess the influence of WWTP discharge on resistome composition across the coastal gradient.

Sampling was conducted across three seasons (*i.e,* spring, summer, and autumn) to capture temporal variation in ARG abundance and spatial distribution patterns. In addition to a broad panel of ARGs covering nine antibiotic classes (beta-lactams, aminoglycosides, sulfonamides, trimethoprim, tetracyclines, macrolides, quinolones, phenicols, and colistin), MGEs namely integrons (*intI1*), and Inc group plasmid markers (*IncN, IncP, IncQ, IncW, IncF*) were also included in the analysis to assess the potential for HGT. The anthropogenic fecal marker *crAss64* was included as an indicator of human fecal contamination, and the 16S rRNA gene was used for normalization of ARG abundances to total bacterial load. The selection of markers was designed to capture both clinically relevant resistance determinants and the genetic vehicles that facilitate their dissemination in environmental settings. For contextualization, resistance mechanisms, genomic location, associated MGEs, and whether they independently confer resistance or modulate existing resistance phenotypes, are listed in Appendix C, Table C2.

Overall trends

Pairwise Spearman rank correlations between sites were uniformly high (rho=0.69–0.92, all $p<0.0001$), indicating that the relative ranking of gene abundance is broadly conserved across the basin regardless of site or sampling month. The highest correlation was observed between the two WWTP effluents (rho=0.906–0.917), confirming that Mungia and Gorliz export a qualitatively similar resistome suggesting the existence of a conserved core resistome

dominated by class 1 integron-associated genes and broad-host-range MGEs across operationally distinct WWTPs.

Despite this apparent structural homogeneity, Non-metric Multidimensional Scaling (NMDS) representation of Euclidean distances between complete 35-gene resistome profiles (stress=0.048, Figure 24), which captures differences in absolute abundance magnitudes across the full gene panel, revealed a spatial structure that is not apparent from pairwise correlations alone. PERMANOVA confirms that sampling site explained 49.9% of total resistome variation (Location: $F=2.74$, $R^2=0.499$, $p=0.040$). However, the Month factor did not reach significance in any PERMANOVA model ($p>0.35$), likely reflecting limited statistical power with n=4 samples per month. Nonetheless, temporal structure is clearly visible in the NMDS ordination, where estuarine and marine waters separate along a gradient that mirrors hydraulic perturbation: spring samples clustered distinctly from summer and autumn, with autumn occupying overlapping ordination space alongside WWTP samples. We also noted that the site effect was substantially amplified under dry-season baseline conditions (spring-summer: Location $F=4.72$, $R^2=0.774$, $p=0.012$), and was largely attributable to the distinctive position of the Bay, whose exclusion reduced the location effect to marginal significance ($p=0.096$), reflecting the high compositional similarity among the three remaining sites.

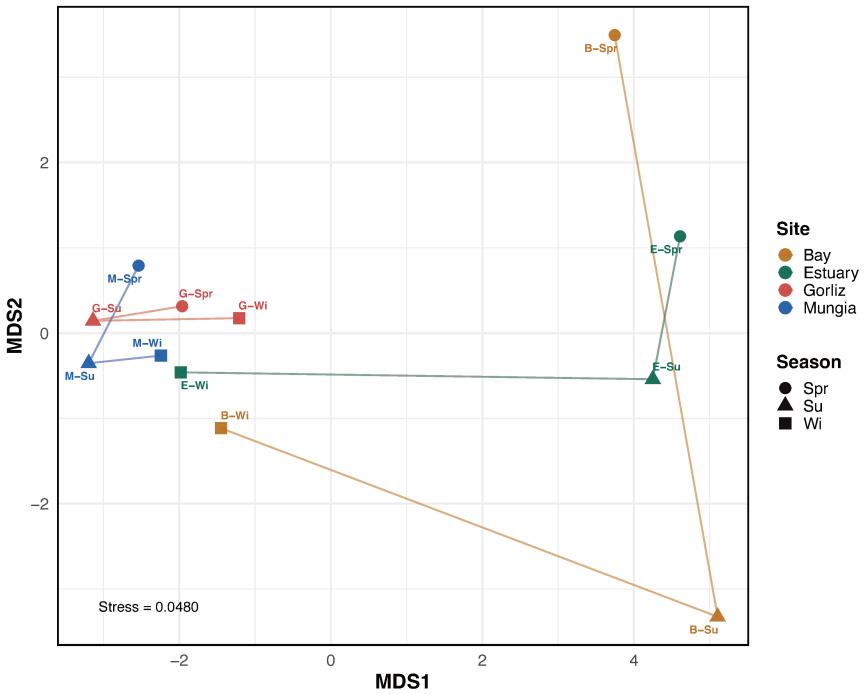

Figure 24. Non-metric Multidimensional Scaling (NMDS) of resistome profiles across sites and seasons

The Bay maintained consistently high Spearman correlations with the Estuary across all sampling months (June/spring: rho=0.885; September/summer: rho=0.937; November/winter: rho=0.882), indicating that both sites share the same relative gene abundance structure throughout the year. However, Euclidean distances between Bay and Estuary profiles ranged from 2.76 in autumn to 4.43 in spring. This seasonal divergence in absolute abundance, greatest under dry-season baseline conditions and minimal during the autumn rainfall event, suggests that Bay maintains site-specific resistome dynamics most evident when, hydrological influence (*i.e.*, precipitation) is lowest.

Hierarchical clustering of log_{10}-normalized abundance profiles across all sites and seasons (Euclidean distance, complete linkage; Figure 25) resolved two gene modules that reappeared consistently across both (i) the inter-WWTP comparison and (ii) the hydraulic continuum analysis. A stable core of 27 genes maintained consistent cluster assignment regardless of whether clustering was performed on the WWTP comparison dataset (Gorliz and Mungia), the hydraulic continuum dataset (Mungia, Estuary and Bay), or the full dataset, designated hereafter as Category 1 (major contributors; n=7 genes) and Category 2 (minor contributors; n=20 genes) based on relative abundance. The remaining 8 genes —*IncP_oriT, aadA_1, aac(6')-Ib_1, aph3-ib, bacA, bla*$_{OXA-48}$*, mcr1, and sul2_2*— showed context-dependent cluster assignment and are discussed separately in the site-specific analyses below.

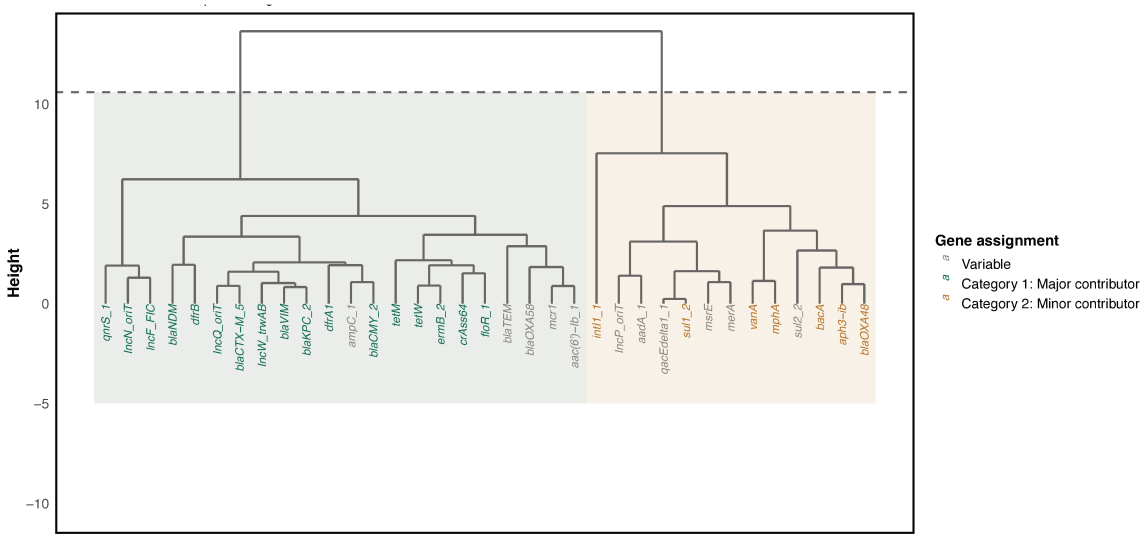

Figure 25. Hierarchical clustering of ARGs and MGE genes across all sampling sites and seasons.
Dendrogram based on Euclidean distance between log_{10}-normalized abundance profiles computed across all sites and month combinations. Clustering was performed using complete linkage. The dashed horizontal line indicates the cut height corresponding to k=2 clusters. Gene labels are colored according to their category assignment

stability across three independent analytical contexts (WWTP comparison, hydraulic continuum, and global dataset): green, Category 2; yellow, Category 1; grey, genes with context-dependent cluster assignment.

The Category 1 (*intI1_1*, *sul1_2*, *qacEΔ1_1*, *merA*, *mphA*, *msrE*, and *vanA*) was characterized by uniformly high abundances across all sites and months, maintaining stable profiles independently of site identity, hydrological state, or distance from WWTP discharge points (Figure 26). This is likely a direct reflection of the conserved architecture of class 1 integrons: *sul1* and *qacEΔ1* are constitutive components of the 3' conserved segment (3'-CS) present in virtually all class 1 integron variants (Stokes & Hall, 1989), with *qacEΔ1* likely representing a co-selected marker rather than an independently selected resistance determinant Gene. *merA* is physically co-located on transposon Tn21, where the mercury resistance operon is linked to the integron backbone (Liebert et al., 1999). The three remaining Category 1 genes (*mphA*, *msrE*, and *vanA*) share the high-abundance, site-independent distribution of the integron-associated core. They are likely maintained by sustained selective pressure in concordance with chemical context and stable broad-host-range plasmid carriage.

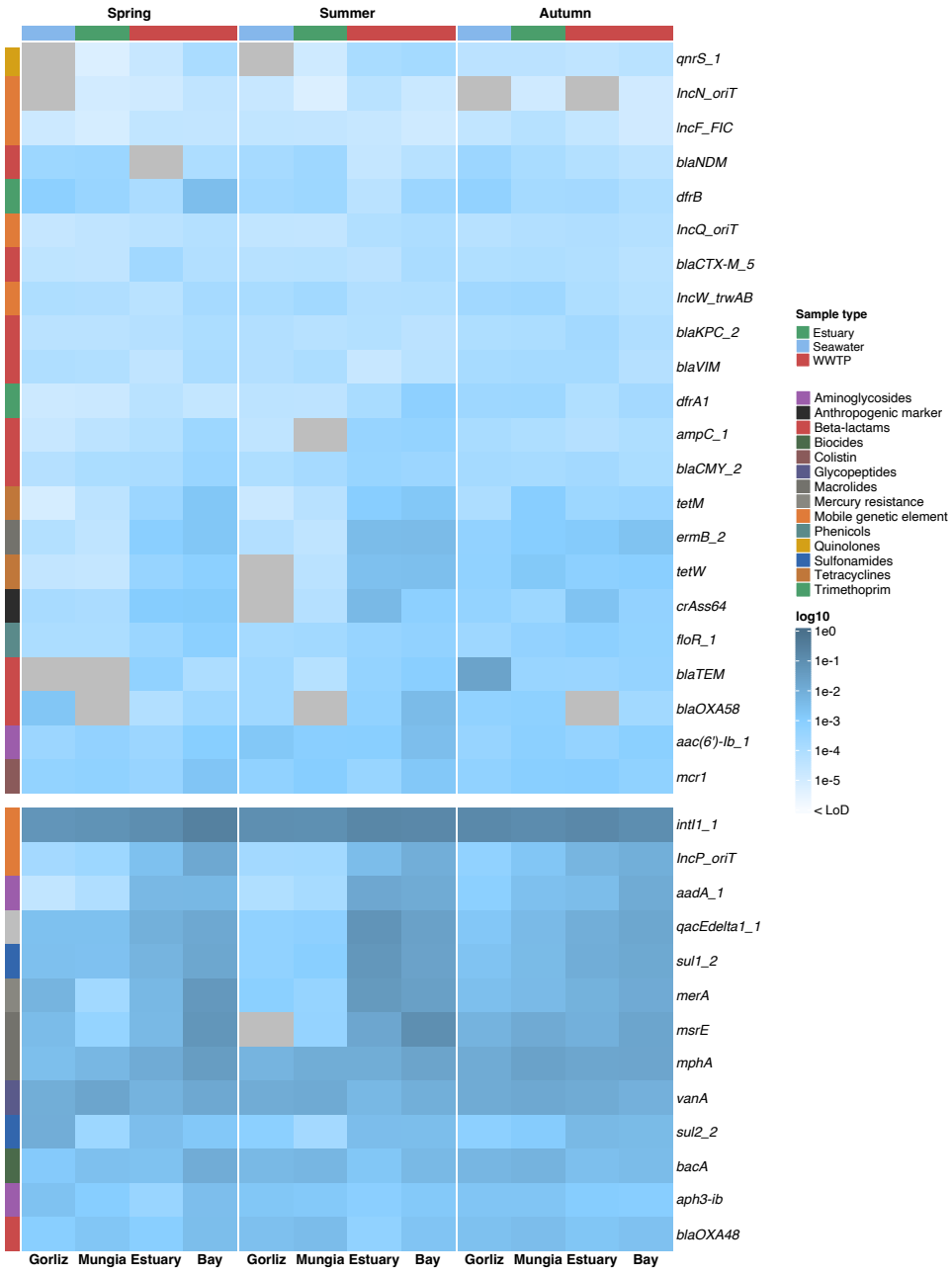

Figure 26. Heatmap of ARG, MGE and anthropogenic markers' abundance across sampling sites and seasons. Log_{10}-transformed abundances normalized to 16S rRNA gene copy numbers. Genes (rows) were clustered using hierarchical clustering (Euclidean distance, complete linkage) and grouped into two categories (k=2), separated by a horizontal gap. The lateral color bar indicates the antibiotic resistance category of each gene. Columns are grouped by season (vertical gaps) and ordered by sample type within each season: Gorliz, Mungia, Estuary and Bay.

The chemical profiling of WWTP effluents revealed a high temporal variation, with no single compound being consistently detected across all sampling campaigns at both plants. The observed variation in contaminant levels contrasts with the stable, high-abundance profiles of Category 1 genes across all months, reinforcing the interpretation that the

integron-associated core reflects the cumulative microbiological record of long-term selective exposure rather than a snapshot of the selective pressures exerted by the chemical environment at the moment of sampling.

Of interest, the detection of macrolides (azithromycin and clarithromycin) and sulfonamides in both WWTPs in at least two sampling campaigns correlated with the abundance of the specific determinants conferring resistance for these antibiotics (macrolides: *mpha, ermB;* sulfonamides*: sul1, sul2)*. Beyond antibiotics, a broad range of CECs detected in these effluents may contribute to co-selection of resistance through cross-resistance mechanisms, efflux pump upregulation, or oxidative stress responses at the sub-inhibitory concentrations present in environmental matrices (Mutuku et al., 2022).

(i) Comparative resistome profiling of Mungia and Gorliz WWTPs

The Gorliz and Mungia WWTP effluents, despite their geographical proximity within the Butroe river basin, differ substantially in catchment, treatment technology, and effluent discharge strategy (Appendix C, Table C1). At the global level, hierarchical clustering of qPCR-derived ARG and MGE abundance profiles revealed a broadly similar resistome composition between both facilities, statistically confirmed by pairwise Spearman correlation (rho>0.9, p<0.0001) and PERMANOVA restricted to the two plants (Location: $F=2.04$, $R^2=0.279$, $p=0.183$), indicating that Mungia and Gorliz are not distinguishable as point sources based on their overall resistome profiles.

The WWTP Category 1 (n=9 genes*: intI1_1, sul1_2, qacEdΔ1_1, aadA_1, merA, vanA, mphA, msrE, IncP_oriT*) were detected at high and relatively uniform abundances in both plants across all sampling months, confirming the treatment-resistant character of the integron-associated core established in the overall analysis. The persistence of *intI1_1* and its 3'-CS-associated markers at comparable abundance levels between Mungia and Gorliz is notable given that Mungia operates UV disinfection whereas Gorliz does not, suggesting that integron-bearing bacterial populations are not efficiently eliminated at the UV doses applied, consistent with previous reports showing limited removal of class 1 integron markers by conventional treatment including UV disinfection (Ma et al., 2011; Zhuang et al., 2015).

Despite this global similarity, differential analysis revealed marked quantitative differences between plants that were strongly modulated by hydrological state (Figure 27). The maximum effect was observed in spring, representing dry-season baseline conditions with minimum antecedent precipitation (7.4 mm/7d). Mungia showed higher abundances for 22 of 35 markers, including heavy metal and disinfectant resistance genes (*merA*, *bacA*), broad-host-range replicons (*IncP_oriT*, *IncW_trwAB*), and multiple beta-lactamase genes (bla_{OXA-48}, bla_{CMY}, bla_{OXA-58},). This pattern is consistent with the higher overall CEC load documented at Mungia during spring and summer alongside its industrial catchment and potential inputs of heavy metal and biocide co-contaminants reflected in the detection of corrosion inhibitors and plasticizer metabolites in its effluent chemical profile. Nonetheless, as discussed in the overall section, these differences more likely reflect the cumulative microbiological record of long-term catchment-specific selective pressure rather than the short-term chemical environment since the overall CEC load increased during summer campaign while the number of genes more abundant at Mungia decreased to 12. By autumn only 3 genes remained higher at Mungia while 27 of 35 markers were statistically similar between plants. This progressive convergence of resistome profiles with increasing precipitation is consistent with the hydrological homogenization effect identified in the NMDS analysis, whereby rainfall-driven inputs from diffuse sources reduce the relative contribution of each plant's catchment-specific signature to the overall effluent resistome.

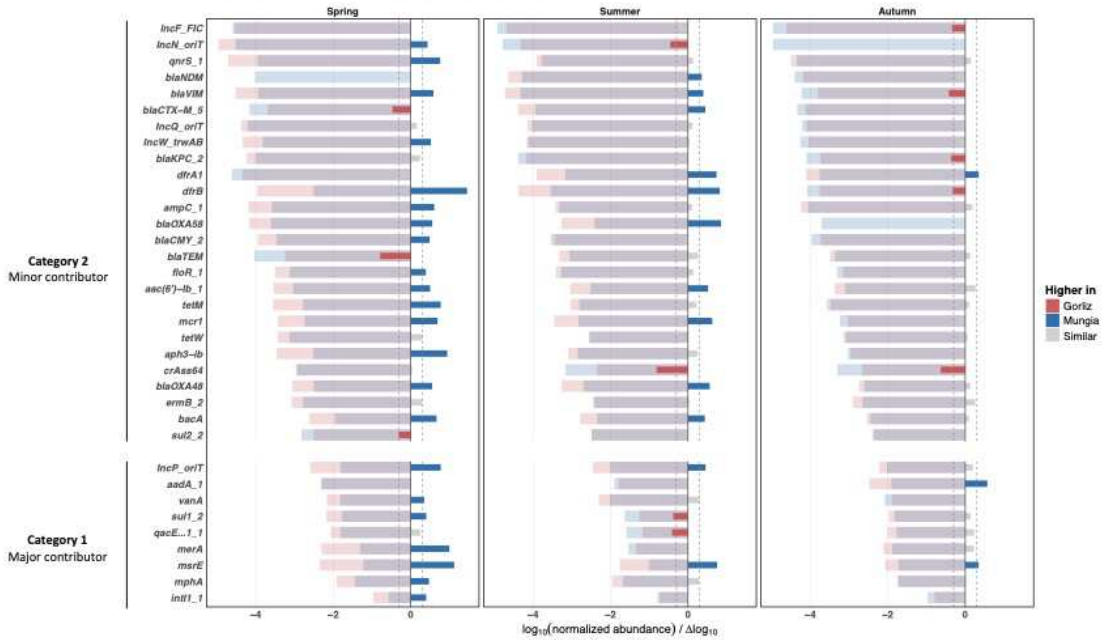

Figure 27. Differential ARG and MGE normalized abundance between Mungia (blue) and Gorliz (red) WWTP effluent across three hydrological sampling campaigns.

The only marker consistently higher at Gorliz was *crAss64*, a crAssphage-derived marker of human fecal contamination (Karkman et al., 2019), showing notably elevated abundances in summer and autumn ($\Delta\log_{10}$=−0.81 and −0.63 respectively), consistent with the seasonal tourist population served by Gorliz whose peak summer presence generates an elevated fecal load along with precipitation events. In autumn, bla_{VIM} and bla_{KPC} were marginally higher at Gorliz ($\Delta\log_{10}$=−0.42 and −0.36 respectively). Their co-clustering with *IncQ_oriT* and *IncW_trwAB* replicons in the hierarchical clustering is consistent with a clinical plasmid input. Nonetheless, the hospital catchment contribution hypothesis cannot be confirmed by the qPCR data alone.

Taken together, the WWTP comparison reveals that both plants release to the environment a qualitatively similar resistome dominated by the integron-associated Category 1, but that quantitative differences (greatest under dry-season baseline conditions and progressively attenuated by precipitation) reflect catchment-specific selective histories: industrial co-contaminants at Mungia driving enrichment of co-resistance and broad-host-range replicon markers, and a higher seasonal fecal load at Gorliz driven by tourism and cumulative precipitation. The detection of carbapenemase resistance genes at both plants, while at low levels of abundance, underscores their role as sources of ARG determinants of clinical concern to the environment.

(ii) ARG and MGE occurrence along the hydraulic continuum and hydrological drivers of resistome variability

Having established the catchment-specific resistome profiles of each WWTP, we next examined the influence of Mungia on the resistome of the downstream receiving environment, sampled at Estuary and Bay. The two gene categories identified in the WWTP comparison recurred consistently in the hydraulic continuum analysis, with 85.7% of genes (30/35) assigned to the same category regardless of analytical context (Figure 28).

The Category 1 (n=10) exhibited consistently high levels of abundance across all sites ($\log_{10}$>−2 at all sampling points). However, it showed some spatial variation. Several genes, such as *merA* and *msrE*, showed Mixed (V-shape) spatial patterns in spring, declining from Mungia to the Estuary but recovering at Bay (Figure 28). This recovery at Bay is not necessarily attributable to additional point-source inputs but could also reflect the distinct marine ecology of the Bay environment: a coastal microbial community with its own sedimentary reservoirs, and community composition that maintains these genes independently of WWTP discharge. The defining characteristic of the Category 1 is therefore its temporal stability and consistently

high abundance floor rather than spatial homogeneity along the hydraulic continuum. This site-independence abundance is again mechanistically consistent with the classic of integron–Tn21 structural backbone, that can be maintained by non-antibiotic co-selective agents (Liebert et al., 1999).

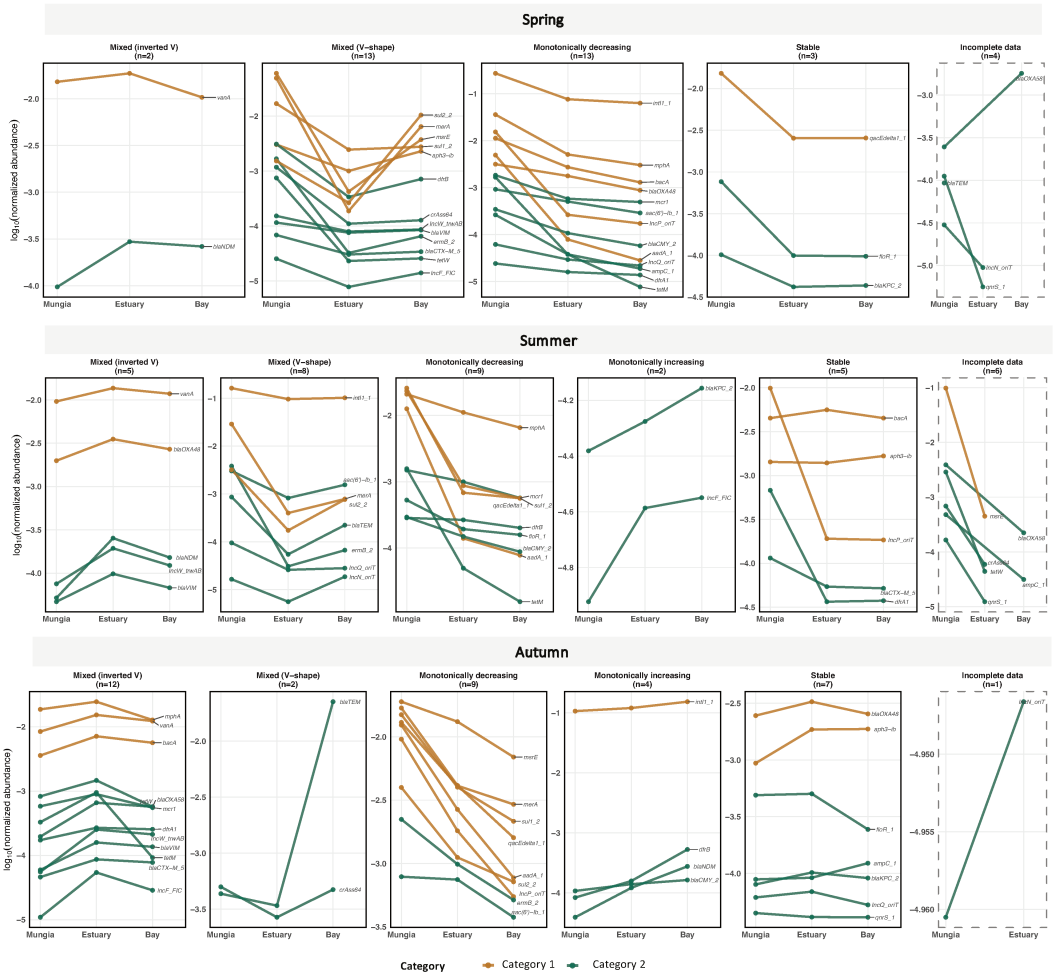

Figure 28. Spatial distribution patterns along the hydraulic continuum Mungia-Estuary-Bay.
Log_{10}-transformed abundances normalized to 16S rRNA gene copy numbers are shown for each sampling season (Spring, Summer, and Autumn). Genes are colored by category: major (orange) and minor contributors (green). A gene was classified as monotonically decreasing or increasing if abundance changed consistently in one direction between all three consecutive sites, with a minimum difference of 5% between each pair; mixed (V-shape); and mixed (inverted V) patterns were assigned when the intermediate site (Estuary) showed the lowest or highest abundance, respectively, exceeding the 5% threshold. Genes were classified as stable when the total range of variation across all three sites was below 0.15 log_{10} units. Genes for which data were not complete at one or more sites are shown separately (incomplete data, dashed panel).

The Category 2 (n=25 genes) displayed a general trend of decreasing abundance from Mungia through the Estuary across spring (n=19) and summer (n=13) sampling campaigns, consistent with a dilution effect (Figure 28). However, again, Bay abundance levels did not

consistently follow this gradient: several genes showed values comparable to or exceeding those of Estuary or even Mungia, establishing Bay as a compositionally distinct coastal node rather than a distal dilution endpoint. This was confirmed by the multivariate analyses described in the overall section. Among the genes that showed pronounced Bay-specific elevation in November were *dfrB* and bla_{TEM} ($\Delta\log_{10}$=+1.82 relative to Estuary), consistent with potential episodic resuspension of contaminated coastal sediments or other diffuse sources as the primary drivers of Bay resistome variability during high-precipitation events. Of note, bla_{NDM} remained consistently higher in the Bay than in the Estuary across all seasons, even exceeding the abundance levels detected in any of the WWTP effluents. The New Delhi metallo-β-lactamase gene (bla_{NDM}) is of major clinical concern, and its dissemination has been widely linked to ISs facilitating its mobility across diverse bacterial taxa (Che et al., 2021). This pattern cannot be attributed to drainage from either point source suggesting that Bay harbors an independent reservoir of bla_{NDM}-carrying bacteria, potentially established in coastal sediments through historical accumulation from multiple diffuse inputs including maritime traffic, recreational bathing, and submarine outfall discharge, or that bla_{NDM} has been acquired by autochthonous marine bacteria through HGT, as documented in coastal environments (Dewi et al., 2020). Romero et al. hypothesized that bla_{NDM} may be maintained via co-selection driven by naturally occurring bleomycin-like molecules. The detection of a carbapenemase of high clinical concern at abundances exceeding those of the most probable point sources in coastal bathing waters warrants targeted surveillance beyond the scope of conventional WWTP monitoring programs.

Permutation testing formally confirmed that Mungia is a significantly stronger predictor of estuarine resistome dynamics than Gorliz under baseline hydrological conditions (spring-summer: rho_diff=0.089, p=0.035, n=9,999 permutations), while this differential was undetectable when autumn was included (rho_diff=0.010, p=0.730). Category-specific tests showed the hydraulic continuum signal concentrated in the Category 2 ((rho_diff=0.153, p=0.088), while the Category 1 showed a consistent inverse pattern (rho_diff=−0.235, p=0.300) with Gorliz being the marginally better predictor for the major integron-associated category. This is consistent with its slightly higher abundances of these markers and the distinct marine ecology of Bay maintaining Category 1 genes through mechanisms independent of either WWTP. The signal did not extend significantly to Bay (spring–summer: rho_diff=0.072, p=0.123), consistent with progressive attenuation of the Mungia influence beyond the estuarine mixing zone and the independent resistome dynamics of the open coastal environment.

The autumn sampling introduced additional complexity, warranting cautious interpretation. Unusually high ARG abundances were observed at the Bay station for several minor Category 2 genes, most notably *bla*$_{TEM}$ (Δlog_{10}=+1.82 relative to Estuary autumn; Figure 28). Notably, gene pattern dynamics shifted markedly from spring to autumn: the number of genes showing increased detection in the Bay rose from 1 to 8, while the stable pattern category tripled, increasing from 4 to 14 classified genes. This rainfall-driven homogenization effect, formally demonstrated by the collapse of the Mungia–Estuary permutation test significance upon inclusion of autumn data (p=0.730), underscores the fundamental limitation of point-in-time sampling strategies for resistome surveillance in open coastal systems and the necessity of integrating hydrological event monitoring into sampling design.

Taken together, the qPCR profiles and multivariate analyses along the Mungia–Estuary–Bay continuum support a two-component model of resistome structuring: an integron–Tn21-anchored core resistome Category 1, and a variable enteric ARG Category 2. The Category 1 is characterized by temporal stability and a consistently high abundance baseline. This category is likely maintained by habitat-specific ecological constraints and selective pressures and represents a major contributor to the HGT of ARGs among bacteria in the environment (Alexander et al., 2020). The enteric ARG Category 2, on the other hand exhibits spatial dynamics driven by point-source hydraulic connectivity from Mungia under baseline conditions and is further reshaped by precipitation-driven mobilization from terrestrial and sedimentary reservoirs. Finally, the consistent detection of clinically relevant ARGs (albeit at low levels of abundance) across estuarine and marine samples suggests the presence of a stable environmental background reservoir, indicating that distinct environments within the same coastal continuum can harbor a shared, persistent resistome fraction.

CHAPTER 4

Characterization of the Mobilizable Plasmidome of a Wastewater-Impacted River Basin: Diversity, Resistance Gene Content and Evolutionary Relationships

The environmental and microbiological characterization of the Butroe river basin presented in Chapter 3 revealed a complex and seasonally variable chemical landscape in the effluents of Gorliz and Mungia WWTPs, alongside a stable resistome dominated by integron-associated genes consistent with sustained anthropogenic selective pressure. These findings establish the context within which plasmid communities develop and circulate in this system and motivate a direct characterization of the mobilizable plasmid pool that this selective landscape shape.

The plasmidome, broadly defined as the overall plasmid content of a microbial community (Norman et al., 2009), encompasses all extrachromosomal replicons regardless of their transfer capacity. Here, we focus specifically on the transferable plasmidome *(i.e.,* the fraction accessible by exogenous plasmid capture mating assays) which represents an epidemiologically key subset of plasmids capable of mediating HGT between environmental and clinical bacterial populations. Plasmids recovered from WWTP-associated environments

have been shown to carry resistance genes of direct clinical relevance on variable Inc group backbones also found in clinical settings, demonstrating the intertwined ecology of plasmids across human and environmental niches (Burgess et al., 2022). Pangenome analysis of plasmid clusters from human bloodstream infections, livestock, and wastewater treatment works revealed shared backbone structures carrying diverse ARGs, with many plasmid backbones detected across species and niches, suggesting a highly dynamic movement of plasmids at greater rates than previously estimated (Matlock et al., 2023).

Characterizing this mobilizable fraction presents inherent methodological trade-offs. Culture-independent metagenomic approaches provide broad coverage but face limitations: chromosomal DNA contamination complicates analysis, assembly of large elements is challenging, and amplification protocols favor small circular elements, underrepresenting large conjugative plasmids (Dib et al., 2015). Culture-based conjugation capture, while biased towards elements transferable to laboratory strains under defined conditions, uniquely recovers complete, active plasmid sequences that can be fully characterized for genetic content, mobility functions and evolutionary relationships. In this study, combination of trimethoprim (TMP) with sulfamethoxazole (SMX) and azithromycin (AZI) were used as capture selecting antibiotics to ensure that the recovered plasmidome is directly relevant to the chemical selective landscape of the sampling sites.

To our knowledge, this chapter presents the first comprehensive culture-based assessment of the mobilizable plasmidome of a complete WWTP-impacted river basin in the Basque Country, integrating two WWTPs with contrasting catchment characteristics —Gorliz (coastal, mixed urban-hospital inputs and seasonal population pressure associated with summer tourism) and Mungia (inland, mixed urban-agricultural catchment)— and their associated estuarine and bay receiving waters. Plasmid diversity, resistance gene content, mobility classification and evolutionary relationships are analyzed within the chemical and microbiological context established in Chapter 3, providing an integrated empirical foundation for understanding how conjugative plasmid communities are shaped by the complex chemical environments characteristic of WWTP-impacted systems.

Objectives

i. To characterize the diversity and general genomic features of the mobilizable plasmidome recovered from WWTP effluents and receiving waters of the Butroe river basin, including plasmid size, topology, mobility classification and replicon typing.

ii. To assess inter-plasmid relatedness and define discrete plasmid entities across sampling sites and seasons, evaluating the spatial distribution and connectivity of plasmid populations within the river basin.

iii. To determine the antimicrobial resistance genes (ARGs) content of the recovered plasmids and evaluate the clinical relevance of the resistance determinants identified.

iv. To reconstruct the evolutionary relationships of the recovered plasmids through relaxase phylogeny, assessing the relative contribution of environmental and clinical plasmid lineages to the mobilizable plasmidome and evaluating the plasmid network structure across sampling sites along the hydraulic continuum.

v. To characterize the broader mobile genetic element landscape associated with the recovered plasmids, including insertion sequences, integrons and other accessory elements contributing to ARG mobilization.

vi. To contextualize the recovered plasmidome within the selective pressure landscape, evaluating whether plasmid diversity, ARGs content and replicon distribution reflect the cumulative catchment-specific selective histories of the two contrasting WWTPs.

Material & Methods

Sampling sites, sampling strategy, and sample processing were as described in Chapter 3. Briefly, water samples were collected from two WWTP effluents (Gorliz and Mungia) and the receiving environments estuary of Plentzia (namely Estuary) and the Plentzia coastal waters of the Bay of Biscay (namely Bay), at four time points across 2024: March, June, September, and November, representing winter, spring, summer, and autumn conditions, respectively. Samples were collected and processed within 24 h of collection. The present chapter focuses on the characterization of the mobilizable plasmidome recovered from these samples through exogenous plasmid capture and subsequent genomic analysis, as described below.

Bacteria and culture conditions

E. coli BW25113 constitutively expressing GFP (gifted by Prof. K. Smalla) was used as the recipient strain. This strain carries chromosomal resistance to kanamycin (50 µg mL^{-1}) and rifampicin (50 µg mL^{-1}), which allowed its selective recovery from mixed mating cultures. The donor community consisted of the total bacterial community present in water samples collected at each sampling point. To prepare the donor community, Hutinel et al. (2021) method was used with modifications. Briefly, immediately after water filtration, cellulose membranes were transferred to 50 mL falcon tubes containing glass beads (5 mm diameter) and vortexed for 10 min to mechanically detach environmental bacteria retained on the membrane surface. The resulting suspension was transferred into a new tube and centrifugated at 2700 x g for 15 min at 4°C. The supernatant was discarded, and the pellet was washed twice with phosphate-buffered saline (PBS, pH 7.4) by centrifugation at 2700 x g for 10 min and resuspended into a final volume 1.2 mL of PBS. An aliquot of 200 µL were used immediately for plasmid capture experiments and the remaining volume was divided into 100 µL aliquots supplemented with sterilized glycerol to a final concentration of 0.2% (v/v) and stored at -80°C.

The recipient strain and the environmental donor community were each cultured *ON* in LB at 30°C with orbital shaking at 220 rpm. Cells were harvested by centrifugation (6,000 × g, 4 min) and washed once with PBS (pH 7.4) and resuspended in the same buffer before use.

Exogenous plasmid capture assay and transconjugant isolation

The recipient strain (*E. coli* BW25113 *gfp*-tagged) was adjusted to OD_{600}=0.5 (~10^8 cells mL^{-1}) and mixed with the environmental donor community in a 1:1 (v/v) ratio. Filter mating

was performed by depositing the mixture onto 0.22 µm cellulose nitrate membranes placed on LB agar plates and incubating at 30°C for 4 h to allow conjugative transfer.

Following incubation, membranes were resuspended in PBS and appropriate dilutions were plated onto CHROMaga MH Orientation (CHROMagar Microbiology, France) plates supplemented with rifampicin (50 µg mL^{-1}) and one of the following selective capture antibiotics: trimethoprim:sulfamethoxazole (TMP:SMX, 2:18 µg mL^{-1}) or azithromycin (AZI, 12 µg mL^{-1}). These selective conditions allowed the recovery of transconjugants that had acquired conjugative plasmids from the environmental donor community. Putative transconjugants were further confirmed by GFP fluorescence screening under blue light illumination, exploiting the constitutive GFP expression of *E. coli* BW25113 to distinguish true transconjugants from donor colonies with intrinsic rifampicin resistance.

Selection of unique transconjugants

For each conjugation experiment, up to four transconjugant colonies were randomly picked from exogenous plasmid capture assay under blue light illumination (Appendix D, Figure D1). Each transconjugant was inoculated into LB supplemented with selective media containing rifampicin and capture antibiotics (*i.e.,* TMP:SMX or AZI) and stored in 20% (v/v) glycerol -80°C.

Antimicrobial susceptibility test

Antimicrobial susceptibility of isolated transconjugants was determined by disc diffusion according to the European Committee on Antimicrobial Susceptibility Testing (EUCAST) guidelines (Matuschek et al., 2014). Briefly, glycerol isolated transconjugants were grown *ON*. Cultures were diluted to an OD_{600}=0.1 in PBS (pH=7.4) and spread with a UV sterilized cotton swab onto Muller Hinton (MH) agar plates. After 15-30 min, a battery of 16 antibiotic discs (DISMED) was placed onto the plate. Assessed antibiotics included: quinolones (nalidixic acid 30 µg, ciprofloxacin 5 µg), macrolides (clarithromycin 15 µg), aminoglycosides (kanamycin 30 µg, streptomycin 10 µg, and gentamycin 10 µg), tetracyclines (tetracycline 30 µg), sulfonamides (sulfadiazine 300 µg), beta-lactamases (amoxicillin 25µg, ampicillin 10 µg, meropenem 10 µg, cefotaxime 30 µg), phenicols (chloramphenicol 30 µg), TMP 5 µg and polymyxins (colistin sulfate 10 µg, polymyxin B 300 international units). After 20 h, inhibition diameters were measured in millimeters and classified as susceptible (S), intermediate (I) or resistant (R) using EUCAST clinical breakpoints for Enterobacterales (v16.0, 2026) if data was available. TMP, sulfadiazine, and clarithromycin were excluded from statistical analyses as

transconjugants were selected on TMP:SMX or AZI-containing media, precluding meaningful interpretation of resistance to these compounds as an independent phenotype.

Transconjugant restriction profiling and sequencing

To avoid redundant sequencing of duplicate transconjugants, all isolates were subjected to plasmid restriction digest profiling prior to sequencing. Briefly, plasmid DNA was extracted from each transconjugant using the GeneJET Plasmid Miniprep Kit (Thermo Fisher Scientific) following the manufacturer's instructions. Purified DNA was digested with three restriction endonucleases (*i.e.,* EcoRI, NdeI and KpnI) and the resulting restriction fragments were resolved by agarose gel electrophoresis (0.8% w/v) at constant voltage. Restriction patterns were compared visually, and only isolates displaying unique restriction patterns were retained for downstream sequencing (Appendix D, Figure D2). When two or more isolates shared an identical restriction pattern, a single representative was selected for sequencing.

The sequencing strategy was determined based on the estimated complexity of the plasmid content of each transconjugant. Isolates suspected to carry a single plasmid inferred from the agarose gel were subjected to plasmid DNA extraction using GeneJET Plasmid Midi kit (Thermo Fisher Scientific). Isolates whose restriction profiles suggested the presence of more than one plasmid were subjected to whole genomic DNA extraction using E.Z.N.A bacterial DNA kit (omega, bio-tek). Both purified DNA samples were prepared and submitted to Eurofins Genomics for long-read sequencing using Oxford Nanopore Technology (ONT).

Genome assembling, annotation and definition of plasmid entities

Assembly of ONT reads was performed using Flye v2.9.6-b1802 (Kolmogorov et al., 2019) or combined assemblers following autocycler methods (Wick et al., 2025). Parameters used were modified to size 500 k as reference genome. Bandage (v0.9.0) visualization program was used to manually assess circularized assembled plasmids (Wick et al., 2015).

To further assess sequence-level redundancy across experiments, sampling sites and timepoints, pairwise genomic distances between all plasmid sequences were estimated using MinHash-based Average Similarity of Hashes (Mash v2.3). Plasmid pairs with a Mash distance <0.001 (corresponding to ≥99.9% average nucleotide identity) were considered to represent the same plasmid entity and were grouped into clonal clusters (CCs) using single-linkage clustering via connected components analysis in igraph (v1.3.5).

Annotation and definition of plasmid entities

Annotation

Prior to comparative genomic analysis, plasmid sequences were reoriented to a common start point using DNAapler v1.3.0, using the *repA* replication initiation gene as the primary anchor. For sequences where *repA* was not detected, DNAapler was run sequentially with -all mode (testing *dnaA, repA*, and *terL*) and, if unsuccessful, with the nearest mode, which orients the sequence to begin at the first coding sequence predicted by Pyrodigal v3.7.1. Reoriented plasmid sequences were annotated using Bakta v1.11.4 (Schwengers et al., 2021) with the full database (v6.0), which provides structural and functional annotation including CDS prediction, non-coding RNA detection, and assignment of gene names and product descriptions based on UniProt, RefSeq, and PGAP references.

Antimicrobial resistance genes were identified using AMRFinderPlus v4.2.7 with the NCBI AMR reference database (2026-01-21.1), applying default identity and coverage thresholds. Replicon typing and plasmid mobility classification were performed using MOB-typer v3.1.9, which assigns Inc group, relaxase type (MOB family), and predicted mobility class (conjugative, mobilizable, or non-mobilizable) based on the MOB-suite database. Insertion sequences were identified and classified using tool mefinder v1.1.2, and the number and family of IS elements per plasmid were recorded. Integrons and associated gene cassettes were detected using IntegronFinder v2.0.2 (Néron et al., 2022) with default parameters; the number of integrons, integron type, and cassette gene content were extracted for each plasmid. Mobile element annotation was additionally complemented by manual inspection of Bakta-annotated products for transposase, integrase, and recombinase functions.

Functional annotation with eggNOG-mapper

Functional annotation of assembled plasmids was performed using eggNOG-mapper v2.1.13 in protein mode (–itype proteins) against a locally installed eggNOG database (v5.0). Input sequences were the predicted protein FASTA files (.faa) generated by Bakta. Taxonomic scope was set to automatic with non-electronic Gene Ontology evidence targeting all orthologues with a seed ortholog e-value threshold of 0.001. Cluster of orthologous groups (COG) functional categories were assigned and grouped into eight broad functional modules for visualization: Unknown function (S), Mobilome & replication (L), Intracellular trafficking (U), Metabolism (C/E/F/G/H/I/P/Q), Regulation (K/T), Cellular processes (D/M/N/O/W/Z), Defense/Resistance (V), and Information storage (J/A/B).

Definition of cargo and backbone genes

Plasmid cargo genes were defined as the sum of non-structural genetic elements predicted to confer adaptive functions to the bacterial host, comprising ARGs identified by AMRFinderPlus, IS identified by MElements, and integron-associated gene cassettes identified by IntegronFinder. Genes encoding plasmid replication, maintenance, transfer, and stability functions were considered part of the plasmid backbone and were excluded from cargo gene counts (San Millan & MacLean, 2017).

Clonal cluster (CC) alignment and intra-cluster variability assessment

Members of each CC were compared to assess genomic inter-cluster genomic variation. To assess intra-cluster genomic variation, multiple sequence alignments were performed with MAFFT v7.526 (–auto –adjustdirection) for each CC. Variable sites including SNPs and indels were extracted from the resulting multiple sequence alignments using *snp*-sites with CDS coordinates from Bakta annotation. When considered, CCs were divided and classified into subclusters and included in posterior analysis as a separate entity. For all comparative analyses, a single representative sequence per CC was retained. In case the number of CDS was variable, the sequence with the highest number of annotated CDS was used as representative.

Whole-genome alignment and chromosomal insertion detection

To identify chromosomal insertions acquired by *E. coli* BW25113 transconjugants during the conjugation experiments, whole-genome assemblies of putative insertion-carrying strains were compared against a reference genome assembled from a non-insertion control strain using number v4.0 (MUMmer4 package). Pairwise alignments were performed with default parameters and alignment differences were characterized using dnadiff, which reports insertions, deletions, and rearrangements relative to the reference. Insertion coordinates were extracted using show-diff and show-coords with a minimum identity threshold of 95%. Inserted regions were annotated using Bakta v1.9 with the full database, and prophage elements within insertions were additionally characterized using PHASTEST (PHAge Search Tool Enhanced System) to classify phage completeness and identify structural and functional genes.

Phylogenetic analysis

To investigate phylogenetic relationships among plasmids, the relaxase aminoacidic sequence was investigated due to its presence in many of the sequences tested and their homology and conservation (Garcillán-Barcia et al., 2009). Sequences were divided into two

major relaxase groups: MOBP and MOBF based on Mob-suite annotations together with Bakta annotations identifying CDS annotated as T-DNA corder endonuclease VirD2, TraI/MobA(P) family conjugative relaxase, plasmid mobilization protein MobA or relaxase/mobilization nuclease domain containing protein. Sequences were aligned using MAFFT v7 algorithm L-INS-i (Katoh & Standley, 2013), cut using trimAl v1.4 using –automated1 option (Capella-Gutiérrez et al., 2009).

Data and statistical analysis

All data processing, visualization, and statistical analyses were performed in R v4.2.3 (R Core Team, 2023) running on macOS. The main packages used included tidyverse v2.0 for data manipulation and visualization, ggplot2 v3.4 for figure generation, ggtree v3.6 and ggtreeExtra v1.8 for phylogenetic tree visualization, gggenes v0.5 for gene map diagrams, ape v5.7 for phylogenetic tree manipulation, patchwork v1.1 for figure composition, and scales v1.2 for axis formatting. MASH distance matrices were computed using MASH v2.3 and imported into R for network analysis using igraph v1.4.

Differences in antimicrobial susceptibility profiles across sampling sites and seasons were assessed using the Kruskal-Wallis test, with post-hoc pairwise comparisons using the Dunn test with Bonferroni correction.

Results & Discussion

Plasmid diversity and general characteristics of the river basin

Transconjugants obtained from exogenous plasmid capture assays

A total of 49 transconjugants from 16 independent mating assays using two different antibiotic capture strategies (*i.e.,* TMP:SMX and AZI) were recovered across sampling site-season combinations spanning four locations: Bay (n=4), Estuary (n=8), Gorliz (n=17), and Mungia (n=20); and four time points: March/Winter (n=16), June/Spring (n=11), September/Summer (n=6), November/Autumn (n=16) representative of each season. Representative plate images under blue light illumination further illustrate site-dependent differences in recovery patterns and phenotypic heterogeneity, with higher diversity observed in Gorliz and Mungia compared to Bay, and a more uniform but resistant-associated phenotype in Estuary samples (Appendix D, Figure D1).

Notably, the proportion of TMP:SMX and AZI-selected isolates was 3:1, being TMP:SMX transferred with the highest success rate (n=37, Table 9). Plasmid capture was uneven across seasons and sites with March being the season at which transconjugants could be captured in the four sites, while September was only represented by two and four transconjugants at Gorliz and Mungia, respectively. Each transconjugant was further confirmed after plasmid extraction and visualization in agarose gel (Appendix D, Figure D2).

To determine unique profiling, each plasmid was digested with three different restriction enzymes and categorized depending on its apparent pattern within each mating experiment. Notably 70% of the resulting transconjugants harbored more than one plasmid during the mating assay highlighting the high co-mobilizable rates of other MGEs. Finally, 33 transconjugants were selected for further whole genome sequencing analysis.

Table 9. Plasmid capture antibiotic strategy.

	Antibiotic capture strategy	
Site	TMP:SMX	AZI
Bay	4	0
Estuary	8	0
Gorliz	9	8
Mungia	16	4

Antimicrobial susceptibility of transconjugants

To functionally validate plasmid transferability and acquired resistance phenotypes, antimicrobial susceptibility testing was performed on all recovered transconjugant isolates by measuring inhibition zone diameters and interpreting results according to EUCAST clinical breakpoints when available for Enterobacteriaceae (Figure 29). Critically, all transconjugants showed co-selection to other antibiotics regardless the selection strategy used.

EUCAST-defined resistance phenotypes were dominated by beta-lactam resistance, with near-universal resistance to amoxicillin and ampicillin across sites and selective conditions. This pattern appears to be largely independent of the relatively low abundances of bla_{TEM} and *ampC* genes detected by qPCR along the hydraulic continuum (Chapter 3), suggesting that phenotypic resistance may be driven by additional beta-lactamase variants not targeted in the molecular assay or by other mobile genetic determinants. The widespread occurrence of resistance to these beta-lactams is commonly described in wastewater environments plasmid-associated (Rizzo et al., 2013).

Cefotaxime resistance although less frequent, was also consistently detected (Figure 29), indicating the presence of clinically relevant third-generation cephalosporin resistance phenotypes within the mobilizable resistome fraction. Resistant transconjugants were recovered from both Mungia WWTP samples collected in winter and estuarine samples collected in spring, suggesting dissemination of third-generation cephalosporin resistance beyond the treatment plant itself. Even though the number of cefotaxime-resistant isolates was lower than that observed for aminopenicillins, third-generation cephalosporin resistance is of particular concern due to its frequent association with Extended-Spectrum Beta-Lactamase (ESBL)-producing Enterobacteriaceae, which are often embedded within multidrug-resistant plasmid backgrounds of clinical relevance (Ojer-Usoz et al., 2014).

Transconjugants captured under TMP:SMX selection displayed slightly more complex resistance profiles than those recovered under AZI selection. Co-occurrence analysis revealed distinct resistance modules associated with each selection regime. The TMP:SMX-selected group exhibited a highly structured co-resistance architecture characterized by strong linkage among aminopenicillins, aminoglycosides, tetracyclines, and chloramphenicol resistance, consistent with class 1 integron-mediated multidrug resistance cassettes. This suggests a highly constrained and modular organization of resistance determinants. The co-expression of resistance to beta-lactams (notably aminopenicillins), in addition to TMP and sulfonamides is mechanistically consistent with the co-occurrence *dfrA1* and *sul1* as canonical class 1

integron cassette components, which are commonly embedded in conjugative plasmids also carrying beta-lactamase genes. The consistent detection of sulfonamide resistance regardless of selective pressure applied is particularly notable: given the tight physical linkage of *sul1* with *intI1* as part of the class 1 integron 3' conserved segment (Stalder et al., 2012), sulfonamide resistance appears to be passively co-mobilized as part of the integron scaffold rather than being independently selected, a pattern that renders *sul1* a reliable functional marker of class 1 integron transfer in anthropogenically impacted environments (Gillings et al., 2015) consistent with the co-clustering of both markers in the treatment-resistant core fraction (Category 1) documented by qPCR in the preceding Chapter 3.

In contrast, the AZI-selected group displayed a more interconnected and less hierarchical co-occurrence network, including strong associations between sulfonamides and polymyxins, and between tetracyclines and trimethoprim resistance. These patterns indicate broader plasmid-mediated co-selection processes, where resistance determinants across unrelated antimicrobial classes are maintained within shared mobile genetic elements.

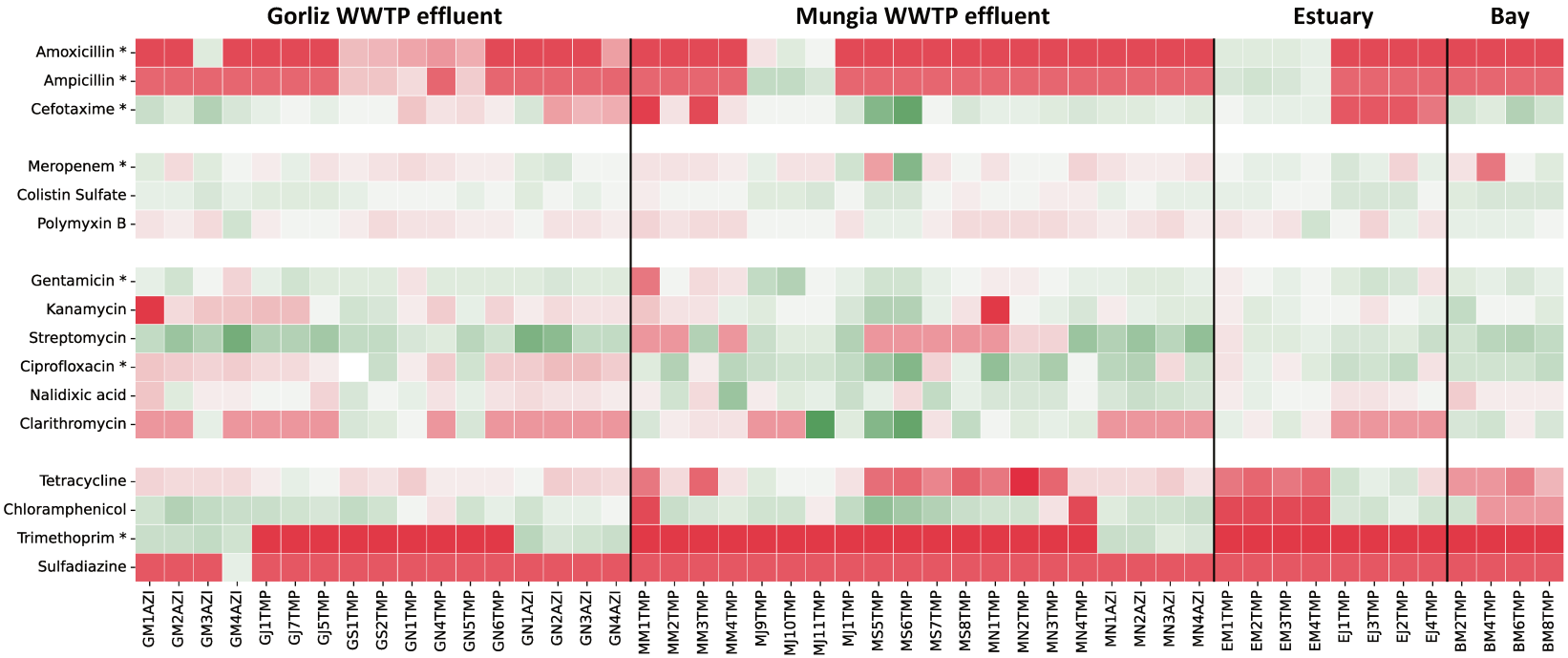

Figure 29. Transconjugant resistance profile.

Heatmap difference in inhibition zone diameter (Δ mm) between each transconjugant and the plasmid-free recipient strain *E. coli* K-12 (BW25113) determined by disk diffusion test. Negative (red) and positive (green) values indicate reduced or increased susceptibility relative to the recipient respectively to a batch of antibiotics. *Available EUCAST clinical breakpoints for Enterobacterales. Vertical black lines separate sampling sites.

Despite a broadly overlapping resistance spectrum across sites, statistical analysis revealed significant site-specific structuring of resistance phenotypes across sites for 7 of the 13 antibiotics tested, with the strongest effects observed for ciprofloxacin (χ^2=20.7, p<0.01), nalidixic acid (χ^2=15.3, p<0.01), and streptomycin (χ^2=13.0, p<0.01).

Fluoroquinolone resistance was more pronounced among Gorliz transconjugants, which may reflect the higher clinical usage pattern, although *qnrS_1* was detected at comparable abundances in both WWTPs by qPCR, indicating that the phenotypic difference likely reflects transfer efficiency or plasmid host range rather than differences in gene abundance or local selection alone. Streptomycin resistance showed the opposite pattern, being more prevalent among Mungia transconjugants. This may indicate selective pressure exerted by agricultural settings and the co-selection of *aadA* gene cassettes carried by class 1 integrons (Binh et al., 2009). Meropenem resistance profiles were comparable between plants, compatible with the low abundances of carbapenemase genes ($bla_{\text{OXA-48}}$, bla_{NDM}, bla_{VIM}, $bla_{\text{KPC_2}}$) detected by qPCR at both sites. These determinants are likely present at low abundance, resulting in transfer frequencies below the detection limit of the mating assay.

The geographic structuring of resistance phenotypes extended beyond the WWTP comparison to the downstream receiving environment. Transconjugants recovered from the estuary displayed resistance profiles overlapping with those of both WWTPs, consistent with its position as a mixing zone receiving inputs from Mungia effluent and diffuse catchment sources. The detection of tetracycline-resistant transconjugants at the estuary is concordant with the qPCR evidence that *tetM* and *tetW* while showing dilution attenuation along the continuum, remain at detectable abundances in estuarine waters, suggesting that conjugation-competent donor populations persist at this site at densities sufficient to sustain plasmid transfer. The absence of AZI-captured transconjugants from Estuary and Bay (Table 7) likely reflects reduced donor density and plasmid transfer efficiency in the more dilute coastal environment rather than the absence of the corresponding resistance determinants, which were detected molecularly by qPCR. Seasonal variation in resistance phenotypes, most pronounced for tetracycline, and the precipitation-driven structuring of profiles at both WWTP sites are consistent with the hydrological confounding effects identified in the qPCR analysis. Particularly, the autumn seasonal variation was attributed to sediment resuspension and storm overflow bypass, supporting the view that hydrological disturbances, rather than seasonality per se, dominate resistome dynamics in impacted catchments (Gao et al., 2025).

The resistance phenotypes documented here reflect the functional expression of ARGs carried by plasmids captured under TMP:SMX and AZI selective conditions and laboratory-based culture methods. Therefore, they should be interpreted as a window into the mobilizable fraction of the resistome rather than a comprehensive survey of ARGs diversity. The qPCR profiles described in the preceding chapter provide the broader quantitative context: the genes most abundantly detected across sites and seasons are not necessarily those represented among the transconjugants, since capture efficiency is inherently constrained by the choice of selective agent, the permissiveness of the recipient strain, and the conjugation conditions employed (Dib et al., 2015). With this caveat in mind, the resistance phenotypes of recovered transconjugants are broadly consistent with the ARGs distribution patterns documented by qPCR and provide functional validation that a subset of the resistance determinants detected molecularly are indeed plasmid-borne and horizontally transferable under the conditions tested.

Mobilizable plasmidome characterization

To resolve the molecular basis underlying the geographically structured resistance phenotypes described above, plasmids successfully transferred to *E. coli* BW25113 recipient strains during filter mating were extracted, sequenced by long-read nanopore sequencing, and assembled into complete or near-complete replicons.

Plasmid identifiers follow a structured nomenclature encoding sampling metadata: the first letter denotes the sampling site (G=Gorliz, M=Mungia, B=Bay, E=Estuary), the second letter denotes the season of collection (M=winter, J=spring, S=summer, N=autumn), followed by an arbitrary transconjugant number and the selective antibiotic used during filter mating (TMP=trimethoprim, AZI=azithromycin). The suffix -pX indicates the plasmid number within a given transconjugant, where multiple plasmids were recovered from the same recipient colony (*e.g.,* GN5TMP-p1 and GN5TMP-p2 denote the first and second plasmid recovered from transconjugant 5, sampled at Gorliz in autumn under TMP selection).

Of the 80 plasmids initially captured across the four sampling sites by restriction pattern analysis, 67 were subjected to long-read sequencing. Following quality filtering which included the exclusion of one putative chromosomal fragment (MN3AZI-p3, 414 kb) and one fragmented inconsistent assembly (BM2TMP-p2, 5.6 kb), the final dataset comprised 65 plasmid sequences recovered from 33 distinct bacterial samples across four sampling sites: Gorliz (n=32), Mungia (n=23), Estuary (n=9), and Bay (n=1). Plasmid sizes ranged from 0.5 to 303 kb (median 51.8 kb, mean 62.7 kb), reflecting the broad size diversity characteristic of environmental plasmid communities (Appendix D, Table D1). Most assemblies were circular (81.5%), consistent with successful complete assembly of closed replicons.

Co-occurrence

Plasmid co-residence was a common feature of the dataset: 20 of the 33 samples (60.6%) harbored more than one plasmid simultaneously. Four samples (GJ1TMP, GN4TMP, GN5TMP, and MN4TMP) carried the maximum of four co-occurring plasmids, while six additional samples (GJ5TMP, GM2AZI, GN6TMP, MJ10TMP, MJ9TMP, and MN3AZI) carried three plasmids each. The co-residence of multiple compatible replicons within the same bacterial host is epidemiologically relevant, as it creates conditions for plasmid-plasmid interactions including mobilization in trans, recombination between mobile elements, and the accumulation of complementary resistance determinants within a single cell (Garcillán-Barcia et al., 2025). Notably, samples carrying four plasmids simultaneously included both large

conjugative elements and smaller non-mobilizable elements, indicating that plasmid co-residence is not restricted to elements of similar size or mobility class (Millan et al., 2014; Shintani et al., 2015).

Mobility classification

In terms of predicted mobility, 47 plasmids (72.3%) were classified as conjugative, 17 (26.2%) as non-mobilizable, and one (1.5%) as mobilizable. Notably, the single mobilizable element (GJ5TMP-p11, ColRNAI, 3.2 kb) carried a MOBP/MOBP dual relaxase, suggesting potential for mobilization in trans by co-resident conjugative plasmids. Seven plasmids exceeded 100 kb in size and are considered megaplasmids, ranging from 109 to 303 kb.

The 65 plasmid sequences were distributed across 12 distinct replicon types (Appendix D, Table D1). IncN was the most prevalent replicon, detected across all sites except Bay (n=17 total), with highest abundance at Mungia (n=7) and Estuary (n=5). IncU plasmids were the second most common (n=11) but were exclusively recovered at Gorliz, suggesting a site-specific enrichment. IncF-complex plasmids (IncFIA, IncFIB, IncFIC, IncFII) were broadly distributed, with IncFII predominating at Mungia (n=6) and IncFIB/IncHI1B elements concentrated at Gorliz. IncP plasmids were detected exclusively at Mungia (n=4). A subset of plasmids (n=14) could not be assigned to a known Inc group, 13 of which were predicted non-mobilizable, carrying either uncharacterized replication clusters (rep_cluster_827, rep_cluster_2350) or lacking recognizable replication protein annotations, indicating either highly divergent sequences or novel plasmid types not yet represented in reference collections. Notably, IncN plasmids are phylogenetically recognized as broad host-range conjugative elements, although their host range is generally considered narrower than that of IncP-1α and IncP-1β plasmids (Yu et al., 2024). Their widespread detection across sites in this study therefore highlights their ecological success in wastewater-associated Enterobacteriaceae communities, consistent with their efficient horizontal transfer and stable maintenance across diverse environmental and clinical backgrounds.

Correlation between size and cargo genes

Plasmid size showed strong positive correlations with all gene cargo metrics assessed by Spearman rank correlation ($p<0.001$) (Figure 30). The strongest association was observed between plasmid size and total gene content ($\rho=0.963$, Figure 30A), followed by IS element count ($\rho=0.794$, Figure 30C), total cargo genes ($\rho=0.753$, Figure 30D), and AMR gene count ($\rho=0.649$, Figure 30B). These results indicate that larger plasmids carry more MGEs and

resistance determinants, consistent with an ongoing process of cargo gene accumulation driven by IS element-mediated recombination events.

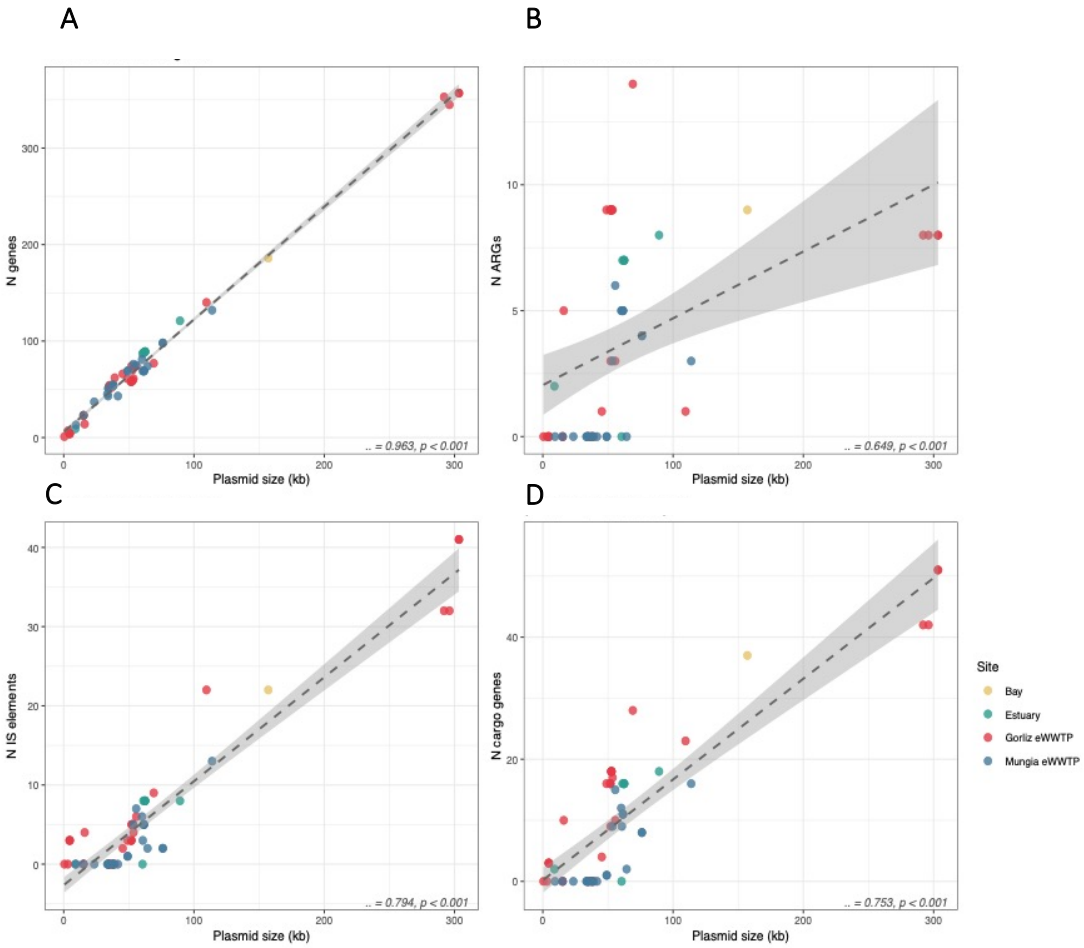

Figure 30. Correlations between plasmid size and gene cargo metrics.

Data across the 65 plasmid sequences recovered in this study. Each panel shows a Spearman rank correlation between plasmid size (kb) and a distinct cargo metric: (A) total number of annotated coding sequences (CDS) as predicted by Bakta; (B) number of ARGs identified by AMRFinderPlus; (C) number of IS elements; (D) total cargo gene count, defined as the sum of ARGs, IS elements, and integron-associated gene cassettes. Points are coloured by sampling site. The dashed line represents a linear regression fit with 95% confidence interval shown in grey. Spearman correlation coefficients (ρ) and associated p-values are shown in each panel.

Functionality analysis

The functional composition of plasmid-encoded genes was assessed by eggNOG-mapper annotation across 64 plasmids (3,559 COG annotations; Figure 31A). The largest functional category across all sites was categorized as Unknown function, consistent with the high proportion of hypothetical proteins typically found in environmental plasmids and reflecting the limited functional characterization of plasmid-borne genes in public databases (Louca et al., 2018). Mobilome and replication functions (*i.e.,* transposases, integrases, replication initiation proteins, and relaxases) constituted the second most represented category, confirming that a substantial fraction of the annotated gene content is dedicated to plasmid maintenance and horizontal transfer. Intracellular trafficking, comprising T4SS components and conjugative transfer genes, ranked third, consistent with the predominantly conjugative character of the recovered plasmids.

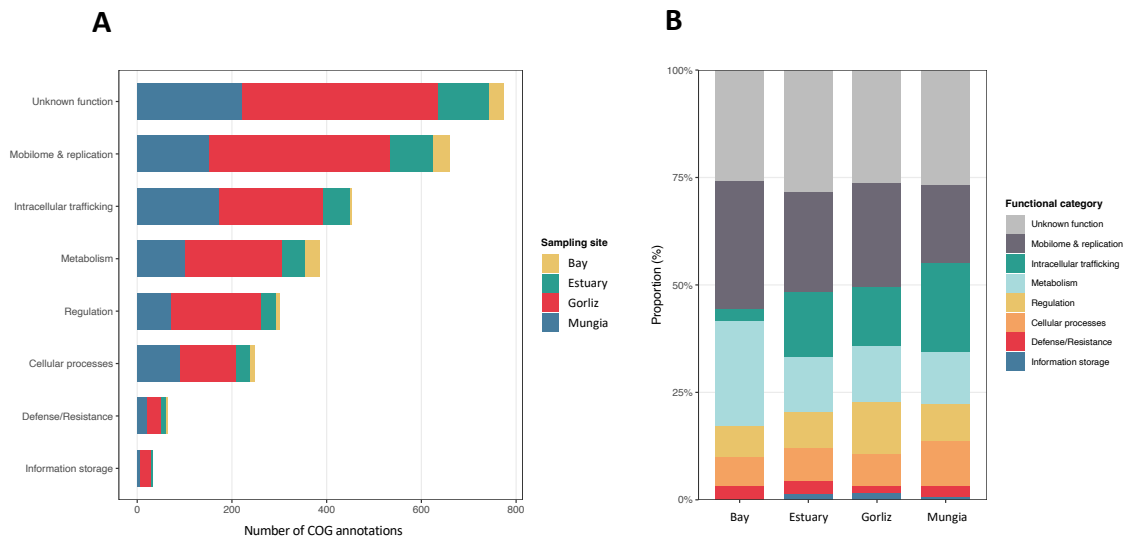

Figure 31. Functional annotation based on eggNOG database of samples by site.

(A) Absolute counts of annotated genes that matched described function in y-axis. (B) Normalized proportion of functional category by site including Bay, Estuary, Gorliz and Mungia.

Comparison of functional profiles across sampling sites revealed broadly similar compositions at Gorliz and Mungia, with "Unknown function" and "Mobilome & replication" dominating in both (Figure 31B). However, Gorliz showed a proportionally higher contribution of Defense/Resistance annotations and Regulation relative to Mungia, consistent with the greater plasmid complexity and size observed at that site. The Bay sample is represented by a single large plasmid (BM4TMP-p12, 303 kb) and its functional profile should therefore be interpreted with caution as it reflects the gene content of one element rather than a site-level

community. Notably, this singleton showed a markedly higher proportion of "Metabolism" annotations relative to the WWTP sites, which may reflect the accessory metabolic cargo characteristic of large IncFIB/IncHI1B megaplasmids (Liang et al., 2022; Ma et al., 2023).

Together, these functional profiles confirm that the recovered plasmidome is dominated by self-transmissible elements with substantial but partially uncharacterized accessory cargo, whose resistance gene content and integron architecture are examined in detail in subsequent sections.

Inter-plasmid relatedness and assignment to plasmid individual identities

Plasmid classification into clusters

Pairwise sequence comparison using Mash distance revealed the presence of 10 clonal clusters (CC) comprising two or more nearly identical plasmids (distance<0.001), suggesting the existence of stable plasmid lineages circulating within the studied population (Table 10). In total, 35 out of 65 assembled plasmids (53.8%) were assigned to one of these clusters, while the remaining 30 (46.2%) were identified as singletons.

Table 10. Clonal cluster (CC) classification.

Clone Cluster (CC)	Cluster size	Members
CC1	8	GJ3TMP, GM2AZI, GM4AZI, GN1AZI, GN2AZI, GN3AZI, GN4TMP, GN6TMP
CC2	4	GN4TMP, GN5TMP, GN6TMP, GS2TMP
CC3	4	MN1AZI, MN3AZI, MN4AZI, MN4TMP
CC4	4	EM1TMP, EM2TMP, EM3TMP, EM4TMP
CC5	3	GN4TMP, GN5TMP, GN6TMP
CC6	3	GN4TMP, GN5TMP, MJ10TMP
CC7	3	MN3AZI, MN4AZI, MN4TMP
CC8	2	GN1AZI, GN2AZI
CC9	2	MJ10TMP, MJ9TMP
CC10	2	MJ10TMP, MN1TMP

The largest cluster, CC1, grouped 8 plasmids recovered exclusively from Gorliz effluent across three sampling seasons (winter, spring, and summer) and with both capture antibiotics strategies (TMP:SMX and AZI), indicating that persisted stably in the environment over at least

nine months. Its capture with two structurally unrelated antibiotics suggests that the selective advantage conferred by plasmid present in CC1 is not restricted to a single resistance class, consistent with their transconjugant broad resistance profiles. Similarly, CC2 plasmids from the same site were recovered at two different time points, further supporting the notion of temporal persistence of established plasmid lineages at Gorliz. In contrast, CC3, CC4, CC5, CC7, CC8 and CC9, were exclusively grouped during the same sampling campaign which may indicate dominance and less diversity at that site and time.

Correction for clonal redundancy revealed that the apparent dominance of Gorliz in plasmid abundance (n=32, 47.8% of total) was substantially reduced when only unique plasmid lineages were considered (n=18 unique, 56.3% clonal redundancy). Only 6 unique plasmid lineages among 16 total captures during autumn sampling (37.5% uniqueness). This pattern, high clonal dominance coinciding with peak precipitation (68.3 mm over 14 days), is consistent with rainfall-driven resuspension of established sediment-associated lineages rather than introduction of novel plasmid diversity, and contrasts sharply with Spring sampling at the same site, where all 10 captured plasmids represented unique lineages (100% uniqueness).

Intra-cluster variability

Pairwise whole-genome comparison using dnadiff (MUMmer4) revealed distinct levels of within-cluster variability across the 10 clonal clusters identified. Five clusters (CC4, CC7, CC8, CC9, and CC10) showed complete sequence identity among all members, indicating clonal dissemination without detectable mutation, and suggesting very recent transmission or shared origin. Note that these correspond to the same sampling campaigns except for CC10 that was detected in winter, spring and autumn seasons. The remaining clusters exhibited varying degrees of divergence, which could be attributed to the accumulation of point mutations, small indels, or the differential acquisition of MGEs.

Three additional clusters exhibited only minor within-cluster variation that could not be attributed to meaningful biological divergence. Cluster CC5 comprised three sequences of near-identical length (4,560–4,568 bp) encoding exclusively ISKpn21 transposase elements, with no ARGs or replication functions detected, consistent with a small autonomous mobile element. Five apparent SNPs identified by *snp*-sites were located entirely within ISKpn21 coding sequences, and four of these represented consecutive single-base changes at positions 6,783–6,786, consistent with a localized sequencing or assembly artefact rather than true nucleotide variation. Cluster CC3 showed no unique genomic regions by pairwise dnadiff

comparison, with only 1–2 minor indels detected in MN4AZI relative to the other three members, associated with slight variation in IS element count (3–5 Tn4380-associated elements per member) rather than any functional gene content difference. Taken together, these seven clusters (*i.e.,* CC3, CC4, CC5, CC7, CC8, CC9, and CC10) represent stably circulating, genetically cohesive plasmid lineages whose inter-sample distribution reflects active dissemination rather than ongoing diversification. Further alignment specific analysis was made to elucidate the differences among two most variable assigned CC (CC1, CC2 and CC6).

Analysis on CC1, the largest cluster, 388 variable sites were detected across the whole-genome alignment, distributed along the plasmid backbone, and associated with variable numbers of IS elements (ranging from 3 to 5 per member), predominantly from the Tn4656 family (Figure 32A). The distribution of SNPs across temporally distinct samples spanning from March to November, is consistent with probable ongoing microevolution of a stably plasmid lineage rather than a single recent transmission event.

Cluster CC6 comprised three prophage-like elements of identical length (15,203 15,204 bp) sharing 0 SNPs and 0 indels across all pairwise comparisons (Figure 32B). However, dnadiff analysis revealed two inversions in the region spanning coordinates 3,615–5,454 in MJ10TMP-p2 relative to both GN4TMP-p3 and GN5TMP-p3. This variable region encodes the tail fiber and tail collar structural proteins (*tfaE*, short tail fiber protein, Tail Collar domain-containing protein), which are direct determinants of phage host range. Notably, all three members encode *pinE* (coordinates ~5,515–6,070), a site-specific DNA recombinase of the invertase family known to catalyze the inversion of tail fiber-encoding segments, thereby enabling reversible switching of host specificity. The detection of this inversion in the sample from Mungia (MJ10TMP) but not in the two samples from the Gorliz estuary (GN4TMP, GN5TMP) suggests that this prophage element may exist in distinct tropism states across sampling sites, potentially reflecting adaptation to different bacterial host communities under contrasting anthropogenic pressures.

Additionally, Cluster CC2 (n=4, IncFIB/IncHI1B) was the most structurally heterogeneous cluster, harboring the highest IS element burden observed across all clusters (32–41 IS elements per member; Figure 32C). Pairwise comparison identified two distinct subclusters in which GN5TMP and GN6TMP showed a region of approximately 11.4 kb absent in GN4TMP nor G6TMP was found to encode five tandem copies of the ISKpn21 transposase, suggesting a recent insertion expansion event in this sublineage. GS2TMP, the most divergent member, additionally carried two unique regions at coordinates 277,683-279,961 and 293,066-296,026,

the latter containing an IS5 family ISKpn26 transposase and an ABC transporter substrate-binding protein, further supporting independent evolutionary trajectories within this cluster. Notably, while GN4TMP, GN5TMP, and GN6TMP shared an identical AMR profile (*qnrB4*, *blaDHA-1*, *qacE*, *sul1*), GS2TMP carried a distinct resistance gene complement (*dfrA15*, *aadA1*, *qacE*, *sul1*) which was absent in the other three members. This difference in ARG content, combined with the structural variation, strongly suggests that GS2TMP represents a divergent variant of the CC2 lineage that has undergone independent acquisition of resistance determinants. This shows a seasonal distinction of the same plasmid.

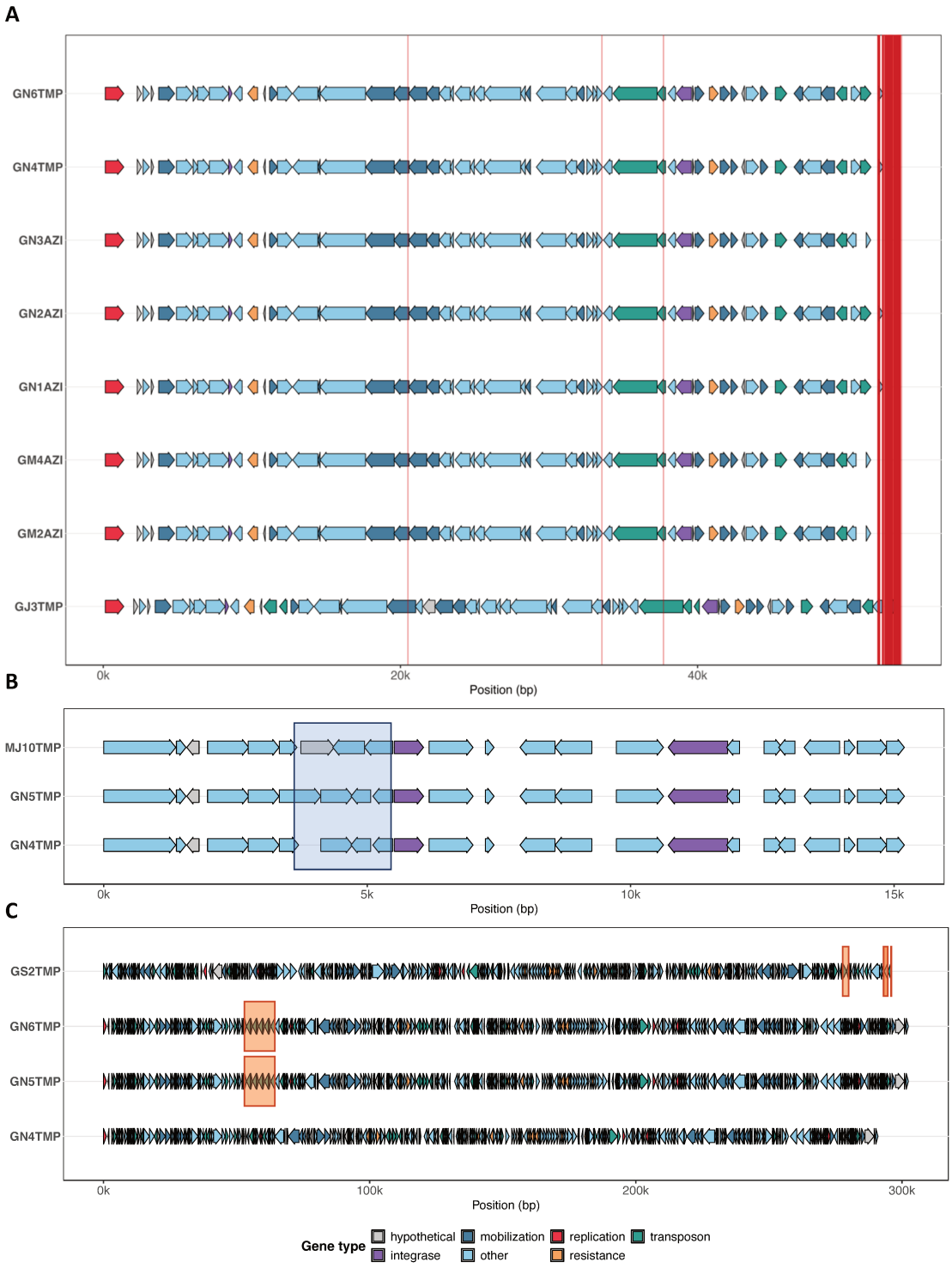

Figure 32. Sequence alignment of selected Clonal Clusters (CCs).

Data identified in the plasmidome from study area (mash<0.001). Gene categories are color-coded as follows: read, replication; blue, mobilization; orange, resistance; teal, transposable elements; purple, integrase/recombinase; grey, hypothetical proteins; light blue, other functions. Vertical red lines indicate single nucleotide polymorphism (SNP) positions detected across the whole-genome alignment. Orange shaded rectangles indicate genomic regions present in a subset of members but absent in others, suggestive of insertion or deletion events. Blue shaded rectangles indicate regions subject to site-specific inversion. Represented cluster correspond to (A) CC1, (B) CC6, (C) CC2.

Across the four sampling sites, a total of 80 plasmids were initially captured by restriction pattern analysis, of which 65 were successfully sequenced and confirmed after quality filtering. Clonal analysis identified 43 unique plasmid lineages, comprising 13 clonal clusters (CCs) and 30 singletons (Table 11).

Table 11. Plasmid recovery and diversity across sampling sites.

Site	Captured plasmid No. (restriction pattern)	Sequenced and confirmed plasmids	Unique lineages
Gorliz	35	32	21
Mungia	29	23	15
Estuary	12	9	6
Bay	4	1	1
Total	**80**	**65**	**43**

Based on these analyses, each cluster was further subdivided into subclusters where biologically relevant differences were identified (Table 12). To avoid redundancy, one representative plasmid was selected per subcluster, resulting in a total of 13 entities used in subsequent analyses, alongside 30 singletons, for a combined dataset of 43 unique plasmid identities. The replicon distribution was largely preserved after collapsing redundant clonal variants into 43 unique plasmid identities, with IncN remaining the most prevalent group (n=12, 27.9%), followed by IncU and IncFII in equal proportion (n=5 each, 11.6%). The reduction in IncN count from 17 to 12 reflects the clonal grouping of related IncN plasmids within shared CCs, while IncU dropped from 11 to 5, consistent with the high clonal relatedness of IncU elements within CC1. This consolidation confirms that the dominance of IncN and IncU backbones in this plasmidome reflects genuine biological prevalence rather than sampling of the same clonal lineage multiple times.

Table 12. Characteristics of representative plasmids for each clonal cluster (CC) detected across sampling sites.

Clonal Cluster (CC)	Representative plasmid	Replication origin	Relaxase	Predicted mobility
CC1a	GJ3TMP-p1	IncU	MOBP	conjugative
CC1b	GN1AZI-p2	IncU	MOBP	conjugative
CC2a	GN5TMP-p7	IncFIB, IncHI1B	MOBH	conjugative
CC2b	GN4TMP-p4	IncFIB, IncHI1B	MOBH	conjugative

CC2c	GS2TMP-p13	IncFIB, IncHI1B	MOBH	conjugative
CC3	MN1AZI-p1	IncP	MOBP	conjugative
CC4	EM2TMP-p3	IncN	MOBF	conjugative
CC5	GN4TMP-p1	-	-	non-mobilizable
CC6	GN4TMP-p3	-	-	non-mobilizable
CC7	MN3AZI-p8	rep_cluster_827	MOBP	conjugative
CC8	GN1AZI-p3	IncN	MOBF	conjugative
CC9	MJ10TMP-p3	IncN	MOBF	conjugative
CC10	MJ10TMP-p4	IncFII	-	non-mobilizable

Plasmid relatedness and network structure across sampling sites

To investigate broader relatedness patterns among the 43 plasmid entities identified in this study, a similarity network was constructed based on pairwise Mash distances, connecting plasmids with a distance between 0.001 and 0.30. This threshold was selected based on the observed bimodal distribution of all pairwise Mash distances (Appendix D, Figure D3). The resulting network revealed that 74.4% of all plasmid entities (n=32) formed a single interconnected main component (Figure 33), while the remaining were distributed across three smaller components (ranging from 2 to 4 sequences) and three fully isolated singletons with no detectable relatedness to any other plasmid in the dataset (Appendix D, Figure D4).

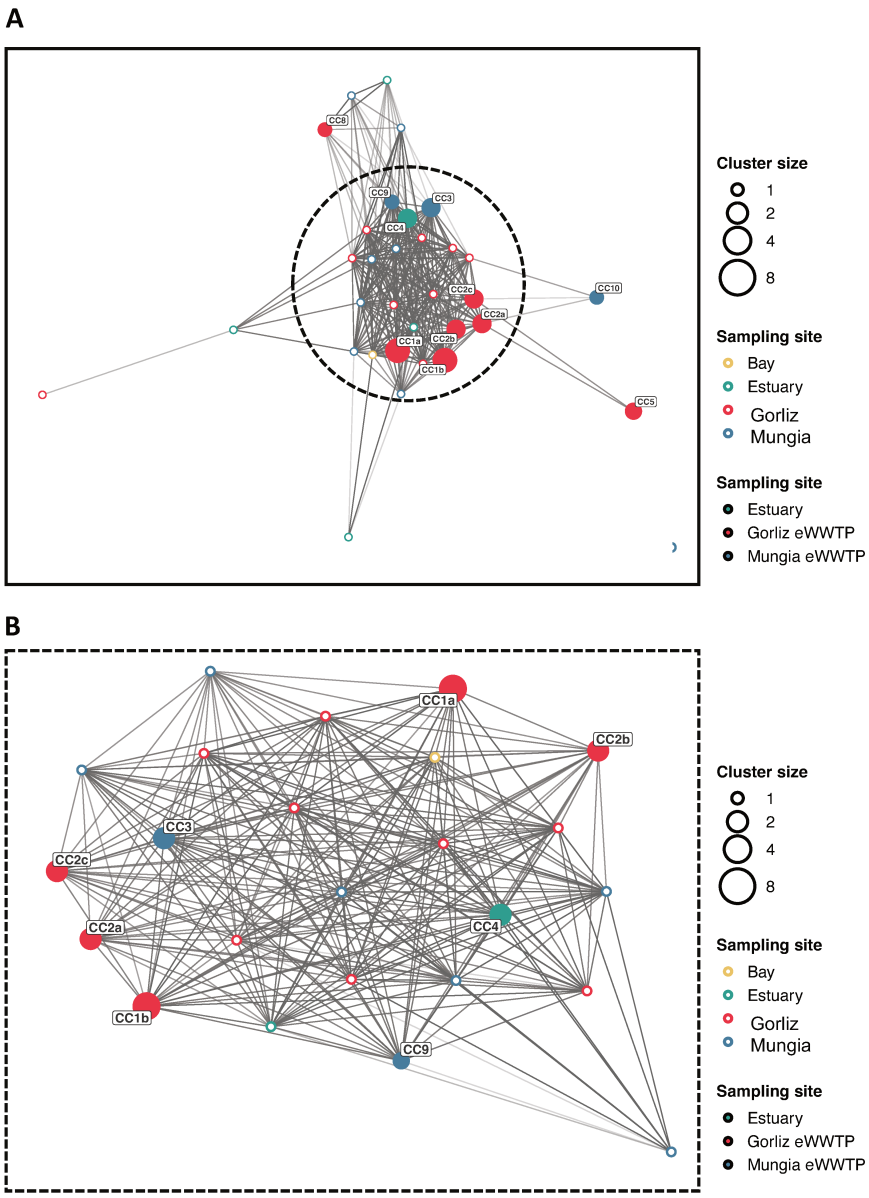

Figure 33. Main MASH network connecting plasmids entities.

(A) Mash network with a distance between 0.001 and 0.30 reduced the main component (74.4%) and (B) zoom into the collapsed interconnected area within the main component.

The high proportion of plasmids forming a single interconnected component contrasts with the fragmented network topology typically observed in globally diverse plasmid datasets (Acman et al., 2020), and instead points to shared evolutionary history among the mobilizable plasmids circulating in this geographically restricted system. Notably, the main component encompassed plasmids from all four sampling sites in the absence of clear geographical clustering. While it might be tempting to attribute this cross-site connectivity to direct hydrological dispersal this explanation is unlikely to account for the similarity between the

two WWTP plasmidomes themselves, as Gorliz and Mungia operate as hydraulically independent systems with no shared receiving water at the point of discharge. Rather, the convergence of plasmid backbones across both WWTPs more plausibly reflects the common anthropogenic selective pressure exerted by the shared human population of the Basque Country, in which antibiotic consumption patterns, clinical practice, and community-associated resistance determinants enter both systems independently through their respective catchments, reflecting the well-documented role of local antibiotic use and community carriage in shaping WWTP influent resistome (Hendriksen et al., 2019). Population size and urban antibiotic pressure have been identified as key deterministic drivers of resistome composition in wastewater treatment systems, operating independently of site-specific hydrological connectivity. Under this interpretation, the shared plasmid backbone pool is a signature of a regionally homogeneous human resistome rather than of active inter-site plasmid dispersal via water flow. Residual cross-site similarity attributable to hydrological transport from Mungia effluent to the estuary and bay may nonetheless contribute to the connectivity observed at the downstream environmental sites. Notably, IncN plasmids occupied the most central positions within the network (highest betweenness centrality), consistent with enterobacteria such as *E. coli, Salmonella enterica and Klebsiella sp*., as the preferred hosts (Eikmeyer et al., 2012) for this Inc type. IncFIB/IncHI1B representatives of CC2 also showed high centrality, reflecting their shared backbone architecture, and suggesting shared mobilization elements.

Other MGEs

Insertion sequences and transposable elements

Insertion sequences (ISs) elements were detected in 58.1% of the plasmids (n=25) with a total of 252 IS elements identified across the dataset, a median of 2 IS per plasmid, and a maximum of 41 in a single element (CC2a, GN5TMP-p7). A total of 41 distinct IS types were identified (including variants), reflecting considerable diversity of transposable elements in the plasmid community. The most prevalent IS element was IS26 identified in 49% of plasmids entities (n=21), followed by IS6100 (33%, n=14), Tn4656 (16%, n=11; Figure 34).

Insertion sequence IS26 is of clinical and ecological relevance, being one of the most prevalent IS elements in enterobacterial clinical isolates, where it actively participates in resistance gene dissemination and plasmid rearrangement (Siguier et al., 2015; Varani et al., 2021). It is known to mediate the capture, amplification, and transfer of ARGs through formation of translocatable units and pseudo-compound transposons. Its predominance in

this dataset, particularly in association with IncN and IncF plasmids carrying multi-drug resistance cassettes, suggests that IS26-mediated recombination may be an important driver of ARG mobilization in this study area. Insertion sequence IS6100 is similarly noteworthy as a key mediator of *qacE* and sulfonamide resistance gene dissemination, being frequently found at the 3'-end of class 1 integrons carrying *qacEΔ1* and *sul1* (Fluit & Schmitz, 2004).

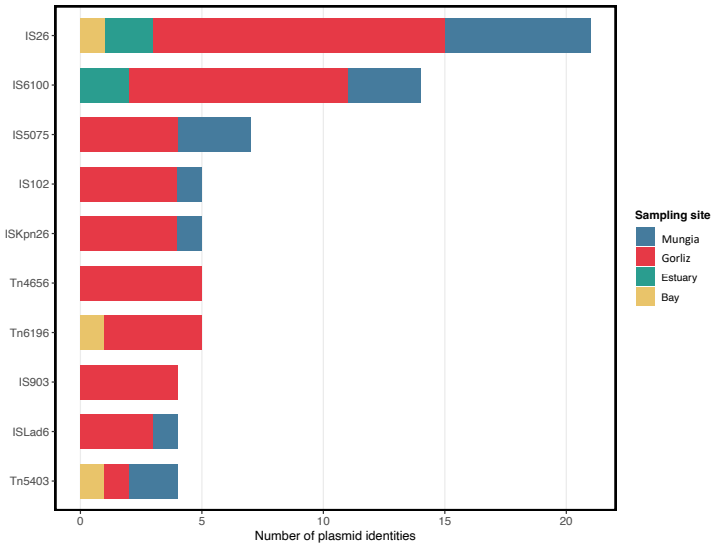

Figure 34. Top ten insertion sequences (IS) and transposon (Tn) elements.
Cumulative barplot showing the total number of unique plasmid identities identified in Mungia (blue), Gorliz (red), Estuary (green) and Bay (yellow).

The strong positive correlation between IS element count and plasmid size (ρ=0.794, p<0.001) observed further points to with a model in which IS element accumulation drives plasmid size increase through successive insertion events, with larger plasmids providing a larger target for IS-mediated recombination and gene capture, a process named as genetic capitalism, by which plasmids bearing ARGs are prone to capture additional resistance genes over time (Baquero et al., 2021).

This pattern was reflected in the distribution of IS elements across sampling sites. WWTP-associated samples harbored the greatest plasmid diversity and IS burden, with Gorliz contributing the largest number of plasmid identities (n=21) and the highest mean IS load (mean=8.2 elements/plasmid), consistent with their role as hotspots for HGT. Mungia showed intermediate values, while Estuary samples were characterized by lower plasmid diversity and IS burden. The single plasmid recovered from the Bay sampling point represented an exceptionally large and IS-rich replicon (157 kb, 22 IS elements), potentially reflecting an advanced stage of IS-driven gene accumulation consistent with the genetic capitalism model;

however, this observation should be interpreted with caution given the limited sample size (n=1).

Integrons and gene cassettes

Class 1 integrons were detected in 46.5% of plasmid identities, with a maximum of two integrons per plasmid and a total of 22 integrons across the dataset. Integron-carrying plasmids were distributed across multiple Inc groups, with IncN (n=8) and IncU (n=5) accounting for the majority, followed by IncFIB (n=4), IncHI1B (n=3), IncFIA and IncFIC (n=2 each), and IncP (n=1). The association between integron carriage and ARGs content was striking. Plasmids carrying at least one integron showed a median of 7.5 ARGs per plasmid and 95% were multi-resistant (≥3 ARGs), compared to only 4.3% multi-resistance among integron-negative plasmids. This near-perfect association confirms that class 1 integrons are the primary platform for ARGs accumulation on the plasmids recovered in this study, consistent with their well-established role as integrative ARGs capture and expression platforms in Gram-negative bacteria (Stalder et al., 2012). The potentially mobile integron collectively provide a reservoir of cassettes associated with ARGs each of which often preceeds an attC recombination site (Stalder et al., 2012)

Eight unique cassette gene profiles were identified across the 20 integron-positive plasmid identities (Figure 35). The most prevalent profile was the simple gene cassette carrying *dfrA1*-like (n=6), conferring TMP resistance, found across multiple sampling sites (*i.e.,* Gorliz, Mungia and Estuary) and conserved in IncN backbone. The high prevalence of this cassette may reflect the use of TMP as a selective agent during plasmid capture and should therefore be interpreted with caution as a measure of environmental abundance. The absence of the canonical 3' conserved segment genes (*qacEΔ1-sul1*) together with the abundance of IS/Tn-associated recombination modules suggest a truncated or complex class 1 integron structure, likely shaped by transposition and recombination events (Gillings, 2014). Two profiles were equally represented with n=4 each: *aac(6')-Ib–blaOXA-1–catB–arr–qacEΔ1*, found exclusively in IncU replicons at Gorliz (CC1a, S7 and S18), conferring simultaneous resistance to aminoglycosides, beta-lactams, phenicols, rifamycins, and QACs; and *qacEΔ1–aadA1–dfrA1*, combining TMP, aminoglycoside, and QACs in a canonical class 1 integron arrangement. A structural variant of the latter, *dfrA1–aadA1–qacEΔ1* (n=2), likely represents the same array in reverse orientation. The *dfrA1–qacEΔ1–aac(6')-Ib–blaOXA-1–catB–arr* profile (IncU) contained a ~14.2 kb sequence region separating two distinct cassette arrays, more consistent with a composite integron structure formed by fusion of two independent

integron elements or insertion of a mobile element between two cassette arrays. The remaining profiles were identified in singletons: *qacEΔ1–dfrA* (GJ1TMP-p3) and *qacF/L–aadA1–cmlA–dfrA1* (BM4TMP-p12).

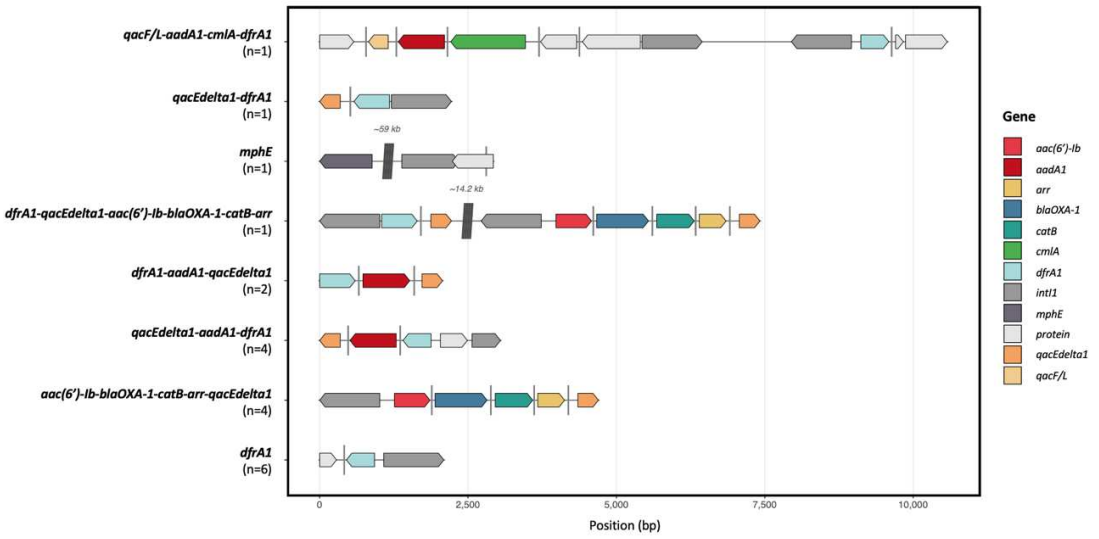

Figure 35. Unique integron diagram cassette gene profiles found in plasmid entities.
Number of plasmid identified with the integron cassette is reported (n=).

Cassette array complexity, measured as the number of attC recombination sites per integron-positive plasmid, ranged from 1 to 5 at Gorliz, with the highest complexity observed mainly in IncU replicons. The single Bay plasmid (BM4TMP-p12) carried 6 attC sites, representing the most complex cassette array in the dataset. Overall, the predominance of *qacEΔ1* and *sul1* as structural components of the 3' conserved segment across virtually all class 1 integrons explains the high prevalence of quaternary ammonium and sulfonamide resistance detected by AMRFinderPlus (Stalder et al., 2012). These resistance determinants are typically embedded within the conserved integron scaffold rather than acquired as independent gene cassettes, consistent with the resistance profiles observed in the transconjugants. Together, these results indicate a high prevalence of integron-associated ARGs linked to mobile genetic elements that facilitate their dissemination. In addition, conserved plasmid backbone modules persistent across the study area may act as stable scaffolds for the progressive accumulation of additional resistance determinants under selective pressure.

ARG content of recovered plasmids

Building on the integron-associated ARGs architecture described above, broader annotation of the full plasmid dataset revealed ten resistance classes across all four sampling sites, with marked differences in prevalence and diversity between locations (Figure 36). At the site level, sulfonamide, beta-lactam, and quinolone resistance were the most widespread classes at Gorliz, followed by QACs resistance. By contrast, Mungia plasmids presented a more restricted resistance profile dominated by sulfonamide and TMP resistance, with quinolone resistance detected in only a single plasmid (*qnrS1*, MN4TMP-p2). Rifamycin resistance was detected exclusively at Gorliz, encoded by the *arr-3* gene cassette within class 1 integrons. This clinically relevant cassette was associated with $bla_{\text{OXA-1}}$*, aac(6')-Ib-cr5,* and *catB3,* demonstrating its incorporation into multidrug resistance cassette arrays that facilitate the co-selection and dissemination of resistance to multiple antibiotic classes. The *arr-3* gene encodes an ADP-ribosyltransferase that confers high-level rifampicin resistance and has been reported predominantly in clinical isolates of Enterobacteriaceae, particularly *Klebsiella pneumoniae*, where it is disseminated within class 1 integron cassette arrays (Elias et al., 2025). Given that rifampicin is used exclusively in clinical settings, its unique detection at Gorliz across seasons is consistent with an active clinical point-source contribution to the local resistance gene pool.

Macrolide resistance determinant *mph(A)* was detected in transconjugants recovered from Gorliz, Mungia and Estuary sites, regardless of whether capture was performed using AZI or TMP selection, suggesting co-selection and co-transfer of macrolide resistance determinants with other ARGs. The highest prevalence was observed at Gorliz (n = 6), consistent with the dissemination of resistance to semisynthetic macrolides and streptogramins commonly associated with clinical settings. Moreover, *mph(A)* was identified together with *mrx(A),* a gene described as encoding a protein required for high-level erythromycin resistance (Partridge, 2011). In parallel, the environmental macrolide resistance determinants *mph(E)* and *msr(E)* were identified in Mungia and Gorliz transconjugants from different sampling seasons, indicating the persistence and temporal circulation of mobile macrolide resistance modules across the study area.

Notably, tetracycline resistance genes *tet(A)* were detected exclusively at the Bay and Estuary sites in winter (Figure 36), associated with large plasmids recovered from those downstream locations. This spatial restriction is consistent with the qPCR evidence showing dilution attenuation of *tetM* and *tetW* along the hydraulic continuum and suggests that

tetracycline selective pressure in the downstream environment, likely driven by diffuse sources such as agricultural residues adsorbing to and remobilizing from organic-rich sediments (Chee-Sanford et al., 2009), that may act on resident microbial communities independently of the WWTP plasmidome. The absence of tetracycline resistance genes in Mungia, in contradiction to its phenotype during the antibiotic susceptibility test, may reflect chromosomally-encoded rather than plasmid-borne determinants that may include tetracycline resistance genes or efflux systems not captured under the mating conditions and analysis employed.

Taken together, the differential ARG content between the two WWTP-captured plasmid populations, despite shared backbone architecture revealed by the similarity network analysis, is most parsimoniously explained by site-specific selective pressure acting on a common regional plasmid pool. This pattern mirrors the architecture described for IncN plasmids from WWTP effluents, which share conserved backbone modules while accommodating diverse accessory resistance modules shaped by local selective pressures (Schlüter et al., 2007). Prior work demonstrates that accessory gene content of environmental plasmids directly reflects the selective pressures of their environment (Gatica & Cytryn, 2013). Here, the co-occurrence at Gorliz of clinically relevant antimicrobial resistance genes across multiple classes together with complex integron cassette architectures, suggests sustained and diverse selective pressures, potentially linked to hospital-associated antibiotic inputs. This environment appears to favor the accumulation and co-localization of clinically relevant ARGs within mobile genetic platforms. In contrast, at Mungia, the predominantly agricultural and urban catchment is associated with plasmids that retain conserved conjugative backbones but display lower overall ARG richness and simpler resistance profiles, with fewer multi-class resistance combinations and reduced integron cassette complexity. This pattern is consistent with a comparatively narrower selective landscape shaping the local resistome structure. The backbone thus acts as a conserved conjugative vehicle whose accessory resistance cargo reflects the local selective environment (Gatica & Cytryn, 2013; Schlüter et al., 2007).

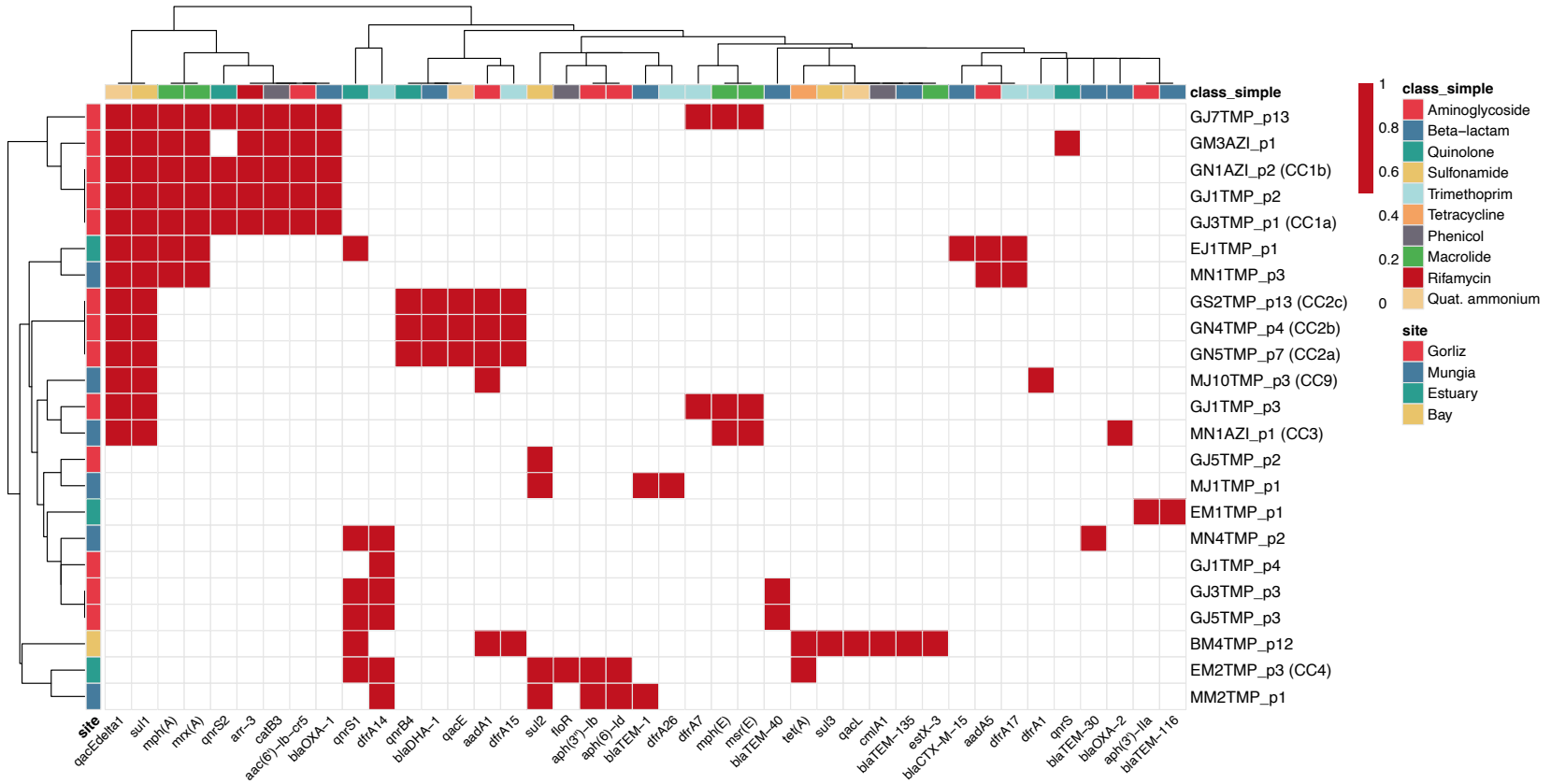

Figure 36. Antimicrobial resistance profile of plasmid bearing-ARGs.

Number of captured ARG-bearing plasmid captured from four different bacterial communities present in Gorliz, Mungia, Estuary and Bay classified by antibiotic class. Heatmap showing presence (colored)/absence (not colored) of ARG conferring resistance to a determined antibiotic class.

To contextualize the backbone conservation of IncN and IncU plasmids within a broader epidemiological framework, it should be noted that despite their co-occurrence and shared conjugative capacity in this river basin, these groups belong to distinct relaxase families: IncN plasmids encode MOBF relaxases while IncU plasmids encode MOBP relaxases phylogenetic implications of this distinction are examined through relaxase sequence analysis in the following section (Garcillán-Barcia et al., 2009).

Relaxase phylogeny and plasmid evolutionary relationships

To investigate the evolutionary relationships among the 65 plasmids recovered in this study, maximum likelihood phylogenetic trees were inferred separately for the two most represented relaxase families represented by 11 plasmid entities each: MOBF and MOBP; based on aligned and trimmed relaxase protein sequences using IQ-TREE2 with automated model selection and 1000 ultrafast bootstrap replicates. Relaxases are the key enzymes that initiate plasmid conjugative transfer by introducing a site-specific nick at the origin of transfer (*oriT*) (Guzmán-Herrador & Llosa, 2019), thereby enabling the mobilization of plasmid DNA during HGT. Relaxase-based mobility (MOB) typing provides a robust framework for plasmid classification, as relaxase phylogeny is largely congruent with the evolutionary history of conjugative transfer systems (Garcillán-Barcia et al., 2009) .

The MOBF relaxase tree revealed a largely unresolved topology consistent with high sequence diversity among plasmids sharing this relaxase family across sites (Figure 37A), reflecting the modular evolution of plasmid backbones driven by recombination and HGT acquisition (Garcillán-Barcia et al., 2009). All 11 plasmids in the MOBF tree carried IncN replicons. Several IncN plasmids carried TMP, sulfonamide, and beta-lactam resistance genes alongside integrons and IS elements, while others lacked detectable ARGs entirely. Notably, within this MOBF group, only metal resistance genes were detected in plasmids from Mungia samples, suggesting site-specific selective pressures shaping accessory gene content. This suggests that ARG acquisition is an independent evolutionary event not correlated with relaxase phylogeny within this family but due to gene cassette capture as described before. Three Beta-lactam variants were detected in the three distinct sampling sites: $bla_{\text{TEM-1}}$ (Mungia), $bla_{\text{TEM-30}}$ (Estuary), and $bla_{\text{TEM-40}}$ (Gorliz). These variants arise from point mutations in $bla_{\text{TEM-1}}$ conferring resistance to beta-lactamase inhibitors such as clavulanic acid, likely selected by amoxicillin-clavulanate use. The detection of similar profile in Mungia and Estuary could suggest shared backbone from which differential selective pressures and HGT events resulted in differential accessory gene acquisition, nonetheless resolution in the tree was

limited. Interestingly, a well-supported clade (bootstrap 100) grouped three IncN plasmids from three different sites (Gorliz, Mungia and Estuary), and time points (winter, spring, and autumn). This is consistent with active inter-site dissemination of a conserved MOBF/IncN backbone and high similarity shown in mash distances distribution.

The MOBP relaxase tree revealed a clearer phylogenetic structure with three well-defined groups (Figure 37B). A basal clade (bootstrap 70) comprised exclusively rep_cluster_827 plasmids, including EM3TMP-p5 (estuary), GM2AZI-p4 (Gorliz), and MN3AZI-p8 (Mungia) representatives. This group lacked detectable ARGs, IS elements, and integrons entirely, representing the most ancestral and cargo-free lineage in the MOBP tree. A second, more derived clade included GJ5TMP-p2 and GJ5TMP-p11 (rep_cluster_827), also largely devoid of ARGs. Moreover, GJ5TMP-p2 was the only Gorliz-derived isolate carrying metal resistance genes (mercury and arsenic resistance), which coincided with a higher number of insertion sequences, suggesting a possible role of IS elements in their acquisition. The most derived and best-supported clade (bootstrap 97–100) showed a clear bifurcation between IncP plasmids and IncU plasmids. The single IncP representative (MN1AZI-p1, CC3) carried macrolide resistance genes [*mph(E)*, *msr(E)*] along with mercury heavy metal resistance associated to integron, while the five IncU plasmids formed a monophyletic group (bootstrap 100). This group comprised plasmids captured along three seasons (winter, spring, and autumn) all carrying a conserved quinolone and aminoglycoside resistance cassette [*qnrS2, aac(6')-Ib-cr5, catB3, qacEΔ1, sul1 and mph(A)*] alongside multiple IS elements (3–9 per plasmid) and integrons, consistent with the clonal CC1 lineage characterized earlier. Within this group, GJ7TMP-p13 stands out as its profile acquired in addition an integron-based ARG capture of *mph(E), msrE* and *dfrA7,* in agreement with previous identified high integron complexity. The progressive increase in ARG content, IS element burden, and integron frequency from the basal rep_cluster_827 clade to the derived IncU clade suggests a stable plasmid lineage and evolutionary trajectory of increasing cargo gene accumulation associated with diversification of the MOBP relaxase lineage in this study area.

Collectively, the relaxase phylogenies provide an evolutionary framework that complements and extends the site-level ARG distribution patterns. The phylogenetic trees indicate that this divergence follows predictable evolutionary trajectories: cargo-free ancestral lineages, represented by the basal rep_cluster_827 and the ARG-free IncN branches, circulate across all sites while derived lineages with accumulated ARG cassettes, IS elements, and integrons are enriched at sites subject to stronger or more clinically derived selective pressure. The monophyletic IncU group at Gorliz, carrying a conserved *qnrS2/aac(6')-Ib-cr5*

cassette alongside high IS element burden, exemplifies a lineage that has undergone recurrent and active cargo accumulation under sustained fluoroquinolone selection, consistent with the clinical and hospital-influenced inputs characterizing that catchment. In contrast, the persistence of cargo-free MOBF/IncN and rep_cluster_827 backbones across all sites, including Mungia and Estuary, supports the view that the regional plasmid pool maintains a reservoir of transfer-competent but resistance-free elements that can serve as vehicles for future ARG acquisition.

A

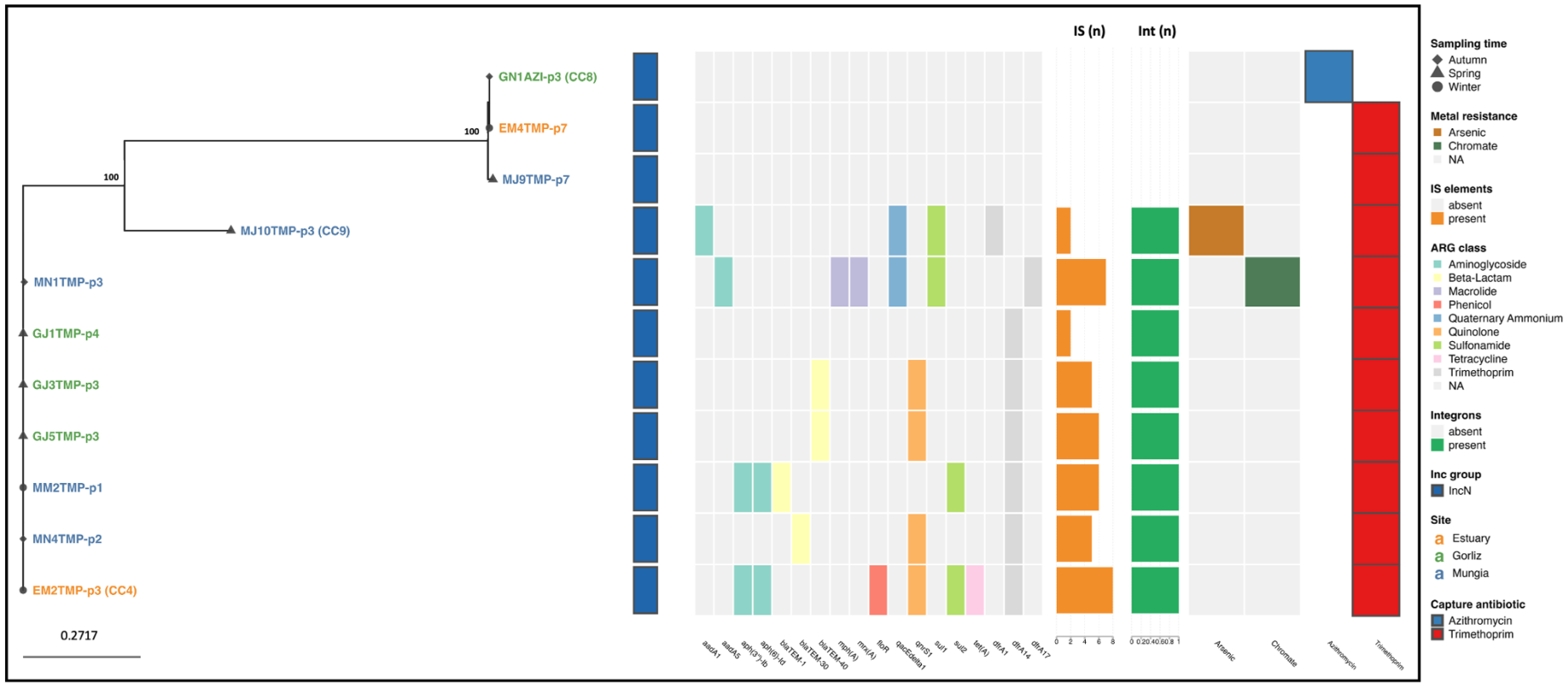

Figure 37 continue

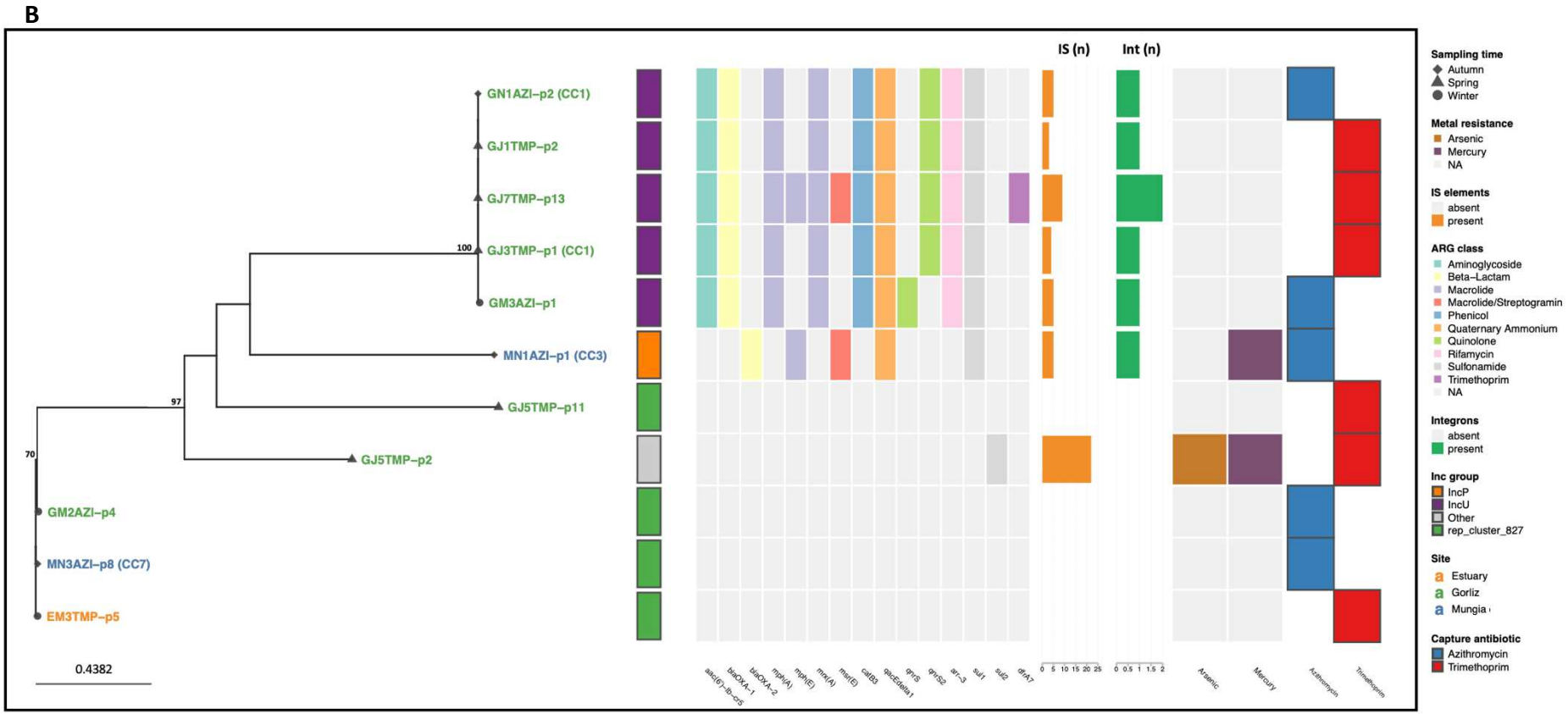

Figure 37. Maximum likehood phylogeny of (A) MOBF relaxase and (B) MOBP-relaxase proteins.

Branch lengths represent substitutions per site. Boostrap values ≥70 are shown at nodes. Tip labels are colored by sampling site. Tip shapes indicate sampling time point. The heatmap shows incompatibility group (Inc), presence/absence of ARG classes, metal resistance genes, IS element count, integron count (Int), and strategy capture antibiotic (trimethorpim:sulfamethoxazole or azithromycin).

Beyond conjugative and mobilizable plasmids

Non-typable plasmid characterization

Ten plasmids in the representative plasmid entities (23.3%) lack detectable replicon sequences by PlasmidFinder and are hereafter referred to as non-typable elements. Difficulties associated to the classification approach based on replicon typing had been previously reported reflecting either the use of novel or divergent replication systems not covered by current databases, or the presence of fundamentally different types of autonomously replicating elements (Shintani et al., 2015).

Among the non-typable elements, two CCs were classified as phage-plasmid elements based on their gene content. Cluster CC5 (representative: GN4TMP-p1, 4.6 kb, n=3) members at Gorliz carries a single annotated CDS corresponding to an integrase of the phage integrase family (COG L), with no detectable replication, transfer, or structural genes, consistent with a minimal satellite phage element or a highly truncated prophage remnant that maintains autonomous replication through an uncharacterized mechanism. Cluster CC6 (representative: GN4TMP-p3, 15.2 kb, n=3) includes members at Gorliz and Mungia and presents a markedly more complex gene repertoire characteristic of phage-plasmid hybrid elements: it encodes a phage integrase (*intE*), an excisionase (*xisE*), a site-specific invertase (*pinE*) responsible for the host-range switching inversion identified in sequence alignment, tail fiber assembly proteins (*tfaE*, *stfP*), the phage kill switch protein Lit, and multiple regulatory genes (*cohE*, *croE*). The co-occurrence of phage structural genes with autonomous replication capacity places CC6 within the emerging category of "phage-plasmids" defined as elements that blur the boundary between temperate bacteriophages and plasmids (Pfeifer & Rocha, 2024) combining phage-derived replication and structural modules with plasmid-like extrachromosomal maintenance. Such elements have been increasingly recognized in environmental metagenomes and clinical isolates, where they may serve as vehicles for HGT independently of both canonical plasmid and phage biology.

The remaining eight non-typable singletons ranged from 0.5 to 41.6 kb and showed diverse functional profiles (Figure 38). GJ1TMP-p6 (39.1 kb) was the only non-typable element with a detectable relaxase (MOBP family), classifying it as a non-typable conjugative plasmid, likely carrying a replicon not covered by current PlasmidFinder databases. In addition, the sequence was compared against the PLSDB database and partial match was observed, corresponding to 35.8% coverage of a reference plasmid from *Cronobacter dublinensis* plasmid. Several larger non-typable elements (MN4TMP-p3, MJ9TMP-p8, GM2AZI-p6) showed functional profiles dominated by Secretion/Trafficking (COG U) annotations, suggesting the presence of T4SS

components and possible conjugative capacity despite the absence of a detectable relaxase, a pattern consistent with MOBH-family or highly divergent transfer systems. MN2TMP-p4 (41.6 kb) showed the most diverse functional profile including metabolic genes, suggesting it may represent a large cryptic plasmid with host-adaptive cargo. Two elements (MN4TMP-p3 and GN5TMP-p2) had no PLSDB hit, representing the most divergent elements in the dataset with no close relatives in public databases.

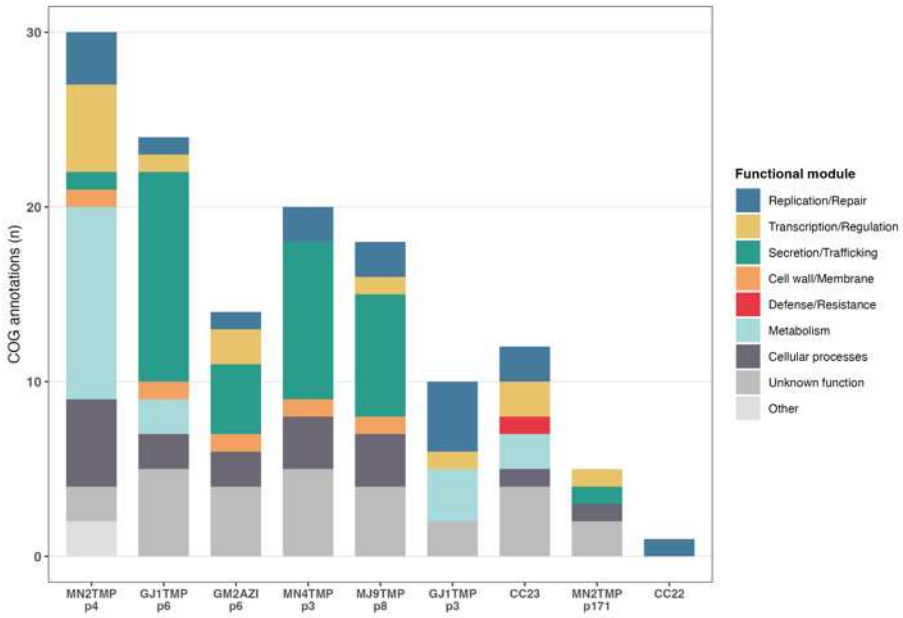

Figure 38. Functional profile of non typable captured plasmids.

Function assignation was based on eggNOG database.

Chromosomic insertion sequences

Whole-genome sequencing of the *E. coli* K-12 BW25113-*gfp* recipient strain following conjugation experiments revealed three independent chromosomal insertions absent from the parental strain, demonstrating that conjugation events from wastewater donors mobilize a broader range of genetic elements beyond plasmids alone (Figure 39). In the GM2AZI experiment, a 30,724 bp insertion carrying hallmark genes of lambda/P2-like prophages (*int, cII, lysB, lysC, gpG, gpV*) was identified and confirmed as an intact prophage by PHASTEST (completeness score 150), with highest similarity to phage 186 (PHAGE_Entero_186_NC_001317, 37 hit genes), a well-characterized P2-like temperate phage of *E. coli* known to serve as helper for P4-like satellite elements (Briani et al., 2001; Nilsson & Haggård-Ljungquist, 2007). This finding is directly relevant to the two P4-like phage-plasmids CC6 identified in this study: the co-circulation of both a P4-like satellite (extrachromosomal) and a compatible P2/186-like helper (integrated) within the same wastewater environment supports

the hypothesis that both elements of the P4-P2 parasitism system are active in WWTP bacterial communities. P2-like phages are prevalent in *E. coli* (Nilsson & Haggård-Ljungquist, 2007), yet their extrachromosomal phage-plasmid form is rarely captured experimentally making the simultaneous detection of both forms in this study particularly noteworthy, given the often underrepresented extrachromosomal phage-plasmid state in conventional genomic surveys.

The GN6TMP insertion (+15,814 bp; Figure 39) is of greatest clinical significance within the resistome context. It encodes the complete AcrEF-TolC multidrug efflux system (*acrE, acrF, acrS*) alongside the global transcriptional regulator *fis*, embedded within a genomic island structure. AcrAB-TolC efflux activity preserves resistance acquisition by plasmid transfer even in the presence of translation-inhibiting antibiotics (Nolivos et al., Science, 2019), and the functionally homologous AcrEF-TolC system confers broad-spectrum resistance to fluoroquinolones, beta-lactams, and other drug classes. Activation of the Cpx response upregulates AcrD-TolC efflux, further linking envelope stress signaling to multidrug resistance (Masi et al., 2017). The HGT of genomic islands carrying intact efflux pump operons alongside conjugative plasmids has been documented in clinical Enterobacteriaceae (Partridge, 2011) but its direct observation in wastewater conjugation experiments is less frequently reported.

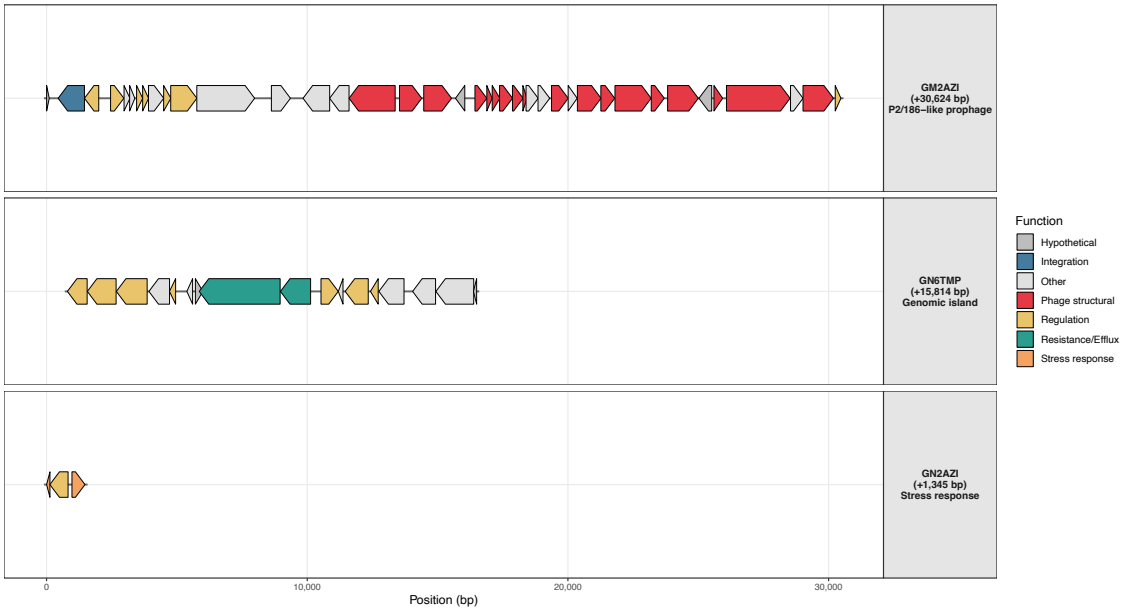

Figure 39. Chromosomal insertion sequences detected in *E. coli* BW25113 transconjugants.

The smallest insertion, detected in the GN2AZI experiment (+1,345 bp, cpxR, cpxP; Figure 39), encodes the CpxAR two-component envelope stress response system. As mentioned, CpxAR controls Fosfomycin resistance in *E. coli* through direct repression of drug uptake transporters. Interestingly, elevated CpxR-P levels reduce conjugation efficiency while simultaneously

conferring increased resistance to aminoglycoside antibiotics, suggesting a complex trade-off between HGT capacity and intrinsic resistance in recipient bacteria acquiring this element.

Collectively, these results demonstrate that environmental bacterial community donors can mobilize not only plasmids but also intact prophages, resistance-encoding genomic islands and regulatory stress-response elements simultaneously, substantially broadening the genetic remodeling potential of recipient bacteria beyond what plasmid transfer alone would predict.

PART IV
GENERAL DISCUSSION

The dissemination of AMR through HGT in environmental settings has emerged as a critical dimension of the global AMR crisis (FAO et al., 2022), yet the contribution of chemical stressors to the acceleration of this process remains challenging. The work presented in this thesis was designed to address this gap by investigating whether CECs routinely present in WWTP effluent can modulate conjugative plasmid transfer, and if so, through what mechanisms, across which plasmid systems, and with what ecological consequences in a real wastewater-impacted river-coastal continuum. The results obtained across the four chapters collectively support the central hypothesis while revealing a complexity that substantially refines it: chemical modulation of conjugative plasmid does occur, it is environmentally relevant at compound-level, and it is mechanistically grounded. However, it is not a uniform or generalizable phenomenon, being compound-specific, plasmid-specific, and ultimately inseparable from the ecological and catchment-level context in which it occurs.

The first challenge confronted by this thesis was the issue of scale. The chemical diversity of the environmental exposome is vast, and classical experimental approaches cannot keep pace with the rate at which new contaminants enter aquatic environments. The ML framework developed in Chapter 1 addressed this bottleneck directly, demonstrating that the capacity of a chemical stressor to modulate conjugative transfer frequency is, to a meaningful degree, encoded in its molecular architecture. Morgan fingerprints emerged as the most informative feature class, along with concentrations and species relation involved in the conjugation process under controlled conditions, captures structure–activity relationships that are not accessible through concentration-based or categorical analyses alone. This finding carries an important mechanistic implication: compounds belonging to entirely different pharmacological or commercial classes can converge on similar biological (Y. Liu et al., 2020) outcomes because they share structural features that interact with conserved elements of the conjugative transfer machinery or its regulatory circuits. The model thus provides a principled basis for chemical prioritization and experimental triage, enabling the identification of compounds most likely to warrant further investigation without requiring exhaustive experimental screening. Its limitations, however, are equally informative. Residual unexplained variance reflects the genuine biological complexity of conjugation dynamics, and the model´s reduced predictive performance at environmentally relevant CECs concentrations directly exposed the critical gap between the current state of the published literature and the experimental data requirements of robust predictive modelling. The reporting bias toward positive outcomes, the scarcity of standardized experimental metadata, and the near-absence of conjugation data at

environmentally realistic concentrations in the training group are not merely technical constraints but a reflection of how the field has historically framed the problem. Closing this gap is a prerequisite for the next generation of predictive tools, and the experimental work of this thesis represents a step in that direction.

The systematic experimental investigation carried out in Chapter 2 provided the most direct and mechanistically detailed test of the central hypothesis. The demonstration that structurally and functionally diverse CECs can promote conjugative plasmid transfer at concentrations between 0.001 and 0.01 μg mL^{-1} establishes unambiguously that the universe of chemical stressors relevant to environmental HGT risk assessment extends well beyond antibiotics. This finding is significant because of the concentration range at which it operates: these are sub-inhibitory, environmentally realistic exposures that would not trigger conventional ecotoxicological endpoints, yet they are sufficient to accelerate the transfer of resistance plasmids between bacterial cells. Equally important is what Chapter 2 revealed about the nature of this effect: it is not uniform, not monotonic, and not explained by a single commonly known mechanism. The magnitude and direction of the modulatory effect were strongly plasmid-dependent, and by introducing a third experimental system in which the IncF plasmid was placed in the UB1637 donor background, it was possible to demonstrate that this differential response is not a property of the donor strain but of the regulatory architecture of the plasmid itself. These differences suggest how the cooperative repressor network governing IncP transfer may amplify small perturbations in regulator activity into large changes in transfer gene expression across the donor population, while the multilayered FinOP-mediated repression and cooperative promoter activation requirements of IncF transfer create a high-threshold circuit that intrinsically buffers against sub-inhibitory chemical stimuli. This mechanistic distinction requires further investigation to elucidate the mechanisms underlying this differential response which is critical for understanding which resistance plasmid families pose the greatest HGT risk under chemical pressure in contaminated environments.

The compound-specific mechanistic investigation further demonstrated diffuse and variable mechanistic pathways. Critically, the consistent dissociation between conjugation-inducing concentrations and those required to elicit detectable bulk stress responses challenges the prevailing mechanistic models in the literature, which have attributed CECs-enhanced conjugation primarily to oxidative stress and membrane disruption (L. G. Li & Zhang, 2023; Y. Liu et al., 2020). It instead points to subpopulation-level processes operating below the detection threshold of bulk assays, a conclusion supported by the population heterogeneity framework: in IncF systems, FinOP-mediated repression ensures that only a small fraction of cells is transfer-

competent at any given time, and chemical perturbation at low concentrations may preferentially activate this pre-existing subpopulation without generating population-wide signals. The high replicate variability and absence of monotonic dose-response relationships observed at low concentrations are consistent with stochastic fluctuations in the proportion of transfer-competent cells rather than with a deterministic concentration-driven response, a distinction with fundamental implications for both mechanistic interpretation and experimental design. Perhaps the most striking single illustration of the inadequacy of single-system risk assessment was the behavior of benzalkonium chloride, which inhibited IncF transfer while strongly inducing IncP transfer at identical concentrations, demonstrating that not only the magnitude but the directionality of the effect is plasmid-specific and that no generalizations across Inc groups can be safely made on the basis of data from a single plasmid system.

The transition from controlled laboratory conditions to the real environmental conditions of the Butroe river basin, undertaken in Chapters 3 and 4, revealed both the ecological relevance and the contextual limits of the laboratory findings. The modest and variable modulatory effect of WWTP effluents tested directly as biological matrices on conjugative transfer indicates that chemical induction of conjugation is unlikely to be the primary driver of ARGs dissemination at the ecosystem scale under ambient conditions. This does not invalidate the mechanistic findings of Chapter 2 but it contextualizes them in an important way: laboratory-demonstrated induction does not translate linearly into equivalent ecosystem-scale effects, and risk communication must reflect this distinction. What the environmental data revealed instead is that the resistome of the basin is shaped primarily by the cumulative selective history of each catchment rather than by instantaneous chemical exposure, and that the integron-plasmid mobilization fraction constitutes the dominant and treatment-resistant vehicle for ARGs capture and dissemination regardless of the specific chemical profile of the effluent. Both WWTPs export this major abundance fraction despite conventional biological treatment, confirming that current wastewater management practices are insufficient to eliminate the primary genetic infrastructure of environmental AMR transfer.

The two catchments shared high similar profiles in the qualitative nature of the resistance determinants they exported. Nonetheless, key divergence was directly traceable to their respective inputs. The industrial catchment at Mungia drove enrichment of co-resistance markers associated with metal and biocide tolerance, illustrating the capacity of non-antibiotic industrial chemical selection to co-select for AMR through shared genetic determinants on mobile elements. This finding connects the chemical exposome data of Chapter 3 directly to the resistance gene content of the mobilizable plasmidome characterized in Chapter 4. The

catchment at Gorliz was associated with carbapenemase genes co-clustering with mobilizable IncQ and IncW replicons of clinical origin, a finding of considerable public health concern given the absence of UV disinfection and advanced tertiary treatment at this facility, with direct marine discharge. Although these genes were presented as minor contributors because of their low abundances, the combination of these factors identifies Gorliz as potentially the higher-risk point source for clinically relevant resistance plasmids entering the coastal environment. Hydrological conditions appear to play a key role in the homogenization of ARG abundances along the hydraulic continuum, consistent with a dilution effect driven by increasing water flow and mixing downstream. However, this dilution signal is gene-dependent, as some resistance determinants appear more sensitive to attenuation than others. This pattern is disrupted by episodic rainfall events, which introduce marked heterogeneity through stormwater overflow and sediment resuspension, effectively overriding the dilution-driven homogenization and weakening the continuity of the resistome along the system.

The molecular characterization of the mobilizable plasmidome in Chapter 4 translated the resistome patterns of Chapter 3 into a plasmid-level understanding of the genetic vehicles through which ARGs circulate in the basin. The recovery of a conserved core plasmid backbone shared across sites and seasons further confirmed the similar qPCR resistome profile characterized in Chapter 3. Mobile genetic elements profiling also confirmed the active conjugative transfer potential of the integron-plasmid axis under real environmental conditions. The inter-site connectivity mediated primarily by IncN replicons establishes a basin-wide dissemination pathway. The site-specific enrichment of IncU at Gorliz and IncP at Mungia demonstrates that replicon distribution is shaped by catchment-level selective pressure rather than by hydrological connectivity alone. The latter finding is particularly significant considering the mechanistic data of Chapter 2: IncP plasmids are also the Inc group most susceptible to CEC-driven transfer induction seen in this study. The relaxase phylogeny further revealed that the two dominant plasmid families (*i.e.,* MOBF/IncN and MOBP/IncU) follow distinct evolutionary trajectories shaped by their respective selective environments, with MOBP/IncU plasmids at Gorliz forming a derived monophyletic lineage with accumulated ARGs cassettes and high IS elements burden consistent with sustained clinical selective pressure. The co-circulation of cargo-free, transfer-competent elements alongside ARG-enriched derivatives within both families represents a standing reservoir for future resistance acquisition, and the detection of integrative elements with evidence of chromosomal insertion among recovered transconjugants demonstrates that the environmental MGE pool of this system extends beyond the plasmid

compartment into bacterial chromosomes, adding a further dimension to the complexity of ARG mobilization in wastewater-impacted coastal environments.

Considered as a whole, the findings of this thesis establish that the environmental dissemination of AMR through conjugative HGT cannot be adequately understood or predicted from any single experimental system, any single compound, or any single scale of analysis. The modulation of conjugative transfer by environmental chemical stressors is real and mechanistically grounded, but it emerges from the intersection of molecular structure, plasmid regulatory architecture, bacterial population biology, and catchment-level selective history in ways that are not reducible to simple concentration–response relationships or generalizable across plasmid types. Risk assessment frameworks that rely on a single plasmid system, a single concentration point, or a single environmental endpoint will systematically mischaracterize the HGT-promoting potential of environmental contaminants (Johnsen & Kroer, 2007; Zhao et al., 2025). Progress in the understanding and governance of environmental AMR requires integrated approaches that operate simultaneously at the molecular, population, and ecosystem scales, and that are embedded within a One Health framework capable of connecting the chemical management of aquatic environments to the surveillance of antimicrobial resistance in clinical, veterinary, and environmental settings. The tools, data, and conceptual frameworks developed in this thesis contribute to that broader effort while making explicit the gaps that future work must address.

PART V
CONCLUSIONS

The main conclusions of this thesis are:

1. A machine learning framework integrating Morgan fingerprints with concentration and experimental metadata predicted CEC effects on conjugative transfer frequency with reasonable cross-validation performance (R^2=0.719), with structural fingerprints as the dominant predictive feature. Performance declined at environmentally relevant concentrations with narrow fold-change ranges, reflecting underrepresentation of this chemical space in training data. **Standardized, systematically generated experimental datasets covering environmentally relevant exposure scenarios are an essential prerequisite for the next generation of predictive HGT risk assessment tools.**

2. Contaminants of emerging concern (CECs)-mediated modulation of conjugative transfer is plasmid-specific, determined by regulatory architecture rather than donor strain identity, as exemplified by a quaternary ammonium disinfectant producing diametrically opposed effects on IncF and IncP conjugation at identical concentrations. **Collectively, these findings establish that conjugation influenced by CECs is more heterogeneous than current models predict,** and that **plasmid Inc group is a critical variable that must be accounted for in any experimental or regulatory framework assessing the HGT-promoting potential of environmental contaminants.**

3. Plasmid-specific variation in chemical sensitivity demonstrates that **single-system conjugation assays are insufficient for comprehensive HGT risk assessment, and conclusions drawn from one incompatibility group cannot be generalized to others.**

4. Wastewater treatment effluent tested directly as biological matrices exerted a modest and variable effect on conjugative transfer, indicating that chemical induction of conjugation is unlikely to be the primary driver of downstream ARG dissemination at the ecosystem scale. **The environmental significance of laboratory-demonstrated CEC-driven HGT induction is therefore mediated by matrix complexity, mixture interactions, and catchment-level context, and does not translate linearly from single-compound assays to environmental exposure conditions.**

5. Both Gorliz and Mungia wastewater treatment plants (WWTP) export a treatment-resistant resistome core dominated by class 1 integron-associated genes and broad-host-range IncP replicons, demonstrating that **conventional biological treatment is insufficient to eliminate the integron–plasmid mobilization module that constitutes the primary vehicle for ARG dissemination in wastewater-impacted aquatic environments.**

6. Catchment identity is a primary determinant of resistome and mobilizable plasmidome composition in WWTP effluent. Industrial inputs in Munguia WWTP drive enrichment of co-resistance markers associated with metal and biocide tolerance.

7. Along the Butroe basin hydraulic continuum, Category 1 (major contributor) ARGs, anchored by integron-associated resistance and co-selection markers, remained detectable in open coastal waters regardless of distance from the discharge point. Category 2 (minor contributor) ARGs showed variable distribution patterns not consistent with simple dilution attenuation, suggesting additional site-specific drivers. Episodic rainfall events introduce substantial variability via storm overflow and sediment resuspension, representing a key confounding factor for coastal resistome surveillance.

8. The mobilizable plasmidome of the Butroe basin is structured into a conserved core backbone and a variable accessory genome shaped by catchment-specific inputs, an organization consistent with the two-component resistome identified metagenomically and confirming active mobilization of resistance genes via the integron–plasmid axis under environmental conditions.

9. Inter-site plasmid connectivity is primarily mediated by IncN replicons circulating across the basin, while site-specific enrichment of IncU at Gorliz and IncP at Mungia demonstrates that **replicon distribution is shaped by catchment-level selective pressure rather than hydrological connectivity alone**. The enrichment of IncP plasmids at the industrially impacted site represents a catchment-specific HGT risk scenario not apparent from resistome profiling alone.

10. The environmental MGE pool of this coastal system extends beyond the plasmid compartment to integrative elements with evidence of chromosomal insertion detected among recovered transconjugants, demonstrating that **ARG transfer in WWTP-impacted environments can involve direct chromosomal integration and is not restricted to plasmid-mediated dissemination.**

PART VI -
APPENDIX

Appendix A

This appendix provides supplementary text, figures and tables supporting the results presented in Chapter 1.

Text A1. Literature Search Strategy and Study Selection

A systematic literature search was conducted in Scopus and the Web of Science (WoS) Collection using Boolean operators. Detailed advanced search for each are detailed below.

Scopus:

TITLE-ABS-KEY (("bacterial conjugation" OR "conjugative transfer" OR "plasmid transfer*" OR "horizontal gene transfer" OR HGT) AND (xenobiotic* OR contaminant* OR pollutant* OR "exogenous compound*" OR exposure OR induc* OR promot* OR inhibit* OR enhance*) AND (plasmid* OR bacteria* OR "antibiotic resistance" OR "resistance gene*")) AND PUBYEAR > 2014 AND PUBYEAR < 2026

Web of Science:

TS = (("bacterial conjugation" OR "conjugative transfer" OR "plasmid transfer*" OR "horizontal gene transfer" OR HGT) AND (xenobiotic* OR contaminant* OR pollutant* OR "exogenous compound*" OR exposure OR induc* OR promot* OR inhibit* OR enhance*) AND (plasmid* OR bacteria* OR "antibiotic resistance" OR "resistance gene*"))

Only articles classified as “Research Articles” in both databases and published between January 1, 2015, and December 10, 2025, were exported to the Rayyan data manager.

Table A1. References from the literature systematic review elected for the study.

No.	Reference.
1	Cao J, Xue B, Yang S, et al. Chlorite and bromate alter the conjugative transfer of antibiotic resistance genes: Co-regulation of oxidative stress and energy supply. J Hazard Mater. 2024;471:134257. https://doi.org/10.1016/j.jhazmat.2024.134257.
2	Chen J, Wang M, Liu H, et al. Novel Substitutes of Phthalate Esters (PAEs) Promote the Propagation of Antibiotic Resistance Genes via Ferroptosis: Implication for the Environmental Safety Evaluation of PAE Substitutes. Environ Sci Technol. 2025;59(39):21052–64. https://doi.org/10.1021/acs.est.5c10489.
3	Cui Y, Gao J, Guo Y, et al. Unraveling the impact and mechanism of antipyretic paracetamol on intergenera conjugative plasmid transfer. Environ Res. 2022;215:114263. https://doi.org/10.1016/j.envres.2022.114263.
4	Ding L, Zhang CM, Jiang HY. Lipid-lowering drug clofibric acid promotes conjugative transfer of RP4 plasmid carrying antibiotic resistance genes by multiple mechanisms. J Hazard Mater. 2025;489:137560. https://doi.org/10.1016/j.jhazmat.2025.137560.
5	Ding P, Lu J, Wang Y, et al. Antidepressants promote the spread of antibiotic resistance via horizontally conjugative gene transfer. Environ Microbiol. 2022;24(11):5261–76. https://doi.org/10.1111/1462-2920.16165.
6	Feng M, Ye C, Zhang S, et al. Bisphenols promote the conjugative transfer of antibiotic resistance genes without damaging cell membrane. Environ Chem Lett. 2022;20:1553–60. https://doi.org/10.1007/s10311-022-01397-x.
7	Gao Y, Guo Y, Wang L, et al. Tebuconazole exacerbates co-occurrence and horizontal transfer of antibiotic resistance genes. Pestic Biochem Phys. 2024;204:106026. https://doi.org/10.1016/j.pestbp.2024.106026.
8	Guo A, Zhou Q, Bao Y, et al. Prochloraz alone or in combination with nano-CuO promotes the conjugative transfer of antibiotic resistance genes between *Escherichia coli* in pure water. J Hazard Mater. 2022;424:127761. https://doi.org/10.1016/j.jhazmat.2021.127761.
9	Guo MT, Zhang GS. Graphene oxide in the water environment could affect tetracycline-antibiotic resistance. Chemosphere. 2017;183:197–203. https://doi.org/10.1016/j.chemosphere.2017.04.145.
10	Guo Y, Gao J, Cui Y, et al. Chloroxylenol at environmental concentrations can promote conjugative transfer of antibiotic resistance genes by multiple mechanisms. Sci Total Environ. 2022;816:151599. https://doi.org/10.1016/j.scitotenv.2021.151599.
11	Han M, Chen Q, Li Z, et al. Cellular mechanism of perfluoroalkyl substances with different chain lengths influence conjugative transfer of antibiotic resistance genes. Environ Int. 2025;204:109810. https://doi.org/10.1016/j.envint.2025.109810.
12	Han Y, Zhou ZC, Zhu L, et al. The impact and mechanism of quaternary ammonium compounds on the transmission of antibiotic resistance genes. Environ Sci Pollut Res Int. 2019;26(27):28352–60. https://doi.org/10.1007/s11356-019-05673-2.

13 He K, Xue B, Yang X, et al. Low-concentration of trichloromethane and dichloroacetonitrile promote the plasmid-mediated horizontal transfer of antibiotic resistance genes. J Hazard Mater. 2022;425:128030. https://doi.org/10.1016/j.jhazmat.2021.128030.

14 Hu Q, Zhang L, Yang R, et al. Quaternary ammonium biocides promote conjugative transfer of antibiotic resistance gene in structure- and species-dependent manner. Environ Int. 2024;189:108812. https://doi.org/10.1016/j.envint.2024.108812.

15 Huang H, Feng G, Wang M, et al. Nitric Oxide: A Neglected Driver for the Conjugative Transfer of Antibiotic Resistance Genes among Wastewater Microbiota. Environ Sci Technol. 2022;56(10):6466–78. https://doi.org/10.1021/acs.est.2c01889.

16 Huang H, Liao J, Zheng X, et al. Low-level free nitrous acid efficiently inhibits the conjugative transfer of antibiotic resistance by altering intracellular ions and disabling transfer apparatus. Water Res. 2019;158:383–91. https://doi.org/10.1016/j.watres.2019.04.046.

17 Jia Y, Wang Z, Fang D, et al. Acetaminophen promotes horizontal transfer of plasmid-borne multiple antibiotic resistance genes. Sci Total Environ. 2021;782:146916. https://doi.org/10.1016/j.scitotenv.2021.146916.

18 Jia Y, Yang B, Shi J, et al. Melatonin prevents conjugative transfer of plasmid-mediated antibiotic resistance genes by disrupting proton motive force. Pharmacol Res. 2022;175:105978. https://doi.org/10.1016/j.phrs.2021.105978.

19 Jiao YN, Chen H, Gao RX, et al. Organic compounds stimulate horizontal transfer of antibiotic resistance genes in mixed wastewater treatment systems. Chemosphere. 2017;184:53–61. https://doi.org/10.1016/j.chemosphere.2017.05.149.

20 Li G, Gao A, Lu XY, et al. Targeting Plasmid Conjugation with Cinnamic Acid: A Novel Approach to Combat Antibiotic Resistance. Engineering. 2025. https://doi.org/10.1016/j.eng.2025.06.040.

21 Li J, Sun D, Wu J, et al. Lithium enhanced plasmid-mediated conjugative transfer of antimicrobial resistance genes in *Escherichia coli*: Different concentrations and mechanisms. Aquat Toxicol. 2025;279:107263. https://doi.org/10.1016/j.aquatox.2025.107263.

22 Li S, Pang J, Liu Y, et al. Baicalin inhibits conjugative transfer of multidrug-resistant plasmid RP4 by regulating autoinducer-2 transporter protein LsrB. Ecotoxicol Environ Saf. 2025;298:118334. https://doi.org/10.1016/j.ecoenv.2025.118334.

23 Li W, Zhang WG, Zhang MS, et al. Environmentally relevant concentrations of mercury facilitate the horizontal transfer of plasmid-mediated antibiotic resistance genes. Sci Total Environ. 2022;852:158272. https://doi.org/10.1016/j.scitotenv.2022.158272.

24 Li YQ, Zhang CM, Liu Y. Antihistamine drug loratadine at environmentally relevant concentrations promotes conjugative transfer of antibiotic resistance genes: Coeffect of oxidative stress and ion transport. J Environ Manage. 2025;376:124430. https://doi.org/10.1016/j.jenvman.2025.124430.

25	Li Z, Gao J, Guo Y, et al. Enhancement of antibiotic resistance dissemination by artificial sweetener acesulfame potassium: Insights from cell membrane, enzyme, energy supply and transcriptomics. J Hazard Mater. 2022;422:126942. https://doi.org/10.1016/j.jhazmat.2021.126942.
26	Liang SZ, Chang YJ, Semaha P, et al. A maverick: Environmentally relevant concentrations of nonylphenol attenuate the plasmid-mediated conjugative transfer of antibiotic resistance genes. Water Res X. 2024;24:100241. https://doi.org/10.1016/j.wroa.2024.100241.
27	Liao J, Huang H, Chen Y. CO2 promotes the conjugative transfer of multiresistance genes by facilitating cellular contact and plasmid transfer. Environ Int. 2019;129:333–42. https://doi.org/10.1016/j.envint.2019.05.060.
28	Liu C, Goh SG, You L, et al. Low concentration quaternary ammonium compounds promoted antibiotic resistance gene transfer via plasmid conjugation. Sci Total Environ. 2023;887:163781. https://doi.org/10.1016/j.scitotenv.2023.163781.
29	Liu C, Zhu X, You L, et al. Per/polyfluoroalkyl substances modulate plasmid transfer of antibiotic resistance genes: A balance between oxidative stress and energy support. Water Res. 2023;240:120086. https://doi.org/10.1016/j.watres.2023.120086.
30	Liu G, Bao Y, Li Y, et al. A Commonly Used Tire Rubber Antioxidant and its Quinone Derivative Facilitate the Conjugative Transfer of Plasmid-Mediated Antibiotic Resistance Genes in *Escherichia coli*. Environ Sci Technol. 2025;59(47):25402–14. https://doi.org/10.1021/acs.est.5c10086.
31	Liu W, Wang Z, Huang Y, et al. Acetylshikonin reduces the spread of antibiotic resistance via plasmid conjugation. Int J Antimicrob Agents. 2024;64(6). https://doi.org/10.1016/j.ijantimicag.2024.107370.
32	Lu J, Wang Y, Jin M, et al. Both silver ions and silver nanoparticles facilitate the horizontal transfer of plasmid-mediated antibiotic resistance genes. Water Res. 2020;169:115229. https://doi.org/10.1016/j.watres.2019.115229.
33	Lu J, Wang Y, Li J, et al. Triclosan at environmentally relevant concentrations promotes horizontal transfer of multidrug resistance genes within and across bacterial genera. Environ Int. 2018;121:1217–26. https://doi.org/10.1016/j.envint.2018.10.040.
34	Lu J, Zhang H, Pan L, et al. Environmentally relevant concentrations of triclosan exposure promote the horizontal transfer of antibiotic resistance genes mediated by Edwardsiella piscicida. Environ Sci Pollut Res Int. 2022;29(43):64622–32. https://doi.org/10.1007/s11356-022-20082-8.
35	Ma J, Huang Z, He Y, et al. Mechanisms for disinfection-driven conjugative spread of antibiotic resistance in drinking water biofilms. J Water Process Eng. 2025;76:108175. https://doi.org/10.1016/j.jwpe.2025.108175.
36	Ma X, Zhang X, Xia J, et al. Phenolic compounds promote the horizontal transfer of antibiotic resistance genes in activated sludge. Sci Total Environ. 2021;800:149549. https://doi.org/10.1016/j.scitotenv.2021.149549.

37 Pu Q, Fan XT, Li H, et al. Cadmium enhances conjugative plasmid transfer to a fresh water microbial community. Environ Pollut. 2021;268:115903. https://doi.org/10.1016/j.envpol.2020.115903.

38 Rong L, Zhang B, Qiu H, et al. Significant generational effects of tetracyclines upon the promoting plasmid-mediated conjugative transfer between typical wastewater bacteria and its mechanisms. Water Res. 2025;287:124290. https://doi.org/10.1016/j.watres.2025.124290.

39 Wang H, Shen X, Zhang C, et al. Effects of plasticizer on removal of antibiotics and antibiotic resistance genes from agricultural soils via soil microbial fuel cells. Pedosphere. 2024;34(6):981–92. https://doi.org/10.1016/j.pedsph.2023.11.001.

40 Wang M, Liu K, Jin W, et al. Mechanistic insight into curcumin-induced conjugative plasmid transfer acceleration: Role of intracellular arginine uptake. Food Microbiol. 2026;133:104895. https://doi.org/10.1016/j.fm.2025.104895.

41 Wang Q, Lu Q, Mao D, et al. The horizontal transfer of antibiotic resistance genes is enhanced by ionic liquid with different structure of varying alkyl chain length. Front Microbiol. 2015;6:864. https://doi.org/10.3389/fmicb.2015.00864.

42 Wang Q, Mao D, Luo Y. Ionic Liquid Facilitates the Conjugative Transfer of Antibiotic Resistance Genes Mediated by Plasmid RP4. Environ Sci Technol. 2015;49(14):8731–40. https://doi.org/10.1021/acs.est.5b01129.

43 Wang X, Yang F, Zhao J, et al. Bacterial exposure to ZnO nanoparticles facilitates horizontal transfer of antibiotic resistance genes. NanoImpact. 2018;10:61–7. https://doi.org/10.1016/j.impact.2017.11.006.

44 Wang Y, Lu J, Mao L, et al. Antiepileptic drug carbamazepine promotes horizontal transfer of plasmid-borne multi-antibiotic resistance genes within and across bacterial genera. ISME J. 2019;13(2):509–22. https://doi.org/10.1038/s41396-018-0275-x.

45 Wang Y, Lu J, Zhang S, et al. Non-antibiotic pharmaceuticals promote the transmission of multidrug resistance plasmids through intra- and intergenera conjugation. ISME J. 2021;15(9):2493–508. https://doi.org/10.1038/s41396-021-01075-w.

46 Wang Y, Yu Z, Ding P, et al. Non-antibiotic pharmaceuticals promote conjugative plasmid transfer at a community-wide level. Microbiome. 2022;10(1):124. https://doi.org/10.1186/s40168-022-01314-y.

47 Wu Q, Du M, Zhang Y, et al. Chlorpyrifos And Chlorpyrifos-methyl Can Promote Conjugative Transfer of Antibiotic Resistance Genes. BIO Web Conf. 2023;59:01015. https://doi.org/10.1051/bioconf/20235901015.

48 Xiong J, Hu S, Xu Z, et al. Different paths, same destination: Bisphenol A and its substitute induce the conjugative transfer of antibiotic resistance genes. Chemosphere. 2024;368:143625. https://doi.org/10.1016/j.chemosphere.2024.143625.

49	Xu J, Ding D, Fan Y, et al. The overlooked risk of horizontal transfer of plasmid-borne antibiotic resistance genes induced by synthetic phenolic antioxidants. J Hazard Mater. 2025;488:137459. https://doi.org/10.1016/j.jhazmat.2025.137459.
50	Xu Y, Yu W, Wang X, et al. Impact of low-dose free chlorine on the conjugative transfer of antibiotic resistance genes in wastewater effluents: Identifying key environmental factors for predictive modeling. J Hazard Mater. 2025;485:136824. https://doi.org/10.1016/j.jhazmat.2024.136824.
51	Xu Z, Hu S, Zhao D, et al. Molybdenum disulfide nanosheets promote the plasmid-mediated conjugative transfer of antibiotic resistance genes. J Environ Manage. 2024;358:120827. https://doi.org/10.1016/j.jenvman.2024.120827.
52	Xu Z, Li S, Ma Y, et al. Role of organophosphorus pesticides in facilitating plasmid-mediated conjugative transfer: Efficiency and mechanisms. J Hazard Mater. 2025;487:137318. https://doi.org/10.1016/j.jhazmat.2025.137318.
53	Xu Z, Xiong J, Li C, et al. Environmental concentrations of per/polyfluoroalkyl substances promote the conjugative transfer of antibiotic resistance genes. Chem Eng J. 2024;498:155500. https://doi.org/10.1016/j.cej.2024.155500.
54	Xu Z, Ma Y, Li S et al. Molybdenum disulfide regulates antibiotic resistance gene conjugative transfer under different light conditions: Oxidative stress and antioxidant response. Chem Eng J. 2025;506. https://doi.org/10.1016/j.cej.2025.160163.
55	Yan X, Liu W, Wen S, et al. Effect of sulfamethazine on the horizontal transfer of plasmid-mediated antibiotic resistance genes and its mechanism of action. J Environ Sci (China). 2023;127:399–409. https://doi.org/10.1016/j.jes.2022.06.014.
56	Yang B, Sun J, Zhu S, et al. Exposure to bisphenol compounds accelerates the conjugative transfer of antibiotic resistance plasmid. Environ Res. 2024;263:120002. https://doi.org/10.1016/j.envres.2024.120002.
57	Yang B, Wang Z, Jia Y, et al. Paclitaxel and its derivative facilitate the transmission of plasmid-mediated antibiotic resistance genes through conjugative transfer. Sci Total Environ. 2022;810:152245. https://doi.org/10.1016/j.scitotenv.2021.152245.
58	Yang S, Cao J, Zhao C, et al. Cylindrospermopsin enhances the conjugative transfer of plasmid-mediated multi-antibiotic resistance genes through glutathione biosynthesis inhibition. Ecotoxicol Environ Saf. 2024;276:116288. https://doi.org/10.1016/j.ecoenv.2024.116288.
59	Yin L, Wang X, Xu H, et al. Unrecognized risk of perfluorooctane sulfonate in promoting conjugative transfers of bacterial antibiotic resistance genes. Appl Environ Microbiol. 2023;89(9):e00533-23. https://doi.org/10.1128/aem.00533-23.
60	Yu K, Chen F, Yue L, et al. CeO2 Nanoparticles Regulate the Propagation of Antibiotic Resistance Genes by Altering Cellular Contact and Plasmid Transfer. Environ Sci Technol. 2020;54(16):10012–21. https://doi.org/10.1021/acs.est.0c01870.

61 Yu Z, Wang Y, Lu J, et al. Nonnutritive sweeteners can promote the dissemination of antibiotic resistance through conjugative gene transfer. ISME J. 2021;15(7):2117–30. https://doi.org/10.1038/s41396-021-00909-x.

62 Zhai H, Guo Y, Zhang L, et al. Presence of bromide and iodide promotes the horizontal transfer of antibiotic resistance genes during chlorination: A preliminary study. Sci Total Environ. 2022;846:157250. https://doi.org/10.1016/j.scitotenv.2022.157250.

63 Zhang G, Li C, Li X, et al. Ibuprofen prevents the conjugative transfer of plasmid-mediated antimicrobial resistance genes. J Glob Antimicrob Resist. 2025;42:10–4. https://doi.org/10.1016/j.jgar.2025.01.012.

64 Zhang H, Song J, Zheng Z, et al. Fungicide exposure accelerated horizontal transfer of antibiotic resistance genes via plasmid-mediated conjugation. Water Res. 2023;233:119789. https://doi.org/10.1016/j.watres.2023.119789.

65 Zhang H, Xu L, Hou X, et al. Ketoprofen promotes the conjugative transfer of antibiotic resistance among antibiotic resistant bacteria in natural aqueous environments. Environ Pollut. 2024;360:124676. https://doi.org/10.1016/j.envpol.2024.124676.

66 Zhang S, Wang Y, Song H, et al. Copper nanoparticles and copper ions promote horizontal transfer of plasmid-mediated multi-antibiotic resistance genes across bacterial genera. Environ Int. 2019;129:478–87. https://doi.org/10.1016/j.envint.2019.05.054.

67 Zhang S, Fang J, Liu H, et al. Enhanced plasmid-mediated conjugative transfer of resistance genes across bacterial species promoted by graphene oxide. Environ Sci: Nano. 2024;11(3):831–45. https://doi.org/10.1039/D3EN00951C.

68 Zhang Y, Rosado-García FM, Puig Peña YP, et al. Sulfonamide metabolites enhance resistance transmission via conjugative transfer pathways. J Hazard Mater. 2025;491:137932. https://doi.org/10.1016/j.jhazmat.2025.137932.

69 Zhao C, Suyamud B, Yuan Y, et al. Effect of non-antibiotic factors on conjugative transfer of antibiotic resistance genes in aquaculture water. J Hazard Mater. 2025;483:136701. https://doi.org/10.1016/j.jhazmat.2024.136701.

70 Zhao H, Liu X, Sun Y, et al. Effects and mechanisms of plant growth regulators on horizontal transfer of antibiotic resistance genes through plasmid-mediated conjugation. Chemosphere. 2023;318:137997. https://doi.org/10.1016/j.chemosphere.2023.137997.

71 Zhao H, Sun Y, Cao X, et al. Effects and mechanisms of chlormequat on horizontal transfer of antibiotic resistance genes through plasmid-mediated conjugation in agro-ecosystems. J Hazard Mater. 2024;479:135639. https://doi.org/10.1016/j.jhazmat.2024.135639.

72 Zhu S, Yang B, Jia Y, et al. Comprehensive analysis of disinfectants on the horizontal transfer of antibiotic resistance genes. J Hazard Mater. 2023;453:131428. https://doi.org/10.1016/j.jhazmat.2023.131428.

73 Zhu S, Yang B, Yu F, et al. Investigation of the impact of widely used pesticides on conjugative transfer of multidrug resistance plasmids. J Hazard Mater. 2024;478:135436. https://doi.org/10.1016/j.jhazmat.2024.135436.

Table A2. Usage group and subgroup categorization. One subgroup may belong to more than one usage group.

Usage group	Usage subgroup
Antimicrobials	Antibiotics
	Disinfectants
	Plant protection products
	Preservatives
Biocides	Disinfectants
	Plant protection products
Disinfection by-products	Inorganic chemicals
	Organic chemical intermediates
Food additives	Additives
	Artificial sweeteners
	Preservatives
Industrial chemicals	Additives
	Endocrine disrupting agents
	Ionic liquids
	Inorganic chemicals
	Organic chemical intermediates
	Pigments
	Pharmaceutical transformation products
	Preservatives
	Rubber additives
	Solvents
Natural products	Additives
	Endocrine disrupting chemicals
	Plant protection products
Nanomaterials	Additives
	Metal nanoparticles
	Metal oxide nanoparticles
Pharmaceuticals non-antibiotics	Anticonvulsants
	Analgesic & Antipyretic
	Antidepressants
	Antihistamines
	Antineoplastic
	Beta-blockers
	Lipid regulators
	Non-steroidal anti-inflammatory drug
	Sleep regulator
	Transformation product
	Contrast agent

Table A3. Performance of linear regression (LR) models predicting the response variable transfer frequency based on reported experimental conditions.

Feature set code	Val RMSE	Val R^2	OF
Time, temperature and species	1.676	-0.659	1.00
Time	1.801	-0.879	1.076
Temperature	1.339	-0.0383	0.30
Species	1.337	-0.0343	0.065

Model performance metrics include the validation coefficient of determination (R^2) and root mean squared error (RMSE). The difference between validation and training performance, denoted as overfitting (OF), is reported for each feature set.

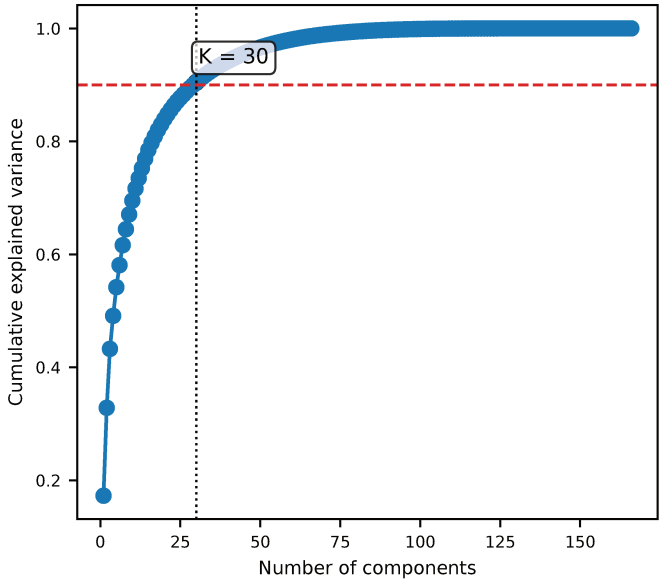

Figure A1. Cumulative explained variance as a function of the number of principal components for MACCs features of elected chemical stressors dataframe.

Appendix B

This appendix provides supplementary figures and tables supporting the results presented in Chapter 2.

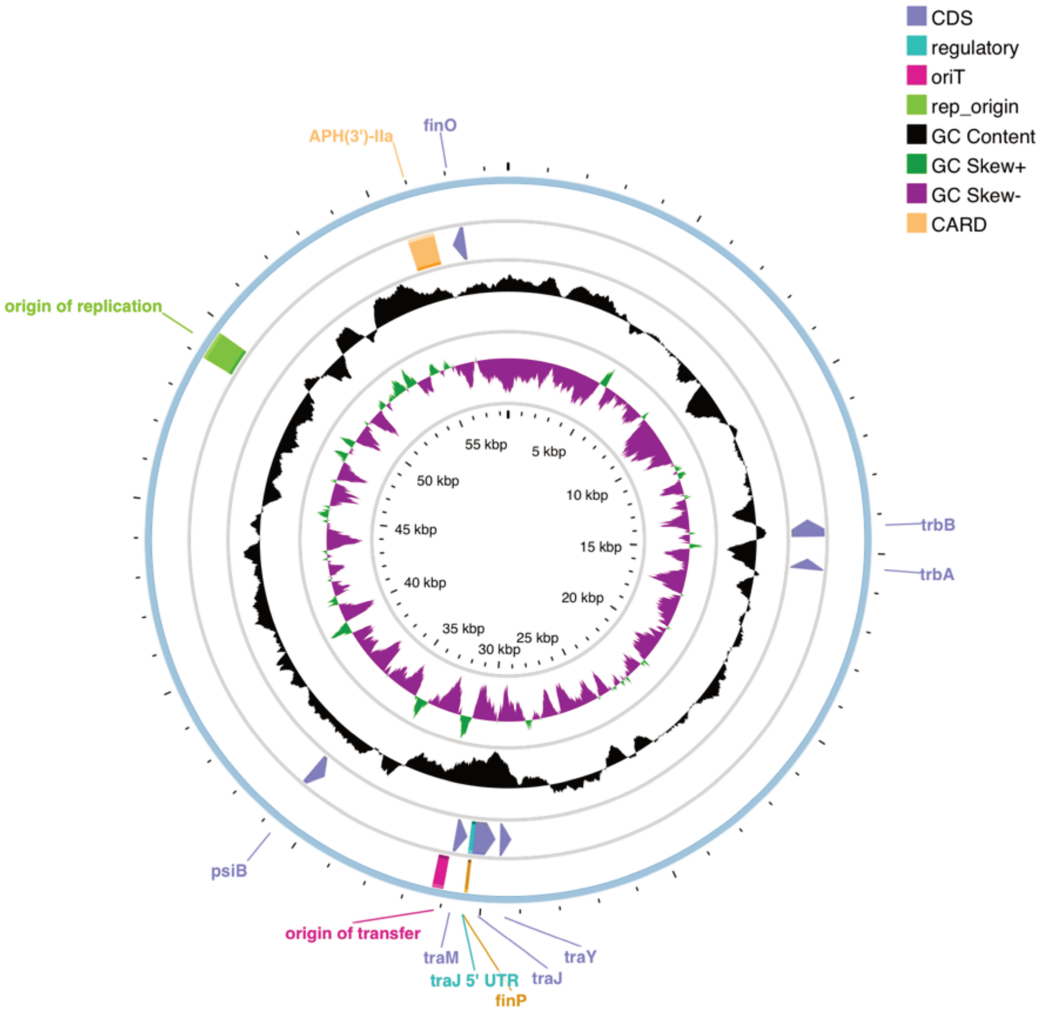

Figure B1. Plasmid genomic map of plasmid IncF used in the study.

Starting from the outermost ring: Backbone, features (+), features (-), GC Content, GC Skew.

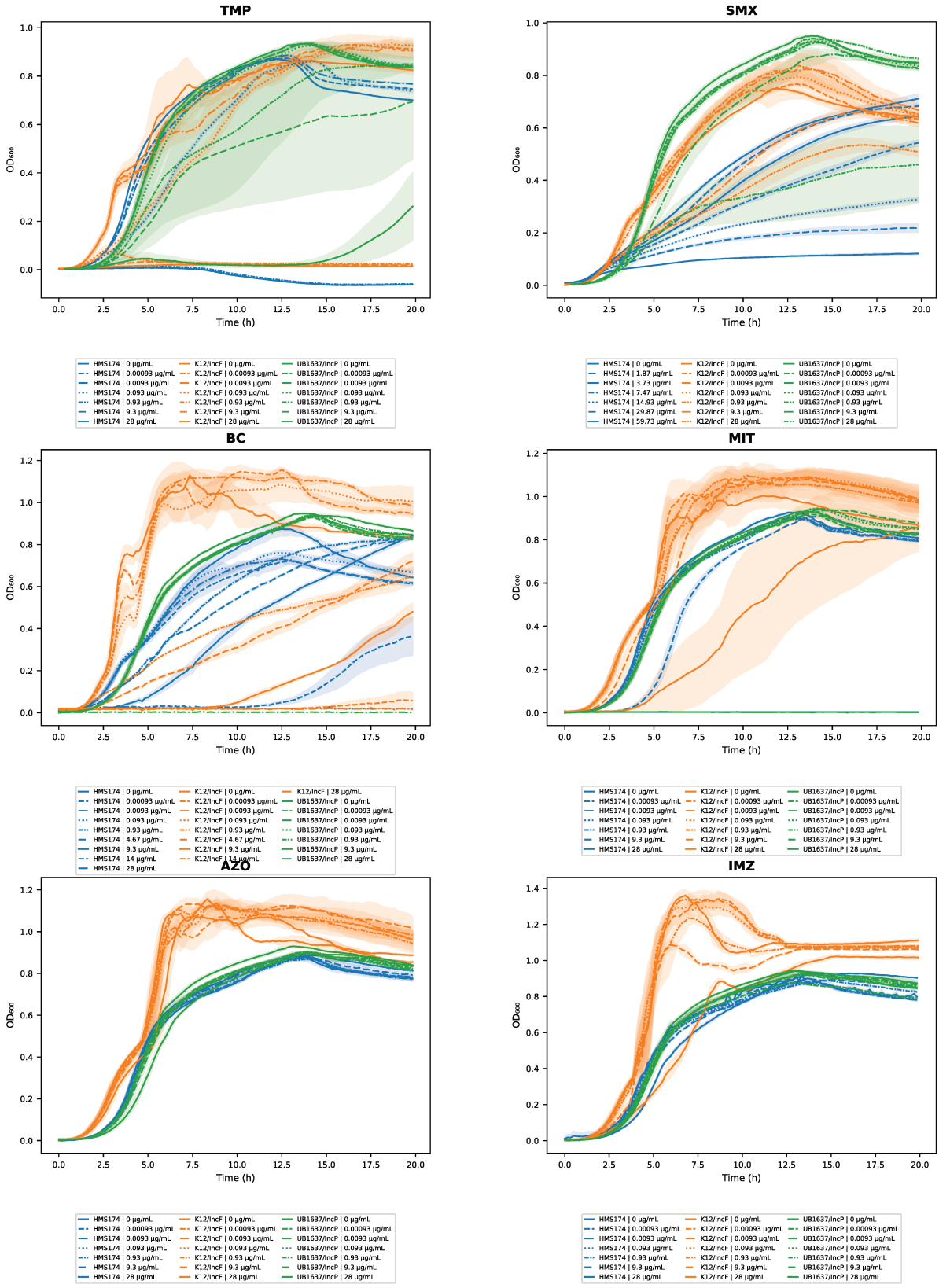

Figure B2 continue

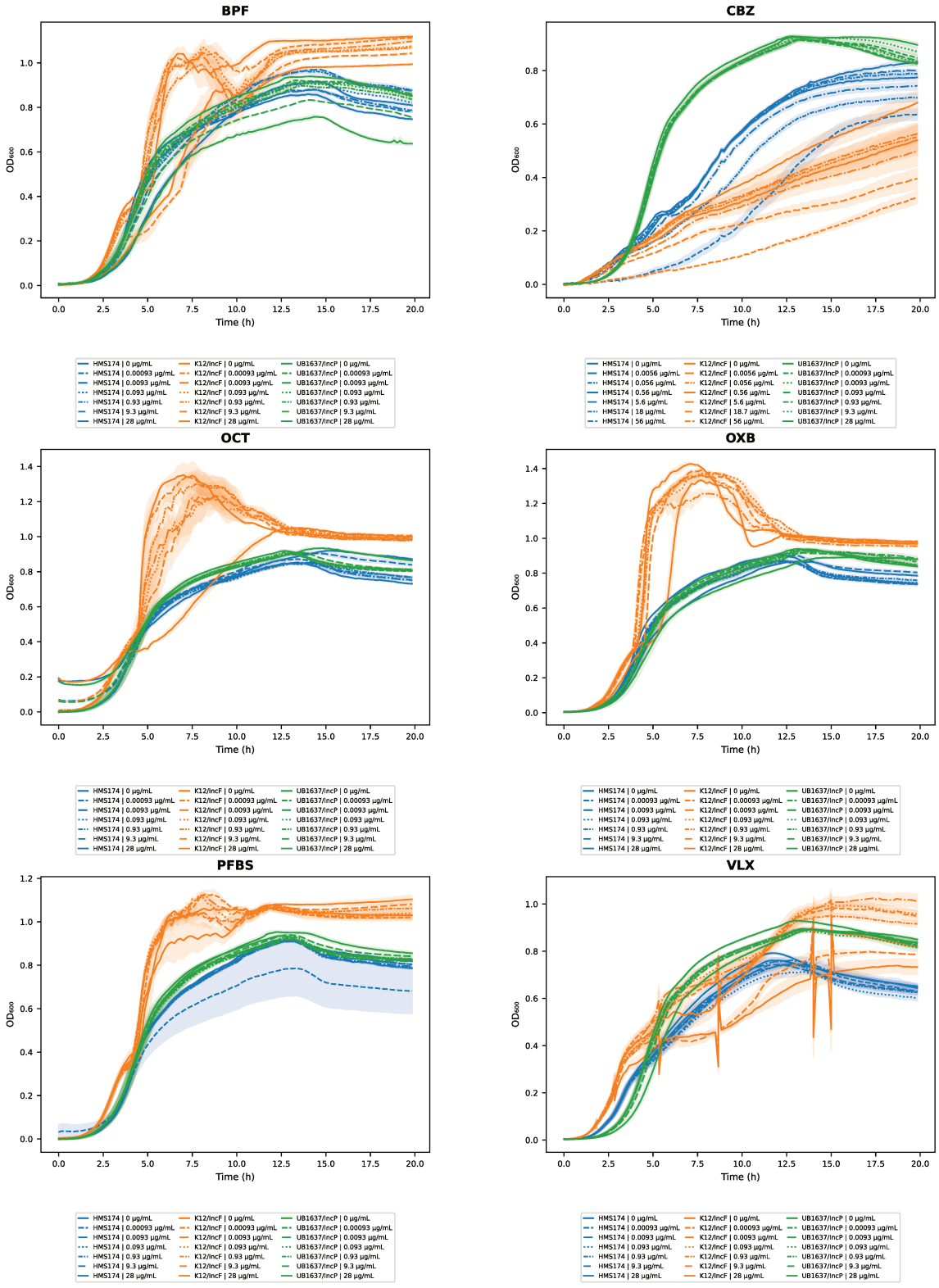

Figure B2. Growth curves of bacterial strains involved in the conjugation experiments.

Measured OD_{600} for 20 h in Recipient strain (*E. coli* HMS174) is colored in blue, donor strain *E. coli* K12/IncF (orange) and donor *E. coli* UB1637/IncP (green) exposed to twelve CECs).

Table B1. Growth inhibition (%) at fixed concentrations extended (AUC- and µ-based).

	E. coli HMS174								*E. coli* K12/IncF								*E. coli* UB1637/IncP							
	AUC (%)				µ (%)				AUC (%)				µ (%)				AUC (%)				µ (%)			
	Concentration (µg mL^{-1})																							
	0.001	0.01	1	10	0.001	0.01	1	10	0.001	0.01	1	10	0.001	0.01	1	10	0.001	0.01	1	10	0.001	0.01	1	10
Antibiotics																								
TMP	0,2	0,02	**103,7**	**104,3**	14,8	22,5	-44,7	-18,30	-1,38	2,76	**95,4**	**96,8**	24,6	**39,6**	n.d.	n.d.	0.5	0.5	**18.7**	**34.9**	6.6	7.7	**56.0**	**56.5**
SMX	*0,00*	*0,00*	*2,6*	***38,2***	*0,00*	*0,00*	*2,00*	***50,6***	-2,89	-9,1	-7,4	22,4	-13,3	-9,96	-15,2	n.d.	3.0	3.9	1.6	12.6	8.0	12.1	13.5	**35.8**
Pharmaceuticals non-antibiotics (P-NAb)																								
CBZ	*2.6*	*2.6*	*3.7*	*12.6*	*0.0*	*0.0*	*0.0*	*10.3*	*13.6*	*13.6*	*16.2*	***31.0***	*17.6*	*17.6*	*17.6*	***32.9***	1.8	1.4	1.5	0.4	7.7	9.6	12.1	11.8
VLX	5,2	2,8	5,77	5,27	15,4	12,1	12,7	10,4	-9,3	-13,0	-6,7	13,1	-3,53	-6,8	-9,4	30	3.4	3.5	3.6	4.7	10.1	11.2	11.2	13.4
Plant Protection Products (PPPs)																								
AZO	-0.2	0.8	1.8	1.0	3.2	4.2	9.8	11.6	-2,5	-5,7	-4,2	-7,1	21,24	16,70	1,95	4,69	3,1	4,2	3,3	4,1	8,6	12,4	10,4	11.9
IMZ	1.5	2.3	2.1	1.9	-6.1	-3.6	9.5	13.7	-2.4	-3.2	2.8	8.9	-0.9	-6.0	3.4	1.6	6.9	2.4	2.0	1.9	10.6	10.2	10.6	12.6
Disinfectants																								
BC	12,3	10,3	9,00	**32,5**	18,5	9	**37,2**	**53,2**	-8,5	-11,1	**52,1**	**83,7**	**33,0**	**30,1**	**90,0**	**88,6**	3.2	2.7	1.9	1.4	8.9	10.7	12.1	17.3
MIT	2.7	2.9	4.0	12.5	6.0	5.8	8.6	2.2	-10,1	-9,5	-6,9	-3,7	-4,7	1,3	7,3	15,1	2.1	1.4	-0.3	-0.5	8.4	9.7	12.0	16.8
Industrial chemicals																								
BPF	-1.2	-0,8	-8.4	-6.5	11.8	16.5	18.6	21.4	0.1	2.7	5.7	19.4	-23.4	-23.5	-6.6	**45.0**	2.2	3.1	5.5	13.1	8.2	12.3	14.0	16.1
PFBS	12.6	0.0	-0.6	-0.3	19.1	2.6	2.9	2.8	-0.7	-1.4	-1.1	-1.2	-14,6	-16.4	-8.7	-7.1	1.5	2.6	1.5	0.3	7.1	9.0	10.3	9.7
Personal care products (PCPs)																								
OCT	-2.1	-0.4	-0.5	-8.0	4.3	5.3	11.5	27.4	-0.2	4.5	0.5	4.5	**50.8**	**71.2**	**64.5**	**77.1**	2.1	1.4	0.8	-0.9	6.8	8.0	7.7	19.8
OXB	3.7	4.2	3.2	-0.2	10.2	11.6	14.8	20.1	-0.9	2.9	-0.2	1.3	0.1	29.9	-2.7	1.8	0.2	1.1	0.4	1.7	6.2	10.3	11.6	17.6

Values represent % inhibition relative to untreated control in LB based on the area under the growth curve (AUC) and maximum specific growth rate (mu) using the Gompertz model. Italic values are values interpolated from fitted 4-parameter logistic model (4PL). Non-italics are directly observed vales. Color labels: yellow>15% inhibition, red>50% inhibition. OCT mu-based values should be interpreted with caution due to artifactual OD_{600} measurements.

Table B2. Conjugation frequency on systems i and ii exposed to 0.01 μg mL^{-1}

		System i K12/IncF					System ii UB1637/IncP				
		Exposure		SEM	Control	SEM	Exposure		SEM	Control	SEM
Ab	TMP	0.50	±	7.3E-02	0.33	7.3E-02	0.055	±	2.5E-02	0.018	3.6E-03
	SMX	0.35	±	3.1E-02	0.28	3.1E-02	0.009	±	8.1E-04	0.004	4.8E-04
P-NAb	CBZ	0.46	±	3.8E-02	0.29	3.8E-02	0.011	±	1.1E-03	0.009	1.5E-03
	VLX	0.38	±	4.7E-02	0.33	4.7E-02	0.010	±	2.6E-03	0.004	9.1E-04
PPP	IMZ	0.42	±	1.1E-01	0.32	1.1E-01	0.012	±	3.1E-03	0.009	3.6E-03
	AZO	0.53	±	5.6E-02	0.36	5.6E-02	0.022	±	1.2E-02	0.020	1.2E-02
Disinfectants	BC	0.32	±	3.4E-02	0.29	3.4E-02	0.014	±	2.5E-03	0.004	1.9E-03
	MIT	0.37	±	4.3E-02	0.21	4.3E-02	0.014	±	1.6E-03	0.005	8.8E-04
Industrial chemicals	PFBS	0.45	±	1.3E-02	0.35	1.2E-02	0.013	±	2.7E-03	0.011	6.0E-03
	BPF	0.67	±	1.9E-02	0.48	1.9E-02	0.013	±	2.0E-03	0.009	1.6E-03
PCP	OCT	0.45	±	1.1E-01	0.36	1.1E-01	0.028	±	1.0E-02	0.012	5.1E-03
	OXB	0.31	±	2.5E-02	0.28	2.5E-02	0.007	±	1.4E-03	0.007	2.0E-03

Systems i used donor *E. coli* K12/IncF and system ii used donor *E. coli* UB1637/IncP as donor of conjugative plasmid to recipient *E. coli* HMS174. Conjugation frequencies are calculated as CFU transconjugants/CFU recipients. Exposure groups include antibiotics (Ab), pharmaceuticals non-antibiotics (P-NAb), plant protection products (PPPs), disinfectants, industrial chemicals, and personal care products (PCPs).

Table B3. Conjugation frequency on systems i and ii exposed to 0.001 µg mL^{-1}

		System i K12/IncF				System ii UB1637/IncP				System iii UB1637/IncF			
		E	SEM	C	SEM	E	SEM	C	SEM	E	SEM	C	SEM
Ab	TMP	0.273	± 2.1E-02	0.271	± 5.1E-03	0.040	± 1.3E-02	0.012	± 4.1E-03	0.234	± 2.7E-02	0.207	± 2.1E-02
	SMX	0.396	± 6.7E-02	0.448	± 1.7E-02	0.010	± 1.3E-03	0.004	± 4.8E-04				
P-NAb	CBZ	0.339	± 6.2E-02	0.361	± 5.2E-02	0.015	± 2.7E-03	0.011	± 6.6E-04	0.389	± 6.8E-02	0.394	± 8.9E-02
	VLX	0.603	± 1.5E-01	0.631	± 8.3E-02	0.023	± 3.6E-03	0.004	± 7.7E-04				
PPPs	IMZ	0.404	± 1.5E-01	0.191	± 5.7E-02	0.010	± 2.9E-03	0.009	± 3.6E-03	0.235	± 8.0E-02	0.258	± 8.7E-02
	AZO	0.233	± 5.0E-02	0.207	± 4.5E-02	0.023	± 9.9E-03	0.016	± 9.0E-03				
Disinfectants	BC	0.472	± 4.8E-02	0.448	± 1.7E-02	0.021	± 1.7E-03	0.009	± 1.2E-03	0.521	± 7.8E-02	0.394	± 8.9E-02
	MIT	0.160	± 6.7E-02	0.161	± 6.9E-02	0.019	± 2.8E-03	0.005	± 6.7E-04				
Industrial chemicals	PFBS	0.421	± 3.3E-02	0.631	± 8.3E-02	0.045	± 2.5E-02	0.011	± 4.3E-03				
	BPF	0.421	± 4.4E-02	0.421	± 3.3E-02	0.003	± 9.7E-04	0.002	± 4.9E-04	0.188	± 4.3E-02	0.258	± 8.7E-02
PCPs	OCT	0.326	± 8.3E-02	0.326	± 1.1E-01	0.021	± 8.2E-03	0.006	± 1.7E-03				
	OXB	0.427	± 1.1E-01	0.386	± 1.2E-01	0.010	± 2.2E-03	0.007	± 2.0E-03	0.520	± 9.0E-02	0.394	± 8.9E-02

Conjugation frequencies are calculated as CFU transconjugants/CFU recipients. Exposure groups include antibiotics (Ab), pharmaceuticals non-antibiotics (P-NAb), plant protection products (PPPs), disinfectants, industrial chemicals, and personal care products (PCPs).

Table B4. Primers for gene expression analysis

Gene		Primer sequence	Target	Related function
rpoS	F	TTTTACCACCAGACGCAAGT	Chromosome	Oxidative stress
rpoS	R	GGAACTGTTATCGCAGGGAG	Chromosome	Oxidative stress
oxyR	F	GATCTTGAGTACCTGGTGGCATTGG	Chromosome	Oxidative stress
oxyR	R	CATCACGCCCAGCTCATCTTCC	Chromosome	Oxidative stress
soxS	F	AACGAATGTTCCGCACGGTGAC	Chromosome	Oxidative stress
soxS	R	CGAGACATAACCCAGGTCCATTGC	Chromosome	Oxidative stress
soxR	F	CGTCCCAATGGCGAGAAGAGTTG	Chromosome	Oxidative stress
soxR	R	AACCAATACATCCGTCCAGTTCGTC	Chromosome	Oxidative stress
sodA	F	GAAAGGCGATAAACTGGCGG	Chromosome	Oxidative stress
sodA	R	GCGCCAGAAATAGCTTCACC	Chromosome	Oxidative stress
sodC	F	GCGCCTCGTCTGAAATCACT	Chromosome	Oxidative stress
sodC	R	TTACACCACAGGCATAGCGT	Chromosome	Oxidative stress
recA	F	GAAGGCGAAATCGGCGACTCTC	Chromosome	Oxidative stress
recA	R	TGAAGATCAGCAGCGTGTTGGAC	Chromosome	Oxidative stress
marA	F	AAAGTGTCAGAGCGTTCGGGTTAC	Chromosome	Oxidative stress
marA	R	ATCTTACGGCTGCGGATGTATTGG	Chromosome	Oxidative stress
ompR	F	CGTTATCTCACCGAACAAGGCTTCC	Chromosome	Oxidative stress
ompR	R	GATTCACGAGTCAGCAGGCGATC	Chromosome	Oxidative stress
umuD	F	GCCCGACGGTACAGCTTATT	Chromosome	SOS response
umuD	R	ACACCAAAGACATCCAGCGT	Chromosome	SOS response
lexA	F	GGTCGTTGTCGCACGTATTG	Chromosome	SOS response
lexA	R	TGAAGCTCTGCTGACGAAGG	Chromosome	SOS response
ompC	F	AAGTAGTAGGTAGCACCAACATCA	Chromosome	Membrane permeability
ompC	R	GGGCGAACAAAGCACAGAA	Chromosome	Membrane permeability
ompA	F	TGAGCCTGGGTGTTTCCTA	Chromosome	Membrane permeability
ompA	R	CAGAGCAGCCTGACCTTCC	Chromosome	Membrane permeability
ompF	F	GGTCTGCGTCCGTCCAT	Chromosome	Membrane permeability
ompF	R	GGTTGCGCCCACTTCA	Chromosome	Membrane permeability
traM	F	GGAGACATGAGGACTGAGAGA	incF-like plasmid	Conjugation
traM	R	GCTTCTTGAACTGGGGCTTC	incF-like plasmid	Conjugation
traJ	F	TGCTCATTCCTATATGCTTCCA	incF-like plasmid	Conjugation
traJ	R	GCTCGTCAAATAGATCTGCTGG	incF-like plasmid	Conjugation
trbB	F	GGTGACAGTAAGGGCAATGC	incF-like plasmid	Conjugation
trbB	R	CTGTTCACCCTGTTGCTGAG	incF-like plasmid	Conjugation
trbA	F	AGCTCGTAACGTCCGGTAAT	incF-like plasmid	Conjugation
trbA	R	TCTCCTGAGCTCACTGGTTT	incF-like plasmid	Conjugation
trbA	F	TGGAAACTCCCCTACCTCTT	incP-like plasmid	Conjugation
trbA	R	CCACACTGATGCGTTCGTAT	incP-like plasmid	Conjugation
korB	F	CTGGTCGGCTTCGTTGTA	incP-like plasmid	Conjugation
korB	R	TGAAGTCACCCATTTCGGT	incP-like plasmid	Conjugation
korA	F	TCGGGCAAGTTCTTGTCC	incP-like plasmid	Conjugation

korA	R	GCAGCAGACCATCGAGATA	incP-like plasmid	Conjugation
trbBp	F	CGCGGTCGCCATCTTCACG	incP-like plasmid	Conjugation
trbBp	R	TGCCCGAGCCAGTACCGCCAATG	incP-like plasmid	Conjugation
trfAp	F	GAAGCCCATCGCCGTCGCCTGTAG	incP-like plasmid	Conjugation
trfAp	R	GCCGACGATGACGAACTGGTGTGG	incP-like plasmid	Conjugation
gapA	F	ACTGACTGGTATGGCGTTCC	Chromosome	Housekeeping
gapA	R	GTTGCAGCTTTTTCCAGACG	Chromosome	Housekeeping
16SrRNA	F	CCTACGGGAGGCAGCAG	Chromosome	Housekeeping
16SrRNA	R	ATTACCGCGGCTGCTGG	Chromosome	Housekeeping

Appendix C

This appendix provides supplementary figures and tables supporting the results presented in Chapter 3.

Table C1. Extended characteristics of Mungia and Gorliz WWTPs.

Feature	Mungia WWTP	Gorliz WWTP	Source
Location	43.361°N, 2.846°W	43.412°N, 2.939°W	EEA (2024)
Design capacity (h.e.)	21,884	44,000	EEA (2024)
Load enering WWTP (h.e.)	19,312	31,399	EEA (2024)
Connected population equivalent (h.e.)	21,616	18,446	URA (2019)
—Permanent residents	13,929	10,446	URA (2019)
—seasonal visitors	Not reported	5,974	URA (2019)
—non-domestic contributors	Industry (Mungia, Gatika)	Hospitality industry	URA (2019)
Annual treated volume	2,600,000	1,700,000	URA (2019)
Max flow rate (m3/h)	650	864	URA (2019)
Primary treatment	Yes	Yes	EEA (2024)
Secondary treatment	Yes (biological)	Yes (biological and physicochemical)	EEA (2024)
UV disinfection	Yes	No	EEA (2024)
N removal	Yes	No	EEA (2024)
P removal	Yes (chemical)	No	EEA (2024)
Storm overflow	Yes (partial treatment)	Yes (partial treatment)	URA (2019)
Discharge point	Butroe river	Bay of Biscay (submarine outfall)	URA (2019)
Receiving water body	Butroe-B (ES111R048020)	Cantabria-Matxitxako (ES111C000030)	URA (2019)

Table C2. Extended information of quantified genes for resistome analysis

Gene	Antibiotic Class	Molecular Target	Role	Functional Dependency	Reference(s)
sul1	Sulfonamides	Dihydropteroate synthase (DHPS)	Primary resistance determinant	Functional as single gene.	Partridge et al. (2002)
qacEΔ1	Biocides (QACs)	Cell membrane	Accessory resistance mechanism	Functional as single gene.	Leelaporn et al. (1994)
aadA	Aminoglycosides (streptomycin, spectinomycin)	30S ribosomal subunit	Primary resistance determinant	Functional as single gene.	Stokes & Hall (1989)
merA	Mercury resistance	Mercuric ions (Hg2+)	Primary resistance determinant	Requires co-expression with merT (transport) and merP (periplasmic binding) for full resistance. Broad-spectrum strains additionally encode merB (organomercury lyase). merA alone confers basal tolerance.	Sotero-Martins et al. (2008)
bacA	Bacitracin	Lipid II cycle / undecaprenyl pyrophosphate (UPP)	Accessory resistance mechanism	Functional as single gene.	El Ghachi et al. (2004)
bla_{TEM}	Beta-lactams (penicillins, early cephalosporins)	Penicillin-binding proteins (PBPs) indirectly	Primary resistance determinant	Functional as single gene.	Bush & Bradford (2016)
ampC	Beta-lactams (cephalosporins, cephamycins)	Penicillin-binding proteins (PBPs) indirectly	Primary resistance determinant	Single functional gene. Inducible chromosomal AmpC in Enterobacter/Citrobacter/Serratia requires regulators AmpR, AmpD, AmpG for full	Jacoby GA (2009)

				induction. In *E. coli ampC* is constitutive and requires no regulatory partners.	
bla_{CMY-2}	Beta-lactams (cephalosporins, cephamycins)	Penicillin-binding proteins (PBPs) indirectly	Primary resistance determinant	Functional as single gene.	Bush & Bradford (2016)
bla_{CTX-M}	Extended-spectrum beta-lactams (ESBLs): oxyimino-cephalosporins, aztreonam	Penicillin-binding proteins (PBPs) indirectly	Primary resistance determinant	Functional as single gene.	Bush & Bradford (2016)
bla_{OXA-48}	Carbapenems (particularly meropenem/ertapenem) ; penicillins	Penicillin-binding proteins (PBPs) indirectly	Primary resistance determinant*	Functional as single gene. Clinical resistance to carbapenems often requires co-production of ESBL or porin loss.	Bush & Bradford (2016)
bla_{OXA-58}	Carbapenems (clinically relevant mainly in Acinetobacter baumannii)	Penicillin-binding proteins (PBPs) indirectly	Primary resistance determinant	Functional as single gene. Over-expression requires IS-provided promoters (ISAba3/ISAba2 upstream); without IS insertion, basal expression may be insufficient for full carbapenem resistance.	Bush & Bradford (2016)
bla_{NDM}	Carbapenems (all beta-lactams except aztreonam)	Penicillin-binding proteins (PBPs) indirectly	Primary resistance determinant	Functional as single gene.	Bush & Bradford (2016)
bla_{VIM}	Carbapenems (all beta-lactams except aztreonam)	Penicillin-binding proteins (PBPs) indirectly	Primary resistance determinant	Functional as single gene.	Bush & Bradford (2016)
bla_{KPC}	Carbapenems (all beta-lactams)	Penicillin-binding proteins (PBPs) indirectly	Primary resistance determinant	Functional as single gene. Tn4401 provides its own promoter; different isoforms have different expression levels.	Bush & Bradford (2016)

aac(6')-Ib	Aminoglycosides (tobramycin, amikacin); Fluoroquinolones (cr variant: ciprofloxacin, norfloxacin)	30S ribosomal subunit (aminoglycosides); DNA gyrase/topoisomerase IV (cr variant)	Aminoglycosides: Primary resistance determinant; Fluoroquinolones (cr): Accessory resistance mechanism	Functional as single gene. The cr variant is a point-mutant allele, not a separate gene. No obligate partner.	Shaw et al. (1993)
aph(3')-Ib	Aminoglycosides (kanamycin, neomycin, paromomycin)	30S ribosomal subunit	Primary resistance determinant	Functional as single gene. No obligate partner.	Shaw et al. (1993)
sul2	Sulfonamides	Dihydropteroate synthase (DHPS)	Primary resistance determinant	Functional as single gene. No obligate partner.	Deng et al. (2015)
dfrA1	Trimethoprim	Dihydrofolate reductase (DHFR)	Primary resistance determinant	Functional as single gene.	Sköld (2001)
dfrB	Trimethoprim	Dihydrofolate reductase (DHFR)	Primary resistance determinant	Functional as single gene.	Kneis et al. (2023)
tetM	Tetracyclines (tetracycline, doxycycline, minocycline)	30S ribosomal subunit	Primary resistance determinant	Functional as single gene.	Roberts (2005)
tetW	Tetracyclines (broad spectrum including doxycycline and minocycline)	30S ribosomal subunit	Primary resistance determinant	Functional as single gene.	Roberts (2005)
ermB	Macrolides, Lincosamides, Streptogramins B (MLSB phenotype)	23S rRNA (50S ribosomal subunit); peptidyl transferase loop	Primary resistance determinant	Functional as single gene.	Roberts (2008)
mphA	Macrolides (14-membered: erythromycin, clarithromycin; 15-membered: azithromycin)	Macrolide 2'-OH group (chemical inactivation)	Primary resistance determinant	*mphA* encodes the resistance enzyme and is functional alone when constitutively expressed. *mphR* (transcriptional repressor) and *mrx* (macrolide-binding protein) are co-transcribed and regulate *mphA* expression	Roberts (2008)

				but are NOT required for phosphotransferase activity.	
msrE	Macrolides & Streptogramins B	50S ribosomal subunit (drug efflux from ribosome vicinity)	Primary resistance determinant	Functional as single gene. Almost invariably co-located with *mphE* on the same plasmid/transposon; *mphE* provides chemical inactivation while *msrE* provides ribosomal protection - they are synergistic but independently functional.	Roberts (2008)
qnrS	Fluoroquinolones (quinolones)	DNA gyrase (GyrA/GyrB) and topoisomerase IV (ParC/ParE)	Accessory resistance mechanism (PMQR)	Functional as single gene.	Jacoby et al. (2006)
floR	Phenicols (chloramphenicol, florfenicol)	50S ribosomal subunit (drug export prevents binding)	Primary resistance determinant	Functional as single gene. No obligate partner. Expression is constitutive.	Cloeckaert et al. (2000)
mcr-1	Colistin (polymyxins: polymyxin B & colistin/polymyxin E)	Lipid A moiety of lipopolysaccharide (LPS) on the outer membrane	Primary resistance determinant	Functional as single gene.	Y. Y. Liu et al. (2016)
vanA	Glycopeptides (vancomycin, teicoplanin)	Peptidoglycan precursor (D-Ala-D-Ala terminus of lipid II)	Primary resistance determinant	It is not functional alone. The VanA phenotype requires the complete van operon: *vanH*, *vanA* and *vanX* are the three essential catalytic genes (minimum for resistance). *vanR* + *vanS* (two-component regulatory system) are required for induction in response to vancomycin. Loss of	(Arthur & Courvalin, 1993)

		any of *vanH, vanA* (ligase), or *vanX* abolishes the mechanism.

Appendix D

This appendix provides supplementary figures and tables supporting the results presented in Chapter 4.

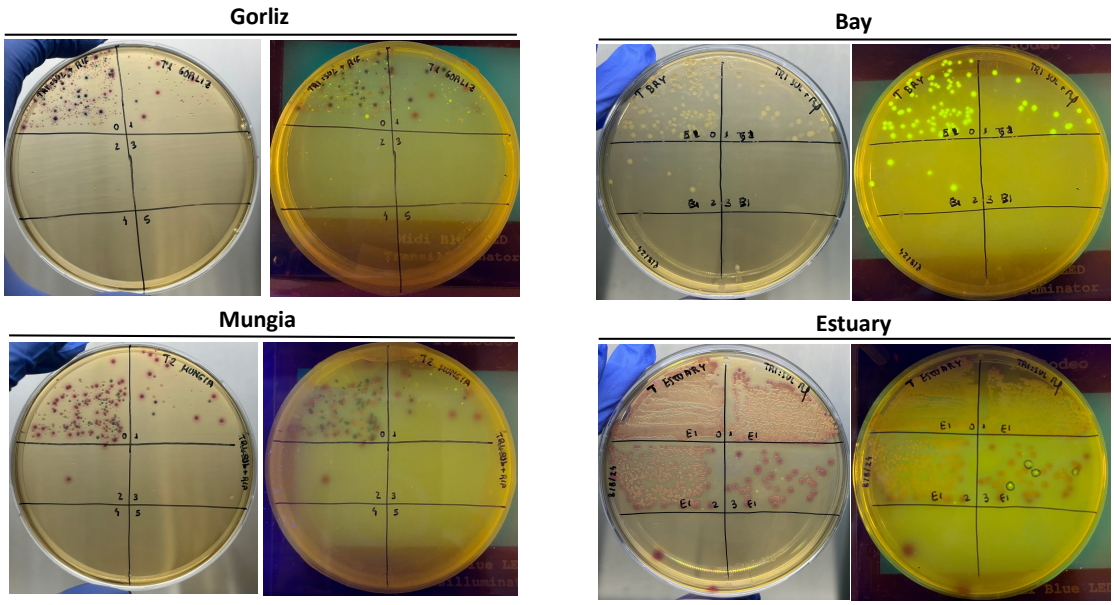

Figure D1. Colony growth of transconjugants obtained from exogenous plasmid capture assays.

Transconjugants were recovered across the four sampling locations (Gorliz, Mungia, Bay, and Estuary). For each site, two representative images are shown corresponding to standard illumination (left) and blue-light illumination (right), allowing visualization of colony morphology and fluorescent signal associated with successful transconjugant recovery.

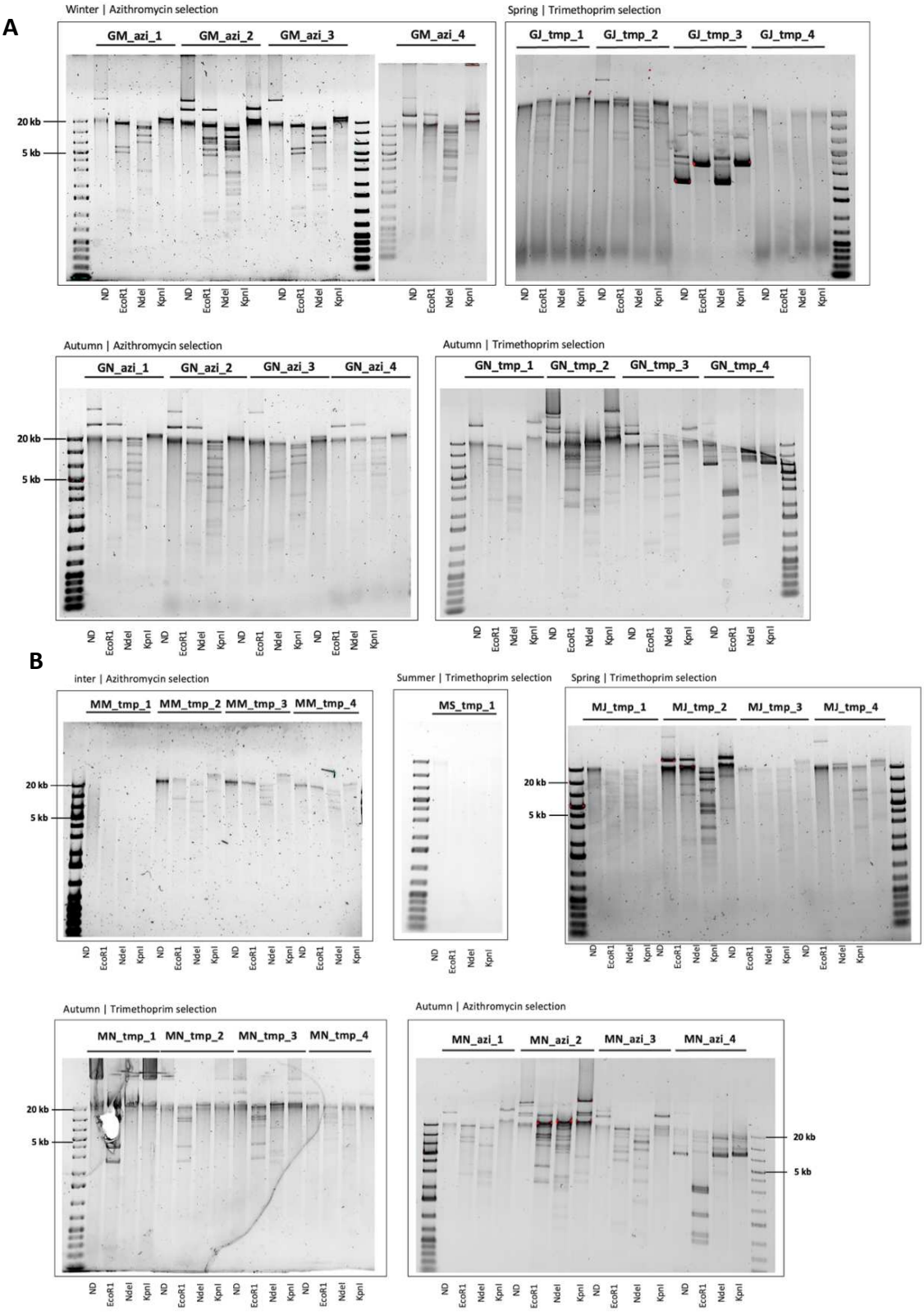

Figure D2. Restriction profiling electrophoresis of DNA from plasmid extractions.
DNA from conjugation experiments with extracted environmental bacterial communities using EcoR1, NdeI and KpnI enzymes. (A) Gorliz and (B) Mungia wastewater treatment plant effluents across different seasons (winter, spring, summer, and autumn) selected with two different antibiotics: trimethoprim (tmp) and azithromycin(azi). ND:Non Digested reference lane.

Table D1. Replicon type number found by site.

Plasmid ID	Site	Season	Selection	Size (kb)	Circularized topology	Replicon type	Relaxase	Predicted mobility
BM4TMP-p12	Bay	Winter	TMP	157	non-resolved	IncFIA,IncFIB,IncFIC	MOBF	conjugative
EJ1TMP-p1	Estuary	Spring	TMP	89.2	circularized	IncFIA,IncFIC	MOBF	conjugative
EM1TMP-p1	Estuary	Winter	TMP	8.9	circularized	rep_cluster_2350	-	non-mobilizable
EM1TMP-p2	Estuary	Winter	TMP	61.2	circularized	IncN	MOBF	conjugative
EM2TMP-p2	Estuary	Winter	TMP	60.5	non-resolved	IncFIA,IncFIC	MOBF	conjugative
EM2TMP-p3	Estuary	Winter	TMP	62.4	NA	IncN	MOBF	conjugative
EM3TMP-p4	Estuary	Winter	TMP	62.4	circularized	IncN	MOBF	conjugative
EM3TMP-p5	Estuary	Winter	TMP	37.9	circularized	rep_cluster_827	MOBP	conjugative
EM4TMP-p5	Estuary	Winter	TMP	62.4	circularized	IncN	MOBF	conjugative
EM4TMP-p7	Estuary	Winter	TMP	35	circularized	IncN	MOBF	conjugative
GN1AZI-p2	Gorliz	Autumn	AZI	52.6	circularized	IncU	MOBP	conjugative
GN1AZI-p3	Gorliz	Autumn	AZI	34.6	circularized	IncN	MOBF	conjugative
GN2AZI-p2	Gorliz	Autumn	AZI	52.6	circularized	IncU	MOBP	conjugative
GN2AZI-p3	Gorliz	Autumn	AZI	34.6	circularized	IncN	MOBF	conjugative
GN3AZI-p1	Gorliz	Autumn	AZI	51.8	circularized	IncU	MOBP	conjugative
GN4TMP-p1	Gorliz	Autumn	TMP	4.6	circularized	-	-	non-mobilizable
GN4TMP-p3	Gorliz	Autumn	TMP	15.2	circularized	-	-	non-mobilizable
GN4TMP-p4	Gorliz	Autumn	TMP	291.9	circularized	IncFIB,IncHI1B	MOBH	conjugative
GN4TMP-p5	Gorliz	Autumn	TMP	52.6	circularized	IncU	MOBP	conjugative
GN5TMP-p2	Gorliz	Autumn	TMP	0.5	non-resolved	-	-	non-mobilizable
GN5TMP-p3	Gorliz	Autumn	TMP	15.2	non-resolved	-	-	non-mobilizable
GN5TMP-p6	Gorliz	Autumn	TMP	4.6	non-resolved	-	-	non-mobilizable
GN5TMP-p7	Gorliz	Autumn	TMP	303.4	non-resolved	IncFIB,IncHI1B	MOBH	conjugative
GN6TMP-p2	Gorliz	Autumn	TMP	4.6	circularized	-	-	non-mobilizable
GN6TMP-p3	Gorliz	Autumn	TMP	52.6	circularized	IncU	MOBP	conjugative
GN6TMP-p4	Gorliz	Autumn	TMP	303.4	circularized	IncFIB,IncHI1B	MOBH	conjugative
GJ1TMP-p2	Gorliz	Spring	TMP	48.9	circularized	IncU	MOBP	conjugative
GJ1TMP-p3	Gorliz	Spring	TMP	16.1	circularized	-	-	non-mobilizable
GJ1TMP-p4	Gorliz	Spring	TMP	45.3	circularized	IncN	MOBF	conjugative

GJ1TMP-p6	Gorliz	Spring	TMP	39.1	circularized	-	MOBP	conjugative
GJ3TMP-p1	Gorliz	Spring	TMP	53.6	circularized	IncU	MOBP	conjugative
GJ3TMP-p3	Gorliz	Spring	TMP	52	circularized	IncN	MOBF	conjugative
GJ5TMP-p11	Gorliz	Spring	TMP	3.2	circularized	ColRNAI_rep_cluster_1987	MOBP, MOBP	mobilizable
GJ5TMP-p2	Gorliz	Spring	TMP	109.6	circularized	IncL/M	MOBP	conjugative
GJ5TMP-p3	Gorliz	Spring	TMP	55.6	circularized	IncN	MOBF	conjugative
GJ7TMP-p13	Gorliz	Spring	TMP	69.1	circularized	IncU	MOBP	conjugative
GS2TMP-p13	Gorliz	Summer	TMP	296.1	non-resolved	IncFIB, IncHI1B	MOBH	conjugative
GM2AZI-p4	Gorliz	Winter	AZI	36.8	circularized	rep_cluster_827	MOBP	conjugative
GM2AZI-p5	Gorliz	Winter	AZI	51.8	circularized	IncU	MOBP	conjugative
GM2AZI-p6	Gorliz	Winter	AZI	35.4	circularized	-	-	non-mobilizable
GM3AZI-p1	Gorliz	Winter	AZI	52.7	circularized	IncU	MOBP	conjugative
GM4AZI-p2	Gorliz	Winter	AZI	51.8	circularized	IncU	MOBP	conjugative
MN1AZI-p1	Mungia	Autumn	AZI	61.5	circularized	IncP	MOBP	conjugative
MN1TMP-p2	Mungia	Autumn	TMP	49	circularized	IncFII	-	non-mobilizable
MN1TMP-p3	Mungia	Autumn	TMP	55.6	circularized	IncN	MOBF	conjugative
MN2TMP-p171	Mungia	Autumn	TMP	9.4	circularized	-	-	non-mobilizable
MN2TMP-p4	Mungia	Autumn	TMP	41.6	circularized	-	-	non-mobilizable
MN3AZI-p4	Mungia	Autumn	AZI	61.5	circularized	IncP	MOBP	conjugative
MN3AZI-p8	Mungia	Autumn	AZI	38	circularized	rep_cluster_827	MOBP	conjugative
MN4AZI-p456	Mungia	Autumn	AZI	60.7	circularized	IncP	MOBP	conjugative
MN4AZI-p7	Mungia	Autumn	AZI	38	circularized	rep_cluster_827	MOBP	conjugative
MN4TMP-p2	Mungia	Autumn	TMP	53.5	non-resolved	IncN	MOBF	conjugative
MN4TMP-p3	Mungia	Autumn	TMP	34.1	non-resolved	-	-	non-mobilizable
MN4TMP-p4	Mungia	Autumn	TMP	61.5	non-resolved	IncP	MOBP	conjugative
MN4TMP-p5	Mungia	Autumn	TMP	38	non-resolved	rep_cluster_827	MOBP	conjugative
MJ10TMP-p2	Mungia	Spring	TMP	15.2	circularized	-	-	non-mobilizable
MJ10TMP-p3	Mungia	Spring	TMP	76.1	circularized	IncN	MOBF	conjugative
MJ10TMP-p4	Mungia	Spring	TMP	49	circularized	IncFII	-	non-mobilizable
MJ1TMP-p1	Mungia	Spring	TMP	113.9	circularized	IncFIA, IncFII, IncFII	MOBF	conjugative
MJ9TMP-p4	Mungia	Spring	TMP	76.1	circularized	IncN	MOBF	conjugative

MJ9TMP-p7	Mungia	Spring	TMP	34.1	circularized	IncN	MOBF	conjugative
MJ9TMP-p8	Mungia	Spring	TMP	33.4	circularized	-	-	non-mobilizable
MS6TMP-p1	Mungia	Summer	TMP	64.3	circularized	IncFII, IncFII	MOBF	conjugative
MM2TMP-p1	Mungia	Winter	TMP	60.2	circularized	IncN	MOBF	conjugative
MM3TMP-p1	Mungia	Winter	TMP	23.4	circularized	IncN	-	non-mobilizable

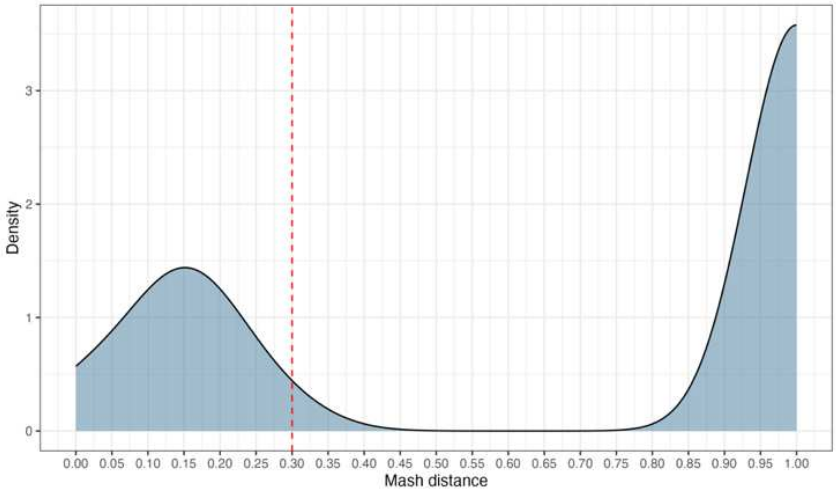

Figure D3. Binomial distribution of MASH distance on sequenced plasmids.

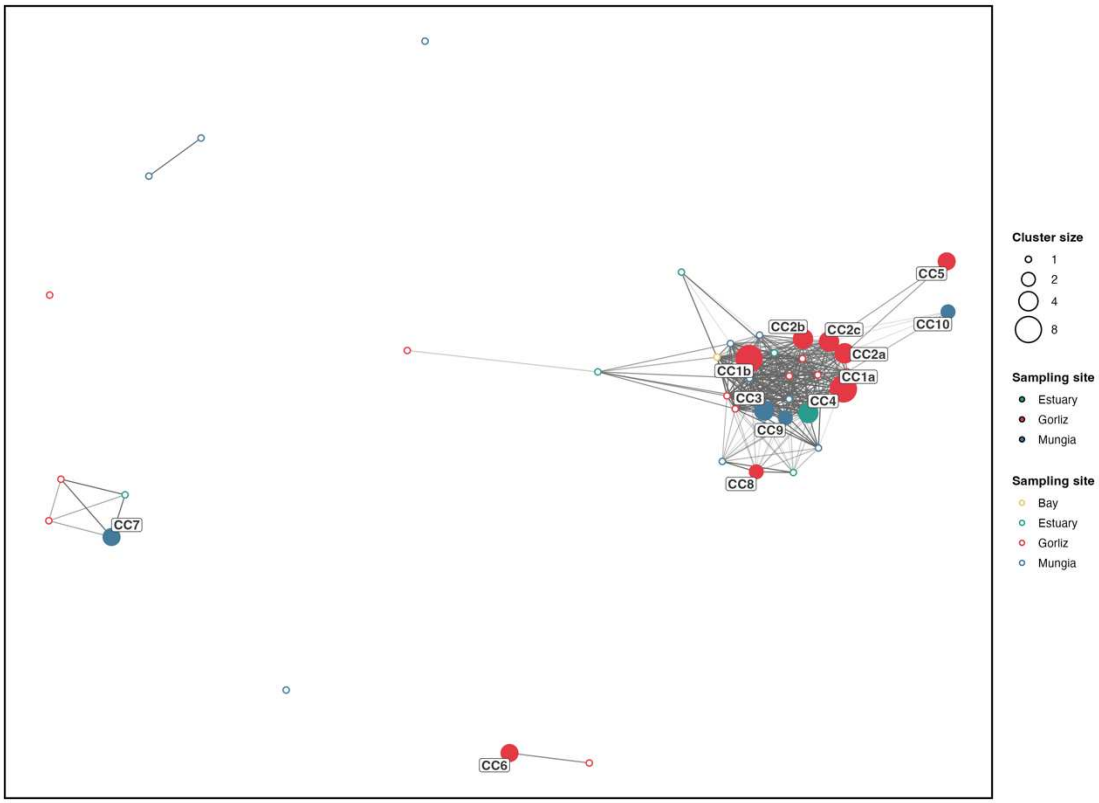

Figure D4. Mash network with a distance between 0.001 and 0.30 integrating all plasmids.

Each node represents a plasmid (n=43), when it belonged to a Clonal Cluster (CC) is indicated along its identifier number based on similarity analysis.

References

Abe, K., Nomura, N., & Suzuki, S. (2021). Biofilms: Hot spots of horizontal gene transfer (HGT) in aquatic environments, with a focus on a new HGT mechanism. In *FEMS Microbiology Ecology* (Vol. 96, Number 5). https://doi.org/10.1093/FEMSEC/FIAA031

Acman, M., van Dorp, L., Santini, J. M., & Balloux, F. (2020). Large-scale network analysis captures biological features of bacterial plasmids. *Nature Communications*, *11*(1). https://doi.org/10.1038/s41467-020-16282-w

Agathokleous, E., & Calabrese, E. J. (2019). Hormesis: The dose response for the 21st century: The future has arrived. In *Toxicology* (Vol. 425). https://doi.org/10.1016/j.tox.2019.152249

Agencia Estatal de Meteorología (AEMET). (2026). *Datos climatológicos — Estación meteorológica Bilbao Aeropuerto (Estación 1082)*. Agencia Estatal de Meteorología, Ministerio Para La Transición Ecológica y El Reto Demográfico.

Agencia Vasca del Agua (URA). (2019a). *RESOLUCIÓN del Director General de la Agencia Vasca del Agua, por la que se REVISA la autorización de vertido de aguas residuales desde tierra al mar, solicitado por el CONSORCIO DE AGUAS BILBAO BIZKAIA al amparo del Decreto 196/1997, de 29 de agosto, que establece el procedimiento para el otorgamiento de autorizaciones de uso en la zona de servidumbre de protección del dominio público marítimo terrestre y de vertido desde tierra al mar.* https://apps.euskadi.eus/y76aaObieeWar/?locale=es

Agencia Vasca del Agua (URA). (2019b). *RESOLUCIÓN del Director General de la Agencia Vasca del Agua, por la que se REVISA la autorización de vertido otorgada al CONSORCIO DE AGUAS BILBAO BIZKAIA para las aguas residuales generadas en la EDAR de Mungia conforme al Reglamento del Dominio Público Hidráulico, en el término municipal de Mungia (Bizkaia).* https://apps.euskadi.eus/y76aaObieeWar/?locale=es

Alav, I., & Buckner, M. M. C. (2024). Non-antibiotic compounds associated with humans and the environment can promote horizontal transfer of antimicrobial resistance genes. In *Critical Reviews in Microbiology* (Vol. 50, Number 6). https://doi.org/10.1080/1040841X.2023.2233603

Alexander, J., Hembach, N., & Schwartz, T. (2020). Evaluation of antibiotic resistance dissemination by wastewater treatment plant effluents with different catchment areas in Germany. *Scientific Reports*, *10*(1). https://doi.org/10.1038/s41598-020-65635-4

Alkorta, I., & Garbisu, C. (2025). Expanding the focus of the One Health concept: links between the Earth-system processes of the planetary boundaries framework and antibiotic resistance. In *Reviews on Environmental Health* (Vol. 40, Number 1). https://doi.org/10.1515/reveh-2024-0013

Álvarez-Rodríguez, I., Arana, L., Ugarte-Uribe, B., Gómez-Rubio, E., Martín-Santamaría, S., Garbisu, C., & Alkorta, I. (2020). Type IV Coupling Proteins as Potential Targets to Control the Dissemination of Antibiotic Resistance. In *Frontiers in Molecular Biosciences* (Vol. 7). https://doi.org/10.3389/fmolb.2020.00201

Andersson, D. I., & Hughes, D. (2011). Persistence of antibiotic resistance in bacterial populations. In *FEMS Microbiology Reviews* (Vol. 35, Number 5). https://doi.org/10.1111/j.1574-6976.2011.00289.x

Arbé-Carton, K., Rey-Sogo, A., Santos-Fernández, N., Altube, O., Garbisu, C., Arana, L., & Alkorta, I. (2023). Development of a high-throughput platform to measure plasmid transfer frequency. *Frontiers in Cellular and Infection Microbiology*, *13*. https://doi.org/10.3389/fcimb.2023.1269732

Arthur, M., & Courvalin, P. (1993). Genetics and mechanisms of glycopeptide resistance in enterococci. In *Antimicrobial Agents and Chemotherapy* (Vol. 37, Number 8). https://doi.org/10.1128/AAC.37.8.1563

Baquero, F., Martínez, J. L., Lanza, V. F., Rodríguez-Beltrán, J., Galán, J. C., San Millán, A., Cantón, R., & Coque, T. M. (2021). Evolutionary Pathways and Trajectories in Antibiotic Resistance. In *Clinical Microbiology Reviews* (Vol. 34, Number 4). https://doi.org/10.1128/CMR.00050-19

Beaber, J. W., Hochhut, B., & Waldor, M. K. (2004). SOS response promotes horizontal dissemination of antibiotic resistance genes. *Nature*, *427*(6969). https://doi.org/10.1038/nature02241

Beltrán de Heredia, I., Garbisu, C., Alkorta, I., Urra, J., González-Gaya, B., & Ruiz-Romera, E. (2023). Spatio-seasonal patterns of the impact of wastewater treatment plant effluents on antibiotic resistance in river sediments. *Environmental Pollution*, *319*. https://doi.org/10.1016/j.envpol.2022.120883

Beltrán de Heredia, I., Sbaffi, T., González-Gaya, B., Di Cesare, A., Sabatino, R., Alkorta, I., & Ruiz-Romera, E. (2025). Comparative analysis of planktonic and sessile microbiomes and associated resistomes in a freshwater ecosystem impacted by municipal wastewater treatment plant discharge. *Journal of Hazardous Materials*, *496*. https://doi.org/10.1016/j.jhazmat.2025.139250

Bengtsson-Palme, J., & Larsson, D. G. J. (2016). Concentrations of antibiotics predicted to select for resistant bacteria: Proposed limits for environmental regulation. *Environment International*, *86*. https://doi.org/10.1016/j.envint.2015.10.015

Benz, F., & Hall, A. R. (2023). Host-specific plasmid evolution explains the variable spread of clinical antibiotic-resistance plasmids. *Proceedings of the National Academy of Sciences of the United States of America*, *120*(15). https://doi.org/10.1073/pnas.2212147120

Berendonk, T. U., Manaia, C. M., Merlin, C., Fatta-Kassinos, D., Cytryn, E., Walsh, F., Bürgmann, H., Sørum, H., Norström, M., Pons, M. N., Kreuzinger, N., Huovinen, P., Stefani, S., Schwartz, T., Kisand, V., Baquero, F., & Martinez, J. L. (2015). Tackling antibiotic resistance: The environmental framework. In *Nature Reviews Microbiology* (Vol. 13, Number 5). https://doi.org/10.1038/nrmicro3439

Berndtson, A. E. (2020). Increasing Globalization and the Movement of Antimicrobial Resistance between Countries. In *Surgical Infections* (Vol. 21, Number 7). https://doi.org/10.1089/sur.2020.145

Binh, C. T. T., Heuer, H., Kaupenjohann, M., & Smalla, K. (2009). Diverse aadA gene cassettes on class 1 integrons introduced into soil via spread manure. *Research in Microbiology*, *160*(6). https://doi.org/10.1016/j.resmic.2009.06.005

Bishop, C. M., Saxe, A. M., McClelland, J. L., Ganguli, S., Pedregosa, F., Varoquaux, G., Gramfort, A., Michel, V., Thirion, B., Grisel, O., Blondel, M., Prettenhofer, P., Weiss, R., Dubourg, V., Vanderplas, J., Passos, A., Cournapeau, D., Brucher, M., Perrot, M., & Duchesnay, E. (2011). Scikit-learn: Machine Learning in {P}ython. *Journal of Machine Learning Research*, *12*.

Blau, K., Jechalke, S., & Smalla, K. (2020). Detection, Isolation, and Characterization of Plasmids in the Environment. In F. de la Cruz (Ed.), *Horizontal Gene Transfer: Methods and Protocols* (Vol. 2075, pp. 39–60). Springer.

Bottery, M. J. (2022). Ecological dynamics of plasmid transfer and persistence in microbial communities. In *Current Opinion in Microbiology* (Vol. 68). https://doi.org/10.1016/j.mib.2022.102152

Breiman, L. (2001). Random forests. *Machine Learning*, *45*(1). https://doi.org/10.1023/A:1010933404324

Briani, F., Dehò, G., Forti, F., & Ghisotti, D. (2001). The plasmid status of satellite bacteriophage P4. In *Plasmid* (Vol. 45, Number 1). https://doi.org/10.1006/plas.2000.1497

Burgess, S. A., Moinet, M., Brightwell, G., & Cookson, A. L. (2022). Whole genome sequence analysis of ESBL-producing *Escherichia coli* recovered from New Zealand freshwater sites. *Microbial Genomics*, *8*(10). https://doi.org/10.1099/mgen.0.000893

Bush, K., & Bradford, P. A. (2016). β-lactams and β-lactamase inhibitors: An overview. *Cold Spring Harbor Perspectives in Medicine*, *6*(8). https://doi.org/10.1101/cshperspect.a025247

Capella-Gutiérrez, S., Silla-Martínez, J. M., & Gabaldón, T. (2009). trimAl: A tool for automated alignment trimming in large-scale phylogenetic analyses. *Bioinformatics*, *25*(15). https://doi.org/10.1093/bioinformatics/btp348

Carver, T. J., Rutherford, K. M., Berriman, M., Rajandream, M. A., Barrell, B. G., & Parkhill, J. (2005). ACT: The Artemis comparison tool. *Bioinformatics*, *21*(16). https://doi.org/10.1093/bioinformatics/bti553

Chaber-Jarlachowicz, P., Gworek, B., & Kalinowski, R. (2025). Removal efficiency of pharmaceuticals during the wastewater treatment process: Emission and environmental risk assessment. *PLOS ONE*, *20*(9 September). https://doi.org/10.1371/journal.pone.0331211

Che, Y., Yang, Y., Xu, X., Brinda, K., Polz, M. F., Hanage, W. P., & Zhang, T. (2021). Conjugative plasmids interact with insertion sequences to shape the horizontal transfer of antimicrobial resistance genes. *Proceedings of the National Academy of Sciences of the United States of America*, *118*(6). https://doi.org/10.1073/pnas.2008731118

Chee-Sanford, J. C., Mackie, R. I., Koike, S., Krapac, I. G., Lin, Y., Yannarell, A. C., Maxwell, S., & Aminov, R. I. (2009). Fate and Transport of Antibiotic Residues and Antibiotic Resistance Genes following Land Application of Manure Waste. *Journal of Environmental Quality*, *38*(3). https://doi.org/10.2134/jeq2008.0128

Chen, T., & Guestrin, C. (2016). XGBoost: A scalable tree boosting system. *Proceedings of the ACM SIGKDD International Conference on Knowledge Discovery and Data Mining*, *13-17-August-2016*. https://doi.org/10.1145/2939672.2939785

Clara, M., Strenn, B., & Kreuzinger, N. (2004). Carbamazepine as a possible anthropogenic marker in the aquatic environment: Investigations on the behaviour of Carbamazepine in wastewater treatment and during groundwater infiltration. *Water Research*, *38*(4). https://doi.org/10.1016/j.watres.2003.10.058

Cloeckaert, A., Baucheron, S., Flaujac, G., Schwarz, S., Kehrenberg, C., Martel, J. L., & Chaslus-Dancla, E. (2000). Plasmid-mediated florfenicol resistance encoded by the floR gene in *Escherichia coli* isolated from cattle. *Antimicrobial Agents and Chemotherapy*, *44*(10). https://doi.org/10.1128/AAC.44.10.2858-2860.2000

Davies, J. (1996). Origins and evolution of antibiotic resistance. In *Microbiología (Madrid, Spain)* (Vol. 12, Number 1). https://doi.org/10.1128/mmbr.00016-10

Dcosta, V. M., King, C. E., Kalan, L., Morar, M., Sung, W. W. L., Schwarz, C., Froese, D., Zazula, G., Calmels, F., Debruyne, R., Golding, G. B., Poinar, H. N., & Wright, G. D. (2011). Antibiotic resistance is ancient. In *Nature* (Vol. 477, Number 7365). https://doi.org/10.1038/nature10388

de Cravalho, A. C. C., da Silva Paganini, W., de Almeida Piai, K., & Bocchiglieri, M. M. (2024). The presence of pharmaceuticals and caffeine in water, as well as the methods used to eliminate them. In *Current Opinion in Environmental Science and Health* (Vol. 39). https://doi.org/10.1016/j.coesh.2024.100550

Deng, Y., Bao, X., Ji, L., Chen, L., Liu, J., Miao, J., Chen, D., Bian, H., Li, Y., & Yu, G. (2015). Resistance integrons: Class 1, 2 and 3 integrons. In *Annals of Clinical Microbiology and Antimicrobials* (Vol. 14, Number 1). https://doi.org/10.1186/s12941-015-0100-6

Dewi, D. A. P. R., Götz, B., & Thomasa, T. (2020). Diversity and genetic basis for carbapenem resistance in a coastal marine environment. *Applied and Environmental Microbiology*, *86*(10). https://doi.org/10.1128/AEM.02939-19

Dib, J. R., Wagenknecht, M., Farías, M. E., & Meinhardt, F. (2015). Strategies and approaches in plasmidome studies-uncovering plasmid diversity disregarding of linear elements? In *Frontiers in Microbiology* (Vol. 6, Number MAY). https://doi.org/10.3389/fmicb.2015.00463

Dimitriu, T. (2022). Evolution of horizontal transmission in antimicrobial resistance plasmids. In *Microbiology (United Kingdom)* (Vol. 168, Number 7). https://doi.org/10.1099/mic.0.001214

Dimitriu, T., Marchant, L., Buckling, A., & Raymond, B. (2019). Bacteria from natural populations transfer plasmids mostly towards their kin. *Proceedings of the Royal Society B: Biological Sciences*, *286*(1905). https://doi.org/10.1098/rspb.2019.1110

Ding, M., Ye, Z., Liu, L., Wang, W., Chen, Q., Zhang, F., Wang, Y., Sjöling, Å., Martín-Rodríguez, A. J., Hu, R., Chen, W., & Zhou, Y. (2022). Subinhibitory antibiotic concentrations promote the horizontal transfer of plasmid-borne resistance genes from Klebsiellae pneumoniae to *Escherichia coli. Frontiers in Microbiology*, *13*. https://doi.org/10.3389/fmicb.2022.1017092

Ding, P., Lu, J., Wang, Y., Schembri, M. A., & Guo, J. (2022). Antidepressants promote the spread of antibiotic resistance via horizontally conjugative gene transfer. *Environmental Microbiology*, *24*(11), 5261–5276. https://doi.org/10.1111/1462-2920.16165

Docampo, L. (1989). Morfometría de las cuencas de la red hidrográfica de Bizkaia (País Vasco, España). *Limnetica*, *5*(1). https://doi.org/10.23818/limn.05.05

Douglas, G. M., & Langille, M. G. I. (2019). Current and promising approaches to identify horizontal gene transfer events in metagenomes. *Genome Biology and Evolution*, *11*(10). https://doi.org/10.1093/gbe/evz184

Doyle, C., Wall, K., Fanning, S., & McMahon, B. J. (2025). Making sense of sentinels: wildlife as the One Health bridge for environmental antimicrobial resistance surveillance. In *Journal of Applied Microbiology* (Vol. 136, Number 1). https://doi.org/10.1093/jambio/lxaf017

Drane, K., Sheehan, M., Whelan, A., Ariel, E., & Kinobe, R. (2024). The Role of Wastewater Treatment Plants in Dissemination of Antibiotic Resistance: Source, Measurement, Removal and Risk Assessment. In *Antibiotics* (Vol. 13, Number 7). https://doi.org/10.3390/antibiotics13070668

Durão, P., Balbontín, R., & Gordo, I. (2018). Evolutionary Mechanisms Shaping the Maintenance of Antibiotic Resistance. In *Trends in Microbiology* (Vol. 26, Number 8). https://doi.org/10.1016/j.tim.2018.01.005

Efron, B., & Hastie, T. (2016). Random Forests and Boosting. In *Computer Age Statistical Inference* (pp. 324–350). Cambridge University Press. https://doi.org/10.1017/CBO9781316576533.018

Eikmeyer, F., Hadiati, A., Szczepanowski, R., Wibberg, D., Schneiker-Bekel, S., Rogers, L. M., Brown, C. J., Top, E. M., Pühler, A., & Schlüter, A. (2012). The complete genome sequences of four new IncN plasmids from wastewater treatment plant effluent provide new insights into IncN plasmid diversity and evolution. *Plasmid*, *68*(1). https://doi.org/10.1016/j.plasmid.2012.01.011

El Ghachi, M., Bouhss, A., Blanot, D., & Mengin-Lecreulx, D. (2004). The bacA gene of *Escherichia coli* encodes an undecaprenyl pyrophosphate phosphatase activity. *Journal of Biological Chemistry*, *279*(29). https://doi.org/10.1074/jbc.M401701200

Elias, R., Modesto, A., Machado, D., Pereira, B., Phelan, J., Melo-Cristino, J., Lito, L., Gonçalves, L., Portugal, I., Viveiros, M., Campino, S., Clark, T. G., Duarte, A., & Perdigão, J. (2025). Dissemination of arr-2 and arr-3 is associated with class 1 integrons in Klebsiella pneumoniae clinical isolates from Portugal. *Medical Microbiology and Immunology*, *214*(1). https://doi.org/10.1007/s00430-024-00814-y

Environmental Protection Agency (EPA), I. (2024). *Innovative Monitoring to Prioritise Contaminants of Emerging Concern for Ireland: Impact*.

European Commission. (2017). *2017 EU One Health Action Plan against AMR*. https://health.ec.europa.eu/antimicrobial-resistance/eu-action-antimicrobial-resistance_en#ref-2017-eu-one-health-action-plan-against-amr

European Council. (1992). *Council Directive 92/43/EEC of 21 May 1992 on the Conservation of Natural Habitats and of Wild Fauna and Flora*.

European Environment Agency. (2026). *Waterbase — UWWTD: Urban Waste Water Treatment Directive. Waterbase reported under UWWTD data call 2023 — Final Public Version*. EEA Datahub. https://doi.org/10.2909/8376be6a-fa06-45f4-bb3b-401dcf4c4fba

European Parliament and Council of the European Union. (2024). *Directive (EU) 2024/3019 of the European Parliament and of the Council concerning urban wastewater treatment*. https://eur-lex.europa.eu/eli/dir/2024/3019/oj/eng

Eustat, I. V. de E. (2020). *Banco de datos o Estadísticas de la C.A. de Euskadi*. Https://Www.Eustat.Eus/Indice.Html.

FAO, UNEP, WHO, & WOAH. (2022). *One Health Joint Plan of Action (2022–2026). Working together for the health of humans, animals, plants and the environment*.

Feng, G., Huang, H., & Chen, Y. (2021). Effects of emerging pollutants on the occurrence and transfer of antibiotic resistance genes: A review. In *Journal of Hazardous Materials* (Vol. 420). https://doi.org/10.1016/j.jhazmat.2021.126602

Feng, M., Ye, C., Zhang, S., Sharma, V. K., Manoli, K., & Yu, X. (2022). Bisphenols promote the conjugative transfer of antibiotic resistance genes without damaging cell membrane. *Environmental Chemistry Letters*, *20*(3), 1553–1560. https://doi.org/10.1007/s10311-022-01397-x

Flores-Vargas, G., Korber, D. R., & Bergsveinson, J. (2023). Sub-MIC antibiotics influence the microbiome, resistome and structure of riverine biofilm communities. *Frontiers in Microbiology*, *14*. https://doi.org/10.3389/fmicb.2023.1194952

Fluit, A. C., & Schmitz, F. J. (2004). Resistance integrons and super-integrons. In *Clinical Microbiology and Infection* (Vol. 10, Number 4). https://doi.org/10.1111/j.1198-743X.2004.00858.x

Friedman, J. H. (2001). Greedy function approximation: A gradient boosting machine. *Annals of Statistics*, *29*(5). https://doi.org/10.1214/aos/1013203451

Gao, F. Z., Hu, L. X., Liu, Y. S., He, L. Y., Bai, H., Qiao, L. K., Chen, Z. Y., Li, P., Ju, F., Guo, J., & Ying, G. G. (2025). The increase in wastewater-sourced resistome elevated the prevalence and risk of riverine antibiotic resistance in wet season. *Environment International*, *203*. https://doi.org/10.1016/j.envint.2025.109769

Garcillán-Barcia, M. P., de la Cruz, F., & Rocha, E. P. C. (2025). The extended mobility of plasmids. In *Nucleic Acids Research* (Vol. 53, Number 14). https://doi.org/10.1093/nar/gkaf652

Garcillán-Barcia, M. P., Francia, M. V., & De La Cruz, F. (2009). The diversity of conjugative relaxases and its application in plasmid classification. *FEMS Microbiology Reviews*, *33*(3). https://doi.org/10.1111/j.1574-6976.2009.00168.x

Garcillán-Barcia, M. P., Redondo-Salvo, S., & de la Cruz, F. (2023). Plasmid classifications. *Plasmid*, *126*. https://doi.org/10.1016/j.plasmid.2023.102684

Gatica, J., & Cytryn, E. (2013). Impact of treated wastewater irrigation on antibiotic resistance in the soil microbiome. In *Environmental Science and Pollution Research* (Vol. 20, Number 6). https://doi.org/10.1007/s11356-013-1505-4

Gillings, M. R. (2014). Integrons: Past, Present, and Future. *Microbiology and Molecular Biology Reviews*, *78*(2). https://doi.org/10.1128/mmbr.00056-13

Gillings, M. R., Gaze, W. H., Pruden, A., Smalla, K., Tiedje, J. M., & Zhu, Y. G. (2015). Using the class 1 integron-integrase gene as a proxy for anthropogenic pollution. *ISME Journal*, *9*(6). https://doi.org/10.1038/ismej.2014.226

Global Coordination and Partnership (GCP). (2025). *Analysis of antibacterial agents in clinical and preclinical development: overview and analysis 2025*.

Graumnitz, S., & Jungmann, D. (2021). *The database "Pharmaceuticals in the Environment". Update for the period 2017-2020*.

Gullberg, E., Cao, S., Berg, O. G., Ilbäck, C., Sandegren, L., Hughes, D., & Andersson, D. I. (2011). Selection of resistant bacteria at very low antibiotic concentrations. *PLoS Pathogens*, *7*(7). https://doi.org/10.1371/journal.ppat.1002158

Gustavsson, M., Käll, S., Svedberg, P., Inda-Diaz, J. S., Molander, S., Coria, J., Backhaus, T., & Kristiansson, E. (2024). Transformers enable accurate prediction of acute and chronic chemical toxicity in aquatic organisms. *Science Advances*, *10*(10). https://doi.org/10.1126/sciadv.adk6669

Guzmán-Herrador, D. L., & Llosa, M. (2019). The secret life of conjugative relaxases. In *Plasmid* (Vol. 104). https://doi.org/10.1016/j.plasmid.2019.102415

Haenelt, S., Richnow, H. H., Müller, J. A., & Musat, N. (2023). Antibiotic resistance indicator genes in biofilm and planktonic microbial communities after wastewater discharge. *Frontiers in Microbiology*, *14*. https://doi.org/10.3389/fmicb.2023.1252870

Han, M., Chen, Q., Li, Z. K., Hu, X. J., Ma, J. C., Qin, C., Gao, Y. Z., Han, M., Chen, Q., Li, Z., Hu, X., Ma, J., Qin, C., & Gao, Y. (2025). Cellular mechanism of perfluoroalkyl substances with different chain lengths influence conjugative transfer of antibiotic resistance genes. *ENVIRONMENT INTERNATIONAL*, *204*. https://doi.org/10.1016/j.envint.2025.109810

Hastie, T., Tibshirani, R., & Friedman, J. (2009). *The Elements of Statistical Learning: Data Mining, Inference, and Prediction (2nd ed.)* (2nd edition). Springer.

He, Z., Dechesne, A., Schreiber, F., Zhu, Y. G., Larsson, D. G. J., & Smets, B. F. (2024). Understanding Stimulation of Conjugal Gene Transfer by Nonantibiotic Compounds: How Far Are We? In *Environmental Science and Technology* (Vol. 58, Number 21). https://doi.org/10.1021/acs.est.3c06060

Headd, B., & Bradford, S. A. (2020). The conjugation window in an *Escherichia coli* K-12 strain with an IncFII plasmid. *Applied and Environmental Microbiology*, *86*(17). https://doi.org/10.1128/AEM.00948-20

Hendriksen, R. S., Munk, P., Njage, P., van Bunnik, B., McNally, L., Lukjancenko, O., Röder, T., Nieuwenhuijse, D., Pedersen, S. K., Kjeldgaard, J., Kaas, R. S., Clausen, P. T. L. C., Vogt, J. K., Leekitcharoenphon, P., van de Schans, M. G. M., Zuidema, T., de Roda Husman, A. M., Rasmussen, S., Petersen, B., … Aarestrup, F. M. (2019). Global

monitoring of antimicrobial resistance based on metagenomics analyses of urban sewage. *Nature Communications*, *10*(1). https://doi.org/10.1038/s41467-019-08853-3

Heuer, H., Binh, C. T. T., Jechalke, S., Kopmann, C., Zimmerling, U., Krögerrecklenfort, E., Ledger, T., González, B., Top, E., & Smalla, K. (2012). IncP-1ε plasmids are important vectors of antibiotic resistance genes in agricultural systems: Diversification driven by class 1 integron gene cassettes. *Frontiers in Microbiology*, *3*(JAN). https://doi.org/10.3389/fmicb.2012.00002

Huang, H., Liao, J., Zheng, X., Chen, Y., & Ren, H. (2019). Low-level free nitrous acid efficiently inhibits the conjugative transfer of antibiotic resistance by altering intracellular ions and disabling transfer apparatus. *Water Research*, *158*, 383–391. https://doi.org/10.1016/j.watres.2019.04.046

Huang, H., Lin, L., Liu, Q., Li, X., Liao, J., Dong, L., Zhang, J., Su, Y., Luo, J., Feng, L., Zheng, X., Guo, J., & Chen, Y. (2025). Hydrogen sulfide drives horizontal transfer of plasmid-borne antibiotic resistance genes in wastewater ecosystems. *Nature Water*, *3*(11). https://doi.org/10.1038/s44221-025-00523-7

Hughes, J., Cowper-Heays, K., Olesson, E., Bell, R., & Stroombergen, A. (2021). Impacts and implications of climate change on wastewater systems: A New Zealand perspective. In *Climate Risk Management* (Vol. 31). https://doi.org/10.1016/j.crm.2020.100262

Hunter, J. D. (2007). Matplotlib: A 2D graphics environment. *Computing in Science and Engineering*, *9*(3). https://doi.org/10.1109/MCSE.2007.55

Hutinel, M., Fick, J., Larsson, D. G. J., & Flach, C. F. (2021). Investigating the effects of municipal and hospital wastewaters on horizontal gene transfer. *Environmental Pollution*, *276*. https://doi.org/10.1016/j.envpol.2021.116733

Inda-Díaz, J. S., Johnning, A., Hessel, M., Sjöberg, A., Lokrantz, A., Helldal, L., Jirstrand, M., Svensson, L., & Kristiansson, E. (2026). Confidence-based prediction of antibiotic resistance at the patient level. *MBio*.

Instituto Nacional de Estadística. (2024). *Estadística de Movimientos Turísticos en Fronteras (FRONTUR)*.

Jacoby, G. A., Walsh, K. E., Mills, D. M., Walker, V. J., Oh, H., Robicsek, A., & Hooper, D. C. (2006). qnrB, another plasmid-mediated gene for quinolone resistance. *Antimicrobial Agents and Chemotherapy*, *50*(4). https://doi.org/10.1128/AAC.50.4.1178-1182.2006

Jiang, Q., Feng, M., Ye, C., & Yu, X. (2022). Effects and relevant mechanisms of non-antibiotic factors on the horizontal transfer of antibiotic resistance genes in water environments: A review. In *Science of the Total Environment* (Vol. 806). https://doi.org/10.1016/j.scitotenv.2021.150568

Johnsen, A. R., & Kroer, N. (2007). Effects of stress and other environmental factors on horizontal plasmid transfer assessed by direct quantification of discrete transfer events. *FEMS Microbiology Ecology*, *59*(3). https://doi.org/10.1111/j.1574-6941.2006.00230.x

Johnston, C., Martin, B., Fichant, G., Polard, P., & Claverys, J. P. (2014). Bacterial transformation: Distribution, shared mechanisms and divergent control. In *Nature Reviews Microbiology* (Vol. 12, Number 3). https://doi.org/10.1038/nrmicro3199

Karkman, A., Pärnänen, K., & Larsson, D. G. J. (2019). Fecal pollution can explain antibiotic resistance gene abundances in anthropogenically impacted environments. *Nature Communications*, *10*(1). https://doi.org/10.1038/s41467-018-07992-3

Katoh, K., & Standley, D. M. (2013). MAFFT multiple sequence alignment software version 7: Improvements in performance and usability. *Molecular Biology and Evolution*, *30*(4). https://doi.org/10.1093/molbev/mst010

Klümper, U., Dechesne, A., Riber, L., Brandt, K. K., Gülay, A., Sørensen, S. J., & Smets, B. F. (2017). Metal stressors consistently modulate bacterial conjugal plasmid uptake potential in a phylogenetically conserved manner. *ISME Journal*, *11*(1). https://doi.org/10.1038/ismej.2016.98

Klümper, U., Maillard, A., Hesse, E., Bayer, F., Houte, S. van, Longdon, B., Gaze, W., & Buckling, A. (2019). Short-term evolution under copper stress increases probability of plasmid uptake. *BioRxiv*.

Klümper, U., Riber, L., Dechesne, A., Sannazzarro, A., Hansen, L. H., Sørensen, S. J., & Smets, B. F. (2015). Broad host range plasmids can invade an unexpectedly diverse fraction of a soil bacterial community. *ISME Journal*, *9*. https://doi.org/10.1038/ismej.2014.191

Kneis, D., Lemay-St-Denis, C., Cellier-Goetghebeur, S., Elena, A. X., Berendonk, T. U., Pelletier, J. N., & Heß, S. (2023). Trimethoprim resistance in surface and wastewater is mediated by contrasting variants of the dfrB gene. *ISME Journal*, *17*(9). https://doi.org/10.1038/s41396-023-01460-7

Kolmogorov, M., Yuan, J., Lin, Y., & Pevzner, P. A. (2019). Assembly of long, error-prone reads using repeat graphs. *Nature Biotechnology*, *37*(5). https://doi.org/10.1038/s41587-019-0072-8

Kostelidou, K., Jones, A. C., & Thomas, C. M. (1999). Conserved C-terminal region of global repressor KorA of broad-host-range plasmid RK2 is required for co-operativity between KorA and a second RK2 global regulator, KorB. *Journal of Molecular Biology*, *289*(2). https://doi.org/10.1006/jmbi.1999.2761

Kwapien, K., Nittinger, E., He, J., Margreitter, C., Voronov, A., & Tyrchan, C. (2022). Implications of Additivity and Nonadditivity for Machine Learning and Deep Learning Models in Drug Design. *ACS Omega*, *7*(30). https://doi.org/10.1021/acsomega.2c02738

Laborda, P., Sanz-García, F., Ochoa-Sánchez, L. E., Gil-Gil, T., Hernando-Amado, S., & Martínez, J. L. (2022). Wildlife and Antibiotic Resistance. In *Frontiers in Cellular and Infection Microbiology* (Vol. 12). https://doi.org/10.3389/fcimb.2022.873989

Larsson, D. G. J., & Flach, C.-F. (2022). Antibiotic resistance in the environment. *Nat Rev Microbiol*, *20*, 257–269.

Lau-Wong, I. C., Locke, T., Ellison, M. J., Raivio, T. L., & Frost, L. S. (2008). Activation of the Cpx regulon destabilizes the F plasmid transfer activator, TraJ, via the HslVU protease in *Escherichia coli*. *Molecular Microbiology*, *67*(3). https://doi.org/10.1111/j.1365-2958.2007.06055.x

Laxminarayan, R., Duse, A., Wattal, C., Zaidi, A. K. M., Wertheim, H. F. L., Sumpradit, N., Vlieghe, E., Hara, G. L., Gould, I. M., Goossens, H., Greko, C., So, A. D., Bigdeli, M., Tomson, G., Woodhouse, W., Ombaka, E., Peralta, A. Q., Qamar, F. N., Mir, F., … Cars, O. (2013). Antibiotic resistance-the need for global solutions. In *The Lancet Infectious Diseases* (Vol. 13, Number 12). https://doi.org/10.1016/S1473-3099(13)70318-9

Leelaporn, A., Paulsen, I. T., Tennent, J. M., Littlejohn, T. G., & Skurray, R. A. (1994). Multidrug resistance to antiseptics and disinfectants in coagulase-negative staphylococci. *Journal of Medical Microbiology*, *40*(3). https://doi.org/10.1099/00222615-40-3-214

Li, J., Li, X., Liu, H., Gao, L., Wang, W., Wang, Z., Zhou, T., & Wang, Q. (2023). Climate change impacts on wastewater infrastructure: A systematic review and typological adaptation strategy. In *Water Research* (Vol. 242). https://doi.org/10.1016/j.watres.2023.120282

Li, L. G., & Zhang, T. (2023). Plasmid-mediated antibiotic resistance gene transfer under environmental stresses: Insights from laboratory-based studies. In *Science of the Total Environment* (Vol. 887). https://doi.org/10.1016/j.scitotenv.2023.163870

Liang, H., Li, X., & Yan, H. (2022). Identification of a Novel IncHI1B Plasmid in MDR Klebsiella pneumoniae 200 from Swine in China. *Antibiotics*, *11*(9). https://doi.org/10.3390/antibiotics11091225

Liebert, C. A., Hall, R. M., & Summers, A. O. (1999). Transposon Tn 21 , Flagship of the Floating Genome . *Microbiology and Molecular Biology Reviews*, *63*(3). https://doi.org/10.1128/mmbr.63.3.507-522.1999

Lin, B., Yan, S., & Zhen, B. (2025). A machine learning method for predicting molecular antimicrobial activity. *Scientific Reports*, *15*(1). https://doi.org/10.1038/s41598-025-91190-x

Liu, G., Thomsen, L. E., & Olsen, J. E. (2022). Antimicrobial-induced horizontal transfer of antimicrobial resistance genes in bacteria: A mini-review. *Journal of Antimicrobial Chemotherapy*, *77*(3). https://doi.org/10.1093/jac/dkab450

Liu, Q., Li, M., Liu, X., Zhang, Q., Liu, R., Wang, Z., Shi, X., Quan, J., Shen, X., & Zhang, F. (2018). Removal of sulfamethoxazole and trimethoprim from reclaimed water and the biodegradation mechanism. *Frontiers of Environmental Science and Engineering*, *12*(6). https://doi.org/10.1007/s11783-018-1048-5

Liu, Y., Tong, Z., Shi, J., Jia, Y., Yang, K., & Wang, Z. (2020). Correlation between exogenous compounds and the horizontal transfer of plasmid-borne antibiotic resistance genes. In *Microorganisms* (Vol. 8, Number 8). https://doi.org/10.3390/microorganisms8081211

Liu, Y. Y., Wang, Y., Walsh, T. R., Yi, L. X., Zhang, R., Spencer, J., Doi, Y., Tian, G., Dong, B., Huang, X., Yu, L. F., Gu, D., Ren, H., Chen, X., Lv, L., He, D., Zhou, H., Liang, Z., Liu, J. H., & Shen, J. (2016). Emergence of plasmid-mediated colistin resistance mechanism MCR-1 in animals and human beings in China: A microbiological and molecular biological study. *The Lancet Infectious Diseases*, *16*(2). https://doi.org/10.1016/S1473-3099(15)00424-7

Louca, S., Polz, M. F., Mazel, F., Albright, M. B. N., Huber, J. A., O'Connor, M. I., Ackermann, M., Hahn, A. S., Srivastava, D. S., Crowe, S. A., Doebeli, M., & Parfrey, L. W. (2018). Function and functional redundancy in microbial systems. In *Nature Ecology and Evolution* (Vol. 2, Number 6). https://doi.org/10.1038/s41559-018-0519-1

Loui, C., Chang, A. C., & Lu, S. (2009). Role of the ArcAB two-component system in the resistance of *Escherichia coli* to reactive oxygen stress. *BMC Microbiology*, *9*. https://doi.org/10.1186/1471-2180-9-183

Lu, J., Peng, Y., Wan, S., Frost, L. S., Raivio, T., & Mark Glover, J. N. (2019). Cooperative function of TraJ and ArcA in regulating the F plasmid tra operon. *Journal of Bacteriology*, *201*(1). https://doi.org/10.1128/JB.00448-18

Lund, D., Parras-Moltó, M., Inda-Díaz, J. S., Ebmeyer, S., Larsson, D. G. J., Johnning, A., & Kristiansson, E. (2025). Genetic compatibility and ecological connectivity drive the dissemination of antibiotic resistance genes. *Nature Communications* , *16*(1). https://doi.org/10.1038/s41467-025-57825-3

Lundberg, S. M., & Lee, S. I. (2017). A unified approach to interpreting model predictions. Advances in neural information processing systems. *Advances in Neural Information Processing Systems*, *30*(2).

Luo, C., Zhang, T., Mustafa, M. F., Li, M., & Xu, S. (2025). Removal efficiency of ARGs in different wastewater treatment plants and their potential risks in effluent. *Npj Clean Water*, *8*(1). https://doi.org/10.1038/s41545-025-00456-4

Ma, L., Qu, Y., Wang, W., & Wang, D. (2023). Characterization of Klebsiella pneumoniae carrying the blaNDM-1 gene in IncX3 plasmids and the rare In1765 in an IncFIB-IncHI1B plasmid. *Frontiers in Cellular and Infection Microbiology*, *13*. https://doi.org/10.3389/fcimb.2023.1324846

Ma, L., Zhang, X. X., Cheng, S., Zhang, Z., Shi, P., Liu, B., Wu, B., & Zhang, Y. (2011). Occurrence, abundance and elimination of class 1 integrons in one municipal sewage treatment plant. *Ecotoxicology*, *20*(5). https://doi.org/10.1007/s10646-011-0652-y

MacFadden, D. R., McGough, S. F., Fisman, D., Santillana, M., & Brownstein, J. S. (2018). Antibiotic resistance increases with local temperature. *Nature Climate Change*, *8*(6). https://doi.org/10.1038/s41558-018-0161-6

Manaia, C. M. (2023). Framework for establishing regulatory guidelines to control antibiotic resistance in treated effluents. In *Critical Reviews in Environmental Science and Technology* (Vol. 53, Number 6). https://doi.org/10.1080/10643389.2022.2085956

Manaia, C. M., Rocha, J., Scaccia, N., Marano, R., Radu, E., Biancullo, F., Cerqueira, F., Fortunato, G., Iakovides, I. C., Zammit, I., Kampouris, I., Vaz-Moreira, I., & Nunes, O. C. (2018). Antibiotic resistance in wastewater treatment plants: Tackling the black box. In *Environment International* (Vol. 115). https://doi.org/10.1016/j.envint.2018.03.044

Mansor, M., & Xu, J. (2020). Benefits at the nanoscale: a review of nanoparticle-enabled processes favouring microbial growth and functionality. In *Environmental Microbiology* (Vol. 22, Number 9). https://doi.org/10.1111/1462-2920.15174

Marçais, G., Delcher, A. L., Phillippy, A. M., Coston, R., Salzberg, S. L., & Zimin, A. (2018). MUMmer4: A fast and versatile genome alignment system. *PLoS Computational Biology*, *14*(1). https://doi.org/10.1371/journal.pcbi.1005944

Masi, M., Réfregiers, M., Pos, K. M., & Pagès, J. M. (2017). Mechanisms of envelope permeability and antibiotic influx and efflux in Gram-negative bacteria. *Nature Microbiology*, *2*(3). https://doi.org/10.1038/nmicrobiol.2017.1

Mathers, A. J., Peirano, G., & Pitout, J. D. D. (2015). The role of epidemic resistance plasmids and international high-risk clones in the spread of multidrug-resistant Enterobacteriaceae. *Clinical Microbiology Reviews*, *28*(3). https://doi.org/10.1128/CMR.00116-14

Matlock, W., Lipworth, S., Chau, K. K., AbuOun, M., Barker, L., Kavanagh, J., Andersson, M., Oakley, S., Morgan, M., Crook, D. W., Read, D. S., Anjum, M., Shaw, L. P., & Stoesser, N. (2023). Enterobacterales plasmid sharing amongst human bloodstream infections, livestock, wastewater, and waterway niches in Oxfordshire, UK. *ELife*, *12*. https://doi.org/10.7554/eLife.85302

Matuschek, E., Brown, D. F. J., & Kahlmeter, G. (2014). Development of the EUCAST disk diffusion antimicrobial susceptibility testing method and its implementation in routine microbiology laboratories. *Clinical Microbiology and Infection*, *20*(4). https://doi.org/10.1111/1469-0691.12373

Mazel, D. (2006). Integrons: Agents of bacterial evolution. In *Nature Reviews Microbiology* (Vol. 4, Number 8). https://doi.org/10.1038/nrmicro1462

McDonnell, A., Countryman, A., Laurence, T., Gulliver, S., Drake, T., Edwards, S., Kenny, C., Lamberti, O., Morton, A., Shafira, A., Smith, R., & Guzman, J. (2024). *Forecasting the Fallout from AMR: Economic Impacts of Antimicrobial Resistance in Humans*. Center For Global Development.

McEwen, S. A., & Collignon, P. J. (2018). Antimicrobial Resistance: a One Health Perspective. *Microbiology Spectrum*, *6*(2). https://doi.org/10.1128/microbiolspec.arba-0009-2017

Memar, M. Y., Yekani, M., Celenza, G., Poortahmasebi, V., Naghili, B., Bellio, P., & Baghi, H. B. (2020). The central role of the SOS DNA repair system in antibiotics resistance: A new target for a new infectious treatment strategy. In *Life Sciences* (Vol. 262). https://doi.org/10.1016/j.lfs.2020.118562

Miao, S., Zhang, Y., Wu, L., Wang, Y., & Zuo, J. (2025). Resistance induction potency assessment of antibiotic production wastewater and associated resistome shaping mechanisms. *Water Research*, *283*. https://doi.org/10.1016/j.watres.2025.123811

Migliore, L., Rotini, A., & Thaller, M. C. (2013). Low doses of tetracycline trigger the E. coli growth: A case of hormetic response. *Dose-Response*, *11*(4). https://doi.org/10.2203/dose-response.13-002.Migliore

Millan, A. S., Peña-Miller, R., Toll-Riera, M., Halbert, Z. V., McLean, A. R., Cooper, B. S., & Maclean, R. C. (2014). Positive selection and compensatory adaptation interact to stabilize non-transmissible plasmids. *Nature Communications*, *5*. https://doi.org/10.1038/ncomms6208

Muoghalu, C., Kaboggoza, H. C., Semiyaga, S., Lebu, S., Liu, C., Niwagaba, C., Nansubuga, F., & Manga, M. (2025). Antibiotic resistant bacteria (ARB) and genes (ARGs) in urban wastewater treatment plants: influencing factors, mechanisms, and removal efficiency. In *Environmental Pollution* (Vol. 383). https://doi.org/10.1016/j.envpol.2025.126851

Murray, L. M., Hayes, A., Snape, J., Kasprzyk-Hordern, B., Gaze, W. H., & Murray, A. K. (2024). Co-selection for antibiotic resistance by environmental contaminants. *Npj Antimicrobials and Resistance*, *2*(1). https://doi.org/10.1038/s44259-024-00026-7

Mutuku, C., Gazdag, Z., & Melegh, S. (2022). Occurrence of antibiotics and bacterial resistance genes in wastewater: resistance mechanisms and antimicrobial resistance control approaches. In *World Journal of Microbiology and Biotechnology* (Vol. 38, Number 9). https://doi.org/10.1007/s11274-022-03334-0

Naghavi, M., Vollset, S. E., Ikuta, K. S., Swetschinski, L. R., Gray, A. P., Wool, E. E., Robles Aguilar, G., Mestrovic, T., Smith, G., Han, C., Hsu, R. L., Chalek, J., Araki, D. T., Chung, E., Raggi, C., Gershberg Hayoon, A., Davis Weaver, N., Lindstedt, P. A., Smith, A. E., … Murray, C. J. L. (2024). Global burden of bacterial antimicrobial resistance 1990–2021: a systematic analysis with forecasts to 2050. *The Lancet*, *404*(10459). https://doi.org/10.1016/S0140-6736(24)01867-1

Néron, B., Littner, E., Haudiquet, M., Perrin, A., Cury, J., & Rocha, E. P. C. (2022). IntegronFinder 2.0: Identification and Analysis of Integrons across Bacteria, with a Focus on Antibiotic Resistance in Klebsiella. *Microorganisms*, *10*(4). https://doi.org/10.3390/microorganisms10040700

Nguyen, A. K., Goering, P. L., Elespuru, R. K., Das, S. S., & Narayan, R. J. (2020). The photoinitiator lithium phenyl (2,4,6-Trimethylbenzoyl) phosphinate with exposure to 405 nm light is cytotoxic to mammalian cells but not mutagenic in bacterial reverse mutation assays. *Polymers*, *12*(7). https://doi.org/10.3390/polym12071489

Niazi, S. K., & Mariam, Z. (2023). Recent Advances in Machine-Learning-Based Chemoinformatics: A Comprehensive Review. In *International Journal of Molecular Sciences* (Vol. 24, Number 14). https://doi.org/10.3390/ijms241411488

Nikaido, H. (2003). Molecular Basis of Bacterial Outer Membrane Permeability Revisited. *Microbiology and Molecular Biology Reviews*, *67*(4). https://doi.org/10.1128/mmbr.67.4.593-656.2003

Nilsson, A. S., & Haggård-Ljungquist, E. (2007). Evolution of P2-like phages and their impact on bacterial evolution. In *Research in Microbiology* (Vol. 158, Number 4). https://doi.org/10.1016/j.resmic.2007.02.004

Norman, A., Hansen, L. H., & Sørensen, S. J. (2009). Conjugative plasmids: Vessels of the communal gene pool. In *Philosophical Transactions of the Royal Society B: Biological Sciences* (Vol. 364, Number 1527). https://doi.org/10.1098/rstb.2009.0037

NORMAN Network. (2025). *NORMAN Substance Database (SusDat)*. https://www.norman-network.com/nds/susdat/

Ochman, H., Lawrence, J. G., & Grolsman, E. A. (2000). Lateral gene transfer and the nature of bacterial innovation. In *Nature* (Vol. 405, Number 6784). https://doi.org/10.1038/35012500

Ojer-Usoz, E., González, D., García-Jalón, I., & Vitas, A. I. (2014). High dissemination of extended-spectrum β-lactamase-producing Enterobacteriaceae ineffluents from wastewater treatment plants. *Water Research*, *56*. https://doi.org/10.1016/j.watres.2014.02.041

Ouzzani, M., Hammady, H., Fedorowicz, Z., & Elmagarmid, A. (2016). Rayyan-a web and mobile app for systematic reviews. *Systematic Reviews*, *5*(1). https://doi.org/10.1186/s13643-016-0384-4

Page, A. J., Cummins, C. A., Hunt, M., Wong, V. K., Reuter, S., Holden, M. T. G., Fookes, M., Falush, D., Keane, J. A., & Parkhill, J. (2015). Roary: Rapid large-scale prokaryote pan genome analysis. *Bioinformatics*, *31*(22). https://doi.org/10.1093/bioinformatics/btv421

Parras-Moltó, M., Lund, D., Ebmeyer, S., Larsson, D. G. J., Johnning, A., & Kristiansson, E. (2025). The transfer of antibiotic resistance genes between evolutionarily distant bacteria. *MSphere*, *10*(6). https://doi.org/10.1128/msphere.00114-25

Partridge, S. R. (2011). Analysis of antibiotic resistance regions in Gram-negative bacteria. In *FEMS Microbiology Reviews* (Vol. 35, Number 5). https://doi.org/10.1111/j.1574-6976.2011.00277.x

Partridge, S. R., Collis, C. M., & Hall, R. M. (2002). Class 1 integron containing a new gene cassette, aadA10, associated with Tn1404 from R151. *Antimicrobial Agents and Chemotherapy*, *46*(8). https://doi.org/10.1128/AAC.46.8.2400-2408.2002

Persson, L., Carney Almroth, B. M., Collins, C. D., Cornell, S., de Wit, C. A., Diamond, M. L., Fantke, P., Hassellöv, M., MacLeod, M., Ryberg, M. W., Søgaard Jørgensen, P., Villarrubia-Gómez, P., Wang, Z., & Hauschild, M. Z. (2022). Outside the Safe Operating Space of the Planetary Boundary for Novel Entities. *Environmental Science and Technology*, *56*(3). https://doi.org/10.1021/acs.est.1c04158

Pfeifer, E., & Rocha, E. P. C. (2024). Phage-plasmids promote recombination and emergence of phages and plasmids. *Nature Communications*, *15*(1). https://doi.org/10.1038/s41467-024-45757-3

Pitout, J. D. D., & Chen, L. (2023). The Significance of Epidemic Plasmids in the Success of Multidrug-Resistant Drug Pandemic Extraintestinal Pathogenic *Escherichia coli*. In *Infectious Diseases and Therapy* (Vol. 12, Number 4). https://doi.org/10.1007/s40121-023-00791-4

Rao, T. V. P., & Kuzminov, A. (2022). Oxidative Damage Blocks Thymineless Death and Trimethoprim Poisoning in *Escherichia coli*. *Journal of Bacteriology*, *204*(1). https://doi.org/10.1128/JB.00370-21

Richardson, S. D., & Ternes, T. A. (2018). Water Analysis: Emerging Contaminants and Current Issues. In *Analytical Chemistry* (Vol. 90, Number 1). https://doi.org/10.1021/acs.analchem.7b04577

Rizzo, L., Manaia, C., Merlin, C., Schwartz, T., Dagot, C., Ploy, M. C., Michael, I., & Fatta-Kassinos, D. (2013). Urban wastewater treatment plants as hotspots for antibiotic resistant bacteria and genes spread into the environment: A review. In *Science of the Total Environment* (Vol. 447). https://doi.org/10.1016/j.scitotenv.2013.01.032

Roberts, M. C. (2005). Update on acquired tetracycline resistance genes. In *FEMS Microbiology Letters* (Vol. 245, Number 2). https://doi.org/10.1016/j.femsle.2005.02.034

Roberts, M. C. (2008). Update on macrolide-lincosamide-streptogramin, ketolide, and oxazolidinone resistance genes. In *FEMS Microbiology Letters* (Vol. 282, Number 2). https://doi.org/10.1111/j.1574-6968.2008.01145.x

Rockström, J., Steffen, W., Noone, K., Persson, Å., Chapin, F. S., Lambin, E., Lenton, T. M., Scheffer, M., Folke, C., Schellnhuber, H. J., Nykvist, B., de Wit, C. A., Hughes, T., van der Leeuw, S., Rodhe, H., Sörlin, S., Snyder, P. K., Costanza, R., Svedin, U., … Foley, J. (2009). Planetary boundaries: Exploring the safe operating space for humanity. *Ecology and Society*, *14*(2). https://doi.org/10.5751/ES-03180-140232

Rodriguez-Grande, J., Garcillan, M. del P., Cruz, F. de la, & Fernandez-Lopez, R. (2023). Fundamental parameters governing the transmission of conjugative plasmids. *BioRxiv*.

Rodríguez-Pérez, R., Miljković, F., & Bajorath, J. (2022). Machine Learning in Chemoinformatics and Medicinal Chemistry. In *Annual Review of Biomedical Data Science* (Vol. 5). https://doi.org/10.1146/annurev-biodatasci-122120-124216

Rogers, D., & Hahn, M. (2010). Extended-connectivity fingerprints. *Journal of Chemical Information and Modeling*, *50*(5). https://doi.org/10.1021/ci100050t.

Rohatgi, A. (2024). *WebPlotDigitizer* (5.2). https://automeris.io/.

Romero, J. L., Grande Burgos, M. J., Pérez-Pulido, R., Gálvez, A., & Lucas, R. (2017). Resistance to Antibiotics, Biocides, Preservatives and Metals in Bacteria Isolated from Seafoods: Co-Selection of Strains Resistant or Tolerant to Different Classes of Compounds. *Frontiers in Microbiology*, *8*. https://doi.org/10.3389/fmicb.2017.01650.

Rozwandowicz, M., Brouwer, M. S. M., Fischer, J., Wagenaar, J. A., Gonzalez-Zorn, B., Guerra, B., Mevius, D. J., & Hordijk, J. (2018). Plasmids carrying antimicrobial resistance genes in Enterobacteriaceae. *Journal of Antimicrobial Chemotherapy*, *73*(5). https://doi.org/10.1093/jac/dkx488.

Ruan, C., Ramoneda, J., Chen, G., Johnson, D. R., & Wang, G. (2021). Evaporation-induced hydrodynamics promote conjugation-mediated plasmid transfer in microbial populations. *ISME Communications*, *1*(1). https://doi.org/10.1038/s43705-021-00057-5.

Sabri, N. A., van Holst, S., Schmitt, H., van der Zaan, B. M., Gerritsen, H. W., Rijnaarts, H. H. M., & Langenhoff, A. A. M. (2020). Fate of antibiotics and antibiotic resistance genes during conventional and additional treatment technologies in wastewater treatment plants. *Science of the Total Environment*, *741*. https://doi.org/10.1016/j.scitotenv.2020.140199.

San Millan, A., & MacLean, R. C. (2017). Fitness Costs of Plasmids: a Limit to Plasmid Transmission. *Microbiology Spectrum*, *5*(5). https://doi.org/10.1128/microbiolspec.mtbp-0016-2017.

Sangurdekar, D. P., Zhang, Z., & Khodursky, A. B. (2011). The association of DNA damage response and nucleotide level modulation with the antibacterial mechanism of the anti-folate drug Trimethoprim. *BMC Genomics*, *12*. https://doi.org/10.1186/1471-2164-12-583.

Schlüter, A., Szczepanowski, R., Pühler, A., & Top, E. M. (2007). Genomics of IncP-1 antibiotic resistance plasmids isolated from wastewater treatment plants provides evidence for a widely accessible drug resistance gene pool. In *FEMS Microbiology Reviews* (Vol. 31, Number 4). https://doi.org/10.1111/j.1574-6976.2007.00074.x.

Schmidt, S. B. I., Rodríguez-Rojas, A., Rolff, J., & Schreiber, F. (2022). Biocides used as material preservatives modify rates of de novo mutation and horizontal gene transfer in bacteria. *Journal of Hazardous Materials*, *437*. https://doi.org/10.1016/j.jhazmat.2022.129280.

Schönenberger, U. T., Beck, B., Dax, A., Vogler, B., & Stamm, C. (2022). Pesticide concentrations in agricultural storm drainage inlets of a small Swiss catchment. *Environmental Science and Pollution Research*, *29*(29). https://doi.org/10.1007/s11356-022-18933-5.

Schwengers, O., Jelonek, L., Dieckmann, M. A., Beyvers, S., Blom, J., & Goesmann, A. (2021). Bakta: Rapid and standardized annotation of bacterial genomes via alignment-free sequence identification. *Microbial Genomics*, *7*(11). https://doi.org/10.1099/MGEN.0.000685.

Shaw, K. J., Rather, P. N., Hare, R. S., & Miller, G. H. (1993). Molecular genetics of aminoglycoside resistance genes and familial relationships of the aminoelycoside-modifying enzymes. *Microbiological Reviews*, *57*(1). https://doi.org/10.1128/mr.57.1.138-163.1993.

Shi, D., Hao, H., Wei, Z., Yang, D., Yin, J., Li, H., Chen, Z., Yang, Z., Chen, T., Zhou, S., Wu, H., Li, J., & Jin, M. (2022). Combined exposure to non-antibiotic pharmaceutics and antibiotics in the gut synergistically promote the development of multi-drug-resistance in *Escherichia coli. Gut Microbes, 14(1). https://doi.org/10.1080/19490976.2021.2018901.*

Shintani, M., Sanchez, Z. K., & Kimbara, K. (2015). Genomics of microbial plasmids: Classification and identification based on replication and transfer systems and host taxonomy. In *Frontiers in Microbiology* (Vol. 6, Number MAR). https://doi.org/10.3389/fmicb.2015.00242.

Siguier, P., Gourbeyre, E., & Chandler, M. (2014). Bacterial insertion sequences: Their genomic impact and diversity. *FEMS Microbiology Reviews*, *38*(5). https://doi.org/10.1111/1574-6976.12067.

Siguier, P., Gourbeyre, E., Varani, A., Ton-Hoang, B., & Chandler, M. (2015). Everyman's Guide to Bacterial Insertion Sequences. *Microbiology Spectrum*, *3*(2). https://doi.org/10.1128/microbiolspec.mdna3-0030-2014.

Simpkin, V. L., Renwick, M. J., Kelly, R., & Mossialos, E. (2017). Incentivising innovation in antibiotic drug discovery and development: Progress, challenges and next steps. In *Journal of Antibiotics* (Vol. 70, Number 12). https://doi.org/10.1038/ja.2017.124.

Sivalingam, P., Sabatino, R., Sbaffi, T., Corno, G., Fontaneto, D., Borgomaneiro, G., Rogora, M., Crotti, E., Mapelli, F., Borin, S., Pilar, A. L., Eckert, E. M., & Di Cesare, A. (2024). Anthropogenic pollution may enhance natural transformation in water, favouring the spread of antibiotic resistance genes. *Journal of Hazardous Materials*, *475*. https://doi.org/10.1016/j.jhazmat.2024.134885.

Sköld, O. (2001). Resistance to trimethoprim and sulfonamides. *Veterinary Research*, *32*(3–4). https://doi.org/10.1051/vetres:2001123.

Smułek, W., & Kaczorek, E. (2022). Factors Influencing the Bioavailability of Organic Molecules to Bacterial Cells—A Mini-Review. In *Molecules* (Vol. 27, Number 19). https://doi.org/10.3390/molecules27196579.

Sotero-Martins, A., De Jesus, M. S., Lacerda, M., Moreira, J. C., Filgueiras, A. L. L., & Barrocas, P. R. G. (2008). A conservative region of the mercuric reductase gene (*merA*) as a molecular marker of bacterial mercury resistance. *Brazilian Journal of Microbiology*, *39*(2). https://doi.org/10.1590/S1517-83822008000200020.

Souza, L. P. de, Sanches-Neto, F. O., Junior, G. M. Y., Ramos, B., Lastre-Acosta, A. M., Carvalho-Silva, V. H., & Teixeira, A. C. S. C. (2022). Photochemical environmental persistence of venlafaxine in an urban water reservoir: A

combined experimental and computational investigation. *Process Safety and Environmental Protection*, *166*. https://doi.org/10.1016/j.psep.2022.08.049.

Stalder, T., Barraud, O., Casellas, M., Dagot, C., & Ploy, M. C. (2012). Integron involvement in environmental spread of antibiotic resistance. In *Frontiers in Microbiology* (Vol. 3, Number APR). https://doi.org/10.3389/fmicb.2012.00119.

Stanton, I. C., Tipper, H. J., Chau, K., Klümper, U., Subirats, J., & Murray, A. K. (2024). Does Environmental Exposure to Pharmaceutical and Personal Care Product Residues Result in the Selection of Antimicrobial-Resistant Microorganisms, and is this Important in Terms of Human Health Outcomes? *Environmental Toxicology and Chemistry*, *43*(3). https://doi.org/10.1002/etc.5498.

Steffen, W., Richardson, K., Rockström, J., Cornell, S. E., Fetzer, I., Bennett, E. M., Biggs, R., Carpenter, S. R., De Vries, W., De Wit, C. A., Folke, C., Gerten, D., Heinke, J., Mace, G. M., Persson, L. M., Ramanathan, V., Reyers, B., & Sörlin, S. (2015). Planetary boundaries: Guiding human development on a changing planet. *Science*, *347*(6223). https://doi.org/10.1126/science.1259855.

Stehle, S., & Schulz, R. (2015). Agricultural insecticides threaten surface waters at the global scale. *Proceedings of the National Academy of Sciences of the United States of America*, *112*(18). https://doi.org/10.1073/pnas.1500232112.

Stokes, H. W., & Hall, R. M. (1989). A novel family of potentially mobile DNA elements encoding site-specific gene-integration functions: integrons. *Molecular Microbiology*, *3*(12). https://doi.org/10.1111/j.1365-2958.1989.tb00153.x.

Strohmeier Gort, A., Ferber, D. M., & Imlay, J. A. (1999). The regulation and role of the periplasmic copper, zinc superoxide dismutase of *Escherichia coli*. *Molecular Microbiology*, *32*(1). https://doi.org/10.1046/j.1365-2958.1999.01343.x.

Su, Z., Chen, L., & Wen, D. (2024). Impact of wastewater treatment plant effluent discharge on the antibiotic resistome in downstream aquatic environments: a mini review. In *Frontiers of Environmental Science and Engineering* (Vol. 18, Number 3). https://doi.org/10.1007/s11783-024-1796-3.

Sünderhauf, D., Klümper, U., Gaze, W. H., Westra, E. R., & van Houte, S. (2023). Interspecific competition can drive plasmid loss from a focal species in a microbial community. *ISME Journal*, *17*(10). https://doi.org/10.1038/s41396-023-01487-w.

Tezel, U., & Pavlostathis, S. G. (2015). Quaternary ammonium disinfectants: Microbial adaptation,Degradation and ecology. In *Current Opinion in Biotechnology* (Vol. 33). https://doi.org/10.1016/j.copbio.2015.03.018.

Thomas, C. M., & Nielsen, K. M. (2005). Mechanisms of, and barriers to, horizontal gene transfer between bacteria. In *Nature Reviews Microbiology* (Vol. 3, Number 9). https://doi.org/10.1038/nrmicro1234.

Touchon, M., Moura de Sousa, J. A., & Rocha, E. P. (2017). Embracing the enemy: The diversification of microbial gene repertoires by phage-mediated horizontal gene transfer. In *Current Opinion in Microbiology* (Vol. 38). https://doi.org/10.1016/j.mib.2017.04.010.

van Bavel, B., Berrang-Ford, L., Moon, K., Gudda, F., Thornton, A. J., Robinson, R. F. S., & King, R. (2024). Intersections between climate change and antimicrobial resistance: a systematic scoping review. In *The Lancet Planetary Health* (Vol. 8, Number 12). https://doi.org/10.1016/S2542-5196(24)00273-0.

Vandecraen, J., Chandler, M., Aertsen, A., & Van Houdt, R. (2017). The impact of insertion sequences on bacterial genome plasticity and adaptability. In *Critical Reviews in Microbiology* (Vol. 43, Number 6). https://doi.org/10.1080/1040841X.2017.1303661.

Varani, A., He, S., Siguier, P., Ross, K., & Chandler, M. (2021). The IS6 family, a clinically important group of insertion sequences including IS26. In *Mobile DNA* (Vol. 12, Number 1). https://doi.org/10.1186/s13100-021-00239-x.

Verlicchi, P., Al Aukidy, M., Galletti, A., Petrovic, M., & Barceló, D. (2012). Hospital effluent: Investigation of the concentrations and distribution of pharmaceuticals and environmental risk assessment. *Science of the Total Environment*, *430*. https://doi.org/10.1016/j.scitotenv.2012.04.055.

Vezeau, N., & Kahn, L. (2024). Spread and mitigation of antimicrobial resistance at the wildlife-urban and wildlife-livestock interfaces. *Journal of the American Veterinary Medical Association*, *262*(6). https://doi.org/10.2460/javma.24.02.0123.

Villa, L., & Carattoli, A. (2020). Plasmid Typing and Classification. In *Methods in Molecular Biology* (Vol. 2075). https://doi.org/10.1007/978-1-4939-9877-7_22.

Virolle, C., Goldlust, K., Djermoun, S., Bigot, S., & Lesterlin, C. (2020). Plasmid transfer by conjugation in gram-negative bacteria: From the cellular to the community level. In *Genes* (Vol. 11, Number 11). https://doi.org/10.3390/genes11111239.

Virtanen, P., Gommers, R., Oliphant, T. E., Haberland, M., Reddy, T., Cournapeau, D., Burovski, E., Peterson, P., Weckesser, W., Bright, J., van der Walt, S. J., Brett, M., Wilson, J., Millman, K. J., Mayorov, N., Nelson, A. R. J., Jones, E., Kern, R., Larson, E., … Vázquez-Baeza, Y. (2020). SciPy 1.0: fundamental algorithms for scientific computing in Python. *Nature Methods*, *17*(3). https://doi.org/10.1038/s41592-019-0686-2.

Wang, Y., Lu, J., Mao, L., Li, J., Yuan, Z., Bond, P. L., & Guo, J. (2019). Antiepileptic drug carbamazepine promotes horizontal transfer of plasmid-borne multi-antibiotic resistance genes within and across bacterial genera. *The ISME Journal*, *13*(2), 509–522. https://doi.org/10.1038/s41396-018-0275-x.

Wang, Y., Lu, J., Zhang, S., Li, J., Mao, L., Yuan, Z., Bond, P. L., & Guo, J. (2021). Non-antibiotic pharmaceuticals promote the transmission of multidrug resistance plasmids through intra- and intergenera conjugation. *The ISME Journal*, *15*(9), 2493–2508. https://doi.org/10.1038/s41396-021-00945-7.

Wang, Z., Walker, G. W., Muir, D. C. G., & Nagatani-Yoshida, K. (2020). Toward a Global Understanding of Chemical Pollution: A First Comprehensive Analysis of National and Regional Chemical Inventories. *Environmental Science and Technology*, *54*(5). https://doi.org/10.1021/acs.est.9b06379.

Wick, R. R., Howden, B. P., & Stinear, T. P. (2025). Autocycler: long-read consensus assembly for bacterial genomes. *Bioinformatics*, *41*(9). https://doi.org/10.1093/bioinformatics/btaf474.

Wick, R. R., Schultz, M. B., Zobel, J., & Holt, K. E. (2015). Bandage: Interactive visualization of de novo genome assemblies. *Bioinformatics*, *31*(20). https://doi.org/10.1093/bioinformatics/btv383.

World Health Organization. (2025). *Global antibiotic resistance surveillance report 2025 Organización Mundial de la Salud*. https://www.who.int/publications/i/item/9789240116337.

Xiong, J., Hu, S., Xu, Z., Li, C., Li, Z., Li, S., Ma, Y., Ren, X., Huang, B., & Pan, X. (2024). Different paths, same destination: Bisphenol A and its substitute induce the conjugative transfer of antibiotic resistance genes. *Chemosphere*, *368*, 143625. https://doi.org/10.1016/j.chemosphere.2024.143625.

Xu, Y. Q., Huo, Z. Y., Bai, Y., Wang, Y., Wang, W. L., Wang, H. Bin, Gao, Y. J., Wang, R. N., Li, C. Y., Liu, H., Huang, W. E., Hu, H. Y., & Wu, Y. H. (2026). Isothiazolinone biocide aggravate disinfection-resistant bacterial fouling on reverse osmosis membranes. *Desalination*, *620*. https://doi.org/10.1016/j.desal.2025.119637

Yang, B., Sun, J., Zhu, S., Wang, Z., & Liu, Y. (2024). Exposure to bisphenol compounds accelerates the conjugative transfer of antibiotic resistance plasmid. *Environmental Research*, *263*, 120002. https://doi.org/10.1016/j.envres.2024.120002.

Yin, L., Wang, X., Xu, H., Yin, B., Wang, X., Zhang, Y., Li, X., Luo, Y., & Chen, Z. (2023). Unrecognized risk of perfluorooctane sulfonate in promoting conjugative transfers of bacterial antibiotic resistance genes. *Applied and Environmental Microbiology*, *89*(9), e00533–23. https://doi.org/10.1128/aem.00533-23.

Yu, Z., Wang, Q., Pinilla-Redondo, R., Madsen, J. S., Clasen, K. A. D., Ananbeh, H., Olesen, A. K., Gong, Z., Yang, N., Dechesne, A., Smets, B., Nesme, J., & Sørensen, S. J. (2024). Horizontal transmission of a multidrug-resistant IncN plasmid isolated from urban wastewater. *Ecotoxicology and Environmental Safety*, *271*. https://doi.org/10.1016/j.ecoenv.2024.115971.

Yu, Z., Wang, Y., Lu, J., Bond, P. L., & Guo, J. (2021). Nonnutritive sweeteners can promote the dissemination of antibiotic resistance through conjugative gene transfer. *The ISME Journal*, *15*(7), 2117–2130. https://doi.org/10.1038/s41396-021-00909-x.

Zhang, H., Song, J., Zheng, Z., Li, T., Shi, N., Han, Y., Zhang, L., Yu, Y., & Fang, H. (2023). Fungicide exposure accelerated horizontal transfer of antibiotic resistance genes via plasmid-mediated conjugation. *Water Research*, *233*, 119789. https://doi.org/10.1016/j.watres.2023.119789.

Zhao, C. D., Suyamud, B., Yuan, Y., Ghosh, S., Xu, X. L., Hu, J. Y., Zhao, C., Suyamud, B., Yuan, Y., Ghosh, S., Xu, X., & Hu, J. (2025). Effect of non-antibiotic factors on conjugative transfer of antibiotic resistance genes in aquaculture water. *JOURNAL OF HAZARDOUS MATERIALS*, *483*. https://doi.org/10.1016/j.jhazmat.2024.136701.

Zhu, S. Y., Yang, B. Q., Jia, Y. Q., Yu, F. Y., Wang, Z. Q., Liu, Y., Zhu, S., Yang, B., Jia, Y., Yu, F., Wang, Z., & Liu, Y. (2023). Comprehensive analysis of disinfectants on the horizontal transfer of antibiotic resistance genes. *JOURNAL OF HAZARDOUS MATERIALS*, *453*. https://doi.org/10.1016/j.jhazmat.2023.131428.

Zhuang, Y., Ren, H., Geng, J., Zhang, Y., Zhang, Y., Ding, L., & Xu, K. (2015). Inactivation of antibiotic resistance genes in municipal wastewater by chlorination, ultraviolet, and ozonation disinfection. *Environmental Science and Pollution Research*, *22*(9). https://doi.org/10.1007/s11356-014-3919-z.